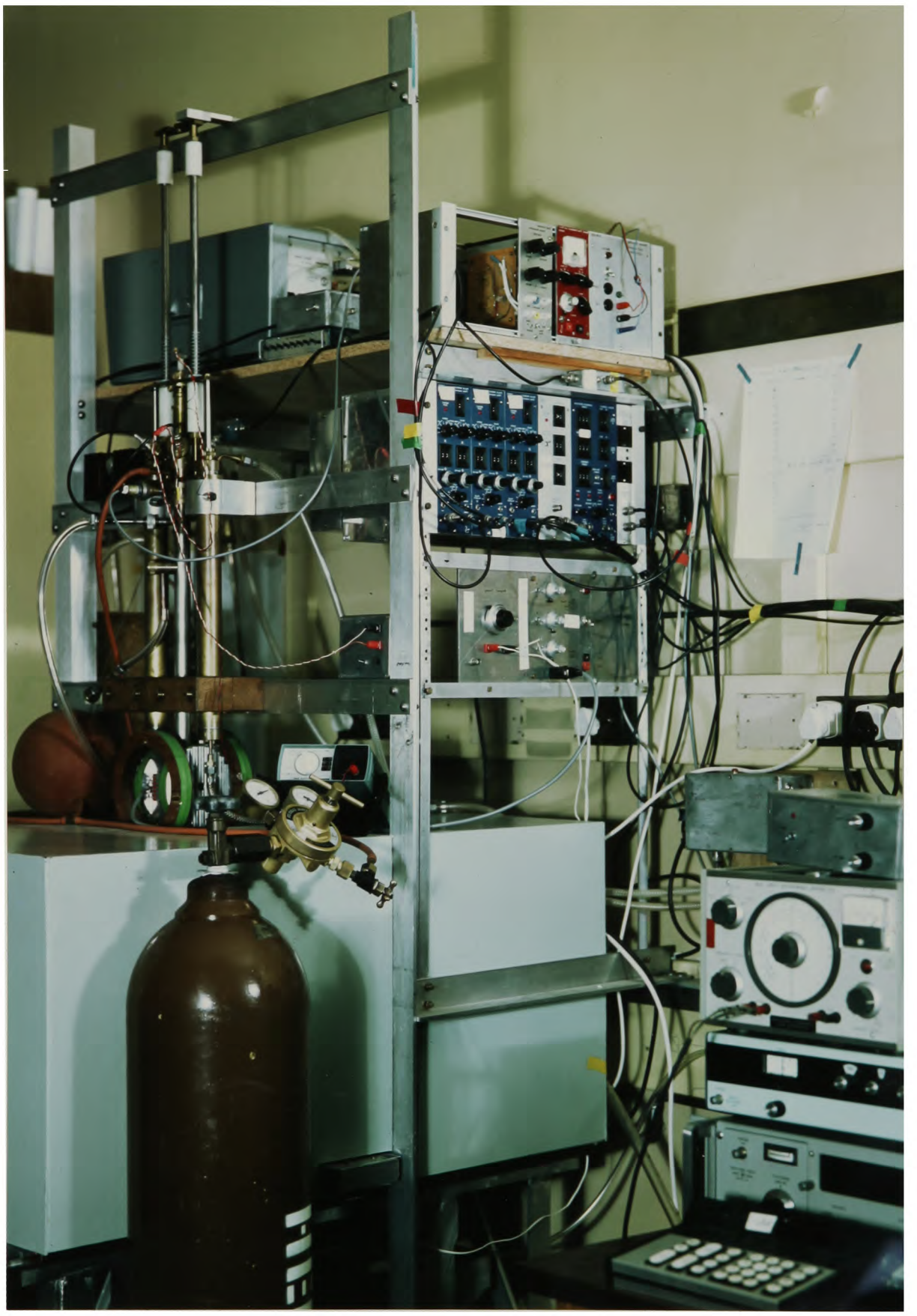


THE APPARATUS

Nuclear Quadrupole Double Resonance

J.P.G. Mailer

This thesis is submitted in partial fulfilment of the requirement for the degree of Doctor of Philosophy in the University of Oxford



Wolfson College

Trinity Term, 1977

CONTENTS

		Page
	CHAPTER I	
	INTRODUCTION	1
	CHAPTER II	
	BASIC THEORIES OF NMR	5
2.1	INTRODUCTION	5
2.2	THE ROTATING FRAME AND THE 90° PULSE (11)	5
2.3	SPIN-SPIN INTERACTIONS AND T_2 (12)	8
2.4	SPIN-LATTICE INTERACTIONS AND T_1	10
2.5	MEASUREMENT METHODS (13)	14
2.6	SPIN TEMPERATURE AND ISENTROPIC DEMAGNETISATION (12)	15
	2.6.1 Spin Temperature	15
	2.6.2 Isentropic Demagnetisation	16
2.7	SPIN MIXING (4)	18
	CHAPTER III	
	THEORY OF NQR, AND THE LEVEL CROSSING METHOD	21
3.0	INTRODUCTION	21
3.1	CLASSICAL INTERACTIONS (15)	21
	3.1.1 Nuclear Quadrupole Moment Tensor Q_{jk}	22
	3.1.2 Electric Field Gradient Tensor V_{jk} (E F G)	23
3.2	QUANTUM-MECHANICAL DEVELOPMENT (15,17)	25
	3.2.1 Spin $I = 1$ (18)	25
	3.2.2 Small Static Magnetic Fields ($\gamma B \ll e^2qQ/h$)	28
	3.2.3 Special Case of $\eta = 0$ $(I = 1)$	29
	3.2.4 General Case $\eta \neq 0$ $(I = 1)$	29
	3.2.5 Large Magnetic Fields $\gamma \hbar B \gg e^2qQ$	
	3.2.6 Spin $\frac{3}{2}$ Case (9)	30
3.3	DETECTION METHODS AND DOUBLE RESONANCE	31
	3.3.1 Pure Quadrupole Resonance	31
	3.3.2 Double Resonance Methods (4)	33
	3.3.3 The Dipolar Bath (12)	39
3.4	SPIN MIXING BY LEVEL CROSSING (4,6)	41
	3.4.1 Polarisation Phase	41
	3.4.2 Irradiation Phase	45
	3.4.3 Detection Phase	45
	3.4.4 Physical Interpretation of Sensitivity	48
	3.4.5 Limitations of the Simple Theory	50

CONTENTS
(continued)

		Page
	CHAPTER IV	
	THE APPARATUS	51
4.1	INTRODUCTION	51
4.2	BRUKER 'MINISPEC' AND MODIFICATIONS TO IT	52
	4.2.1 Modifications	54
4.3	NMR TANK CIRCUIT	55
	4.3.1 Minispec/Tank Circuit Connection Network	56
4.4	CRYOSTAT AND TEMPERATURE CONTROL SYSTEM	59
	4.4.1 Introduction	59
	4.4.2 Construction	60
	4.4.3 Performance	62
	4.4.4 Temperature Sensors	64
	4.4.5 Temperature Control Unit	65
	4.4.6 Storage Dewars	64
	4.4.7 Internal Fittings	68
4.5	SYSTEM CYCLE CONTROLLER	68
	4.5.1 Central Control Module	68
	4.5.2 Operation	68
	4.5.3 Pulse Generator Modules	70
	4.5.4 Use of the Controller	70
4.6	THE QUADRUPOLE IRRADIATION SYSTEM	73
	4.6.1 R.F. Power Amplifier	74
	4.6.2 NQR Irradiation Coil (Upper Coil)	77
	4.6.3 Field Calibration	77
4.7	UPPER STATIC MAGNETIC FIELD CONTROL UNIT	79
	4.7.1 Field Calibration	81
4.8	CHART RECORDER CONTROL UNIT	83
4.9	NMR MAGNET, MAIN FRAME, AND TRANSIT MECHANISM	83
	4.9.1 NMR Magnet	83
	4.9.2 Apparatus Main Frame	86
	4.9.3 Sample Transit Mechanism - Operation	87
4.10	PERFORMANCE DATA: NQR SPECTROMETER MARK II	90

LIST OF PLATES

Plate 1	NMR Coil Former and Tank Circuit	91
Plate 2	Cryostat - Dewar Vessel	92
Plate 3	Cryostat - Flow Control Insert	92
Plate 4	Helium Storage Dewar and Hydraulic Lifting Mechanism	93
Plate 5	NMR Magnet (During Installation)	94
Plate 6	View of Main Frame Assembly without the Magnet	95
Plate 7	Sample Transit Mechanism, Internal Support Tube and RF Coils	95
Plate 8	Details of Transit Mechanism and Cryostat Top Plate Connections	96
Plate 9	Telescopic Exchange Gas Sealing Tube	96

CONTENTS
(continued)

		Page
CHAPTER V		
	DOUBLE RESONANCE BY CONTINUOUS COUPLING	97
5.1	INTRODUCTION	97
5.2	CONTINUOUS COUPLING THROUGH ν_0 ALONE	98
	5.2.1 Irradiation of ν_+	99
	5.2.2 Irradiation of ν_-	100
	5.2.3 Generalization of Continuous Coupling to the Case of $I > 1$	104
5.3	CONTINUOUS COUPLING THROUGH ν_+ AND ν_-	104
	5.3.1 Experimental	107
5.4	DETECTION OF NATURALLY ABUNDANT DEUTERIUM NQR	114
	5.4.1 Natural Abundance ^2D Spectra in HCOOH	114
5.5	CONCLUSION	116
5.6	FACTORS AFFECTING NITROGEN NQR SENSITIVITY	117
	5.6.1 Experimental Observations	120
	5.6.2 Continuous Coupling of ν_0 and Nitrogen NQR	123
5.7	CONCLUSION	130
CHAPTER VI		
	USES OF HIGH-SENSITIVITY NQR	131
6.1	INTRODUCTION	131
6.2	D-D AND H-D INTERACTIONS IN AMIDE GROUPS AND WATER MOLECULES	131
	6.2.1 Conclusions	140
6.3	NQR SPECTRUM OF LANTHANUM NICOTINATE DIHYDRATE (LND)	142
	6.3.1 Structure of LND	143
	6.3.2 Hydrogen-Bonding in Related Pyridine-Ring Compounds	145
6.4	CORRELATION BETWEEN NITROGEN COUPLING CONSTANTS AND HYDROGEN BOND LENGTH IN PYRIDINE DERIVATIVES	147
6.5	CONCLUSIONS	150

CONTENTS
(continued)

		Page
	CHAPTER VII	
	QUADRUPOLE RESONANCE IN SPIN $\frac{3}{2}$ NUCLEI	151
7.1	INTRODUCTION	151
7.2	ZEEMAN NQR IN SPIN $\frac{3}{2}$ POWDERS	152
	7.2.1 Theory	153
7.3	LEVEL CROSSING AND THE SPIN $\frac{3}{2}$ NUCLEUS	156
	7.3.1 Level Crossing Calculations	159
	7.3.2 Double Irradiation Effects	162
	7.3.3 Continuous Coupling Effects	165
7.4	EXPERIMENTAL INVESTIGATION OF NaOH AND ITS DERIVATIVES	170
	7.4.1 Comparative Studies	175
	7.4.2 The Hydrates of NaOH	176
	7.4.3 Structures of NaOH and its Hydrates	179
	7.4.4 Water Molecules and Assignment of the HDO Spectrum of $NaOH.4H_2O$	182
7.5	CONCLUSIONS	183
	CHAPTER VIII	
	RELAXATION TIMES AND RELATED PROBLEMS	185
8.1	INTRODUCTION	185
8.2	RELAXATION TIMES AND THE DRLC METHOD	185
	8.2.1 Proton (P-Spin) Spin-Lattice Relaxation Time T_1	185
	8.2.2 Proton Dipolar T_1 (T_{1D})	186
	8.2.3 Q Spin Relaxation Times	186
	8.2.4 T_1 and the NQR Experiment	186
8.3	FACTORS AFFECTING T_1 AND T_{1D}	187
	8.3.1 Paramagnetic Relaxation[64]	188
	8.3.2 Phonon-Induced Relaxation	190
	8.3.3 The T_1 Minimum Prediction	191
8.4	EXPERIMENTAL OBSERVATIONS	195
8.5	CONCLUSION	197
	CHAPTER IX	
	SUCCESSES, FAILURES AND THE FUTURE	199
9.1	GENERAL CONCLUSIONS	199
9.2	LIMITATIONS OF THE APPARATUS	200
9.3	FUTURE DEVELOPMENTS	200
	9.3.1 The Single Transit Spectrometer	202
	9.3.2 High-Speed Passage	204
	9.3.3 Electromagnetic Field Switching	205
9.4	EPILOGUE	209

CONTENTS
(continued)

		Page
	APPENDICES	210
App. 1	TUNED CIRCUITS	210
	A.1 Damped Oscillations	210
	A.2 Parallel Tuned Circuit - Driven by a Generator	212
	A.3 Tank Circuit used in NMR Detection System	216
	A.4 Summary	222
App. 2	LIST OF COMPONENTS	224
	REFERENCES	225

ACKNOWLEDGEMENTS

Many people have helped me during the course of this work, but I should like to thank the following in particular.

Prof. B. Bleaney, for extending to me the facilities of the Clarendon laboratory.

Dr. D.T. Edmonds, for his excellent supervision and constant enthusiasm, even in the face of adversity.

Dr F.N.H. Robinson, for much useful advice.

Tony White, Shaul Goren and Alex Mackay, for sharing my problems as other members of our group.

Prof. Abragam, for his book[12].

The technical and research staff of the Clarendon Laboratory, including Ray Hewitt, Harold Lock, John Siertsema, David Smith, Bill Turner and John Ward.

The S.R.C. Permanent Magnet Centre, Sunderland Polytechnic.

For financial support, I wish to thank the Science Research Council, who funded the project and gave me a studentship, and also Oxford University Board of Graduate Studies, the Scott Fund and Wolfson College.

Finally, I must thank Ina Godwin for turning my grubby scribblings into this fine typescript.

NUCLEAR QUADRUPOLE DOUBLE RESONANCE

J.P.G. Mailer, Wolfson College

A thesis submitted for the degree of Doctor of Philosophy
in the University of Oxford, Trinity term 1977

ABSTRACT

The basic theories of Nuclear Quadrupole Resonance are outlined, together with some basic NMR theory and its application to double resonance techniques.

An improved design of spectrometer using double resonance is presented, including a description of a new flow cryostat which can operate down to 4.2°K with low (250 cc/hour) consumption of liquid He. The whole apparatus may be used to detect NQR signals in solids over the frequency range 100 kHz - 5 MHz.

The theory of double resonance with spin mixing by continuous coupling (DRCC) is developed and illustrated by experiments performed on HCOOD, HDO and several nitrogen-containing compounds, including Imidazole. Further experiments were then carried out on samples dilute in deuterium, including the detection of NQR in formic acid (HCOOH) due to naturally abundant deuterium. Other experiments on proton-deuteron interactions in amide groups and in water molecules are also described and compared with results previously published on fully-deuterated amides and D_2O as a water of crystallisation in L-serine hydrate.

The NQR spectrum of Lanthanum Nicotinate Dihydrate is obtained using F.M. techniques and related to its structure.

The theory of Zeeman NQR in spin $\frac{3}{2}$ nuclei is developed with reference to the double resonance technique, and the measured quadrupole coupling constants of ^{23}Na and ^{2}D in NaOH and some of its hydrates are discussed.

Finally, some standard theories concerning proton relaxation times in solids at low temperatures (4°K-300°K) are outlined and related to some measured relaxation times, illustrating their significance to the double resonance technique.

The concluding chapter outlines a speculative proposal for a new spectrometer design.

ABBREVIATIONS AND SYMBOLS

SYMBOL	MEANING
B , B_0 , B_1	Magnetic field
Cycle Time	The time to complete one experimental measurement using D R L C
D R C C	Double resonance with spin mixing by continuous coupling
D R L C	Double resonance with spin mixing by level crossing
D R R F	Double resonance with spin mixing in the rotating frame
E F G	Electric field gradient
E N D O R	Electron nuclear double resonance
eq	V_{zz}: strength of E F G
eQ	Nuclear quadrupole moment
e^2qQ	The product of the above. Energy of nuclear quadrupole interaction
e^2qQ/h	Quadrupole interaction in kHz
F I D	Free induction decay
F M	Frequency modulation
$\mathcal{H}$	Hamiltonian (operator)
I	Nuclear spin (operator)
L N D	Lanthanum nicotinate dihydrate
m , M	(Nuclear) magnetic moment
N M R	Nuclear magnetic resonance
N Q R	Nuclear quadrupole resonance
O X Y Z	Laboratory frame coordinate system
O X′ Y′ Z	Rotating frame coordinate system
P P	Peak-to-peak
P spins	Spins used for detecting N Q R/spin $\frac{1}{2}$
Q spins	Spins to be examined in N Q R/spin ≥ 1
R F	Radio frequency (irradiation)
T_1	High field spin-lattice relaxation time
T_{1D}	Dipolar (low) field spin-lattice relaxation time
T_2	Spin-spin relaxation time
Up time	Time when N Q R sample is held in low field region
Z N Q R	Zeeman nuclear quadrupole resonance
γ	gyromagnetic ratio
ν	$\gamma/2\pi$
μ	magnetic moment

SYMBOL	MEANING
ν	absorption frequency
ν^+ , ν^- , ν^0	N Q R frequencies of a spin 1 nucleus
ν_q	N Q R frequency of a spin $\frac{3}{2}$ nucleus (zero field)
η	Asymmetry parameter of E F G
(θ , ϕ)	Polar coordinates
θ	Temperature
ρ	(a) $(1 + \frac{1}{3} \eta^2)^{\frac{1}{2}}$; (b) Charge density.
τ	Time interval, correlation time
π }	Parts of final measured P spin magnetisation:
Δ }	π does not depend directly on the Q spins

CHAPTER I

INTRODUCTION

The field of nuclear quadrupole resonance is a relatively new one, the first successful experiment having been performed in 1951 by DEHMELT and KRUGER[1]. For many years, however, pure quadrupole resonance studies were restricted to the heavy elements and the halogens, especially chlorine, which has a large quadrupole moment.

Pure quadrupole resonance in light nuclei only became a routine experimental possibility with the development of the techniques of Nuclear Quadrupole Double Resonance from 1962 onwards[2]. The technique of nuclear quadrupole double resonance with spin mixing by level crossing, the topic of this thesis, was first described in 1969 in the Ph.D Thesis of KOO[3], a student of E.L. HAHN at Berkeley. Subsequently, this method was developed in the Clarendon Laboratory in the research group of D.T. EDMONDS, and is described in several papers[4-6].

All nuclei with spin $I \geq \frac{1}{2}$ have a magnetic moment and those with $I \geq 1$ also have a quadrupole moment. If a sample containing an assembly of nuclei with non-zero spin is immersed in a magnetic field $\underline{B}$, a characteristic set of energy levels will be generated. The values of these energy levels will depend on the magnetic moment, quadrupole moment, applied magnetic field and on the chemical environment of the nucleus under study. Under suitable conditions, electromagnetic radiation of the appropriate frequency may cause transitions of the nucleus between its allowed energy levels. This phenomenon of Nuclear Spin Resonance[7] may be divided into two main categories, depending on the conditions under which it is observed.

If the magnetic energy term $\underline{\mu} \cdot \underline{B}$ (where $\underline{\mu}$ = magnetic moment) $\gg e^2qQ$ (the energy of the quadrupole interaction) the phenomenon is called Nuclear Magnetic Resonance (NMR). For spin $I = \frac{1}{2}$, there is no quadrupole moment,

and one may only use NMR to investigate the nucleus in question. If, however, $e^2qQ \gg \underline{\mu} \cdot \underline{B}$, the phenomenon is called Nuclear Quadrupole Resonance (NQR): NQR can be performed when $\underline{B} = 0$ and the magnetic energy term is zero. Both these phenomena are useful probes of the chemical structure of materials, because the precise absorption frequencies and relaxation times that one may measure depend critically on the immediate molecular environment of the nucleus under study.

For example, an NMR study of the protons ($I = \frac{1}{2}$) in ethanol (CH_3CH_2OH) reveals[8] a closely-spaced three-line multiplet spectrum. The largest line corresponds to the protons of the $-CH_3$ group, the middle line to the protons of $-CH_2$ and the smallest line to the $-OH$ group protons. The differences in the chemical environments of the three types of proton reveal themselves as shifts in the observed absorption frequency $\sim 10^{-4}$ of the mean absorption frequency of protons. This effect is known as the chemical shift. NMR lines in liquids are particularly sharp, and measurements of chemical shifts in large values of applied field ($\underline{B} \sim 2\text{-}5$ T) reveal much about the chemical structure of the molecules.

Alternatively, if we perform an NQR study in zero magnetic field (so that magnetic energy terms may be ignored) of (say) CD_3CD_2OD, we would observe an absorption spectrum due to the deuterium ($I = 1$), which would be a direct result of the chemical structure of the molecule. We would be restricted to examining solid d-ethanol, because an NQR experiment provides information about the electric field gradient at the nucleus in question. Rapid thermal motions in liquids (Brownian motion) remove all asymmetry from molecular electric field gradients, and the quadrupole energy, e^2qQ, becomes zero. Returning to our thought-experiment on d-ethanol, we would expect to see a complete spectrum of lines from all the deuterium sites in the solid, with a broad grouping into CD_3, CD_2 and OD deuterons. From

these we could deduce the strength and symmetry of the field gradients at all the sites in the molecule. A direct comparison can then be made with the calculations of the structural chemist, because electric field gradients are essentially an average of $(3z^2-r^2)/r^5$ over the molecular wave function - an easier parameter to calculate than the chemical shift, for example, especially for light elements with their simpler electron orbitals.

However, an experimental investigation of pure NQR of light elements in powder solids had to wait for the development of sensitive double resonance methods. Our method is generally applicable to low-frequency NQR (100 kHz - 5 MHz) and has been demonstrated in ^{2}D, ^{10}B, ^{11}B, ^{14}N, ^{17}O, ^{23}Na, ^{25}Mg and ^{27}Al [9]. Since many organic materials contain ^{14}N, ^{1}H and ^{16}O, much data has been collected in recent years[4,9] on organic molecules, much of it from samples in which ^{2}D is substituted for ^{1}H and some in which ^{17}O is substituted for ^{16}O.

Analysis of deuterium spectra is especially useful, since ^{2}D has only a single 1s electron, and its ground state is well removed from its excited states. The spherical charge distribution of a 1s electron contributes nothing to the electric field gradient at the ^{2}D nucleus, and hence ^{2}D NQR probes only the field gradients due to external atoms or molecules.

Nuclear Quadrupole Double Resonance relies heavily on the sister technique of NMR for its sensitivity, and for this reason we must begin by describing the simpler theories of NMR, to the extent that is necessary for an understanding of the experimental method.

The aim of this work has been to advance our knowledge of the method of Nuclear Quadrupole Double Resonance, from a practical point of view, so that it may be applied to a wider range of nuclei and molecules.

This thesis may be divided broadly into two parts. The first part, consisting of Chapters II, III, IV and Appendix I, describes the basic

theories and terminology used in our technique, and includes a detailed description of a new spectrometer built during the course of this research, designed to make the best use of the theories as we presently understand them.

The rest of the thesis describes a series of experiments carried out in order to improve our understanding of the method. Chapter V develops the ideas of continuous coupling, especially as applied to deuterium N Q R, and Chapter VI describes a series of experiments using these new methods. Chapter VII develops the theory of Zeeman N Q R in spin $\frac{3}{2}$ nuclei, and applies it to an investigation of NaOH and some of its hydrates. Chapter VIII outlines some of the theories of relaxation times in solids and describes some experiments performed at 4.2°K which revealed relatively small changes in relaxation times compared to 77°K.

Chapter IX forms a conclusion, and sums up the successes and failures of the last three years as I see them. It also includes a speculative proposal for a new design of spectrometer, which might solve some of the problems which we did not overcome.

CHAPTER II

BASIC THEORIES OF NMR

2.1 INTRODUCTION

Nuclear quadrupole resonance spectroscopy has been performed principally in two ways — continuous wave NQR (including also pulsed NQR) and NQR by double resonance. The former is outwith the scope of this thesis, but will be discussed briefly in Chapter III.

The methods we employ are known as Nuclear Quadrupole Double Resonance with spin mixing by Level Crossing (DRLC) and with spin mixing by Continuous Coupling (DRCC). Other double resonance methods also exist, and are referred to in Chapter III.

Double Resonance techniques all employ two types of spin, viz the 'P spins' which are abundant and the 'Q spins' which may be rare and whose quadrupole spectrum we wish to measure. We always end an experimental cycle by performing a Nuclear Magnetic Resonance (NMR) experiment to measure the magnetisation of the P spins. Several of the fundamental ideas of double resonance come from the field of NMR, and we thus begin this thesis with a summary of the theories of NMR and develop the ideas which we will later use to describe the NQR double resonance techniques.

2.2 THE ROTATING FRAME AND THE 90° PULSE[11]

Any nucleus having a non-zero spin $\underline{I}$ will have an associated magnetic moment $\underline{m} = \gamma \hbar \underline{I}$, where γ = magnetogyric ratio of the nucleus.

Classically speaking, if a magnetic moment $\underline{m}$ is placed in a magnetic field $\underline{B}_0$, a couple is exerted on it given by:

$$\underline{C} = \underline{m} \times B_0 \qquad \ldots (2.1)$$

The angular momentum of the nucleus is then caused to change by this couple at a rate:

$$\frac{d}{dt}(\underline{I}\hbar) = \underline{C} = \underline{m} \times B_0$$

or

$$\frac{d\underline{m}}{dt} = \gamma \underline{m} \times B_0 . \qquad \ldots (2.2)$$

This equation indicates that the angular momentum $\underline{I}\hbar$ of the nucleus presses about $\underline{B}_0$ at a uniform angular velocity $-\gamma B_0 = \omega_L$ (the Larmor frequency).

It is convenient to change to a coordinate system rotating at angular velocity $\underline{\omega}$ with respect to the laboratory. Then if $\partial\underline{m}/\partial t$ represents the rate of change of $\underline{m}$ in this new coordinate system (Ref. (11), Appendix A)

$$\frac{d\underline{m}}{dt} = \frac{\partial \underline{m}}{\partial t} + \underline{\omega} \times \underline{m} . \qquad \ldots (2.3)$$

Using this in equation (2.2), we have

$$\frac{\partial \underline{m}}{\partial t} = \gamma \underline{m} \times \underline{B}_0 - \underline{\omega} \times \underline{m}$$

$$= \gamma \underline{m} \times \left(\underline{B}_0 + \frac{\underline{\omega}}{\gamma} \right)$$

$$= \gamma \underline{m} \times \underline{B}_{eff} . \qquad \ldots (2.4)$$

We may write $\frac{\underline{\omega}}{\gamma} = -\underline{B}'$, and $(\underline{B}_0 - \underline{B}') = \underline{B}_{eff}$, the effective field in the rotating frame. Clearly, if $\underline{\omega} = \underline{\omega}_L$, $\underline{B}' = \underline{B}_0$, $\underline{B}_{eff} = 0$ and $\frac{\partial \underline{m}}{\partial t} = 0$. $\underline{m}$ is then constant in time.

We now additionally apply a small oscillating magnetic field $\underline{B}_1 \cos \omega t$ in the plane normal to $\underline{B}_0$, which is circularly polarised so that the oscillating field is of constant magnitude B_1 and rotates at rate $\underline{\omega}$ about $\underline{B}_0$. [A plane polarised field may be considered as two contra-rotating circularly polarised components, so no generality is lost.]

In the frame rotating at $\underline{\omega}$ about $\underline{B}_0$, the effective magnetic field is now made up as in Fig.2.1, since $\underline{B}_1$ is now constant. With

$$\underline{B}_{eff} = \left(\underline{B}_0 + \frac{\underline{\omega}}{\gamma} \right) + \underline{B}_1 \qquad \ldots (2.5)$$

and

$$\frac{\partial \underline{m}}{\partial t} = \gamma \underline{m} \times \underline{B}_{eff} \qquad (2.4)$$

$\underline{m}$ will thus precess about $\underline{B}_{eff}$ (in the rotating frame) with an angular velocity $-\gamma \underline{B}_{eff}$. If $\underline{B}_1$ is switched on at time $t = 0$, and if $\underline{m}$ is initially aligned along $\underline{B}_0$ then as t increases, $\underline{m}$ will precess about $\underline{B}_{eff}$ until it reaches maximum angle 2θ with $\underline{B}_0$, before beginning to return, where (Fig.2.2)

$$\tan\theta = \frac{B_1}{B_0 - B'} = \frac{B_1}{B_0 + \omega/\gamma} \quad . \qquad \ldots (2.6)$$

If $\underline{B}_0 = -\omega/\gamma$, i.e. $\omega = \omega_L$, then $\theta = \pi/2$ and the maximum angle $2\theta = \pi$: i.e. $\underline{m}$ can turn right round till it is anti-parallel to $\underline{B}_0$. This can only happen when ω is very close to ω_L; for otherwise, with $B_1 \ll B_0$, θ is a very small angle. This is a forced resonance condition.

If we define $\omega_1 = -\gamma B_1$, then $\tan\theta = \frac{\omega_1}{\omega_L - \omega}$ and the resonance is of width $\approx \omega_1$.

At resonance

$$B_{eff} = B_1$$

$$\theta = \frac{\pi}{2}$$

and

$$\frac{\partial \underline{m}}{\partial t} = \gamma \underline{m} \times \underline{B}_1 = -\underline{m} \times \underline{\omega}_1 \quad .$$

Suppose now we apply $\underline{B}_1$ for some time t. If $\underline{m}$ is initially aligned along $\underline{B}_0$, then, when $\underline{B}_1$ has been applied for a period τ from $t = 0$ to $t = \tau$, with $\underline{\omega} = \underline{\omega}_L$, $\underline{m}$ will be at an angle α to B_0 where

$$\alpha = -\gamma B_1 \tau \quad .$$

If $\alpha = \frac{\pi}{2}$, then $|\tau| = \frac{\pi}{2\gamma B_1}$. Such a burst of radiation is called a '90° pulse'. If $|\tau| = \frac{\pi}{\gamma B_1}$, $\alpha = \pi$ and we have a '180° pulse'.

We have so far considered a classical situation in which a system of non-interacting magnetic moments are subjected to various magnetic fields.

Quantum mechanically, the angular momentum of each nuclear spin is quantised, and its projection on $\underline{B}_0$ is also quantised, forming magnetic

energy levels given by $E_m = -\underline{m} \cdot \underline{B}_0 = -\gamma\hbar m B_0$, where m is the 'magnetic quantum number. Allowed transitions are given by $\Delta m = \pm 1$, or $\hbar\omega = -\gamma\hbar B_0$. In other words, $\omega = \omega_L$, as in the classical case.

A large assembly of spins, in states of different m-values will give rise to a net macroscopic moment $\underline{M}$, where $\underline{M} = N_1\underline{m}_1 + N_2\underline{m}_2 + \ldots$ with $\underline{m}_1$, $\underline{m}_2$ etc. being allowed values of $\underline{m}$ in the field $\underline{B}_0$, and $N_1, N_2, \ldots$ are the occupation numbers of the states $\underline{m}_1$, $\underline{m}_2 \ldots$ [$\underline{m} = |I,m\rangle$].

So long as the interactions between spins are small, $\underline{M}$ will behave as the classical moment outlined above.

2.3 SPIN-SPIN INTERACTIONS AND T_2 [12]

If there were no other forces acting, the magnetic moment $\underline{M}$ prepared by a 90° pulse would continue to rotate (in the laboratory frame) about the direction of $\underline{B}_0$ indefinitely. However, each spin will experience a slightly different value of B_0, due to both inhomogeneity of the applied field and the varying magnetic effects of neighbouring spins. As a result, each spin will precess at a slightly different rate, so that the various individual moments that make up $\underline{M}$ will become non-parallel. The net effect is that the spins fan out in the $X'Y'$ plane of the rotating frame until the vector total represented by $\underline{M}$ becomes zero.

Definitions

If the total net magnetisation at some time is $\underline{M}$, made up of N spins each of moment $\underline{m}$, we may define:

$$\left.\begin{aligned} &\underline{M}_0 = N\underline{m} && \text{(all } \underline{m}_i \text{ parallel)} \\ &\underline{M} = \sum_{i=1}^{N} \underline{m}_i && \text{(}\underline{m}_i \text{ non-parallel)} \\ &M_p = \text{component of } \underline{M} \text{ parallel to } \underline{B}_0 \\ &\underline{M}_T = \text{(vector) components of } \underline{M} \text{ perpendicular to } \underline{B}_0 \end{aligned}\right\} \quad \ldots (2.7)$$

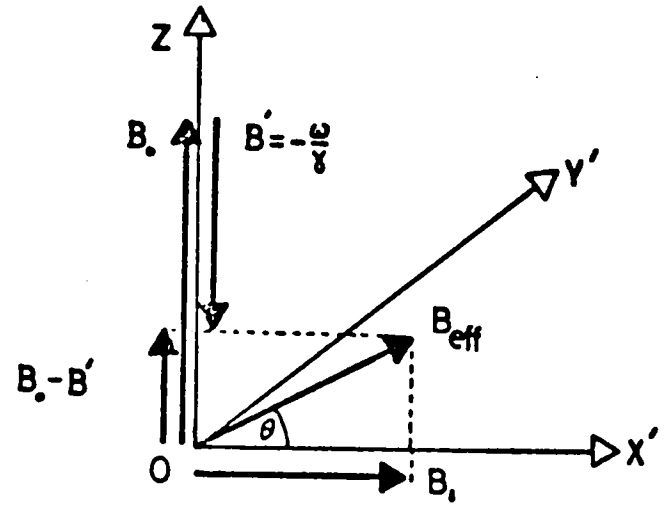


Fig. 2.1 : Fields in the Rotating Frame

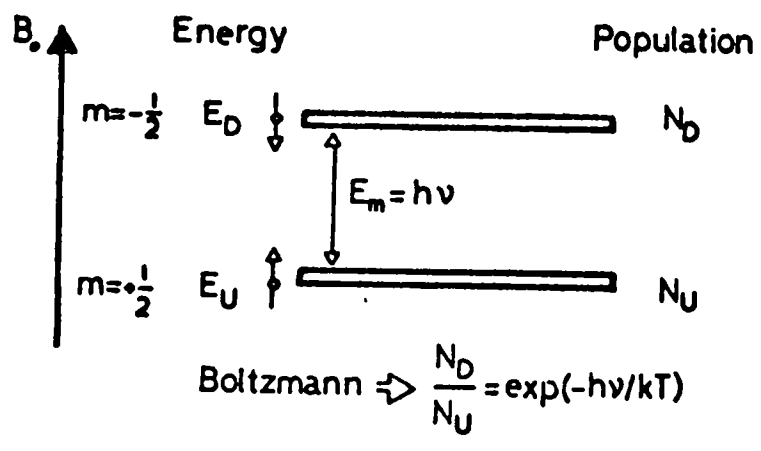


Fig. 2.3 : Magnetic energy (spin=$\frac{1}{2}$) levels

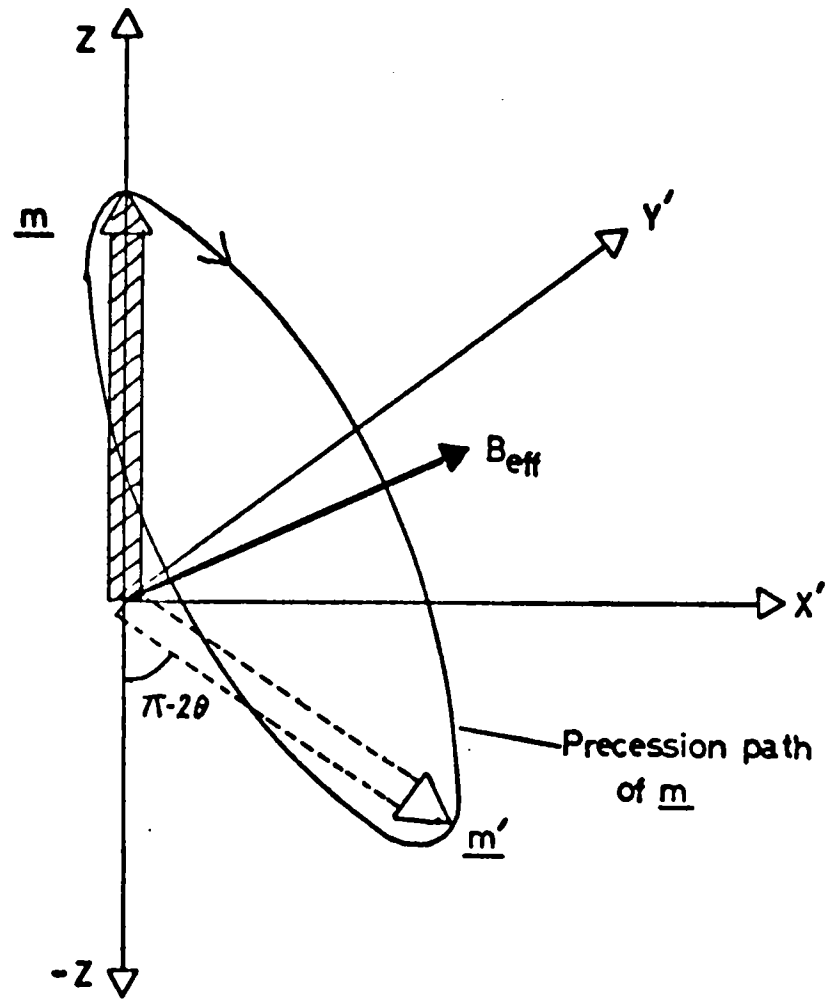


Fig. 2.2 : Precession of m in the rotating frame

Immediately following a 90° pulse, we have $M_p = 0$ and $\underline{M}_T = \underline{M}_0$ (fixed in the rotating frame, precessing about $\underline{B}_0$ in the laboratory frame)

We may define the Spin-Spin relaxation time T_2 thus: (where t represents time)

$$\underline{M}_T = \underline{M}_0 \cdot F(t/T_2) \qquad \ldots (2.8)$$

So that, for $t \gg T_2$, $\underline{M}_T \approx 0$, T_2 in solids is typically 10-30 μsec.

Note: Spin-Spin interactions involve no net transfer of energy into or out of the spin system, merely a redistribution of order within the spin system.

2.4 SPIN-LATTICE INTERACTIONS AND T_1

We now consider the statistical behaviour of this assembly of spins. As stated earlier, different values of the magnetic quantum number m correspond to different values of magnetic energy E_m, where $E_m = -\gamma\hbar m B_0$.

If the assembly of spins obeys Boltzmann statistics then, at some temperature T, the populations of these different energy levels will be given by P_m, where

$$P_m \propto \exp(-E_m/kT) = \exp(+\gamma\hbar m B_0/kT) \quad . \qquad \ldots (2.9)$$

The net macroscopic magnetisation of a sample containing N spins will then be given by M, where

$$M = N\gamma\hbar \frac{\sum_{m=-I}^{+I} m \exp(\gamma\hbar m B_0/kT)}{\sum_{m=-I}^{+I} \exp(\gamma\hbar m B_0/kT)} \qquad \ldots (2.10)$$

Since $\gamma\hbar B_0/kT$ is almost always small for nuclear moments (e.g. for protons, with $B_0 = 1T$, $T = 50^\circ K$, $\gamma\hbar B_0/kT = 6.5 \times 10^{-6}$) we can expand linearly and then

$$M = \frac{N\gamma^2\hbar^2 B_0}{kT} \frac{\sum_{-I}^{+I} m^2}{2I+1} = \frac{N\gamma^2\hbar^2 I(I+1)}{3kT} B_0 \qquad \ldots (2.11)$$

For example, for $I = \frac{1}{2}$ (Fig.2.3), we have two states: $m = +\frac{1}{2}$ and $m = -\frac{1}{2}$ and we have two energy levels $E_D = +\frac{1}{2}\gamma\hbar B_0$ and $E_u = -\frac{1}{2}\gamma\hbar B_0$.

Then

$$M = \frac{N\gamma^2\hbar^2\frac{3}{4}}{3kT} = \frac{N\gamma^2\hbar^2}{4kT} B_0 = \chi_0 B_0$$

[N.B. χ_0, the nuclear susceptibility, is very small (3.5×10^{-21} MKS/kg)].

For protons, say, in equilibrium at a temperature T in field B_0

$$\frac{N_D}{N_u} = \exp -(E_D - E_u)/kT = \exp(-h\nu/kT).$$

For B_0 = 1 Tesla, ν = 40 MHz and $T = 77°K$.

$$\frac{N_D}{N_u} = .999975, \quad \text{i.e.} \quad N_D \approx N_u \approx \frac{N}{2} \quad \text{where} \quad N = N_D + N_u$$

and

$$\frac{N_u - N_D}{N_u} = 2.5 \times 10^{-5},$$

i.e. only $\sim 10^{-5}$ of all protons present make up the net magnetisation.

Thus we see that

(a) An isolated set of spins can absorb energy (say from a 180° pulse) which would align any net $\underline{M}$ anti-parallel to $\underline{B_0}$. Equivalent to $N_D > N_u$.

(b) A set of spins in equilibrium with an environment at temperature T has only a small population difference between the two levels, and $N_u > N_D$.

To reconcile these two views of the spins we introduce the spin-lattice relaxation time T_1, as a mechanism which tends to re-order a set of spins such as (a) into a distribution such as (b), in a time span $\approx T_1$.

Put another way, if a set of spins, randomly oriented, is put into a magnetic field $\underline{B_0}$ at time $t = 0$, they will acquire a net magnetisation $\underline{M_p}$ parallel to $\underline{B_0}$ according to the rule

$$\underline{M_p} = \underline{M_0}(1 - \exp(-t/T_1)) \qquad \ldots (2.12)$$

where $\underline{M_0}$ is the equilibrium value given in equation (2.11) above, and $\underline{M_p}$ will not exceed $\underline{M_0}$. If, by means of a pulse of radiation, $\underline{M_p}$ is changed to some other value $\underline{M'}$, it will return to the equilibrium value $\underline{M_0}$ according to $\underline{M_p} = \underline{M_0} - M'e^{-t/T_1}$.

In solids at low temperatures, T_1 can be minutes or even hours. It is thus possible to define a separate spin temperature θ_s for a two-level system where

$$k\theta_s = \frac{E_m}{\ell n(N_u/N_D)} \qquad \ldots (2.13)$$

θ_s is established in a time $\approx T_2 \ll T_1$ and $\theta_s \rightarrow \theta_{lattice}$ in a time $\approx T_1$. The spin-lattice relaxation process requires a net loss of energy by the spins to the lattice.

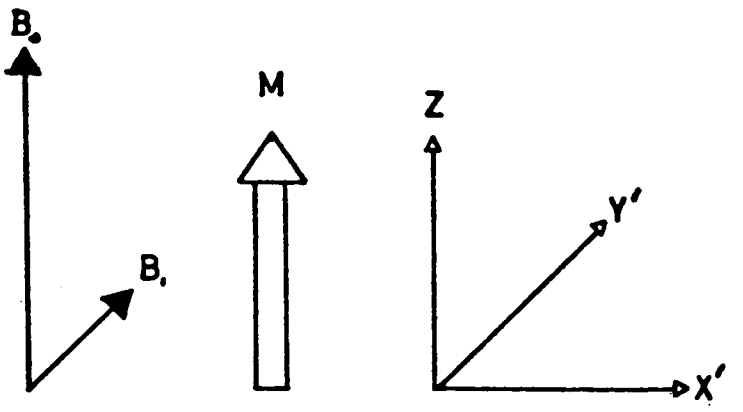
Energy is trapped in the spin system by a 90° pulse because, in general, $T_1 \gg T_2$, and the amount of energy trapped is proportional to the angle between $\underline{M}$ and $\underline{B}_0$.

Summary (see also Fig.2.4)

1. A spin system in a magnetic field $\underline{B}_0$ acquires a small net magnetisation $\underline{M}_0$.
2. It acquires this $\underline{M}_0$ in a time $\approx T_1$ and this equilibrium value of $\underline{M}_0$ is dependent on both the lattice temperature and $\underline{B}_0$.
3. If the equilibrium is disturbed — say by a 90° pulse — the spins re-distribute their orientations among themselves at a rate T_2, but may remain for some time in a state of non-equilibrium with the lattice — they have a different spin temperature.
4. While not in equilibrium with the lattice, energy is stored in the spin system, and the amount of this energy is dependent on the angle between $\underline{M}$ and $\underline{B}_0$.
5. In a time $\approx T_1$, the spin system will return to equilibrium with the lattice (i.e. at same temperature as the lattice), radiating energy (as heat) to the lattice.

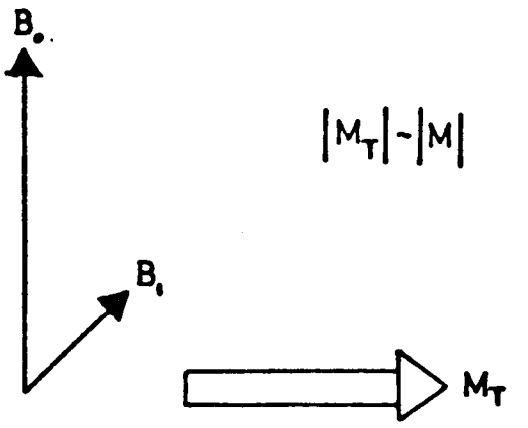
Notes T_2 processes involve no energy transfer to the lattice — this takes place only at T_1 rates.

The fan-out of the spins following a 90° pulse involves a transfer of energy from the spins to the radiation field, i.e. net power is emitted by the spins and may be observed as a free induction decay in a pick-up coil whose axis is perpendicular to $\underline{B}_0$.



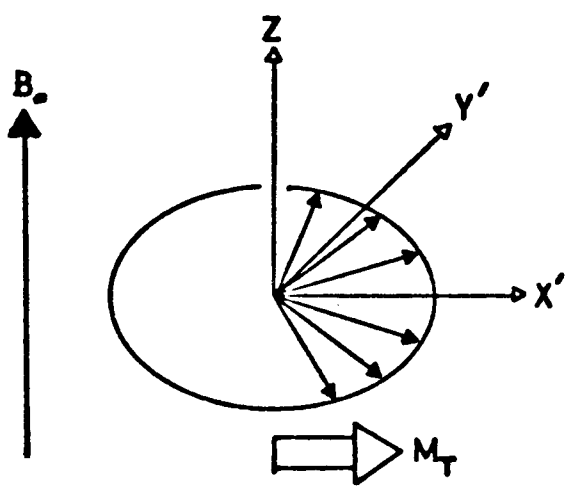
1. Just before applying B_1

$\theta_s = \theta_L$: Time $t = 0$



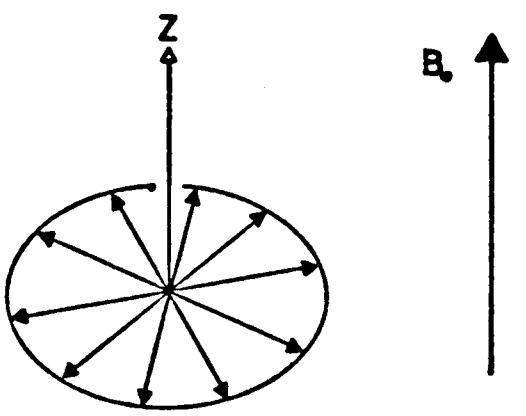
2. End of 90° Pulse

θ_s not defined : $t = \tau_{90}$



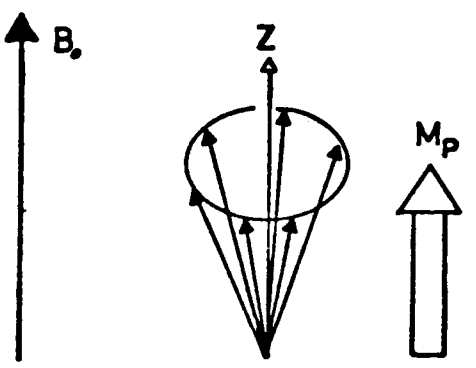
3. Spins begin to dephase

θ_s becomes defined : $t \sim T_2$



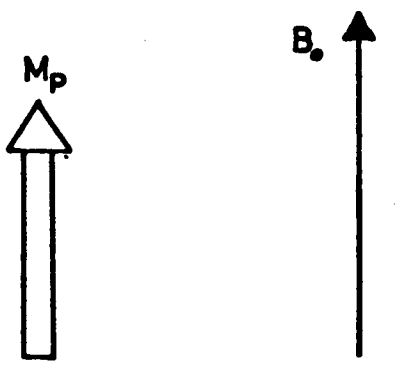
4. Spins fully dephased

$\theta_s \gg \theta_L$: $t \sim 3T_2$



5. Spins realigning along B_0 (Z)

$\theta_s \rightarrow \theta_L$: $t \sim T_1$



6. Spins realigned : $M_P = M$

$\theta_s = \theta_L$: $t \gg T_1$

Fig. 2.4 : A 90° Pulse & its effects
(Rotating frame : $T_1 \gg T_2$)

2.5 MEASUREMENT METHODS[13]

As shown before, the net magnetisation of a sample of nuclear spins is very small and the nuclear susceptibility is also very small, so that conventional static susceptibility measurements are not possible.

In practice, R.F. methods are used to detect NMR signals. If the spin sample is made part of the tank circuit of an oscillator, we can make use of the Q of that circuit to discriminate in favour of R.F. at the resonant frequency, say by detecting the change in Q as the sample absorbs R.F. when an applied field is swept through the nuclear resonance value. (Continuous wave NMR).

Alternatively (pulsed NMR), the free induction decay from the sample is picked up by the inductance coil of a tank circuit resonant at ν_L (the Larmor frequency).

It is to be remembered that the magnetisation $\underline{M}_T$ prepared by a 90° pulse will (in the laboratory frame) precess around $\underline{B}_0$ at frequency ω_L, and will generate an R.F. voltage in a coil whose axis is perpendicular to $\underline{B}_0$ (induction). The amplitude of this R.F. will decrease as the spins dephase and the net magnetisation disappears. This is the source of the free induction decay signal.

The size of the free induction decay signal is proportional to the net magnetisation $\underline{M}_0$ induced in the sample before application of the 90° pulse.

Note: In order to obtain the maximum signal, it is necessary to apply the 90° R.F. pulse for a time τ short compared to T_2, since the spins dephase in times $\approx T_2$. The length of a 90° pulse is given by $\tau = \frac{\pi}{2\gamma B_1}$. Thus if $\tau \approx 2\,\mu$sec and $\gamma/2\pi$ (protons) = 4.25 kHz/Gauss, then B_1, the peak R.F. field, is

$$B_1 \approx 30 \text{ Gauss}$$

This high field is obtained by driving a parallel tuned circuit at resonance, and making use of the current-amplifying effect of the circuit Q (see Appendix I) - if I amps flow from the signal generator into the tuned circuit, QI will circulate in the tank circuit itself, [ref.(11), p.241]

The same tuned circuit is then used to pick up the free induction decay signal, which is typically a few mV in amplitude[12, p.72] and feed it to a tuned preamplifier stage in the detection system of the NMR apparatus. Again, the Q of the circuit helps to discriminate in favour of photons at the Larmor frequency, rather than thermal (noise) photons.

The Bruker 'Minispec' is a commercially-available fixed-frequency NMR spectrometer which generates an intense burst of R.F. radiation at the Larmor frequency. This can be adjusted in length to give a 90° pulse (~ 5 μs long in our apparatus).

The Bruker also contains a sensitive radio receiver, which amplifies and detects the free induction decay and presents it for display on an oscilloscope. It also gates a section of the amplified F.I.D. and averages it to present the result as a D.C. output voltage.

The D.C. voltage is a function of the magnetisation M_0 present in the sample before application of the 90° pulse, and is linear with M_0 unless the amplifier is saturated by an over-large signal (see Apparatus section).

2.6 SPIN TEMPERATURE AND ISENTROPIC DEMAGNETISATION[12, Chp.5]

2.6.1 Spin Temperature

As stated earlier, spin temperature θ_s may be defined for a two-level system in terms of the populations of the two levels (Fig.2.3), i.e.

$$\frac{N_D}{N_u} = \exp\left[-\frac{(E_D - E_u)}{k\theta_s}\right] = \exp\left[-\frac{\Delta E}{k\theta_s}\right]$$

For a magnetic system, ΔE is given by:

$$\Delta E = -\gamma\hbar B_0 \Delta m = \gamma\hbar B_0$$

when $\Delta m = -1$ and θ_s may always be defined.

For a 3 (or more) level system, θ_s may only be defined if the populations of all the levels obey Boltzmann statistics (Fig.2.5).

It follows that, if N_1 is changed (say) then <u>both</u> N_2 and N_3 must change if θ_s is to be definable. Since, in general the energy levels are not equally spaced, this is not possible without some exchange of energy with the lattice. Thus a spin temperature is not always definable for a quadrupolar system.

However, if we only consider two levels at a time, we can always define an apparent spin temperature for those two levels alone. This is an alternative way of describing the populations of the levels, and does not imply a real temperature for the system as a whole. If we refer to the levels in Fig.2.5, non-equilibrium values of N_1, N_2 and N_3 would result in three (different) apparent spin temperatures defined by the equations on the right of Fig.2.5.

2.6.2 Isentropic Demagnetisation

If a two level spin system is in equilibrium at a temperature θ_s in a field B_0, and B_0 is changed to a new value B' in such a way that entropy is conserved, the spin temperature must also change, for entropy S is a function $S(\frac{B}{\theta})$ of B and θ only. Thus if B is decreased, θ must also decrease. This process is known as isentropic demagnetisation and can be used for obtaining very low spin temperatures (below $0.1^\circ K$). For if

$$B_0 = 1\ T\ ,\quad B' = 10^{-3}\ T\ ,\quad \theta_s = \theta_L = 77^\circ K$$

then

$$\theta = \frac{B'}{B_0}\,\theta_s = 0.077^\circ K\ .$$

The spin temperature is reduced far below the lattice temperature θ_L by the demagnetisation, and can only return to equilibrium with θ_L at a rate T_1, or, more accurately, at a rate T_{1D}, the spin-lattice relaxation

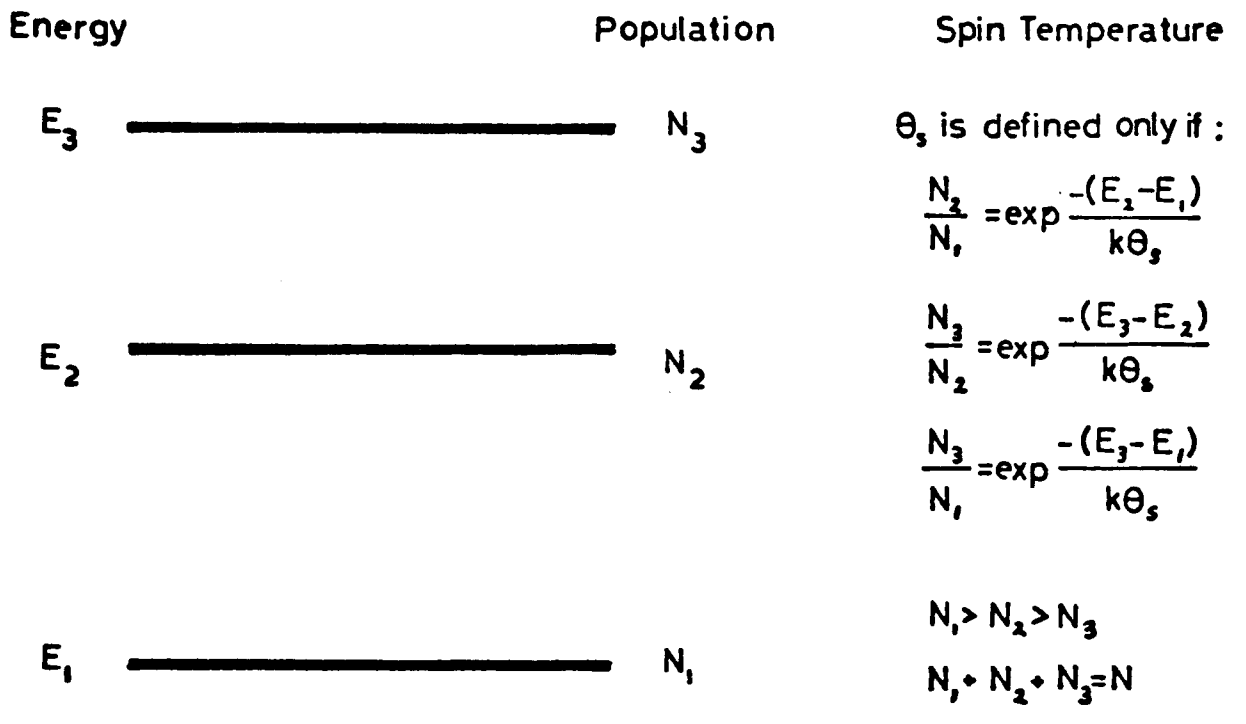


Fig.2.5: Spin Temperature in a Spin 1 system

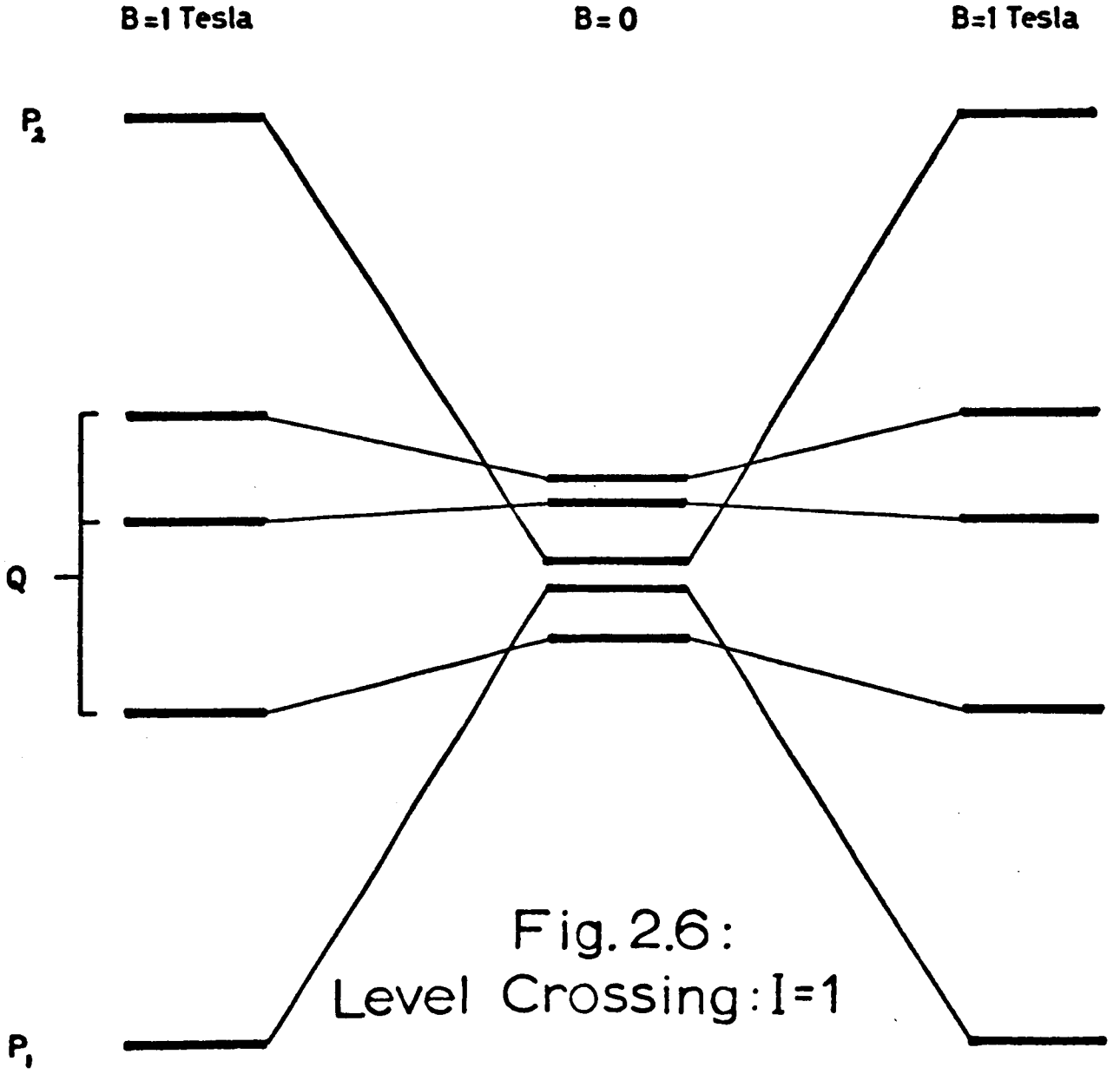


Fig.2.6: Level Crossing: I=1

time in zero applied field. 'D' implies T_1 in the dipolar fields due to the magnetic moments of the spins. Generally T_{1D} is much shorter than T_1 in large applied fields, but large differences in this respect occur between different materials.

Thus, if a sample is magnetised, in equilibrium in a magnetic field B_0, and is removed isentropically from B_0, its spin temperature must drop. Further, if a sample is removed entirely from B_0, any spin will only experience local fields due to other nearby nuclei (typically a few Gauss).

Since these fields are randomly oriented, the sample will consist of randomly oriented spins, and will have no net magnetisation. However, the magnetic order represented by the high-field magnetisation has changed into 'thermal' order represented by the new low temperature[14].

The process may be reversed by returning the sample to the high field, when the magnetisation will be found to have returned (without waiting any period $\sim T_1$).

Some loss usually does occur, however, due to absorption of heat from the lattice while in the low magnetic field. This process is accelerated if T_{1D} is much shorter than T_1. (In most cases T_1 increases in higher values of magnetic field - see Chapter VIII).

2.7 SPIN MIXING[4, p.246]

If we have a sample containing two spin species, P and Q, where P are a two-level system (say protons) and Q are a quadrupole system (3 or more levels), we may examine what occurs when such a sample is moved from a high to a low-field region.

Firstly, the sample is left for a long ($\geq T_1$ of protons) time in a high field B_0. All the spins are then in equilibrium at the lattice temperature θ_L. If the sample is then moved adiabatically into a low (near zero) field region, the proton system demagnetises and acquires a new (very low) spin temperature.

The quadrupole system also demagnetises to a new (but different) spin temperature. If, during this move, the proton energy splitting should become equal to one of the quadrupole energy splittings, energy may be transmitted between the two spin systems via the radiation field (i.e. by emitting and absorbing photons). This process occurs in times $\approx T_2$, since it is a spin-spin interaction.

If the apparent spin temperature of the two quadrupole levels in question is much higher than the (real) temperature of the proton system, energy (heat) is transferred from the quadrupoles to the proton bath until an 'equilibrium' is reached corresponding to some common temperature θ, which is 'real' for the protons and 'apparent' for the two quadrupole levels under discussion.

The above simply means that the population <u>difference</u> between the two quadrupole levels is <u>increased</u> by resonant emission of photons to the proton bath.

It may be seen (Fig.2.6) that all three levels of a spin 1 quadrupole system will, in turn, be affected by the proton bath, as it collapses to near-zero splitting. When the system arrives in zero field, there will, in general, be no definable spin temperature for the quadrupole system as a whole.

<u>Such interaction processes are referred to as level crossings.</u>

If nothing disturbs either the quadrupoles or protons while in zero field, a return to the high field will involve more level crossings, in reverse order, and further changes of populations. The final, measurable, magnetisation of the protons is a function of all the level crossings, and is discussed further in Chapter III.

If, however, while in zero field, the quadrupole system is made to absorb energy by irradiation at one of the quadrupole resonance frequencies,

the population structure of the quadrupole levels will be changed, and this will produce a different (lower) net magnetisation of the protons after the level crossings during the return to high field.

This difference is what constitutes our NQR 'signal'.

Double resonance by level crossing (DRLC) is the name given to this measurement procedure, and is applicable whenever the lowest quadrupole frequency (in zero field) is $\geqslant 200$ kHz.

An additional complication arises when the lowest quadrupole frequency is $\leqslant 200$ kHz, for the net proton splitting in 'zero' applied field in fact consists of a broad absorption from $0 \rightarrow 200$ kHz or more, due to the spread of internal local fields experienced by the protons.

Part of the quadrupole system is then capable of exchanging photons with the proton system at all times while in low fields, and the apparent temperatures of these low quadrupole levels are always held very close to the real temperature of the proton bath.

This situation occurs in deuterium NQR, when ν_0 is always in the range 10 - 50 kHz, and is referred to as double resonance with continuous coupling (DRCC). This generally results in much higher sensitivity than DRLC.

CHAPTER III

THEORY OF NQR, AND THE LEVEL CROSSING METHOD

3.0 INTRODUCTION

We now develop the theory of the quadrupole interaction itself, beginning from a classical point of view, extending this with quantum mechanical arguments and then proceeding to discuss detection methods. We complete the chapter by developing the numerical theory of level crossing.

3.1 CLASSICAL INTERACTIONS[15]

We begin by considering the classical interaction between a nuclear charge distribution $\rho(\underline{r})$ and an external electrostatic potential $V(\underline{r})$, where $\underline{r}$ is a position vector in some fixed frame of reference. In Cartesian coordinates, $\underline{r} = (x_1, x_2, x_3)$.

The interaction Hamiltonian is given by

$$\mathcal{H} = \int \rho(\underline{r}) \cdot V(\underline{r})\, d^3\underline{r} \,. \qquad \ldots (3.1)$$

We expand $V(\underline{r})$ as a power series about the nuclear centre of mass, $\underline{r} = \underline{r}_0$. Then

$$\mathcal{H} = \int \rho(\underline{r}) \left\{ V_0 + \sum_j \left(\frac{\partial V}{\partial x_j}\right)_0 x_j + \tfrac{1}{2} \sum_{j,k} \left(\frac{\partial^2 V}{\partial x_j \partial x_k}\right)_0 x_j x_k + \ldots \right\} d^3(\underline{r}) \qquad \ldots (3.2)$$

or

$$\mathcal{H} = ZeV_0 + \sum_j P_j \left(\frac{\partial V}{\partial x_j}\right)_0 + \tfrac{1}{2} \sum_{j,k} Q'_{jk} \left(\frac{\partial^2 V}{\partial x_j \partial x_k}\right)_0 + \ldots \qquad \ldots (3.3)$$

where

$$Ze = \int \rho(\underline{r}) d^3(\underline{r}) \quad = \text{nuclear charge (not a function of } \underline{r})$$

$$P_j = \int \rho(\underline{r}) x_j\, d^3(\underline{r}) \quad = \text{nuclear electric dipole moment (vector)}$$

$$Q'_{jk} = \int \rho(\underline{r}) x_j x_k\, d^3(\underline{r}) = \text{nuclear electric quadrupole moment (tensor)}$$

The time-average charge distribution of the nucleus satisfies inversion symmetry, i.e. $\rho(\underline{r}) = \rho(-\underline{r})$, and hence the electric dipole moment is zero. Similarly, the octupole term $\int \rho(\underline{r}) x_j x_k x_\ell d^3(\underline{r})$ (also an odd function) is zero.

Thus the only orientation-dependent terms are the quadrupole and subsequent terms based on even functions of the components of $\underline{r}$.

$$\underline{\text{Orders of magnitude}} \begin{cases} r_n \approx \text{nuclear radius} \approx 10^{-12}\,\text{cm} \\ r_e \approx \text{electron orbit radius} \approx 10^{-8}\,\text{cm} \end{cases}$$

(a) Electrostatic term $= ZeV_0 \approx Ze\,\frac{e}{r_e} \approx 10^{-5}\ \text{cm}^{-1}$ (visible light)

(b) Quadrupole term $= Q'_{jk}V_{jk} \approx \left(Ze\,r_n^2\right) \cdot \left(\frac{e}{r_e^3}\right)$

$\approx 10^{-13}\,\text{cm}^{-1}$ (radio frequency)

(c) 16-pole term $\approx 10^{-21}\,\text{cm}^{-1} \sim 1\,\text{Hz}.$

Thus 16-pole and higher terms can be ignored because of the very low interaction energies involved, and the quadrupole term is the only significant electrical orientation-dependent term, i.e.

$$\mathcal{H}_Q = \tfrac{1}{2} \sum_{jk} Q'_{jk} V_{jk} \qquad \left(\text{where} \quad V_{jk} = \left(\frac{\partial^2 V}{\partial x_j \partial x_k}\right)_0\right) \qquad \ldots (3.4)$$

and V_{jk} is an electric field gradient (E F G).

3.1.1 Nuclear Quadrupole Moment Tensor Q_{jk}

Q'_{jk} is symmetric ($Q'_{jk} = Q'_{kj}$) and hence has six independent terms. We may define a simpler, traceless tensor:

$$Q_{jk} = 3Q'_{jk} - \delta_{ij} \sum_n Q'_{nn} \qquad \ldots (3.5)$$

We may then rewrite (3.4) as:

$$\mathcal{H}_Q = \tfrac{1}{6} \sum_{jk} Q_{jk} V_{jk} + \tfrac{1}{6}\,\text{Tr}(Q'_{jk}) \cdot \text{Tr}(V_{jk}) .$$

The second term involves only traces of tensors, and hence is independent of orientation. It is thus a constant for any energy transition, and may thus be neglected. The quadrupole Hamiltonian is thus reduced to

$$\mathcal{H}_Q = \tfrac{1}{6} \sum_{jk} Q_{jk} V_{jk} \qquad \ldots (3.6)$$

By symmetry, the nuclear spin axis must form one of the principal axes of the tensor, Q_{jk}, and (classically speaking) the nuclear charges

precess rapidly about this axis. External fields interact with the time-average components of the quadrupole tensor. Since the nucleus is cylindrically symmetric about this axis, the off-diagonal elements of Q_{jk} must average to zero; furthermore, if Z is the nuclear spin axis, $Q_{xx} = Q_{yy}$. Since $Tr(Q_{jk}) = 0$, we must also have

$$Q_{zz} = -2Q_{xx} = -2Q_{yy}$$

and thus there is only <u>one</u> independent parameter in the quadrupole moment tensor.

This parameter, the nuclear electric quadrupole moment, Q is defined by:

$$eQ = \int \rho_{II}(\underline{r})(3z^2 - r^2)\, d^3\underline{r} \qquad \ldots (3.7)$$

Where $\rho_{II}(\underline{r})$ represents the expectation value of $\rho(\underline{r})$ in the nuclear spin state $I_z = I\hbar$. Thus Q is the expectation value of Q_{zz} in that nuclear spin state.

Q determines the departure of the nucleus from spherical symmetry. Q has the dimensions of area, and $Q > 0$ indicates a 'cigar-shaped' or prolate spheroid, while $Q < 0$ indicates an oblate or 'disc-shaped' nucleus.

3.1.2 Electric Field Gradient Tensor V_{jk} (E F G)

V_{jk} is symmetric, but not necessarily traceless, for by Poissons' equation $\nabla^2 V = \sum_j V_{jj} = -\rho/\varepsilon_0$.

However, only s-electrons have a non-zero probability of being at the nucleus - and they have a spherically symmetric charge distribution, so that they do not contribute to V_{jk}.

Hence V_{jk} may be transformed into a traceless tensor by adding a spherically symmetric quantity, leaving the quadrupole Hamiltonian unaffected.

By choosing suitable axes (the principal axes of the E F G), say by rotational transformations from arbitrary axes, V_{jk} may be made diagonal.

We then have

$$V_{jk} = 0 \quad \text{for} \quad j \neq k.$$

$$V_{xx} + V_{yy} + V_{zz} = 0 \qquad \text{(Laplace's Equation)} \qquad \ldots (3.8)$$

Only two parameters are required to specify V_{jk} fully. By convention, we take

$$|V_{zz}| \geq |V_{yy}| \geq |V_{xx}|$$

and define

$$eq = V_{zz} = \text{'strength of electric field gradient'} \qquad \ldots (3.9)$$

$$\eta = \frac{|V_{yy}| - |V_{xx}|}{|V_{zz}|} = \text{'asymmetry parameter'} \qquad \ldots (3.10)$$

$0 \leq \eta \leq 1$ and η determines the degree of departure from cylindrical symmetry, i.e. $\eta = 0$

$$\Rightarrow |V_{yy}| = |V_{xx}|$$

$\Rightarrow$ cylindrical symmetry about z axis.

The case $\eta = 1$ corresponds to $V_{xx} = 0$, $V_{yy} = -V_{zz}$. The geometry is more difficult to visualise - a rotation of $\pi/2$ in the yz plane produces a sign reversal in the EFG.

One may say that a regular tetrahedron, having equal positive charges $+e$ at two corners, and equal negative charges $-e$ at the other two, will generate an EFG with $\eta = 1$ at the centre of symmetry of the tetrahedron.

Thus, to completely specify the nuclear quadrupole energy levels, we must know eQ, eq, η and the angles describing the relative orientations of the principal axes of the quadrupole moment tensor and the principal axes of the electric field gradient.

Quadrupole resonance in powder samples gives only two independent parameters $-\eta$ and e^2qQ. The orientations of the principal axes of the EFG relative to the crystalline axes may be deduced from single-crystal experiments, but this information is not generally necessary in order to achieve a good understanding of the powder specimen spectra.

Nuclear quadrupole moments (Q above) do not depend on chemical environment, but only on nuclear species. Q is essentially a constant for a given nucleus (in its ground state) whatever molecule it may be found in. Thus by measuring e^2qQ, we obtain a relative measure of eq for the same nucleus in different environments, and thus have a probe of the electronic structure at a given nuclear site in a molecule.

3.2 QUANTUM-MECHANICAL DEVELOPMENT[15,17]

We transform the quadrupole Hamiltonian (3.6) into operator form by changing variables from position $\underline{r}$ to the nuclear spin operators $\underline{I}$ (and I_{xyz})[16]. Then

$$\mathcal{H}_Q = \frac{eQ}{2I(2I-1)} (V_{xx}I_x^2 + V_{yy}I_y^2 + V_{zz}I_z^2) \qquad \ldots (3.11)$$

or, using η, eq and the shift operators I^+ and I^-

$$\mathcal{H}_Q = \frac{e^2qQ}{4I(2I-1)} \left(3I_z^2 - I^2 + \frac{\eta}{2} (I_+^2 + I_-^2)\right) \qquad \ldots (3.12)$$

i.e. a knowledge of the quantum numbers I and m specifies the quadrupole tensor Q_{ij} completely (for a given nuclear species of known quadrupole moment Q).

Only nuclei with spin $I \geq 1$ can have a quadrupole moment, since spins $I = 0$ or $\frac{1}{2}$ must have a spherically symmetric charge distribution. (The two allowed states of a spin $I = \frac{1}{2}$ nucleus differ only by spin reversal, not charge distribution.)

The work in this thesis is concerned with the cases $I = 1$ (nitrogen and deuterium) and $I = \frac{3}{2}$ (sodium, ^{11}boron and potassium, for example).

3.2.1 Spin I = 1 [18]

The operator I^2 has a constant eigenvalue of 2, since $\langle I,m|I^2|I,m\rangle = I(I+1) = 2$. Hence we can write:

$$\mathcal{H}_Q = \frac{e^2qQ}{4} \left\{3I_z^2 - 2 + \frac{\eta}{2} (I_+^2 + I_-^2)\right\}.$$

In terms of the three spin states of I_z, labelled by $|m\rangle = |+1\rangle$, $|0\rangle$, $|-1\rangle$ taken along the principal axes of the electric field gradient, we have

$$\mathcal{H}_Q = \frac{e^2qQ}{4}\begin{pmatrix} 1 & 0 & \eta \\ 0 & -2 & 0 \\ \eta & 0 & 1 \end{pmatrix}$$

This may be simply diagonalised to give

$$\mathcal{H}_Q = \frac{e^2qQ}{4}\begin{pmatrix} 1-\eta & 0 & 0 \\ 0 & -2 & 0 \\ 0 & 0 & 1+\eta \end{pmatrix} \qquad \ldots (3.13)$$

in terms of the new eigenstates $|B\rangle$, $|0\rangle$ and $|A\rangle$, where

$$\left.\begin{aligned} |B\rangle &= \frac{1}{\sqrt{2}}\left(|+1\rangle - |-1\rangle\right) \\ |0\rangle &= |0\rangle \\ |A\rangle &= \frac{1}{\sqrt{2}}\left(|+1\rangle + |-1\rangle\right) \end{aligned}\right\} \qquad \ldots (3.14)$$

(These states transform under rotations in a way analogous to the P electronic wavefunctions: i.e. $-|B\rangle$, $i|A\rangle$ and $|0\rangle$ transform like x,y,z.)

There are thus three energy levels, and three allowed transition frequencies (Fig.3.1). Electromagnetic radiation of the appropriate frequency will induce transitions between levels. Since the electric dipole moment of the nucleus is zero, transitions are induced by the magnetic component of the radiation acting on the magnetic dipole moment of the nucleus.

The electromagnetic field may be treated as a perturbation on the quadrupolar Hamiltonian $\mathcal{H}_Q$ which becomes

$$\mathcal{H} = \mathcal{H}_Q + \mathcal{H}'$$

where

$$\mathcal{H}' = -\gamma\hbar\underline{B}_1 \cdot \underline{I} \qquad \ldots (3.15)$$

and $\underline{B}_1 = (B_{1x}, B_{1y}, B_{1z})$ = magnetic field, (RF).

Using the coordinate system (x,y,z) defined by the principal axes of the electric field gradient, the components of $\underline{I}$ referred to the manifold $\{|B\rangle, |0\rangle, |A\rangle\}$ become:

$$
\begin{array}{c}
\qquad\quad |B\rangle \quad |0\rangle \quad |A\rangle \\
I_x = \begin{pmatrix} 0 & 0 & 0 \\ 0 & 0 & i \\ 0 & -i & 0 \end{pmatrix} \begin{matrix} |B\rangle \\ |0\rangle \\ |A\rangle \end{matrix} \\
I_y = \begin{pmatrix} 0 & i & 0 \\ -i & 0 & 0 \\ 0 & 0 & 0 \end{pmatrix} \\
I_z = \begin{pmatrix} 0 & 0 & -i \\ 0 & 0 & 0 \\ i & 0 & 0 \end{pmatrix}
\end{array} \qquad \ldots (3.16)
$$

When $\underline{B}_1$ is a magnetic field oscillating at one of the transition frequencies ν^+, ν^- or ν^0, the probability of a transition between states $|m\rangle$ and $|n\rangle$ is proportional to[12, p.28]

$$T_{mn} \propto |\langle m|\mathcal{H}|n\rangle^2| \qquad \ldots (3.17)$$

Since $\mathcal{H}_Q$ is diagonal in the representation $\{|B\rangle, |0\rangle, |A\rangle\}$ only $\mathcal{H}'$ contributes to the transition probability.

$$T_{mn} \propto |\langle m|\gamma\hbar B_1 \cdot \underline{I}|n\rangle|^2 \ . \qquad \ldots (3.17)$$

From the forms of the matrices of $\underline{I}$, it is apparent that only the x-component of B_1 is effective in coupling the states $|0\rangle$ and $|A\rangle$ (the ν_+ transition). Similarly, B_{1y} excites ν_- and B_{1z} excites ν_0. From the form of T_{mn} it is seen that the transition probabilities depend on the squares of the magnitudes of the components of $\underline{B}_1$.

Thus, if we have polarised radiation, where $\underline{B}_1 = (0,0,B_1)$ say, and apply this to a single crystal sample, we may, by comparing line intensities while rotating the crystal, find the directions of the principal axes of the electric field gradient and relate these to the crystal axes.

When the irradiation is isotropic ($B_{1x}^2 = B_{1y}^2 = B_{1z}^2$), all transitions are equally probable. With polarised radiation and a polycrystalline sample roughly equal numbers of crystallites will have suitably oriented axes, and

all transitions will be detected. However, if $\underline{B}_1$ is strong enough, a given transition will become saturated in some crystallites before others, due to more favourable orientation. This can lead to broadening of the absorption lines at high power levels.

Since all our experiments are performed on polycrystalline samples, the differences in the relative intensities of ν^+, ν^- and ν^0 that we measure are mainly due to level crossing effects, and not transition probabilities. For this reason, intensity information in double resonance must be interpreted with care.

3.2.2 Small Static Magnetic Fields ($\gamma B \ll e^2qQ/h$)

If a small static magnetic field $\underline{B}_z$ is applied to a nucleus of spin $\underline{I}$, a Zeeman energy term is introduced into the Hamiltonian. We again write the Hamiltonian as

$$\mathcal{H} = \mathcal{H}_Q + \mathcal{H}_z$$

where $\mathcal{H}_z = -\gamma\hbar \underline{B}_z \cdot \underline{I}$ (as in equation (3.15)).

When the spin $\underline{I} = 1$, $\mathcal{H}_z$ has no diagonal elements (as shown by equations (3.16)), and hence $\mathcal{H} \approx \mathcal{H}_Q$ to first order and the energy levels are unaffected. The quadrupole levels are said to be quenched. $\mathcal{H}_z$ does have off-diagonal elements, however, and we may use second-order non-degenerate perturbation theory to calculate the small energy shifts ΔE that do occur. The shift in level $|m\rangle$ is given by

$$\Delta E_m = \sum_{k \neq m} \hbar^2 \gamma_Q^2 \frac{|\langle m|\underline{B}_z \cdot \underline{I}|k\rangle|^2}{E_m - E_k} \qquad \ldots (3.18)$$

where γ_Q = gyromagnetic ratio of the quadrupole nucleus and E_m and E_k are unperturbed energies. The summation is over all states $|k\rangle \neq |m\rangle$

3.2.3 Special Case of $\eta = 0$ ($I = 1$)

In this case the states $|A\rangle$ and $|B\rangle$ become degenerate and equation (3.18) can no longer be used. Use of degenerate perturbation

theory reveals that the two levels are unquenched and behave like the states $|+1\rangle$ and $|-1\rangle$. The expectation value of the operator I_z is no longer zero, and the two degenerate levels $|+1\rangle$ and $|-1\rangle$ diverge with applied magnetic field with the characteristic gyromagnetic moment of the nucleus in question.

3.2.4 General Case $\eta \neq 0$ $(I = 1)$

For single crystals, the absorption lines are shifted as explained above. For polycrystalline samples, since the sizes of the shifts depend on the relative orientations of the applied magnetic field and the principal axes of the E F G, the overall effect is to broaden the resonance lines asymmetrically. The general effect of the perturbation is for energy levels to repel one another, closely spaced levels being mutually repelled more than distantly spaced levels. As a result (Fig.3.1) level $|A\rangle$ moves up, level $|B\rangle$ moves down and level $|0\rangle$ moves very slightly down. For small η, $\nu^+ \sim \nu^- \gg \nu^0$ and level $|0\rangle$ is almost unaffected by the perturbation. ν^+ is increased and ν^- is decreased (ν_0 also increases).

NEGITA[19] calculated the full effect of a magnetic field on a powder sample spectrum, and concluded that ν^+ is broadened asymmetrically to the high frequency side and ν^- is broadened asymmetrically to the low frequency side.

This conclusion is confirmed by experiments and can be used, particularly in deuterium N Q R, in identifying which lines are ν^+ and which are ν^- in a complex spectrum. Relative amounts of shift can be used as a guide to linking together ν^+ and ν^- from the same site.

3.2.5 Large Magnetic Fields $\gamma\hbar B \gg e^2qQ$

Under these conditions the quadrupole states are unquenched and magnetic transitions are the main feature of the spectrum. The experiment is then usually referred to as N M R rather than N Q R.

3.2.6 Spin $\frac{3}{2}$ Case[9]

In zero applied magnetic field, the quadrupole Hamiltonian is given by

$$\mathcal{H}_Q = \frac{e^2qQ}{12}\left\{3I_z^2 - \frac{15}{4} + \frac{\eta}{2}(I_+^2 + I_-^2)\right\}. \qquad \ldots (3.19)$$

Writing this in matrix form for the base states $|\frac{3}{2}\rangle$, $|\frac{1}{2}\rangle$, $|-\frac{1}{2}\rangle$, $|-\frac{3}{2}\rangle$ we obtain

$$\mathcal{H}_Q = \frac{e^2qQ}{12}\begin{pmatrix} 3 & \sqrt{3}\eta & 0 & 0 \\ \sqrt{3}\eta & -3 & 0 & 0 \\ 0 & 0 & -3 & \sqrt{3}\eta \\ 0 & 0 & \sqrt{3}\eta & 3 \end{pmatrix}$$

This may be simply diagonalised to give

$$\mathcal{H}_Q = \frac{e^2qQ}{12}\begin{pmatrix} 3 & 0 & 0 & 0 \\ 0 & -3 & 0 & 0 \\ 0 & 0 & -3 & 0 \\ 0 & 0 & 0 & 3 \end{pmatrix}\sqrt{(1 + \tfrac{1}{3}\eta^2)}$$

in terms of the new eigenfunctions ψ_1, ψ_2, ψ_3 and ψ_4, where

$$\psi_1 = -b|\tfrac{3}{2}\rangle + a|-\tfrac{1}{2}\rangle$$

$$\psi_2 = a|\tfrac{3}{2}\rangle + b|-\tfrac{1}{2}\rangle$$

$$\psi_3 = b|\tfrac{1}{2}\rangle + a|-\tfrac{3}{2}\rangle$$

$$\psi_4 = a|\tfrac{1}{2}\rangle - b|-\tfrac{3}{2}\rangle$$

and a and b are given by

$$a = \left(\frac{\rho-1}{2\rho}\right)^{\frac{1}{2}} \quad : \quad b = \frac{\eta}{\sqrt{6\rho(\rho-1)}} \quad : \quad \rho = \sqrt{1 + \tfrac{1}{3}\eta^2}$$

There are thus two doubly degenerate levels and a single transition frequency at

$$\nu = \nu_q = \frac{e^2qQ}{2h}\rho\,. \qquad \ldots (3.20)$$

As a result, e^2qQ and η cannot be separately determined. When a small D.C. magnetic field is applied, however, the levels diverge (Fig.3.2) in a way characteristic of both η and the gyromagnetic ratio γ. The

analytical treatment of this system is somewhat complex, and numerical methods must be used to analyse a powder spectrum. This is left until Chapter VII.

3.3 DETECTION METHODS AND DOUBLE RESONANCE

3.3.1 Pure Quadrupole Resonance

We have seen that a quadrupolar nucleus immersed in an electric field gradient will have a characteristic set of absorption lines situated (in most cases) in the radiofrequency region of the electromagnetic spectrum.

For example, chlorine ($I = \frac{3}{2}$) has a single absorption usually near 35 MHz. Sodium ($I = \frac{3}{2}$) has an absorption usually in the 1-2 MHz region. Nitrogen ($I = 1$) has three absorption frequencies usually between 1 and 4 MHz, but ν_0 can be as low as 100 kHz. Deuterium ($I = 1$) also has three absorptions. ν^+ and ν^- are usually 100 - 200 kHz, with $\nu_0 \sim 10 - 20$ kHz.

These figures[4] show part of the range of quadrupole frequencies, and indicate some experimental difficulties.

(a) 'Continuous wave' techniques of NQR, where a sample is included inside the inductance of a tank circuit, which forms part of a variable-frequency super-regenerative oscillator, are most suitable for nuclei like chlorine, where the NQR frequencies are ≥ 20 MHz, but may be used for nitrogen NQR at 3 MHz[20]. The method relies on thermal equilibrium in the sample causing a population difference between levels, so that, when the oscillator is driven through a quadrupolar frequency, power is absorbed by the sample, and the resultant change in R.F. level of the oscillator is detected. This was the first form of 'pure' NQR.

Since this method relies on population differences between spin energy levels which are maintained by thermal contact with the lattice, it is restricted to high-frequency NQR measurements. A large energy splitting is required to maintain a relatively large population difference at high

temperatures. High temperatures (~ 300°K) generate many thermal photons and produce more thermal noise, so that the signal/noise ratio of the detection system is low. If the temperature is lowered, either to improve signal/noise or to improve the population differences for small quadrupole energy splittings, one is limited by saturation effects. The T_1 of the quadrupole nucleus increases as the temperature falls, which means that a longer time is required for equilibrium to be established between the quadrupole and the lattice. As a result, the quadrupoles absorb energy from the R.F. field, until the populations of the two irradiated levels become equal (saturation); further absorption is then very slight, because of the very slow transfer of energy to the lattice.

Since 'continuous wave' NQR relies on detecting the power absorbed by the sample from the detection system (usually a resonant circuit), and power ceases to be absorbed when saturation occurs, the detection system ceases to operate at the onset of saturation. Thus if the population difference between the energy levels of interest is low, and the T_1 of the quadrupole nucleus is long, the signal/noise ratio of a C.W. technique will be very bad, due to the rapid onset of saturation. For this reason, reducing the temperature does not aid sensitivity.

(b) Pulsed Continuous Wave NQR (similar to pulsed NMR)

This method can also be used for nitrogen NQR[21]. A high-power R.F. pulse at the quadrupole frequency is applied to the sample, and the resulting free induction decay (or spin echo) of the precessing quadrupolar spins is detected, or not observed if the irradiation pulse frequency is not a quadrupole resonance frequency. Thus in this case the apparatus detects power emitted by the sample.

Again, small population differences and available signal/noise ratios severely limit the detail which can be observed in such spectra, and work is restricted to frequencies of NQR ≥ 500 kHz.

Neither of these methods is thus suitable for deuterium NQR. Early work on deuterium was done by observing quadrupole effects as a perturbation on the NMR levels of the nucleus in a large magnetic field[22]. This work requires single-crystal specimens, but can be very accurate, although analysis of complex spectra can be tedious.

Powder samples can be used for NMR studies, but the resulting lines are broad due to the angle-dependent energies of different crystallites, and the data produced is of low precision.

NMR studies have also been done on nitrogen[23], but larger fields are required (because of the larger quadrupole splitting) and again, single crystals are required for good precision.

3.3.2 Double Resonance Methods[4]

The difficulties of low frequency NQR were largely overcome by the development of double-resonance methods.

In all such methods, samples must contain at least two nuclear spin species. One (henceforth called the P spins) which has a large gyromagnetic ratio, no quadrupole moment and is relatively abundant in the sample, is to be the detection medium. The other (or others), called the Q spins, have a low gyromagnetic ratio or are rare in the sample, or both.

It is easy to polarise the P spins by immersing them in a large magnetic field, because of the resulting large energy splitting, and it is also easy to measure their magnetisation, say by using a 90° pulse. It is difficult (in isolation) to polarise the Q spins because of their small energy splitting and their total magnetisation is normally small.

The general principals of double resonance are outlined in Fig.3.3 and may be divided into three phases.

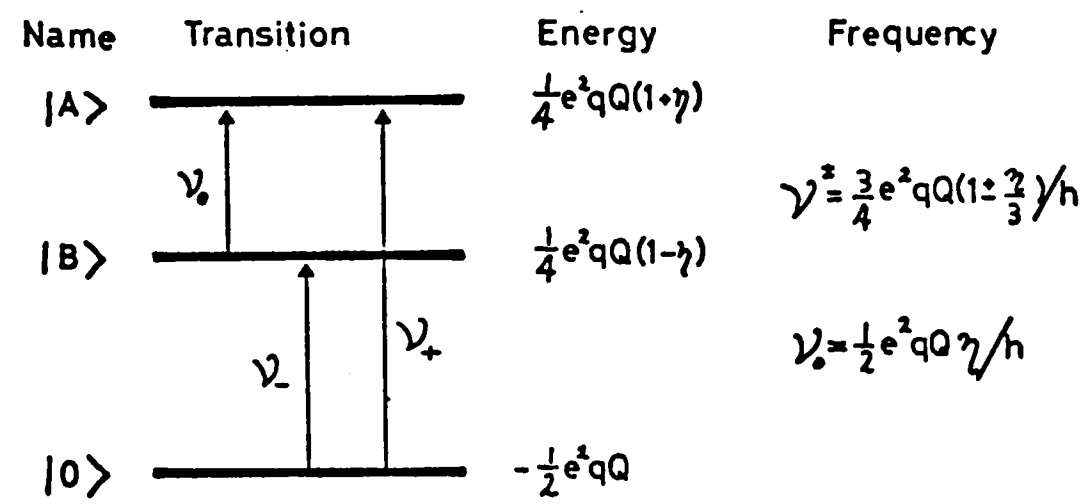


Fig.3.1 : Energy levels : Spin 1

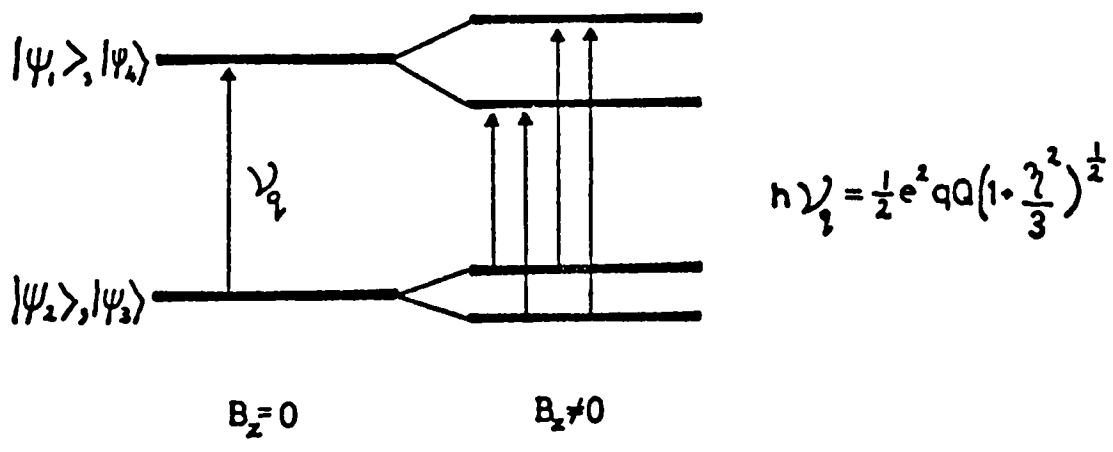


Fig.3.2 : Energy levels : Spin $\frac{3}{2}$

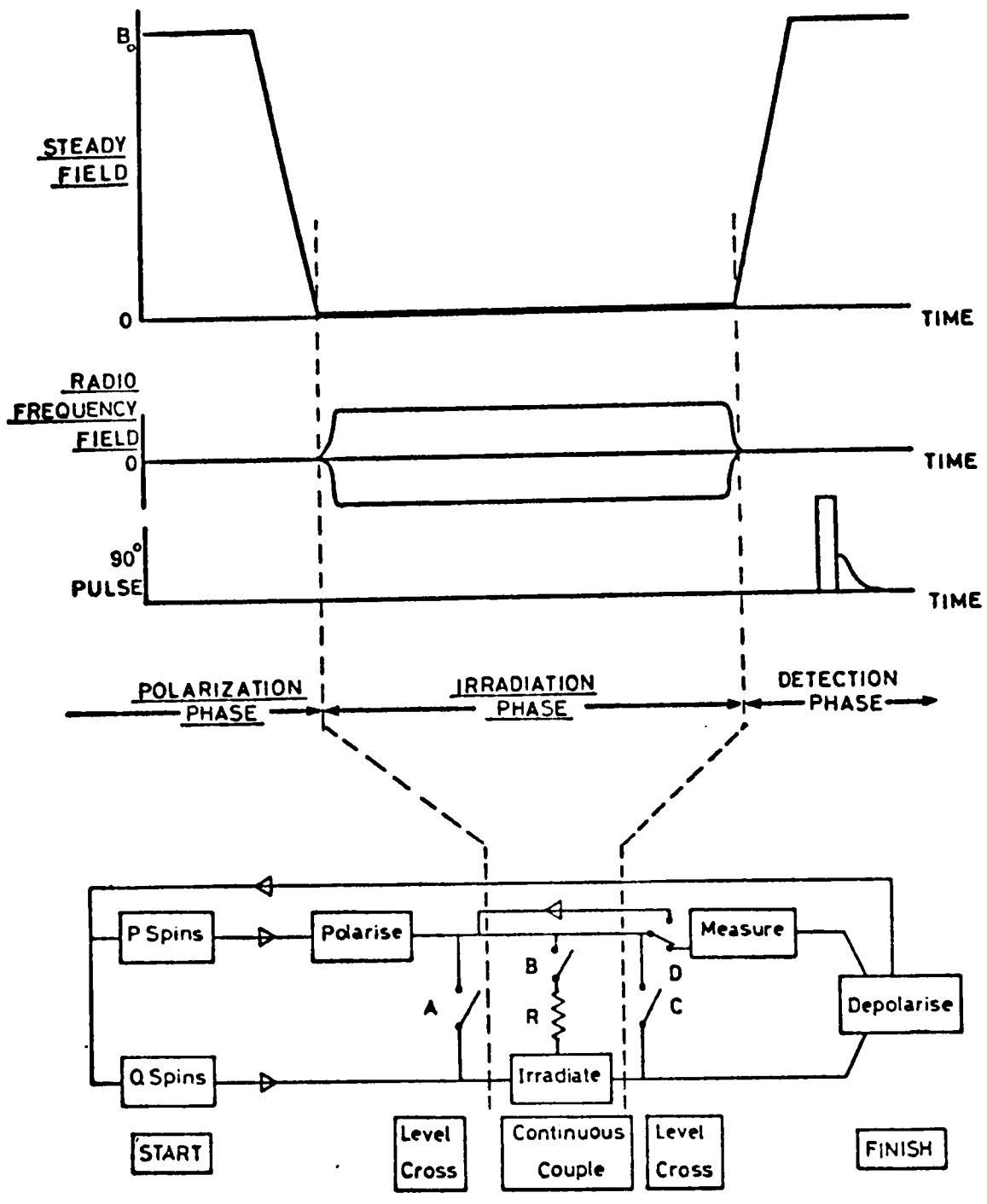


Fig.3.3 : Events during an experimental cycle

(a) Polarisation Phase

At a time $t = 0$, the sample is immersed in a strong magnetic field. The P spins acquire a relatively large magnetisation at a rate $\sim T_1(P)$. As shown earlier, if the number of P spins is $\sim N$, then the population difference between the two magnetic states of the P spins is $\sim N \times 10^{-5}$. The Q spins will also acquire a small magnetisation if $T_1(P) \geq T_1(Q)$, but this is usually insignificant due to the much smaller energy splittings of the Q spins in the field.

At a time $t \approx T_1(P)$, the sample is removed from the magnetic field and level crossings occur (as shown earlier). This may be pictured as closing switch A momentarily between the P and Q spins. As a result, the population differences between the various Q spin levels are increased: i.e. the apparent spin temperatures of pairs of Q spin levels are decreased by 'thermal' contact with the cold P spins during level crossing. At the end of the polarisation phase, switch A opens, and the Q spins are isolated from the P spins, prepared in their 'polarised' state.

(b) Irradiation Phase

During this phase, an R.F. magnetic field is applied to the sample. If the frequency of the R.F. corresponds to a transition in the Q spin system, power can be absorbed by the Q spins. Assuming that $T_1(Q)$ is long when $B_0 \sim 0$, the Q spins may absorb power until the populations of the two Q spin states, thus connected, are made equal, but absorption then ceases (saturation).

During the irradiation phase, one may have some direct coupling between the P spins and Q spins, indicated by switch B. If switch B is always 'closed', then resistor R indicates the strength of this continuous coupling — this is always the case when doing deuterium NQR, and there are ways of varying the 'size' of R experimentally. As the irradiation

frequency $\rightarrow 0$, $R \rightarrow 0$, and we always detect direct absorption by the P spins at low irradiation frequencies. This is explained further under the heading 'Double Resonance by Continuous Coupling' or 'D R C C'.

If switch B is always open, then the experiment is called 'Double Resonance by Level Crossing' or "D R L C".

Other double resonance methods employ ways of closing switch B, such as Double Resonance in the Rotating Frame (D R R F) due to HARTMANN and HAHN[2], but this method employs large magnetic fields, and single crystals are required. There is also Double Resonance in the Laboratory Frame (D R L F) [24,25], but this is not suitable for integer spin quadrupole nuclei such as nitrogen. These two methods are both more complicated than D R L C and have limitations as outlined above. They do not form part of the work of this thesis.

The advantage of all these continuous coupling techniques is that one can avoid most of the problems of saturation. For most samples $T_1(Q)$ is long, but $T_{1D}(P)$ [the dipolar (zero) field T_1 of the P spins] is relatively short. If $T_{1D}(P)$ is long, then the P spins will be at a very low spin temperature when $B_0 = 0$, due to their large abundance (large 'specific heat'). If the energy that is put into the Q spins can be fed through into the P spins at a rate faster than $T_1(Q)$ by means of some form of spin-spin coupling, saturation does not occur or occurs after much more net energy has been absorbed through the Q spins.

Thus if $T_{1D}(P)$ is short, energy fed into the Q spins passes to the P spins via R and switch B and then rapidly to the lattice. If $T_{1D}(P)$ is long, the energy stays in the P spin system, but raises its spin temperature gradually (due to its large specific heat) until eventually the P spin system becomes saturated (when its spin temperature $\rightarrow \infty$). In both cases, much more energy can be absorbed by the whole spin system (P + Q)

than can be absorbed by the Q spins alone. Since it is the absorption, or non-absorption of energy by the Q spins that one wishes to detect, some form of continuous coupling will obviously aid this detection.

Continuous coupling is of special use when the Q spins are rare. It has been possible to detect naturally abundant deuterium (0.015%) NQR in HCOOH [10] by DRCC and naturally abundant ^{17}O (0.03%) NQR in several organic solids by DRLF [26].

When continuous coupling is weak or not present, one can enhance sensitivity by multiple level crossing, indicated by switch D and the return path. After irradiation, the sample is moved into a sufficiently large field for level crossing to occur again (switch C), and then the irradiation phase is repeated. In this way, the energy put into the Q spins (to saturation) is shunted back to the P spins by the level crossing, which also repolarises the Q spins so that they can absorb more energy. Repetition of the process transfers more energy into the whole system (P + Q) than a single cycle could.

(c) Measurement Phase

After one or more irradiation phases, the sample is finally returned to the large field B_0, and level crossings during that passage (indicated by switch C) ensure a transfer of 'heat' from the Q spin system to the P spin system. Finally, the remaining magnetisation of the P spins is measured, say by using a 90° pulse, and the size of the free induction decay is recorded.

If, during the irradiation phase, the Q spins absorbed energy from the R.F. magnetic field, that absorption of energy will appear as a rise in the spin temperature of the P spin system. This is recorded as a decrease in the size of the free induction decay, indicating a decrease in the net remaining magnetisation of the P spins when they return to the large field.

If no energy has been absorbed by the Q spins during irradiation, the final measured P spin magnetisation will be larger.

After the measurement and recording phase, the P spins are depolarised completely by applying a long chain of closely spaced 90° pulses. It is desirable, but not essential, to also completely depolarise the Q spin system. However, this is difficult to arrange experimentally and is not usually done.

After depolarisation, one returns to the beginning and repeats the whole cycle; by changing the R.F. irradiation frequency and recording the F I D during each cycle, one can scan through a complete quadrupole spectrum.

The methods used by the apparatus described in this thesis are double resonance with spin mixing by level crossing (D R L C) and by continuous coupling (D R C C) .

In D R L C, the experimental sequence is as described above, with switch B (Fig.3.3) always open. The Q spins normally form ≥ 10% of the sample, and absorption during the irradiation phase is limited by Q spin saturation.

D R L C can detect quadrupole resonances in the range 250 kHz - 5 MHz with a sensitivity which is almost independent of frequency. The first level crossings (switch A) polarise the quadrupole levels as if all the Q splittings were ≈ 40 MHz (the P spin splitting in $B_0 \sim 1$ Tesla), whatever the Q spin splittings actually are. The population difference between two Q spin levels, say, 1 MHz apart, is as large as if the splitting were 40 MHz. The Q spins can then absorb radiation until the difference between the populations of the levels becomes zero (saturation). The heat thus absorbed by the Q spins is then passed to the P spin system during the second level crossing, and the resultant P spin magnetisation is recorded. The number of Q spins present limits the sensitivity, as explained in the section on level crossing calculations.

When one or more of the Q spin absorption frequencies lies below ~250 kHz, the Q spin system may become thermally linked to the P spin system during the irradiation phase (switch B in Fig.3.3 closed). The mechanism of this coupling is through the P spin dipolar bath and the effect is known as continuous coupling.

3.3.3 The Dipolar Bath[12, Chpt.IV]

The assembly of P spins is able to absorb R.F. power directly when the irradiation frequency is low.

If one first considers a set of P spins isolated from each other, but thermally linked to a non-magnetic lattice, in an external field of 5 G, then they are able to absorb power at a frequency of (exactly) 21.29 kHz, since each spin experiences a field of (exactly) 5 G. The P spins, however, are not isolated from each other, since T_2 is finite. Spin-Spin interactions occur at a rate $\approx T_2$, corresponding to a 'spread' in frequencies $\approx 1/T_2$. For solids with $T_2 \sim 10\ \mu s$, $1/T_2$ is ≈ 100 kHz (say). The spin-spin interaction may be pictured as a magnetic effect. The P spins are all magnetic dipoles, and are surrounded by a magnetic dipole field proportional in strength to $1/r^3$, where r is the distance from a given spin. If a second spin is sufficiently close to the first spin, it will experience this magnetic dipole field due to its neighbour, and its energy levels will be split by it. Similarly, the energy levels of the first spin will be split by the magnetic dipole field of the second spin.

When one extends these ideas to N spins in an interacting assembly, each spin experiences a net field due to the effects of all its neighbours, although the value of this field will vary from spin to spin. Thus an assembly of spins in zero applied field will be able to absorb energy over a range of frequencies corresponding to the range of fields within the spin bath.

Such an assembly is called a dipolar spin bath and has a finite frequency width Δf, extending in general over a range $\Delta f \approx \frac{1}{T_2}$ (12, p.46). If a small static magnetic field is applied, then the spin bath may absorb power over a range of frequencies $\approx \Delta f$ centred on the Larmor frequency in the field. Theory predicts[33] that the zero-field linewidth Δf_0 is wider than the Zeeman linewidth (in a field) by a factor $\sqrt{\frac{10}{3}} = 1.83$.

The range of frequencies Δf may be written, using the gyromagnetic ratio of the P spins, as a range of magnetic fields. One may then define the local field B_L of the spin bath, being the root mean squared internal field, e.g. for protons in ice Ih, $\Delta f \approx 150\,\text{kHz} \approx 30\,\text{G}$ and $B_L \simeq 10\,\text{G}$. Individual spins experience fields in the range 0 to $\sim 3 B_L$, and a short T_2 corresponds to a large B_L.

The absorption of R.F. power by an assembly of dipoles in zero or small applied D.C. field can be described by a function of the form:[27,33]

$$A(\nu) = (h\nu \cdot \left(\frac{h\nu}{kT_s}\right) \cdot f(\nu)\, B_1^2 \qquad \ldots (3.21)$$

where $h\nu$ = energy of one photon

$\frac{h\nu}{kT_s}$ = relative probability of stimulated absorption over stimulated emission (T_s = spin temperature)
= population difference between two levels

B_1 = amplitude of applied R.F. field

$f(\nu)$ = transition matrix element distribution function.

In zero applied field, $f(\nu)$ is Gaussian in shape, having a maximum at zero frequency, and a standard deviation $\approx \gamma_p B_L$ [γ_p = gyromagnetic ratio of P spins $\div 2\pi$].

In a small D.C. field B_0, $f(\nu)$ breaks up into peaks at 0, γB_0, $2\gamma B_0$, $3\gamma B_0$, etc., but the peaks are not resolved for $B_0 < B_L$, and the effect is simply to shift the broad peak of $f(\nu)$ slightly to higher frequency. For $B_0 \gg B_L$, the peak at $\nu = \gamma B_0$ (the Larmor frequency) dominates the spectrum.

The absorption spectum of a dipolar bath thus has the form of Fig.3.4. Two experimental spectra of this type appear in Fig.5.5. Proton dipolar baths are typically between 100 and 200 kHz wide.

If a quadrupole splitting is thus $< 250\,kHz$, a Q spin may be able to take part in a mutual spin flip with a member of the P spin dipolar bath. Heat absorbed by the Q spin system may thus leak directly into the P spin system during the irradiation phase.

This effect is called continuous coupling and the strength of this coupling depends on both the extent of the P spin bath, which in turn depends on B_L, and on the absorption frequencies of the Q spin system. Continuous coupling can also be induced or improved by applying small D.C. magnetic fields — this is the subject of Chapter V.

3.4 SPIN MIXING BY LEVEL CROSSING[4,6]

Following closely the theory as laid out by EDMONDS[4], we will now consider the sequence of events associated with one experimental cycle of the DRLC method, taking the particular case of protons for the P spins and spin 1 quadrupoles (such as nitrogen) for the Q spins.

We shall assume that both sets of spins have long T_1's and (at first) that T_{1D} of the protons is also long. We shall now consider what happens to the populations of the various spin energy levels as we take the sample through the three phases of Fig.3.3.

3.4.1 Polarisation Phase

The sample is placed in a large field B_0 for a time $t \gg T_1(P)$. The populations of the various levels are as shown in Fig.3.5. The P spins come to thermal equilibrium with the lattice at temperature θ_L. The equilibrium values of P_+ and P_- are then given by the Boltzmann distribution:

$$\frac{P_-}{P_+} = \exp\left(-\frac{h\nu_p}{k\theta_L}\right) = 1 - \frac{h\nu_p}{k\theta_L} \quad \left(\text{since } \frac{h\nu_p}{k\theta_L} \ll 1\right) \qquad \ldots (3.22)$$

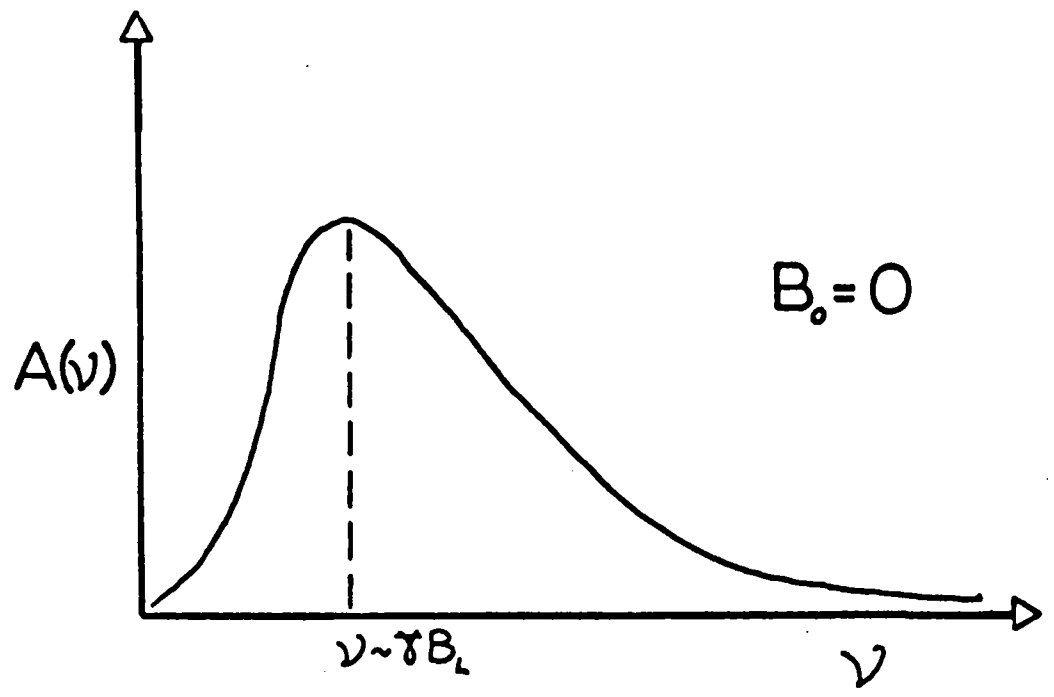


Fig. 3.4 : Dipolar Bath absorption

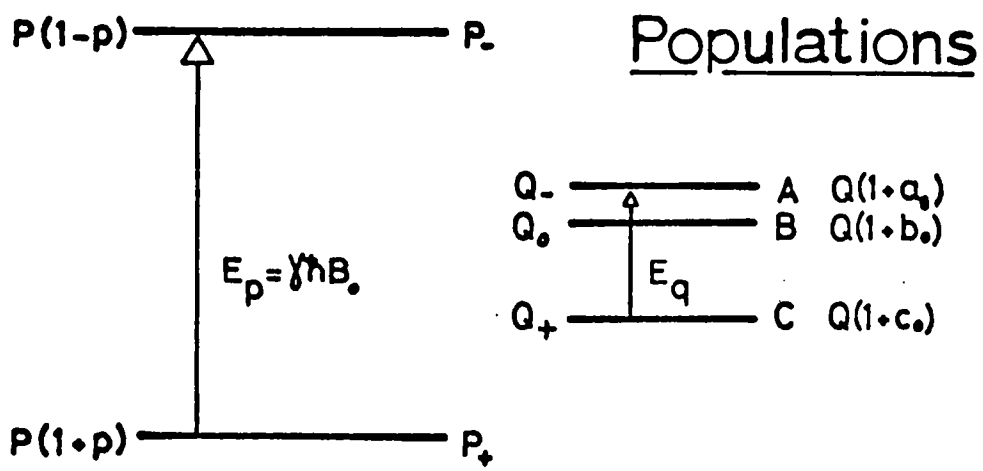


Fig. 3.5 : Before first level crossing $E_P > E_Q$

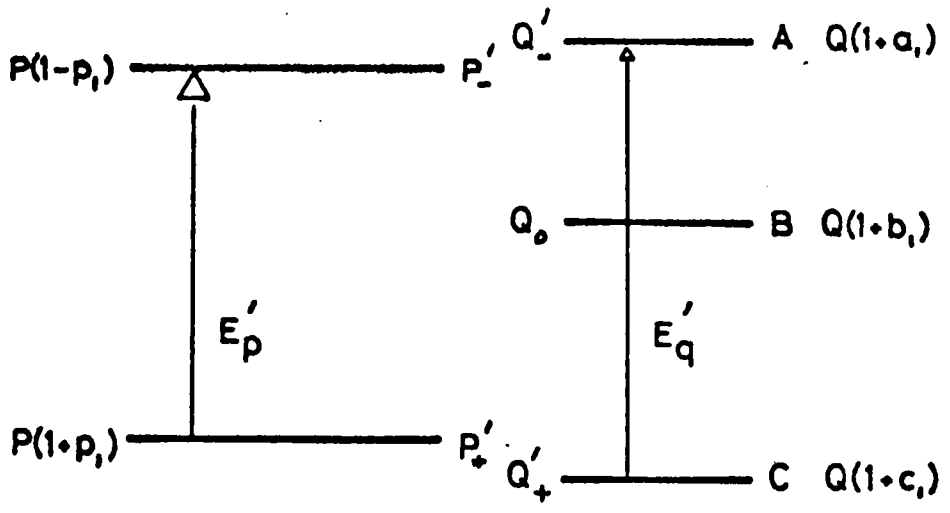


Fig. 3.6 : After first level crossing $E'_P < E'_Q$

The Q spins also come to equilibrium with the lattice (if $t \gg T_1(Q)$) but the energy splitting E_Q is so small that we may say that $Q_- = Q_+ \ (= Q_0)$.

The sample is now removed from the magnetic field so that the P spin level splitting $h\nu_p$ decreases to the small value characteristic of the dipolar spin bath. The Q spin splittings also change with the removal of the field, but they do not collapse to zero. The first level crossing occurs when $h\nu_p = \hbar\gamma B_0 = E_Q(B_0)$. Fig.3.6 shows the populations of the various levels immediately after this first level crossing, between the P spins and the quadrupole levels A C The level crossing occurs in a time $\sim T_2$ (characteristic of the PQ system) and consists of a large number of mutual spin flips, the A C levels emitting a photon of energy $h\nu_q$ and the P spins absorbing a photon of energy $h\nu_p = h\nu_q$, so that energy is conserved.

The populations of the levels after this first level crossing are described[5] by the following equations:

$$(P_+ + P_-) = (P'_+ + P'_-) = 2\ N_P \qquad \ldots (3.23)$$

$$(Q_+ + Q_-) = (Q'_+ + Q'_-) = 2\ N_Q \qquad \ldots (3.24)$$

(By conservation of the total numbers of spins)

$$(Q_- + P_-) = (Q'_- + P'_-) \qquad \ldots (3.25)$$

(Conservation of energy: energy lost by the Q spins = energy gained by P spins, in isolation from the lattice and the level Q_0.)

$$\frac{P'_-}{P'_+} = \frac{Q'_-}{Q'_+} \ . \qquad \ldots (3.26)$$

The P spins come to thermal equilibrium with the two Q spin energy levels A and C. The new spin temperature of the P spins now equals the apparent spin temperature of the levels A and C. There is no spin-spin coupling to the level Q_0 and hence the 'polarised' levels A and C have a lifetime $\approx T_1(Q)$, which is assumed long.

Solving equations (3.23) - (3.26), we obtain

$$P'_{\pm} = \frac{N_P}{N_P + N_Q} \; (P_{\pm} + Q_{\pm})$$
$$Q'_{\pm} = \frac{N_Q}{N_P + N_Q} \; (P_{\pm} + Q_{\pm}) \qquad \ldots (3.27)$$

As B_0 decreases further, the P spin splitting becomes equal, in turn, to the other two Q spin energy splittings; when all three level crossings have occurred, the field B_0 falls to zero, and the polarization phase is complete. To simplify calculations, we shall rewrite the population equations (3.27) in terms of population differences p, a, b and c[6], as also defined in Fig.3.5. We now have the total numbers of spins given by:

$$N_P = P(1-p) + P(1+p) = 2P$$
$$N_Q = Q(1+a) + Q(1+b) + Q(1+c) = 3Q$$

and $a+b+c = 0$ (conservation of Q spins).

Equation (3.22) can be rewritten as

$$\frac{P_-}{P_+} = \frac{1-p}{1+p} \approx 1 - 2p = 1 - \frac{h\nu_p}{k\theta_L} \; .$$

Thus

$$p = \frac{h\nu_p}{2k\theta_L} \approx 10^{-5} \quad \text{for} \quad \nu_p = 40\,\text{MHz} \; , \; \theta_L = 77^\circ\text{K} \; .$$

Equations (3.27) may be rewritten as

$$\left.\begin{aligned} p_1 &= Xp_0 + \tfrac{1}{2}(1-X)(c_0 - a_0) \\ a_1 &= a_0 - \tfrac{1}{2}X(2p_0 + a_0 - c_0) \\ c_1 &= c_0 + \tfrac{1}{2}X(2p_0 + a_0 - c_0) \end{aligned}\right\} \qquad \ldots (3.28)$$

where subscript 0 refers to populations before and subscript 1 to populations after the level crossing. The equations are given in terms of the parameter X, where

$$X = \frac{P}{P+Q} \; .$$

Before the first level crossing, the initial conditions are

$$p_0 = p \text{ (thermal, } B_0 = 1 \text{ Tesla)} \approx 10^{-5}$$
$$a_0 = b_0 = c_0 = 0 \; .$$

After the first level crossing, the populations are given by (Fig. 3.6) p_1, a_1, b_1 $(= b_0 = 0)$ and c_1, and these form the initial conditions for a second level crossing. After the third level crossing, the polarisation phase is complete, and the populations of the various levels are described by p', a', b', and c' : where

$$\left.\begin{aligned} a'/p &= -\tfrac{3}{4} X^3 - X \\ b'/p &= +\tfrac{3}{4} X^3 - \tfrac{1}{2}X^2 \\ c'/p &= +\tfrac{1}{2} X^2 + X \\ p'/p &= \tfrac{3}{4} X^3 - \tfrac{1}{4} X^2 + \tfrac{1}{2} X \end{aligned}\right\} \quad \ldots (3.29)$$

These values are plotted out in Fig.3.7 as a function of R, where

$$R = N_P/N_Q = 2P/3Q \ .$$

3.4.2 Irradiation Phase

The sample is now polarised and the applied field falls to zero. R.F. irradiation is applied to the sample, and this may or may not affect the Q spin populations a', b', c'. The P spin population is not affected provided we do not irradiate the dipolar bath. We denote the populations at the end of the irradiation phase by p'', a'', b'', c''. If we do not irradiate a Q spin transition, $p'' = p'$, $a'' = a'$ etc. If we do irradiate a Q spin transition, then we alter the populations of the two levels in question. For example, if we irradiate the transition A C to saturation, we make the populations of levels A and C equal. Level B is unaffected. Then:

$$\begin{aligned} a'' = c'' &= \tfrac{1}{2}(a' + c') \\ b'' &= b' \\ p'' &= p' \ . \end{aligned}$$

3.4.3 Detection Phase

After irradiation, the sample is returned to the large field $B_0 \sim 1$ Tesla. On the way, three more level crossings occur, this time in reverse order. Three further applications of equations (3.28), using p'', a'', b''

and c'' as initial conditions result in a final P spin population given by

$$p''' = (\tfrac{3}{4}X^3 - \tfrac{1}{4}X^2 + \tfrac{1}{2}X)p'' + \tfrac{1}{2}(1-X)\left[-(\tfrac{3}{4}X^2+1)a'' + (\tfrac{3}{4}X^2 - \tfrac{1}{2}X)\,b'' + (\tfrac{1}{2}X+1)c''\right] \quad \ldots (3.30)$$

This may be written as

$$p''' = \pi(p'') + \Delta(a'', b'', c'') \quad \ldots (3.30')$$

Since $p'' = p'$ for D R L C, $\pi(p'')$ is a function only of the original polarisation of the P spins and the spin ratio X. It is unaffected by any irradiation.

$\Delta(a'', b'', c'')$ is the 'useful' part of p'', which depends on the quantities a'', b'' and c''.

All 'triple dash' quantities refer to the stage in the experiment when the sample has returned to $B_0 \sim 1$ Tesla, immediately before measurement of magnetisation by the 90° pulse — which effectively measures p'''.

After this measurement, a 'comb' of 90° pulses is applied which demagnetises the sample ($p = 0$), and a new experimental cycle begins.

In the absence of irradiation (at a transition frequency) $a'' = a'$, $b'' = b'$, $c'' = c'$, as already stated. Substituting equations (3.29) into the expression for Δ (3.30') we obtain

$$\Delta(a',b',c') = \tfrac{1}{2}[X(1-X)][\tfrac{9}{8}X^4 - \tfrac{3}{4}X^3 + 2X^2 + X - 2]\,p \quad \ldots (3.31)$$

This is plotted against R in Fig.3.8.

It can be seen that Δ decreases with increasing R (fewer Q spins). Δ represents that part of the P spin polarisation which is passed to the Q spins during magnetisation, remains there during irradiation, and is passed back to the P spins during remagnetisation.

As the number of Q spins decreases, their 'thermal capacity' or ability to store magnetisation, also decreases, and hence $\Delta(a', b', c')$ decreases.

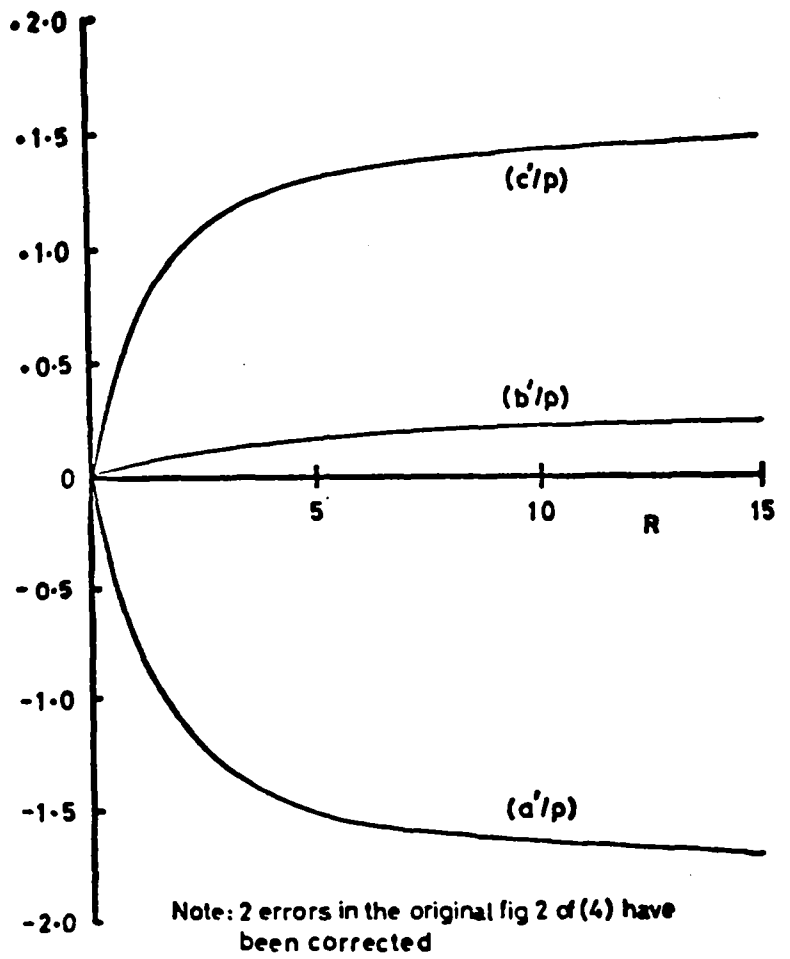


Fig.3.7: Population constants after polarisation (from(4))

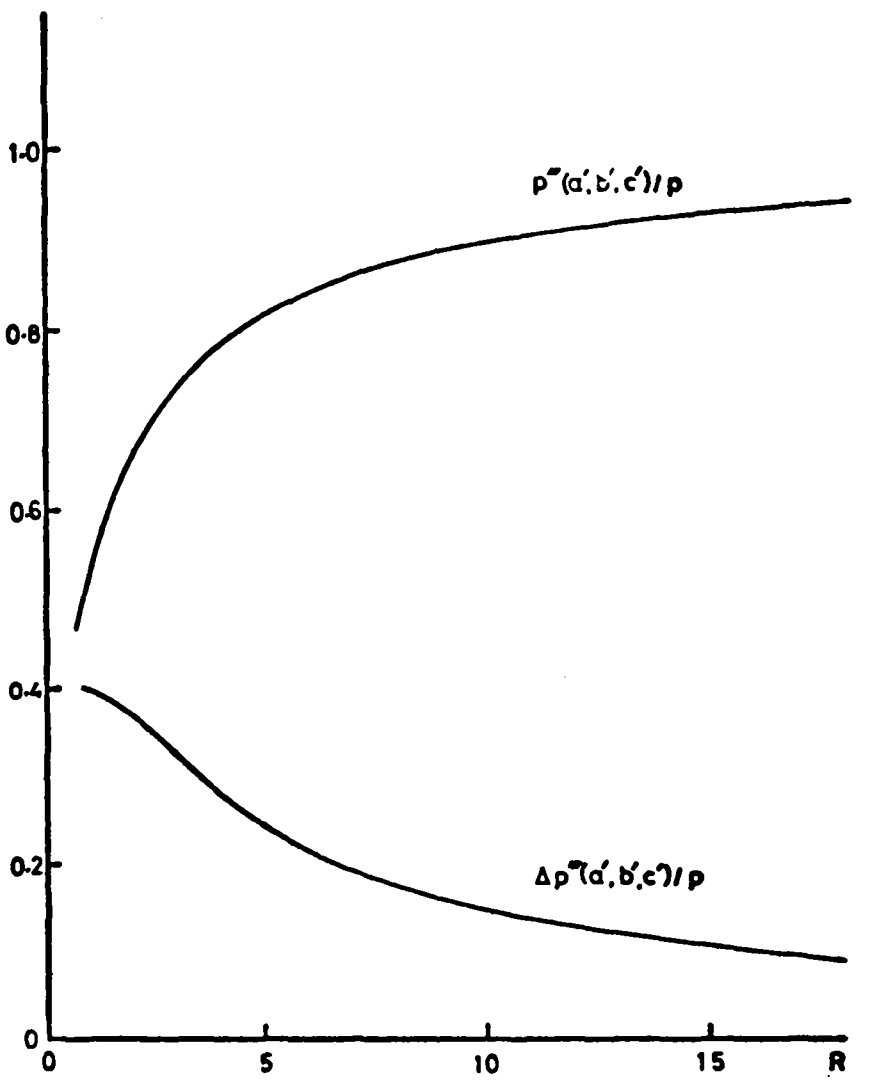


Fig.3.8: Δ & p''' for P spins, no irrad. (from (4))

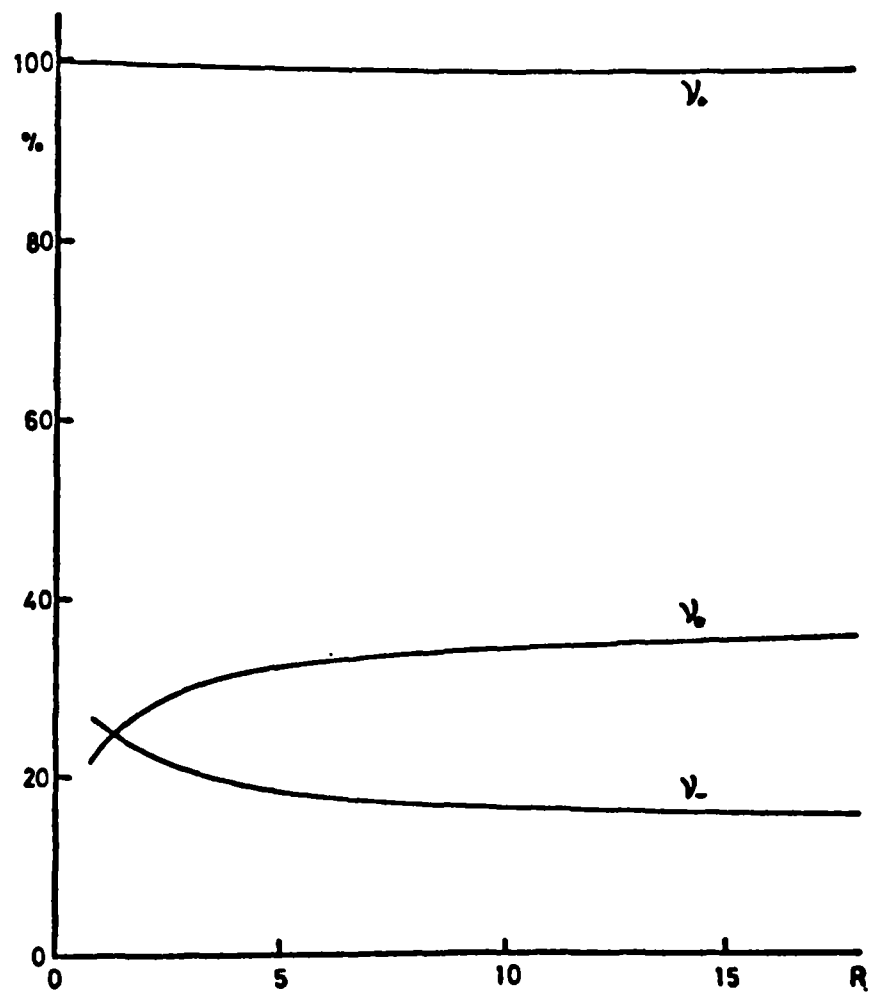


Fig.3.9: %age of Δ which can be destroyed by irradiation (from(4))

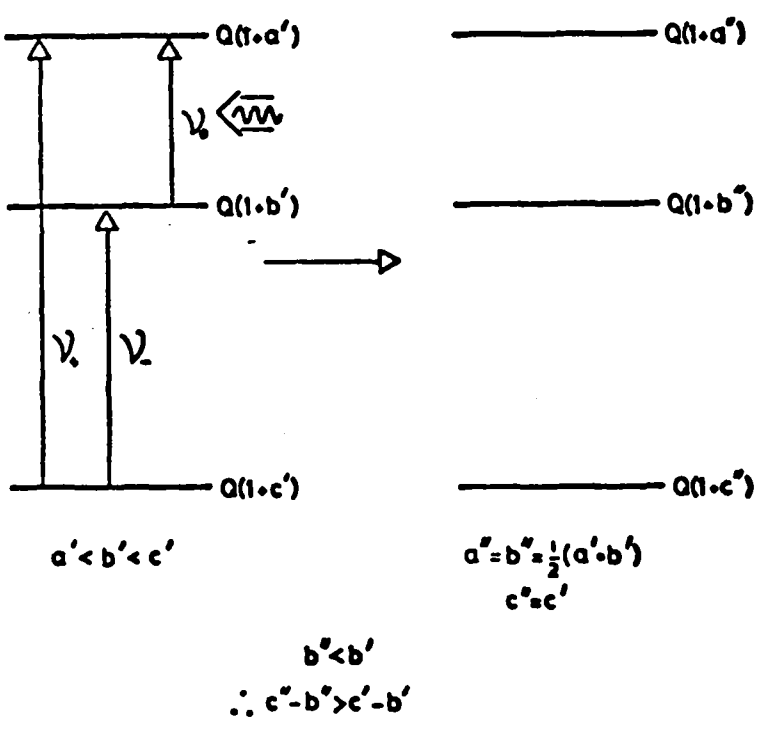


Fig.3.10: Effect on ν- of double irradiation at

Figure (3.9) shows the percentage of Δ that may be destroyed by irradiating ν^+, ν^- or ν^0 to saturation.

Figures 3.8 and 3.9 define the sensitivity of the method. The size of a quadrupole absorption, as detected, depends both on the fraction $\frac{\Delta p^{iv}}{\Delta(a',b',c')}$ and on the ratio $\frac{\Delta(a',b',c')}{p'''}$, where Δp^{iv} indicates the value of Δ after irradiation of a quadrupole transition to saturation.

For example, if $T_{1D}(P)$ is fast, then $p''' \approx \Delta$, because p'' (equation (3.30) is ≈ 0 since the spin temperature of the P spins rises rapidly in zero field to $\approx 77°K$. This effect may be induced (if T_{1D} is long) by irradiating the sample at $\sim 50\,kHz$, thereby inducing the P spins to absorb power until $p'' \approx 0$. Sharing the irradiation phase between 50 kHz and a second frequency ν_Q will thus aid the sensitivity of detection for the quadrupole transitions.

Sensitivity is thus best defined by the ratio $\Delta p^{iv}/\Delta(a',b',c')$, since this is independent of T_{1D} effects.

3.4.4 Physical Interpretation of Sensitivity

It can be seen that the sensitivity of detection of Q spin transitions depends entirely on the polarisation built into the Q spins by the P spins during the demagnetisation phase. This polarisation is independent of the actual Q spin splittings and depends only on the ratio of spins R, and the polarisation p of the P spin system in the large field B_0, at lattice temperature θ_L.

The greater the polarisation built into a pair of Q spin levels, the larger the number of spin flips that can be induced by irradiation before saturation occurs, and thus the greater the final effect on the P spin system.

The remagnetisation phase provides a useful means of transferring the information in the Q spins back to the P spins. The final measurement

is performed on the P spins only, using a 90° pulse + F I D or other means, thus allowing use of a simple fixed-frequency N M R spectrometer.

For example, if we increase p by either increasing B_0 or decreasing θ_L or both, we can extend the useful measurement range to higher values of R (lower percentage of Q spins). Other factors also influence this improvement, but the higher value of B_0 is of significance. It is not necessary even to polarise and detect (90° pulse) in the same field B_0. Another scheme suggested (by E.L. Hahn) a 10 T superconducting magnet for polarisation, and a simple 0.5 T (permanent) magnet for detecting the result, using a single uni-directional passage of the sample.

Figure (3.9) indicates that the sensitivity of detection for ν_0 and ν_- is much less than that of ν_+. This effect is readily observed in practice, but can be somewhat overcome by double irradiation techniques.

For example, if it is desired to improve detection of ν_-, the irradiation period is chopped, so that for part of the time the ν^0 transition is saturated, and for the rest of the time the ν^- transition is stepped through. This has the effect of equalising the populations of levels A and B (Fig.3.10) making $a'' = b'' = \frac{1}{2}(a' + b')$ and hence of increasing the population difference $c'' - b''$ [reference (4), corrected for a printer's error].

Thus the number of spin flips which can now be induced by irradiating ν^- to saturation is larger, and the final measured change in Δ is increased.

Similarly, irradiation of ν^- while scanning through ν^0 will improve the sensitivity of detection for ν^0. Double irradiation can thus be used for associating lines in a complex spectrum into triplets. Irradiation of a given ν^0 can only affect the corresponding ν^- (and ν^+), not any other site. (Double irradiation tends to decrease the size of the ν^+ absorption).

3.4.5 Limitations of the Simple Theory

The simple theory outlined above must be modified to take account of the polycrystalline nature of the sample.

Firstly, the quadrupole energy levels may be affected by a magnetic field in such a way that different crystallites experience level crossings in different sequences of time, depending on crystal orientation, thus affecting the population equations during the polarisation phase. This effect is particularly important in the case of large unquenched spins $\geq \frac{5}{2}$ (the $I = \frac{3}{2}$ case is dealt with later).

Secondly, during irradiation, a given transition will saturate at different R.F. intensity levels in different crystallites, depending on crystallite orientation. This is because the irradiation is polarised (non-isotropic) and, as shown earlier, (pp. 27-28), a ν^+ transition (say) is only affected by the R.F. component in a certain direction relative to the E F G principal axes. For some crystallites this component will be large, and for others small or zero. Thus the true saturation behaviour of poly-crystalline samples will be more complex than previously outlined. These deductions are made for the case $I = 1$, but are generally true for all I.

These effects, and some others, lead to modifications of the simple theory, but do not detract from its main conclusions.

CHAPTER IV

THE APPARATUS

4.1 INTRODUCTION

Following several years of successful operation of a nuclear quadrupole double resonance spectrometer, it was decided that a new, more flexible apparatus would be constructed, in order to extend the range of compounds to which the DRLC method could be applied.

Principally, the new spectrometer would be capable of working at temperatures down to 4.2°K, in the expectation that the low temperature would increase the proton T_1 of certain compounds to 30 seconds or more, which is necessary, if the DRLC method as described here is to work successfully.

Given our experience with the Mark I spectrometer, several other additions and refinements to the apparatus design were also made.

(1) The proton NMR section of the apparatus would work at 39.6 MHz (corresponding to a magnetic field of 0.93 T), to give a better signal/noise than the Mark I.

(2) The dewar system was designed not to exceed 1" total diameter, so that a readily-available 1.125" pole gap NMR permanent magnet could be employed.

(3) Given (2) and the 4.2°K requirements, it was decided to employ a flow cryostat design, allowing additionally for operation at any temperature between 4.2°K and 350°K by means of a controlled heater winding.

(4) Since a 'zero static field' or small preset static field must be provided during irradiation, a 3-dimensional field control unit was designed to allow control of the magnetic field in the region of the upper coil between zero and 100 Gauss in the horizontal plane, and/or up to 40 Gauss vertically - parallel to the R.F. coil.

(5) With an eye on ease of construction by other researchers it was decided, as far as possible, to use 'off the shelf' units in assembling the spectrometer.

(6) Throughout design and construction, reliability was a prime concern, since it was intended to fully automate the apparatus, to allow unattended operation for up to 36 hours at a time.

A block diagram of the complete system appears in Fig.4.1, and Fig. 4.2 outlines the experimental measurement sequence, with its control analogue.

The following sections give brief descriptions of the components of the system and finally we present a table of normal performance data.

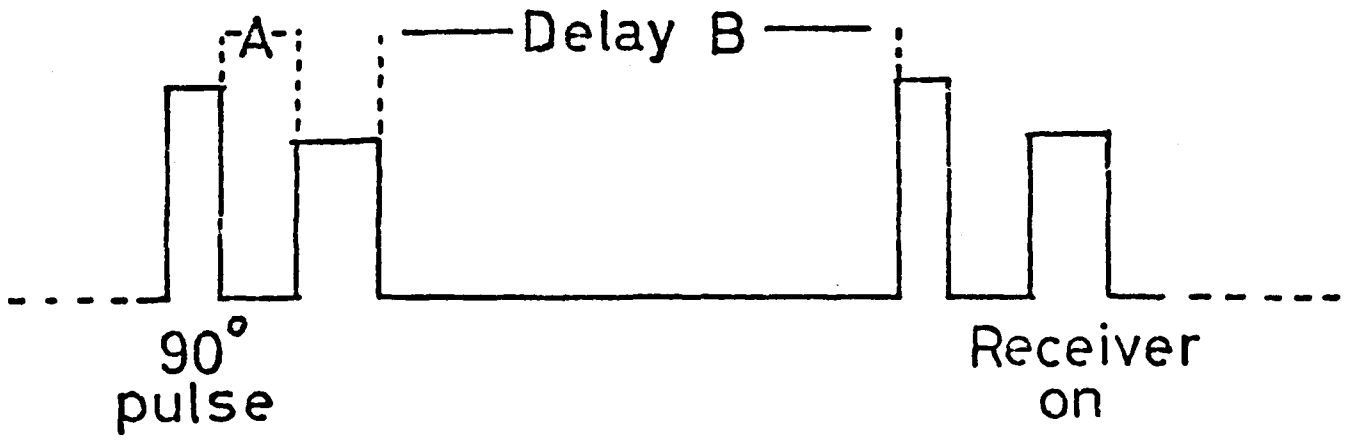
4.2 BRUKER 'MINISPEC' AND MODIFICATIONS TO IT

The NMR spectrometer section of the apparatus consists of a standard Bruker 'Minispec' P.40, with some small modifications.

The block diagram of the unit is reproduced in Fig.4.3.

A crystal-controlled oscillator generates R.F. at 9.9 MHz, which is then amplified, multiplied up ×4 in frequency to 39.6 MHz and fed to an R.F. power amplifier which generates 150 V pp into 50 Ω.

The crystal frequency is also fed to a chain of dividers, so that control pulses at 1 MHz, 100 kHz etc... 1 Hz are also generated. These are controlled by the 'Program' module which gates the 39.6 MHz R.F. in order to generate a '90°' pulse (or a 180° pulse, or a combination of these), and determines the operation of the receiver and signal evaluation sections so that the correct measuring sequence is obtained.



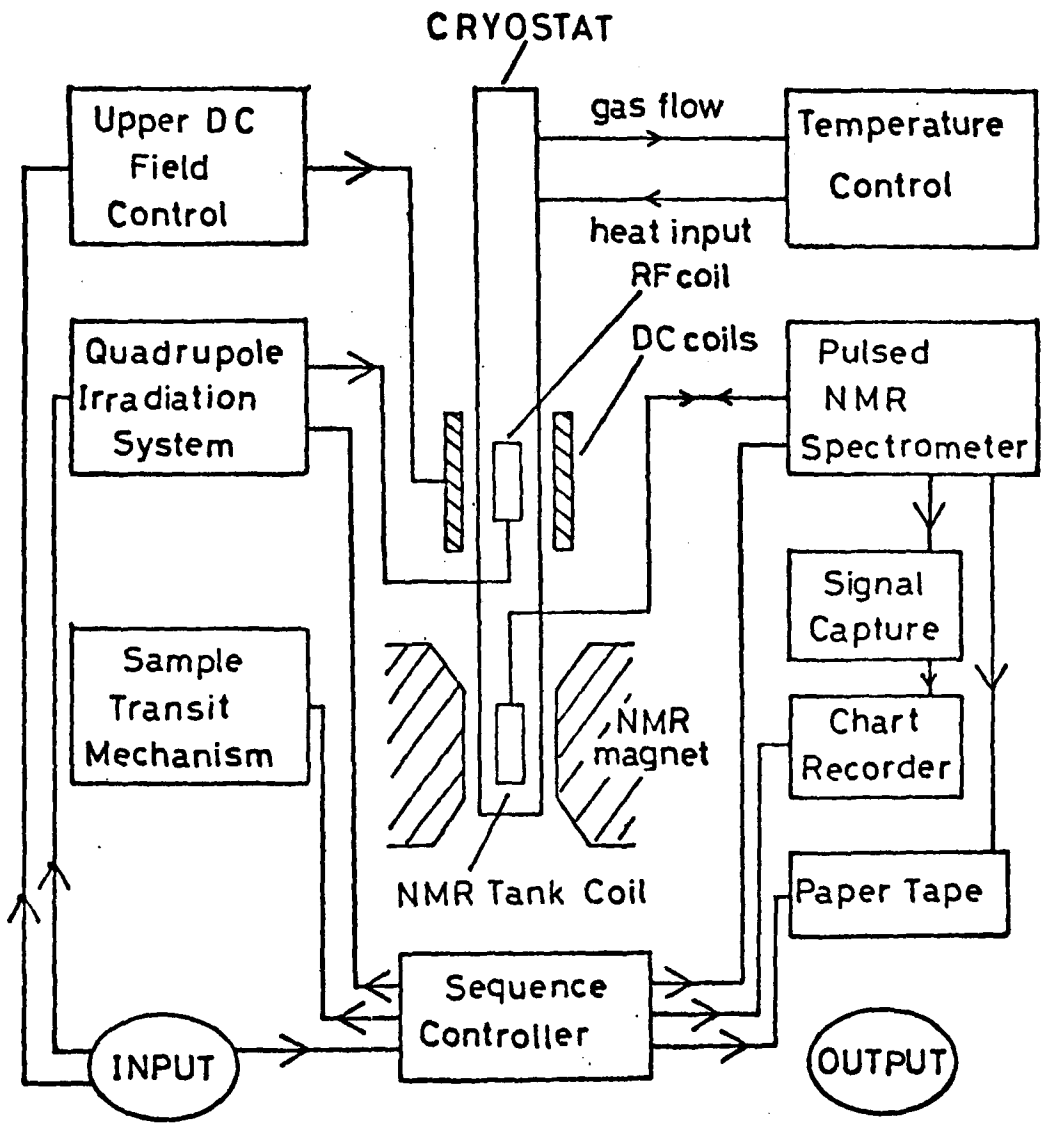


Fig.4.1: NQR Spectrometer - Block diagram

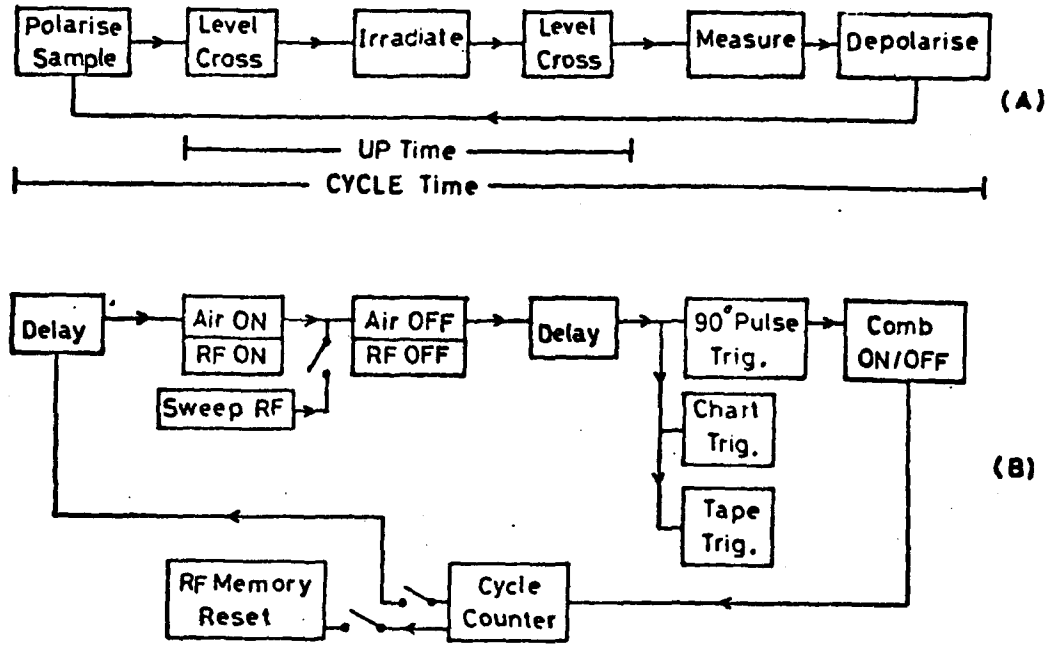


Fig.4.2: (A) Experimental Sequence
(B) Control Analogue

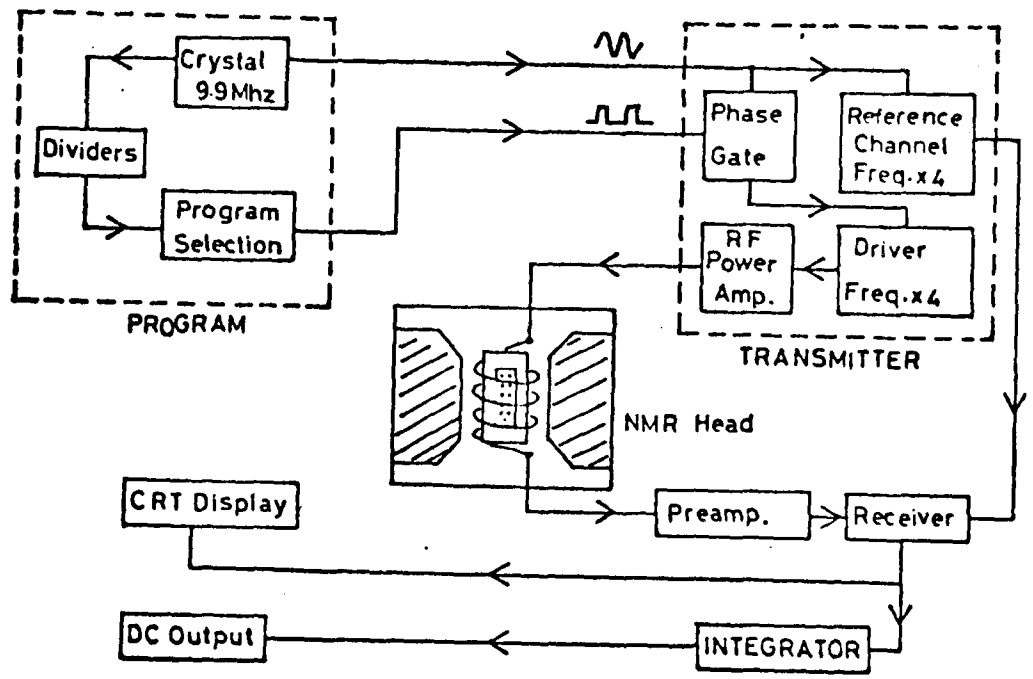


Fig.4.3: Block diagram of Minispec P40 (from Bruker)

The program can be set up with delay B from 1 ms to 100 sec. Delay A is normally fixed, and adjusted to the minimum value that gives a 'zero' output with no sample inside the tank circuit, i.e. delay A = receiver dead time.

The Minispec also provides other built-in programs, such as 90° - Delay - 180° - Measure, but these are not used in NQR spectroscopy.

The measurement section of the Minispec consists of a tuned pre-amplifier followed by a gated receiver which detects the free induction decay and converts this into an R.F. envelope signal, either by feeding it to a diode detector stage, or by feeding it through a phase sensitive detector.

The envelope signal is then passed to a gated integrator, which generates a D.C. voltage proportional to the size of the free induction decay. From the Minispec this D.C. signal is passed to an FET Sample-and-Hold gate, where it is held until it is recorded on the chart recorder.

The free induction decay signal is also available for display on a suitably triggered oscilloscope.

4.2.1 Modifications

The Minispec is controlled by a front panel switch which selects either 'Periodic' or 'Single Shot' operation — i.e. either a chain of 90° pulses and measurements, separated by a controlled delay, or a single 90° pulse and measurement.

For external control, logic gates were connected in parallel with this switch, so that 'Periodic' or 'Single Shot' operation is selected by external control pulses. The 'single shot' allows a single measurement of sample magnetisation after an externally fixed time interval, and the periodic setting, with a 1 ms separation between 90° pulses, generates a comb during the 'on' pulse (usually 1 sec on) which effectively demagnetises any sample with a $T_1 \geq 100$ ms.

To summarise: By application of a single trigger pulse to the unit, the Minispec, by means of a 90° pulse and its receiver/integrator, measures the magnetisation of the sample, and presents the result as an analogue voltage in the range 0 → 1.000 volts, for recording both on a chart recorder and a digital voltmeter.

The application of a longer gate pulse (1 sec) causes the Minispec to 'free-run' and apply a large number (1000) of 90° pulses to the sample, demagnetising it.

4.3 NMR TANK CIRCUIT

The tank circuit used in this apparatus is based on the Bruker Minispec design (Fig.4.4). The detailed analysis of the performance of such a circuit is left to Appendix 1, but may be summarised as follows: the parallel resonant circuit formed by L, and the capacitor network has a high impedance at resonance, which is matched to the 50 Ω input/output line by the capacitive divider network. The metal oxide resistor R does not vary appreciably with temperature, and hence the circuit Q is held approximately constant.

When constructing the tank circuit, considerable care is needed in the choice of components, given the following constraints on its operation:

1. Resonant frequency. This is fixed at 39.6 MHz by the Minispec P.40.
2. Circuit Q. We require a high Q to aid detection, and to ensure a short 90° pulse.
3. Line matching. This must be ~50 Ω for efficient matching to the transmitter.
4. Voltage ratings. The high Q and capacitive transformer ensure a high voltage (~1 kV) across the inductance L.
5. Temperature. The components must be stable through repeated temperature cycles to 4°K, and must not vary excessively in value when the temperature is changed.

Given these constraints, we employ silver mica fixed capacitors for their temperature stability. Rated at 500 V D.C., we use two 39 pF capacitors in series for C_3, and a single 220 pF capacitor for C_2. C_1 is a 10 pF Jackson Subminiature Tetfer (P T F E insulated) trimmer, rated at 1.2 kV, allowing tuning over the range 37-41 MHz. The ratio $C_3/(C_1 + C_2) \simeq 7$ determines the voltage step-up ratio of the capacitive transformer. With 150 volts peak input, approximately 1 kV is generated across C_3, necessitating the choice of high-voltage types.

Having fixed the capacitor values, the required inductance of L is fixed at ~0.6 μH. Fig.4.6 shows a sketch of the coil former unit. Constructed of P T F E and machined from the solid, it consists of a sample space and a 17.5 turn spiral groove in which a 1.0 mm wide bare copper tape is wound, forming the coil. The trimmer is fitted inside the sample space, below the sample position, and the other components are mounted below. When warm (300°K), the trimmer may be adjusted (using a special tool) from the top of the cryostat. The complete assembly is a slide fit inside the cryostat sample space.

To prevent excessive heat leaks, the tank circuit is connected to the top of the cryostat using miniature 50 Ω stainless steel clad coaxial cable, from where normal 50 Ω coaxial cable leads to the transmitter. Since this cable has a capacitance of ~100 pF, and has higher losses than a copper equivalent, it is undesirable for it to be included in the tank circuit, where large R.F. currents flow. It is for this reason that we mount all capacitors inside the cryostat, close to the coil. Losses are thus kept to a minimum, and a high Q is easier to obtain.

4.3.1 Minispec/Tank Circuit Connection Network (Fig.4.5)

This circuit[28] makes use of the nonlinear properties of forward-biased diodes to ensure correct interconnection of the tank circuit, transmitter and receiver. It operates as follows:

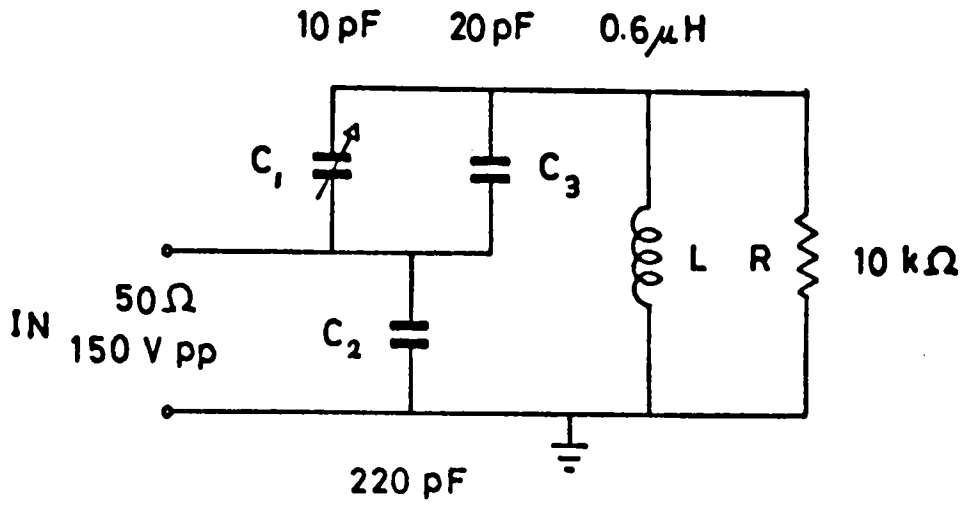


Fig.4.4: NMR Tank circuit

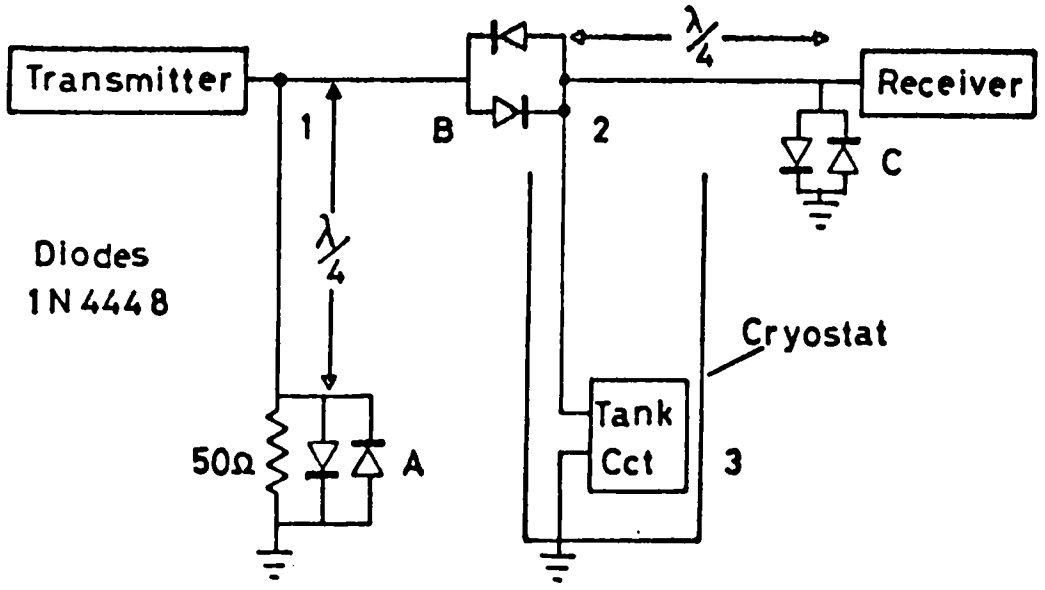


Fig.4.5 : Interconnections

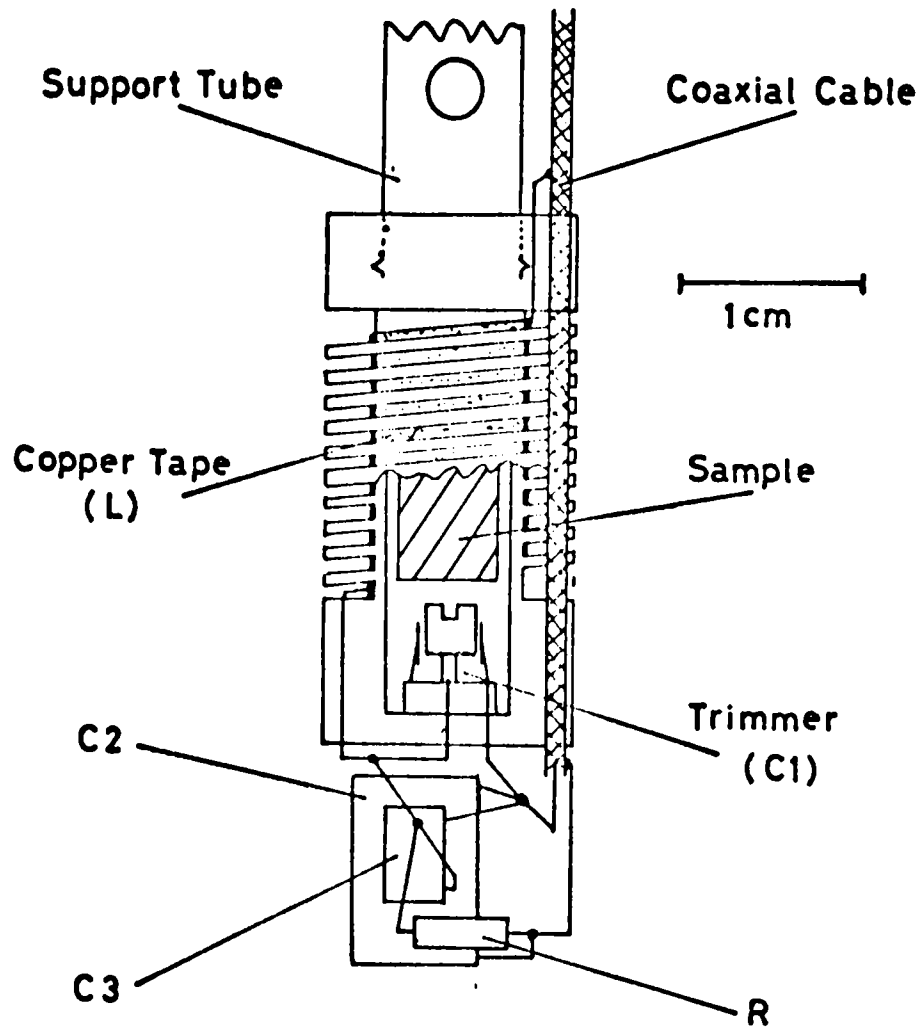


Fig.4.6: NMR Coil former and components

(1) Transmitter on - high voltage pulse out - diodes all short circuit. The short circuit at A reflects as an open circuit at (1), the other end of the $\lambda/4$ transmission line, so that no power flows down this line. The short circuit at C also reflects as an open circuit at (2), so that no power flows to the receiver. The short at B allows R.F. to pass down to the tank circuit (3).

(2) Transmitter off - low voltage noise and leakage past the gate at the transmitter output and the free induction decay (low voltage) at the tank circuit (3). Diodes all open circuit.
The transmitter noise passes down to A and is absorbed in the 50 Ω load. It cannot pass through B. The free induction decay similarly cannot pass B, but it does pass into the preamplifier of the receiver since the diodes C are open circuit.

4.4 CRYOSTAT AND TEMPERATURE CONTROL SYSTEM

The cryostat design is to be published in the Journal of Physics E, but we will repeat the description here, as publication will be in early 1978.

4.4.1 Introduction

A flow cryostat differs from the more usual cryogenic dewar vessel in that no liquid refrigerant is stored within it. The experimental chamber is cooled by drawing past it a flow of liquid refrigerant or its cold vapour which is stored in a separate dewar vessel. By controlling the flow rate of the refrigerant and the power input to an electrical heater wound directly upon the experimental chamber, any temperature between room temperature and the boiling point of the refrigerant may be maintained.

The advantages of a flow cryostat over the conventional dewar vessel are:-

(i) Any temperature intermediate between the boiling point of the refrigerant and room temperature may be maintained as mentioned above.

(ii) Because no liquid refrigerant is stored, the outer diameter of the cryostat need be only one or two cm larger than that of the working chamber which may be important in experiments in confined spaces such as magnetic resonance experiments performed between the pole tips of a magnet or in a magnetic solenoid.

(iii) With proper heat exchangers the total enthalpy of the refrigerant may be utilized rather than merely the latent heat, which makes for efficient use of refrigerant.

(iv) The cool-down or warm-up time of the experimental chamber may be rapid as there is little heat storage. For example from 300 K to 4 K using liquid helium may be of order ten minutes.

A flow cryostat with an outer dimension of 1" has been described before[29].

The additional features of the present design may be summarised as follows:

(1) Ease of top loading whilst at low temperature.

(2) Through-flow of refrigerant. The tail of the cryostat may be directly inserted into the refrigerant storage dewar, thus eliminating the need for a transfer line and its associated high heat leak.

(3) The top of the cryostat is uncluttered, due to the simple coolant exit tube.

(4) A large experimental volume is available.

4.4.2 Construction

The construction is illustrated in Fig.4.7. The inner and outer diameters are those used in our cryostat but are not critical provided that thin wall stainless steel and high conductivity copper are employed and that adequate gaps are allowed between coaxial cylinders. The cryostat is seen to consist of two parts, an outer vacuum jacket and a flow control insert which are joined at the top by means of a bolted flange with a rubber O-ring seal.

The lower part of the vacuum jacket has a copper radiation shield (o/d 2.22 cm) within the vacuum space which is brazed to the copper joining piece to ensure good thermal contact. The radiation shield is thus cooled by the refrigerant gas immediately it has passed by the experimental chamber through heat exchange between the refrigerant and the copper joining piece. The bellows inserted in the innermost tube is necessary to compensate for differential thermal contraction between brass and stainless steel.

The gas flow control insert consists of the copper experimental chamber suspended from the top flange by a thin wall stainless steel tube. As in all cryostat construction for use with magnetic fields, non-magnetic stainless steel is used. The stainless steel suspension tube carries two

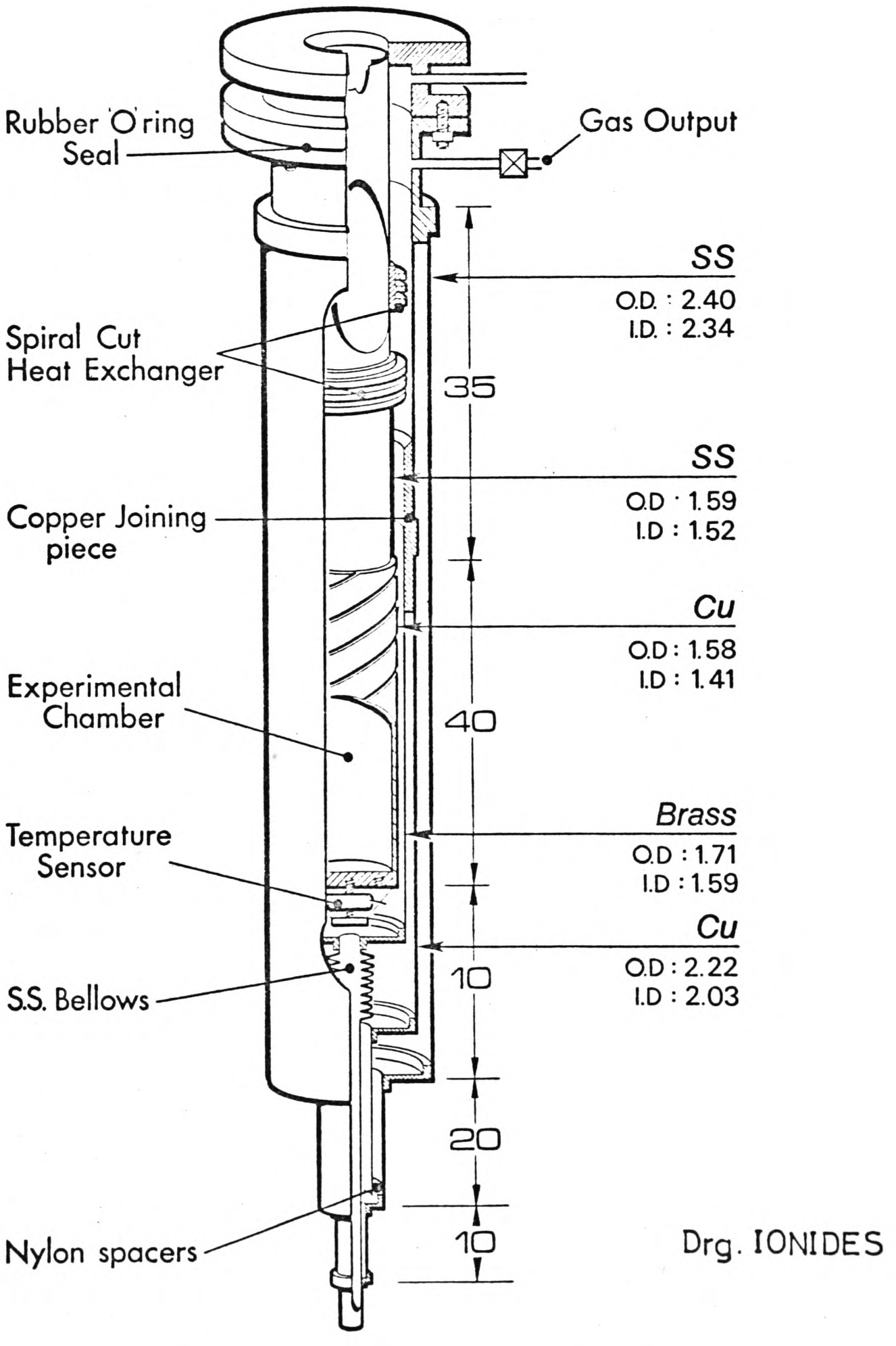


Fig.4.7: Cryostat Dimensions in cm.

copper collars with deep spiral grooves cut in them to ensure that the refrigerant gas makes good thermal contact both with this tube and also with the inner wall of the vacuum jacket.

The experimental chamber is a loose fit in the vacuum jacket and is made of high conductivity copper. In its outer surface is cut a triple start spiral of pitch a few cm so that the refrigerant, in passing along the spiral, makes excellent thermal contact with the chamber. A temperature sensor (in our case a forward-biassed silicon diode) is attached to the bottom plate of the experimental chamber and closely thermally linked to it, (Fig.4.8). It is important that this sensor be shielded from direct thermal contact with the refrigerant. A bifilar loop of manganin resistance wire is wound within one of the spiral grooves and the wires from the temperature sensor are led up another. The sensor and heater are connected to an external temperature control unit.

The refrigerant gas emerges from the top of the cryostat near room temperature and is pumped through a precision 12 turn needle valve by a simple oil free neoprene diaphragm pump. The needle valve is by-passed by a standard gas flow valve for initial fast cooling and then the desired temperature is held approximately by adjusting the needle valve with the by-pass valve closed. The fine temperature control consists of a simple electronic controller which senses the voltage across the forward-biassed silicon diode (IS 44) and holds this constant by controlling the power fed to the 60 Ω bifilar heater. A temperature stability of ± 0.1 K is thus easily attained.

4.4.3 Performance

In the temperature range 300 K to 77 K the refrigerant used is liquid nitrogen contained in a glass bucket dewar below the cryostat which is vertical. To maintain 77 K the liquid consumption is about 60 ml/hour

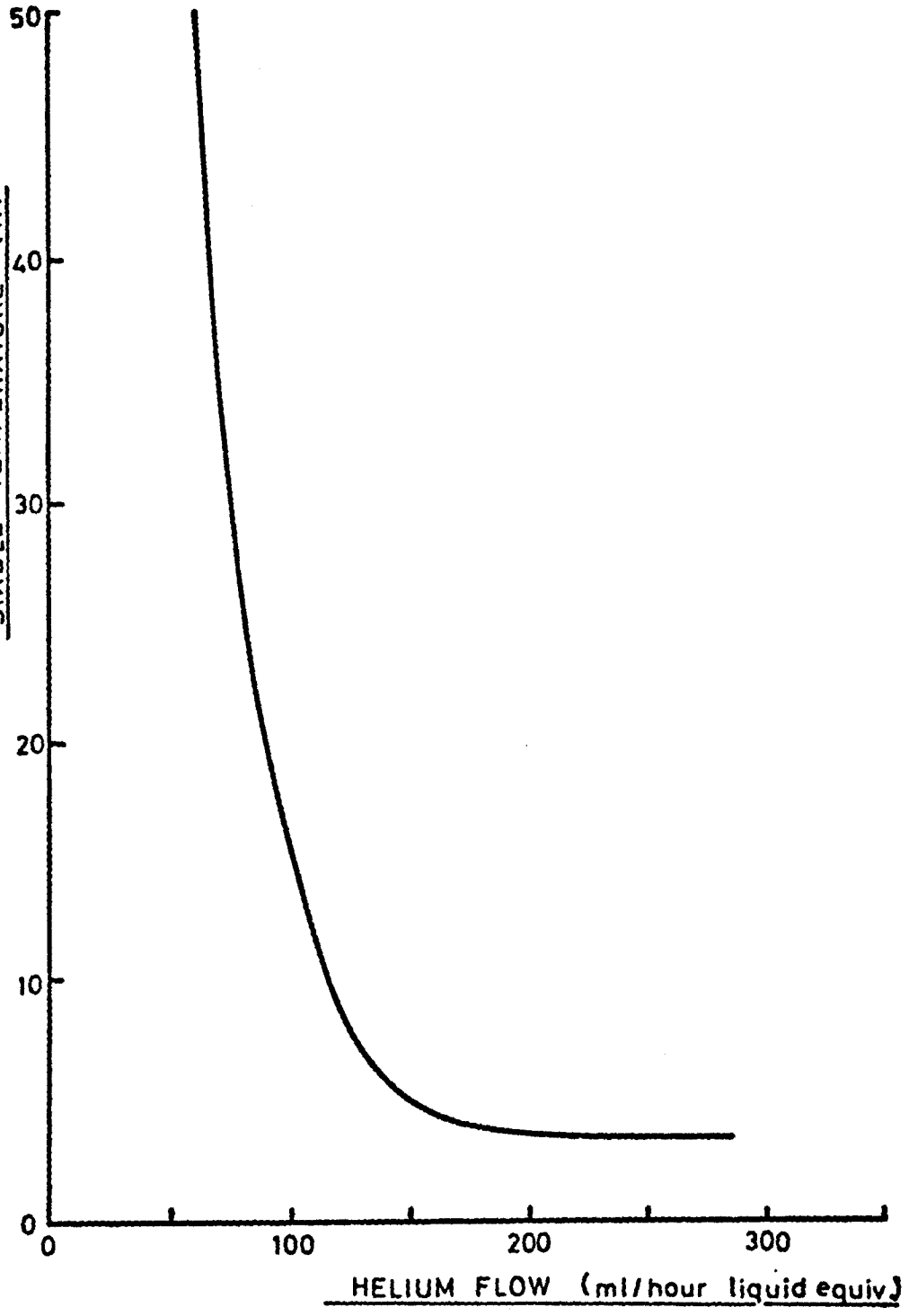


Fig.4.9: Helium consumption

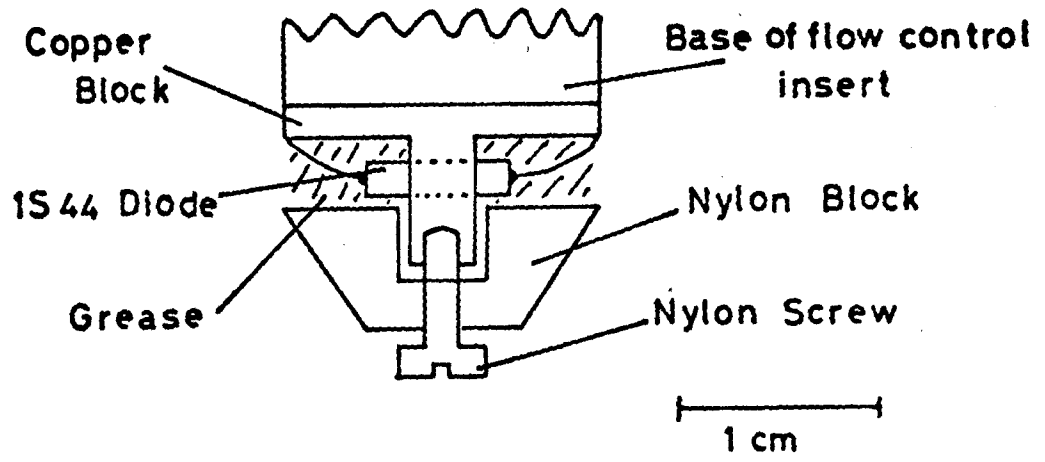


Fig.4.8: Temp. sensor mounting

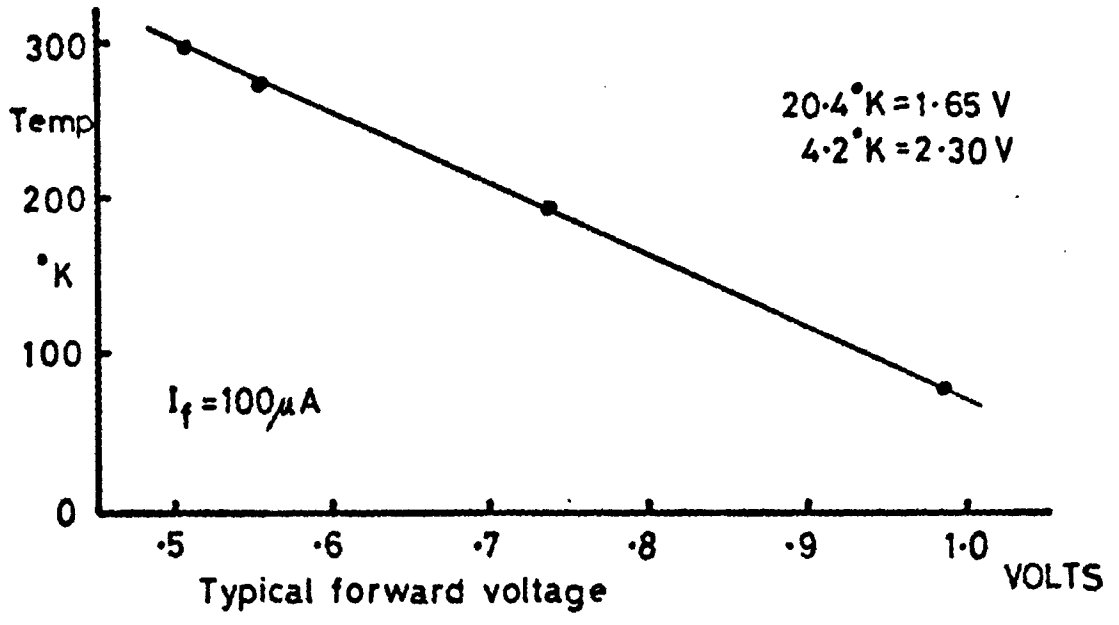


Fig.4.10: 1S44 Temp. characteristic

(gas flow about 0.6 ℓ/min) with no deliberate heat input into the experimental chamber. At higher temperatures the consumption is less. The temperature rise along the length (40 cm) of the experimental chamber is about 1 K.

In the temperature range 77 K to 4 K liquid helium is used as refrigerant and is stored in a simple, purpose built storage dewar of total height 34 cm, diameter 25 cm and helium storage capacity 5 ℓ. The direct boil-off-rate of the storage dewar is almost independent of the cryostat flow rate and is equivalent to 80 mℓ/hour of liquid.

The helium flow rate through the cryostat required to maintain temperatures between 50 K and 3.5 K is shown in Fig.4.9. At 4.2 K the flow through the cryostat is equivalent to 160 mℓ/hour liquid, making a total liquid refrigerant loss of 240 mℓ/hour. At these lowest temperatures the temperature gradient along the experimental chamber rises sharply and may reach ½ K/cm. At 25 K the flow through the cryostat is reduced to 80 mℓ/hour liquid equivalent making a total liquid refrigerant loss of 160 mℓ/hour.

4.4.4 Temperature Sensors

IS 44 Silicon Diodes are used as temperature sensors for all experiments. When forward-biassed with a current of ~100 μA, the D.C. forward voltage depends on temperature. Between 300°K and 70°K, the voltage is a linear function of temperature (Fig.4.10). Below 70°K, the characteristic is nonlinear, but calibration at 4.2°K and 20.4°K gives two additional reference points on the temperature scale, allowing an estimate of temperatures in that range. Small variations between diodes require that every diode must be individually calibrated before use.

In addition to the control sensor, a second diode is mounted on the lower end of the sample holder rod, so that a continuous check on the sample temperature is possible.

4.4.5 Temperature Control Unit

To maintain temperatures other than 4.2°K or 77°K, controlled heat is supplied to the copper experimental chamber via the 60 Ω bifilar manganin resistance wire heater. The control unit which does this is illustrated in Fig.4.11 (based mainly on a unit from our Electronics Workshop[30]).

The first stage compares the sensed temperature to a reference and an output proportional to the difference is fed to a variable gain amplifier. The next stage either integrates the signal or controls the response with an externally set time constant. The next stage ensures that an output only results if the sensed temperature is below the selected value, and the final stage is a power amplifier to drive the necessary current (up to 300 mA) into the 60 Ω load.

The circuit is perhaps over-complicated for the use it is put to, but was a simple adaptation of an existing unit.

In use, one presets the refrigerant flow to a suitable value for the temperature required (as given by Fig.4.9, say) sets the desired temperature and waits until stability is achieved (usually ~10 minutes, depending on the experimental cycle in use). The thermal mass of the copper experimental chamber effectively damps out small temperature oscillations due to bubbles of liquid etc.

4.4.6 Storage Dewars

As mentioned earlier, liquid nitrogen is stored in a simple 10 ℓ glass bucket dewar, into which the cryostat tail is inserted. The top of the dewar is loosely plugged with polystyrene, to reduce direct boil-off.

The helium storage dewar is illustrated in Fig.4.12, and the coupling on to the cryostat tail is shown in Fig.4.13. The whole system is designed to be helium gas tight, so that all the helium refrigerant used can be recovered and fed into the laboratory recovery system.

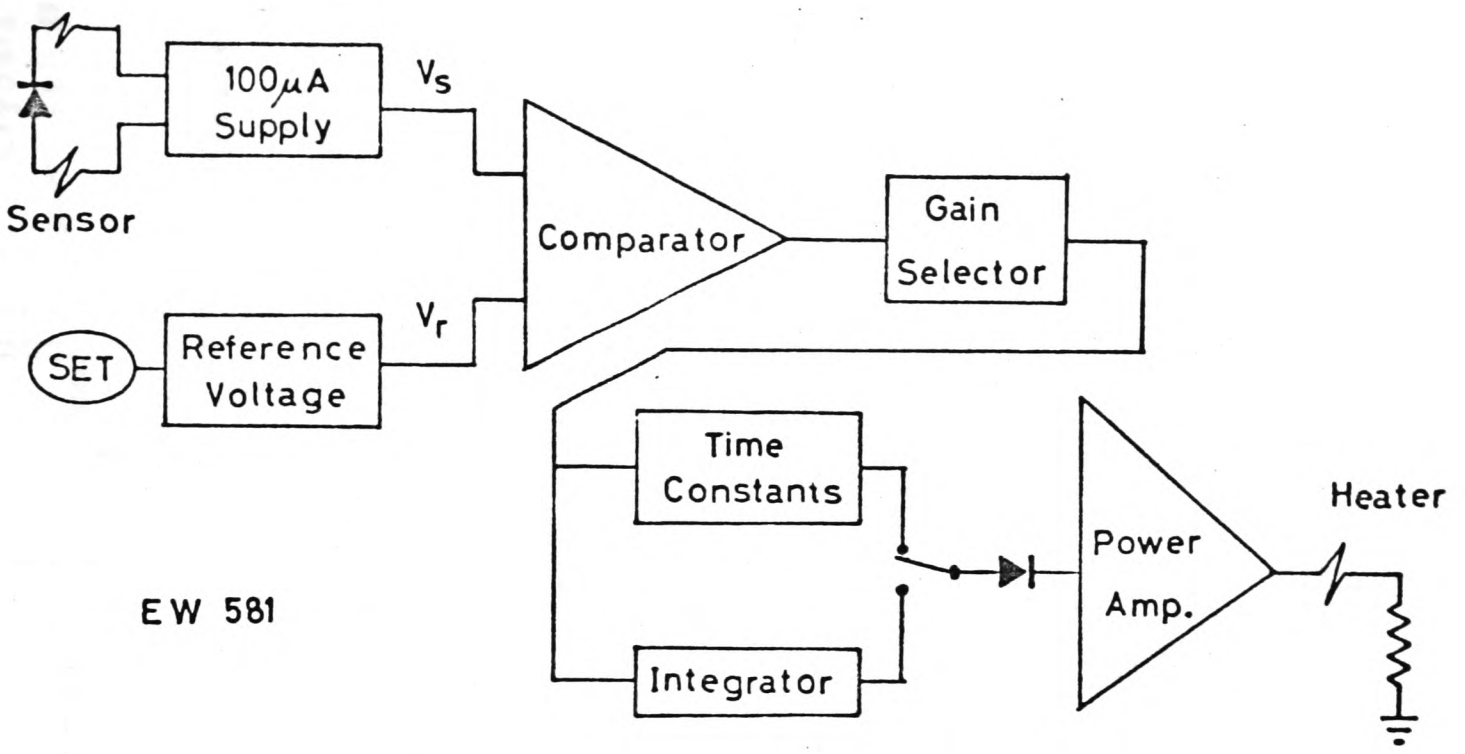


Fig.4.11: Temperature control unit

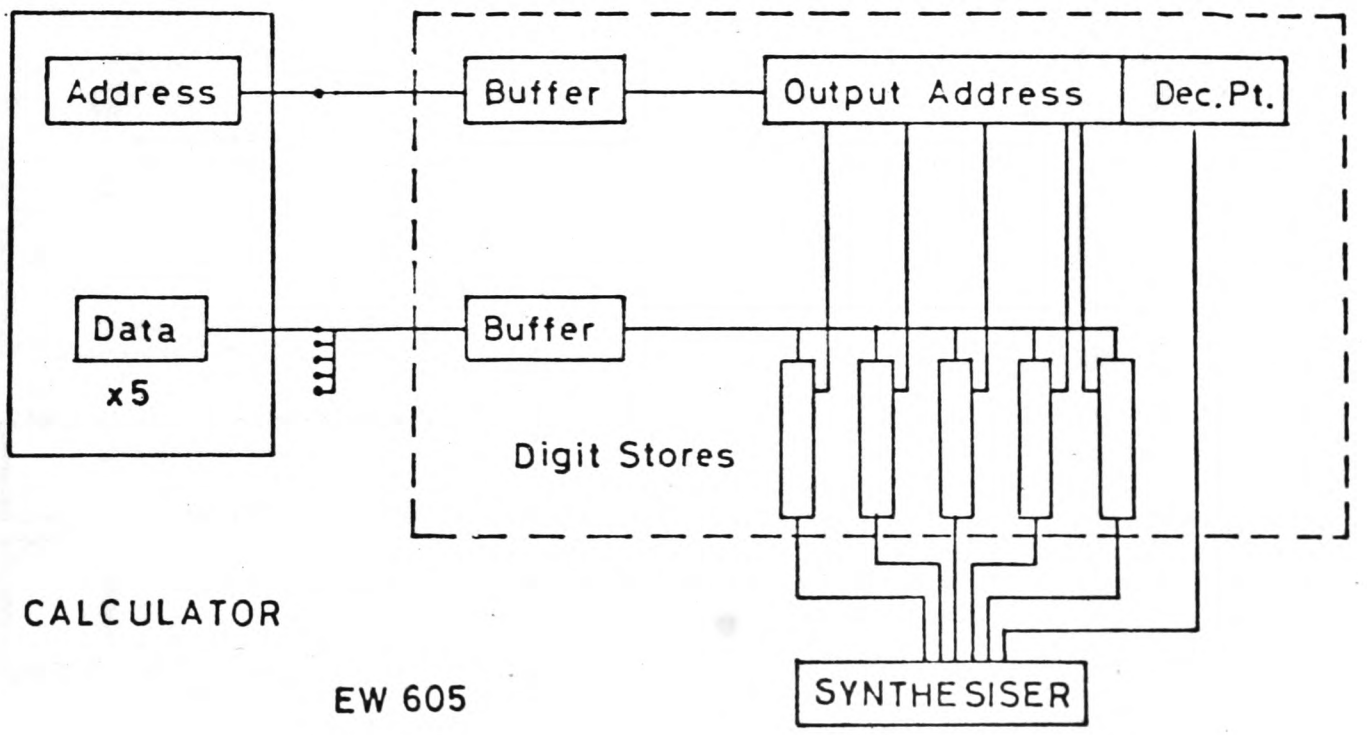


Fig.4.16: Calculator / Synthesiser interface

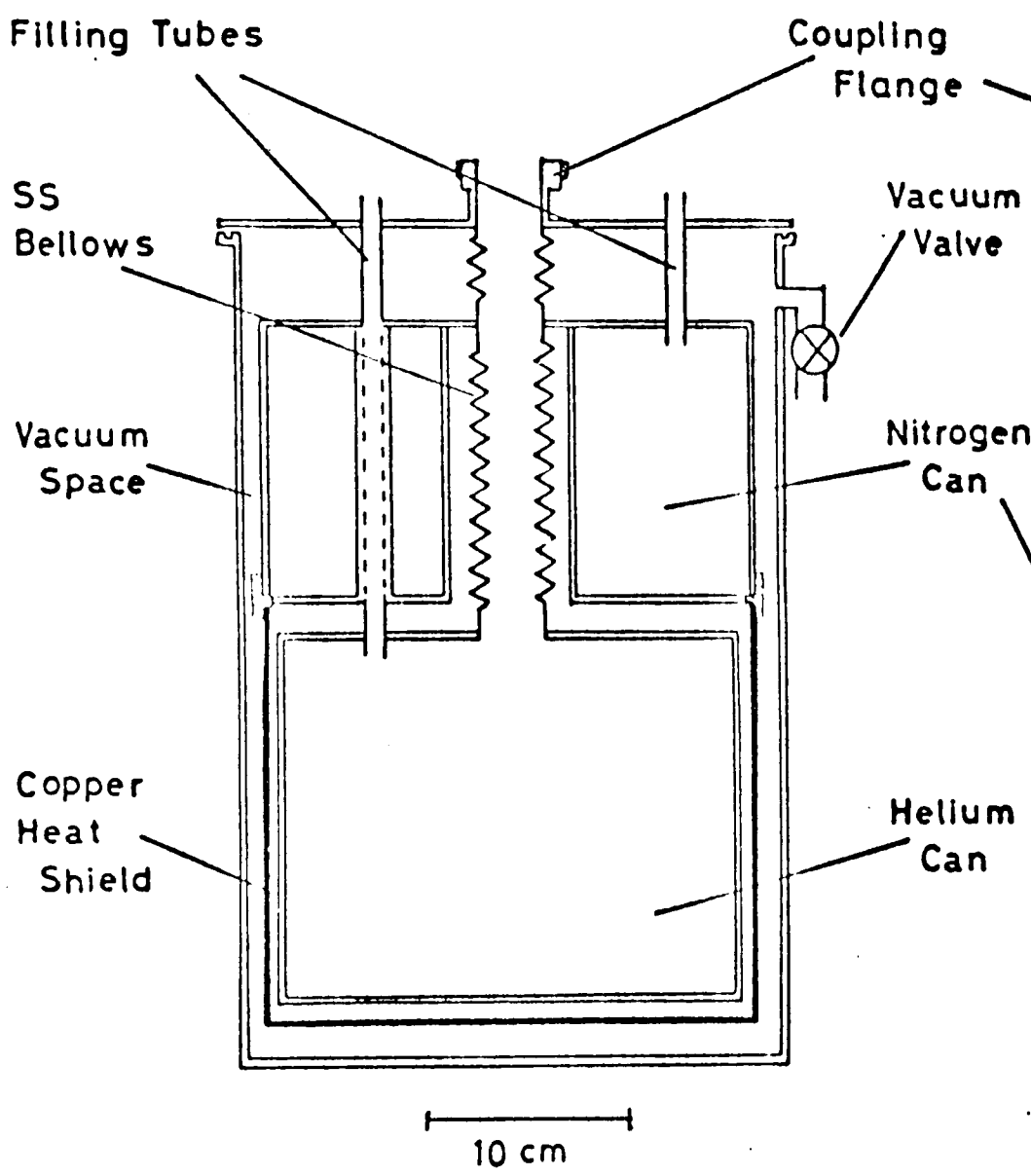


Fig.4.12 : Helium storage dewar

Design M.R. Wells

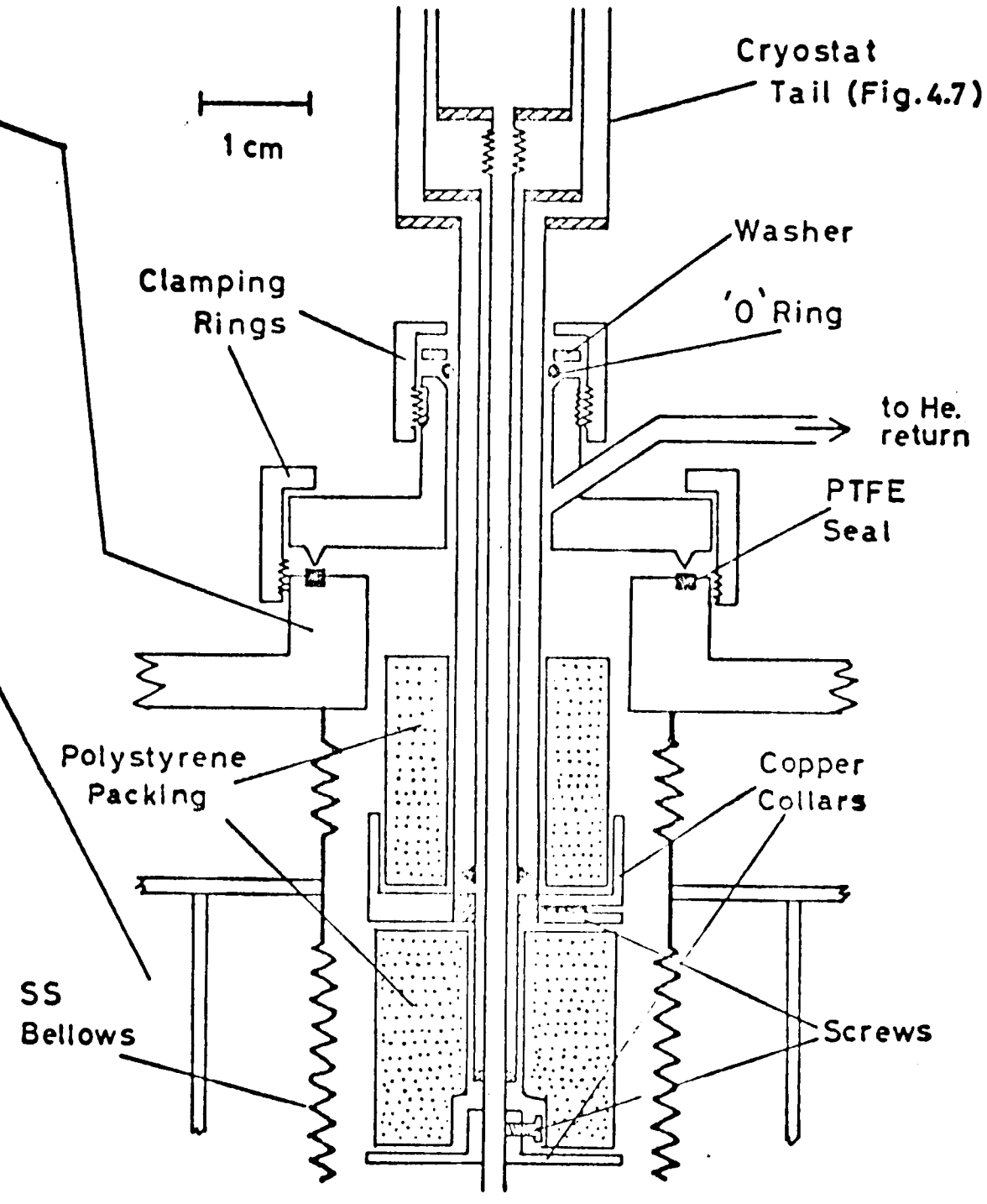


Fig.4.13 : Cryostat/Dewar Seal

4.4.7 Internal Fittings

Internal components - NMR tank circuit and NQR irradiation coil - are mounted on a perforated thin-wall german silver tube, which is attached to the lower fixed cross-plate of the sample transit mechanism.

The two coil formers are designed to be a sliding fit inside the inner copper can of the cryostat. The coaxial leads to the coils are attached to the perforated tube, and led up to sealed BNC sockets fitted above the cross-plate.

Helium exchange gas is piped into the space between the cryostat inner wall and the perforated support tube. Passing down through this space, gas passes through the perforations into the sample space, and hence up to the sample insertion hole, permitting the whole experimental volume to be flushed with helium.

4.5 SYSTEM CYCLE CONTROLLER

The control system for the spectrometer is based on the design of TAYLOR, BOOTH and ALLEN[31] and was developed and built in the Clarendon Laboratory Electronics Workshop by W.J. Siertsema (Ref. No. EW612).

The system works on the 'count down' principle, and consists of a central control module linked to a number of peripheral pulse generator units.

4.5.1 Central Control Module

This unit generates a 10 MHz clock signal which may, if desired, be locked to an external 5 MHz master clock via a phase lock loop. The 10 MHz signal is divided down in stages to give clock pulses at 100 ns, 1 µs, 10 µs, 100 µs, 1 ms, 10 ms, 100 ms and 1 s intervals, which are fed via bus-bars to the other units in the system, and are used to define all time intervals.

4.5.2 Operation

The central control module generates a delay of 1-999 seconds, followed

by a chain of commands to individual pulse generator units. This we shall call one cycle. When the command chain is complete, the controller returns to the delay mode, and a new cycle commences. The controller can be set up to generate 1-999 cycles, before stopping and issuing a pulse. This set of cycles shall be referred to as a sequence . The 'sequence complete' pulse may be used to reset other equipment and/or restart a new sequence in the controller. This sequence facility may be disabled, and the controller then free runs, generating cycles indefinitely.

The 'command chain' is preset by the operator, and consists of a set of instructions to individual pulse generator units, each of which is identified by an address in the range 1-9. We normally only employ four pulse generators, with addresses 1-4.

The simplest possible command chain would be 'operate the pulse units in the order 1-2-3-4 and then return to the delay mode'. The controller passes from unit to unit in numerical order.

Alternatively, the controller can be programmed to repeat a given address or set of addresses a given number of times (2-999). Examples of this would be:

1-2-(3-3-3-3)-4

or 1-([2-3]-[2-3]-[2-3])-4

One may also arrange to repeat two addresses (or sets of addresses) a number of times, such as: 1-(2-2-2)-(3-3-3)-4

or 1-([2-3]-[2-3])-([3-4]-[3-4])-5

If two addresses are to be repeated, then they will both be repeated the same number of times.

The operation of the control system is started or stopped by a simple manual push button, and always begins with the command chain.

4.5.3 Pulse Generator Modules

Up to 9 of these may be driven by one control module, but only 3 or 4 are necessary for the NQR spectrometer.

Each pulse generator is identified by its address (1-9). When the controller emits a command 'operate address 2' (say) then all pulse units with that address are initiated (normally only one unit, but two or more are allowed).

A pulse unit is set up to generate a delay followed by a pulse, each being timed from the central clocks, and set up in the form (1-99) × (chosen clock interval/100 ns - 1 s) + (analogue) 10 - 100 ns. This output is fed to a power amplifier stage which can generate up to 14 volts o/c or 8 volts into 50 Ω. The pulse can be positive or negative-going and the output can be switched over to give the complementary form.

If more than one pulse unit has the same address, then the address is not 'complete' until both units have completed their delay+pulse.

A block diagram of the controller, together with some sample outputs is given in Fig.4.14.

4.5.4 Use of the Controller

An indicator panel continuously displays the 'state' of the control system, counting up the seconds of the main delay and the number of cycles completed.

Address 1. This pulse unit is a specialised one, used to control the sample transit mechanism and irradiation system. It provides three fixed-amplitude outputs consisting of:

(a) A positive output, on for the full duration of address 1 (set up by (b)) which operates the solenoid air valve to move the sample up out of the magnet. The sample returns to the magnet when it is switched off. This output also drives a relay, which connects an R.F. input to the R.F. power amplifier.

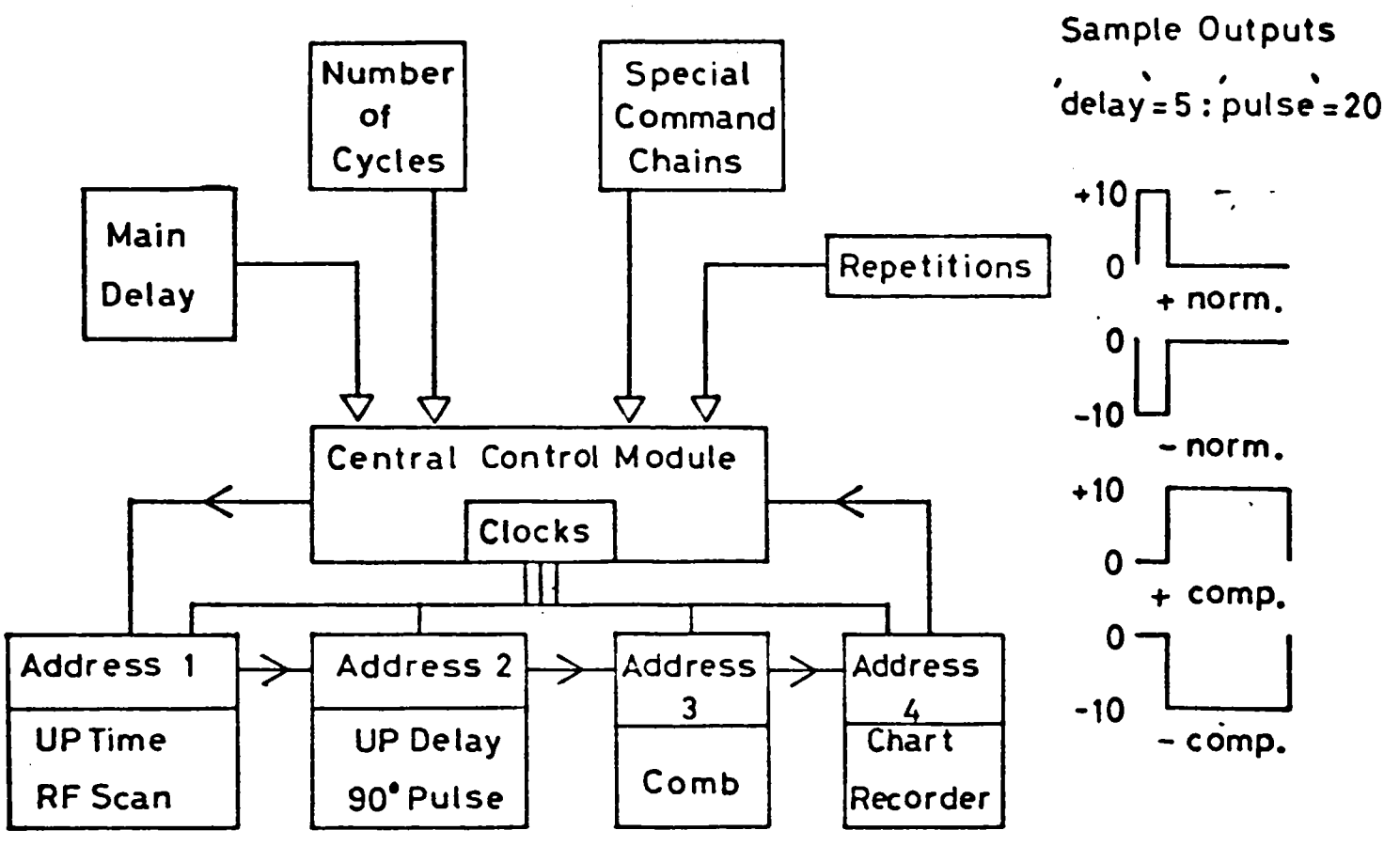


Fig.4.14: Control System-block diagram

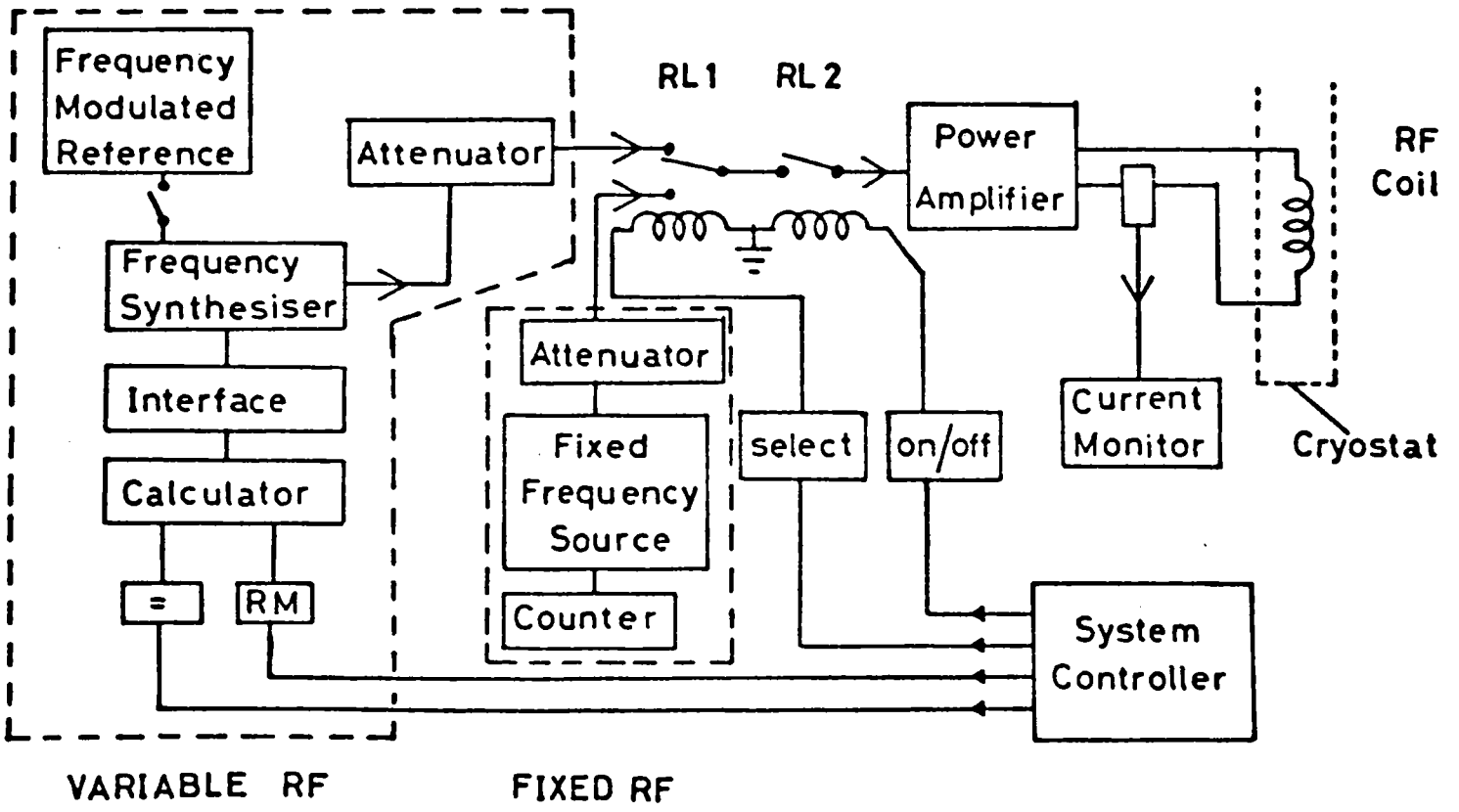


Fig.4.15: Quadrupole irradiation system

(b) A delay of 0.1 - 9.9 seconds, followed by a number (1 - 99) of pulses of 100 ms duration, separated by intervals of 0.1 - 9.9 seconds. This chain may be used to step the R.F. frequency control unit (synthesiser).

(c) A square wave of 0.5 or 1 second period, on from the end of the delay in (b) until the end of address 1. This is used to drive the relay which switches between two sources of R.F. energy, before being fed to the power amplifier. (For double irradiation purposes).

Address 2. A standard unit. This generates a 1.1 second delay (time for the sample to move back into the magnet) followed by a 0.5 second pulse. The leading edge of this pulse triggers the Minispec 90° pulse and opens the sample-and-hold gate which records the D.C. output voltage generated by the Minispec as a measure of the magnetisation of the sample (size of the free induction decay). The trailing edge of the pulse triggers a digital paper tape punch linked to the digital voltmeter inside the Minispec, and thus the magnetisation measurement is also captured in digital form. The trailing edge also closes the sample-and-hold gate.

Address 3. A two second delay (to allow the tape punch to operate) followed by a one second pulse. This drives the Minispec into its 'periodic' mode, so that it generates a chain of 90° pulses 1 ms apart. This 'comb' demagnetises the sample ready for a new cycle.

Address 4. A 100 ms delay, followed by a 100 ms pulse, which triggers the chart recorder control unit and causes the magnetisation measurement in the sample-and-hold gate to be recorded on the chart.

4.6 THE QUADRUPOLE IRRADIATION SYSTEM (Fig.4.15)

This consists of two main parts.

(a) Variable Frequency Source

An Advance model 161 desk calculator is interfaced to a Pacific Instruments Model 1028A programmable frequency synthesiser using an interface unit designed by our Electronics workshop (Ref. EW 605). The result is that the number displayed by the calculator always equals the output frequency (in kHz) of the synthesiser. This is fairly simple to achieve, since both units operate on B.C.D. code, and one has merely to capture and hold the logic voltages feeding the calculator display and connect the held voltages to the synthesiser control inputs (see Fig.4.16).

To change the frequency, an external pulse operates a reed relay connected in parallel with the '=' key. If we then enter the sequence '145 + 5 =' on the keyboard, the display will read '150'. When the '=' key is operated again, the display changes to '155', and so on. One may thus simply store the irradiation frequency information for an experimental run. A chain of pulses may alternatively be fed to the calculator, so that a scan of frequencies is fed to the sample during irradiation.

If another number is stored in the calculator memory, this can be recalled at any time by operation of the "RM' [Read Memory] key.

By storing the starting frequency of a run in the memory and suitably programming the system controller to carry out a sequence of a given number of cycles, one can thus scan the same spectrum repetitively, for signal averaging purposes, for example.

The frequency synthesiser normally generates output by counting an internal 1 MHz crystal oscillator, multiplying or dividing to produce the required output frequency. If an external 1 MHz source is used, the synthesiser will generate all frequencies as proportions of this reference.

Furthermore, if the reference is frequency modulated at a low frequency (20 Hz, say), the output will also be modulated, provided the modulation swings are not too large (< 1% say). In this way we can generate a synthesised frequency modulated R.F., and this is of great use in certain experiments. The external source was designed by Dr F.N.H. Robinson and built by the author.

(b) Fixed Frequency Source

This consists simply of an Airmec oscillator Type 304 A, with built-in attenuator. This source is only used for 'Double Irradiation' experiments when we desire to irradiate a sample simultaneously at two different frequencies, one of which is fixed and the other being the usual frequency scan.

The 'select' relay is then switched either once or twice per second between the two sources.

The ON/OFF relay is activated in parallel with the air solenoid drive, so that RF is only applied to the upper coil when the sample is in it. If this is not done, some RF can be picked up by the NMR spectrometer, through the tank circuit, causing noise.

4.6.1 R.F. Power Amplifier

A preset voltage input (from the synthesiser via the 50 Ω attenuator) must generate a fixed output current, in order to generate a fixed R.F. field in the upper coil. Since the impedance of this coil is nearly all reactive (L = 3.2 μH , R = 0.1 Ω) , the applied output voltage must increase with frequency, i.e. since

$$Z_L = \omega L$$

$$V_{out} = I_{out} Z = I_{out} \omega L \ .$$

Thus we require an amplifier with a frequency-independent mutual conductance, to generate a fixed output current for a fixed voltage input.

The circuit, due to EDMONDS[4], for an amplifier which does this fairly simply, is shown in Fig.4.17(a). T_1 and T_2 provide bias voltages to the push-pull double cascode amplifier $T_3 - T_6$.

The input is a 50 Ω/200 Ω commercial balanced matching transformer. The 11 Ω non-inductive resistors provide series feedback to fix the mutual conductance at $\sim \frac{1}{11}$ amps/volt.

The output balanced transformer matches the output to the irradiation coil.

Since the load is almost all inductance, the voltage required for a given output current rises almost linearly with frequency. For 1 amp output current, 100 volts is needed at 5 MHz, or 20 volts at 1 MHz.

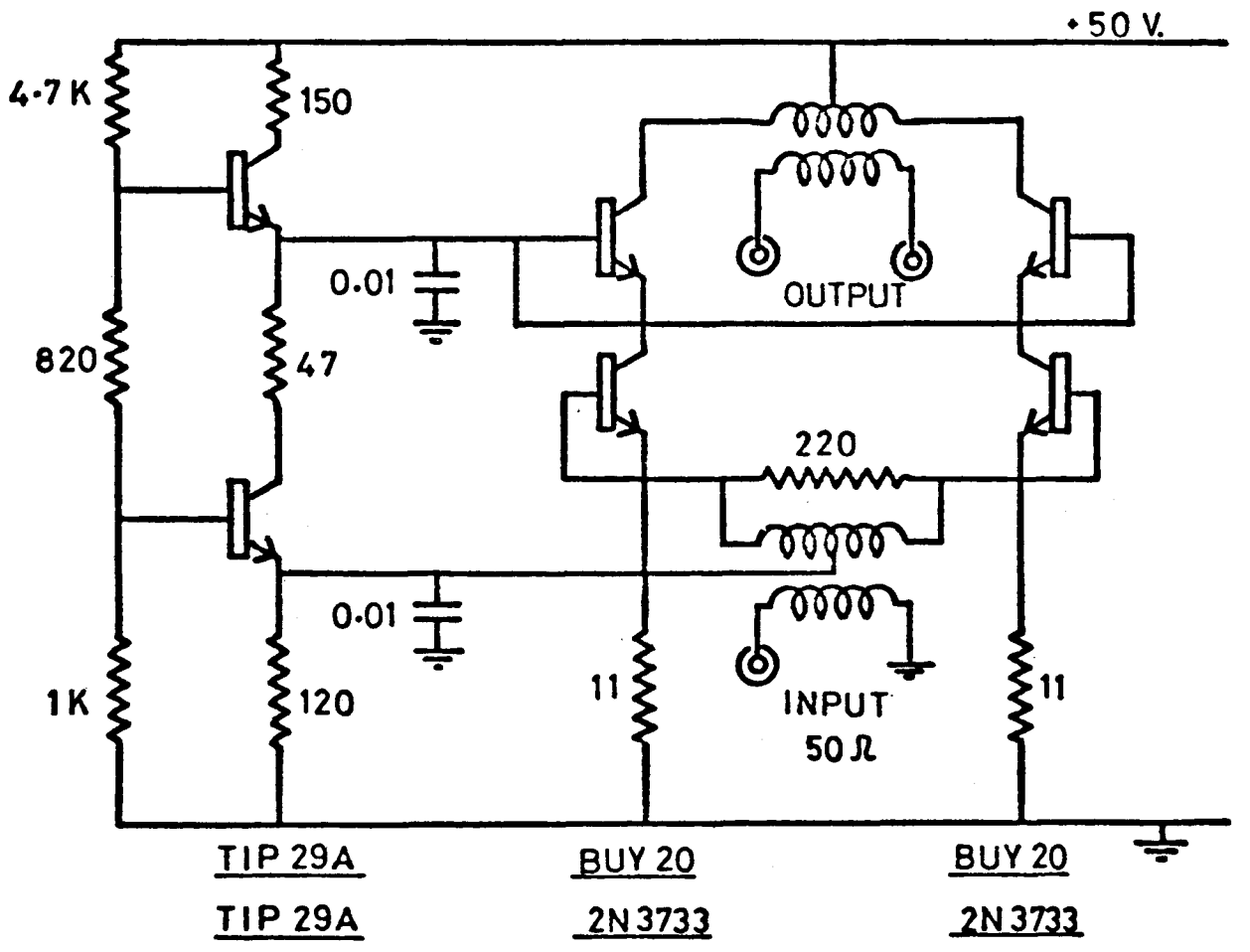
Thus since the power supply is rated at 50 volt, 1.2 amps, the maximum voltage to the output transformer is ~48 volts (peak) (before distortion sets in). A step up of 2:1 will thus produce ~100 volts peak, 0.6 amp maximum, corresponding to ~ 3.5 Gauss peak R.F. field up to 5 MHz.

Changing the output turns ratio to, say, 1:1, would give up to ~50 volts peak at ~1 amp peak, which would allow undistorted peak currents in the coil of up to 1 amp (6.5 Gauss) at up to 2.5 MHz.

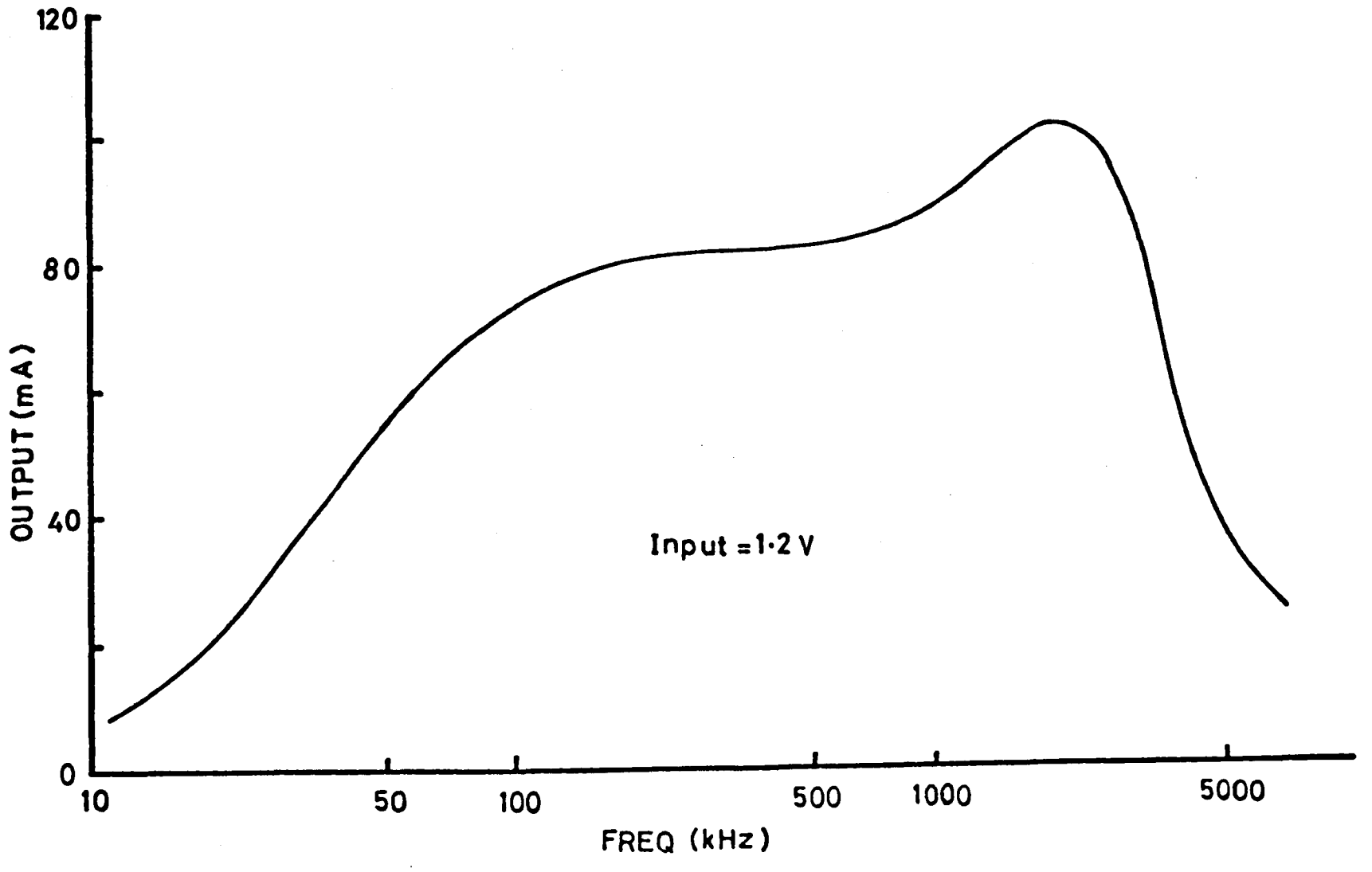
A current probe directly monitors the output at all times.

The output power is limited mostly by the efficiency of the amplifier heat sinks, and is ~60 watts (1.2 amps at 50 volts) on this model.

A plot of the output current for a fixed input voltage as a function of input frequency appears in Fig.4.17(b).



(a)



(b)

Fig. 4.17: RF Power Amplifier (from (4)) and performance

4.6.2 N Q R Irradiation Coil (Upper Coil) (Fig.4.18)

This consists of 40 turns of 1.5 mm copper tape on a 1 cm diameter nylon former, held in place with G.E. varnish. The coil has an inductance of ~3.2 μH.

Two lengths of miniature stainless steel 50 Ω coaxial cable are used to connect the amplifier output to the coil. Use of two cables reduces the effective capacitance in parallel with the coil, so that the self-resonant frequency of the coil/cable network is raised (to ~ 9.6 MHz in this case). The irradiation system (and hence the whole spectrometer) is limited to working below this frequency, since only small R.F. magnetic fields can be generated by the coil above its resonant frequency, due to the large (capacitive) impedance which is presented to the amplifier at such frequencies.

4.6.3 Field Calibration (Fig.4.19)

It is necessary to know the R.F. magnetic field which the apparatus generates. This was measured as follows:

First, a small solenoid (25 turns on $\frac{3}{8}$" former) was wound, and the field generated by it, per amp of D.C. current, measured, using a Bell Gaussmeter (Hall effect).

Secondly, a smaller test coil was wound (10 turns on a $\frac{1}{4}$" former). This was inserted inside the solenoid, and the output voltage generated by it measured for various R.F. currents and frequencies.

Since flux ϕ for a solenoid is given by

$$\phi = K N A I$$

N = number of turns, A = cross-section area, I = current, K = geometry constant ≈ 1.

$$\frac{d\phi}{dt} = KNA \frac{dI}{dt} .$$

Thus if $I = I_0 e^{i\omega t}$

$$\frac{d\phi}{dt} = KNA\, I_0\, e^{i\omega t} \cdot i\omega$$

$$= i\omega KNAI .$$

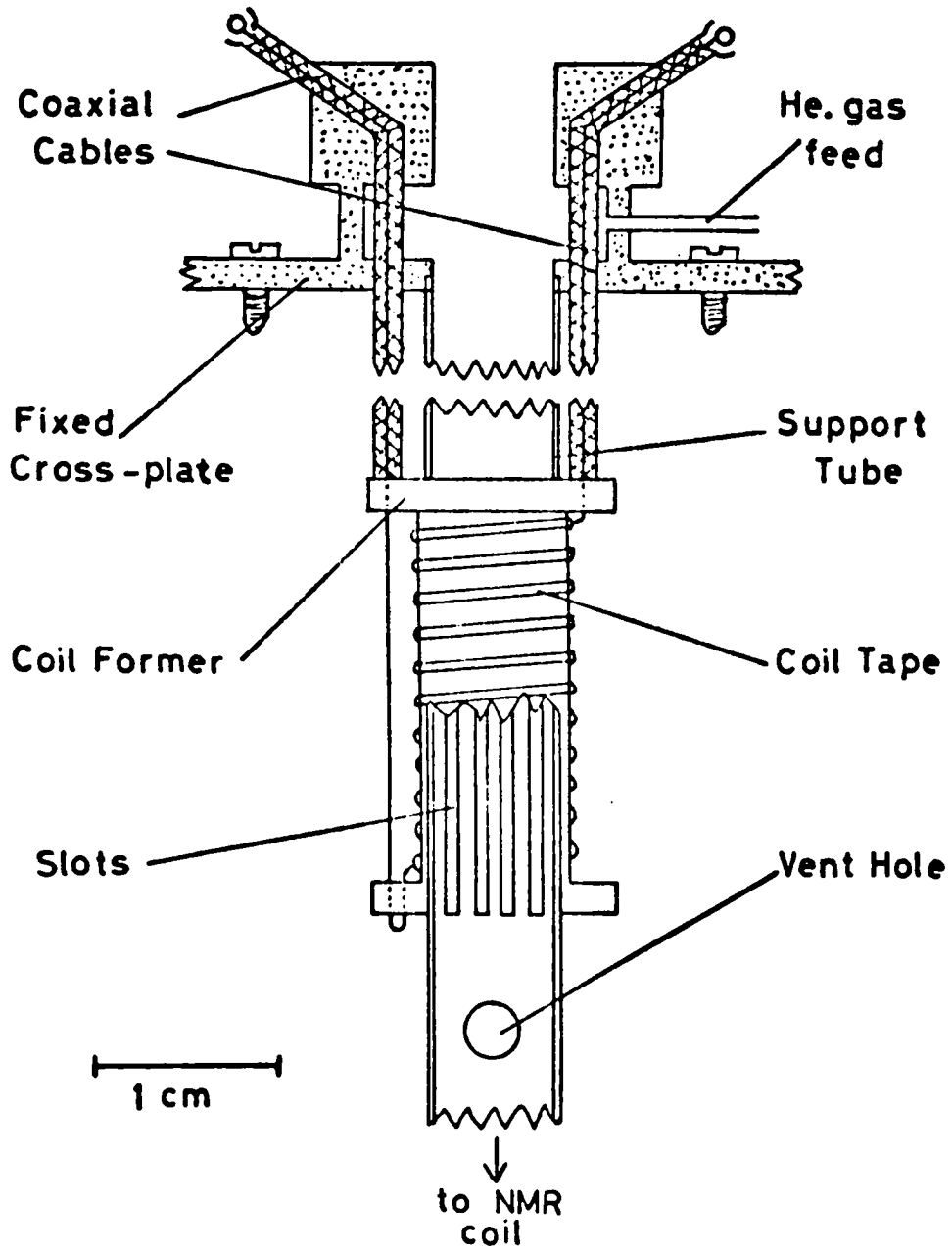


Fig.4.18: NQR Irradiation coil & Top plate fittings

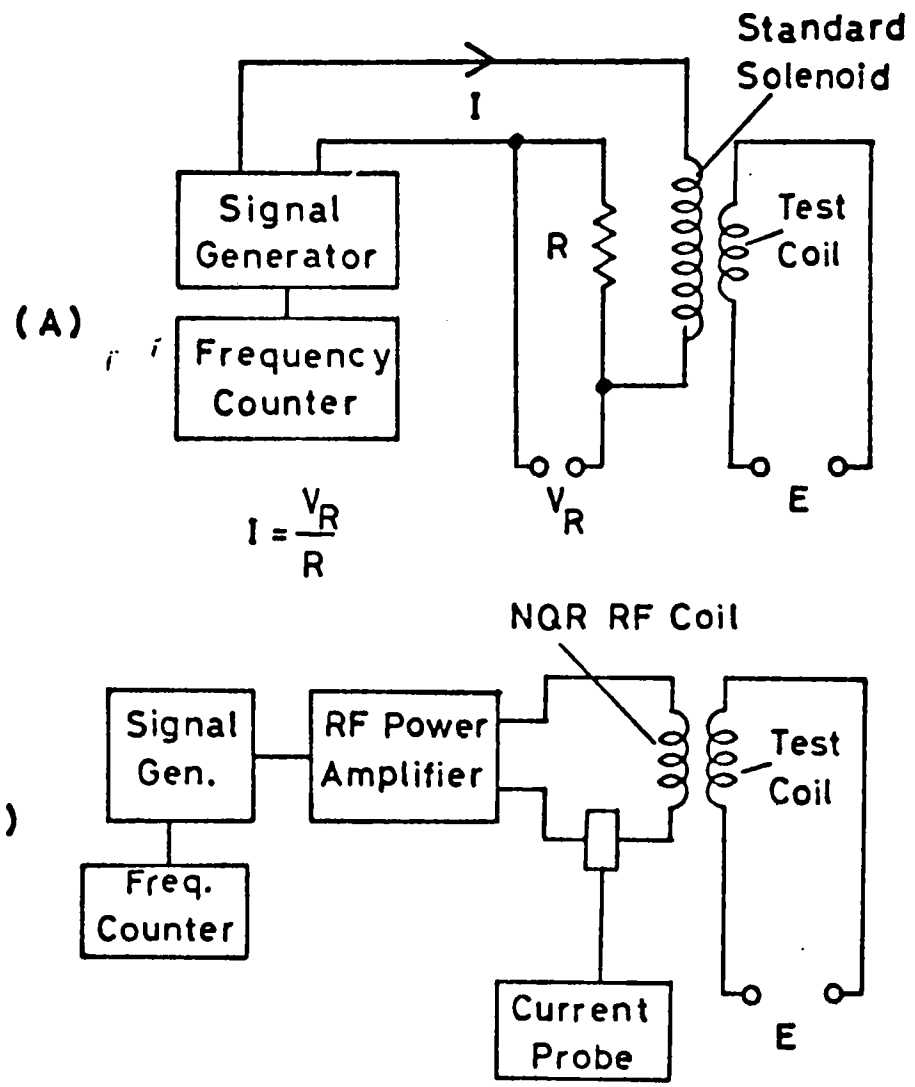


Fig.4.19: (A) Calibration of test coil
(B) Measurement of RF magnetic fields

and since E, the emf generated in a circuit subject to a magnetic flux ϕ is given by

$$E = -M \frac{d\phi}{dt} \qquad \text{where } M = \text{mutual inductance.}$$

$$E = -i\, M\omega KNAI$$

$$\propto \omega I \qquad\qquad MKNA = \text{constant};$$

Thus, knowing ω and I for the solenoid, a plot of E versus ωI should produce a straight line - the calibration line for the test coil.

Since we already know the Gauss/amp of the solenoid, we can convert I (amps) into field units. Thus we have an R.F. field probe which can be inserted into an uncalibrated solenoid. By measuring E on an oscilloscope and ω on a frequency meter we can obtain a direct measure of the R.F. magnetic field inside the solenoid, A simultaneous measurement of the current fed to the solenoid gives the ratio Gauss/amp for the unknown coil.

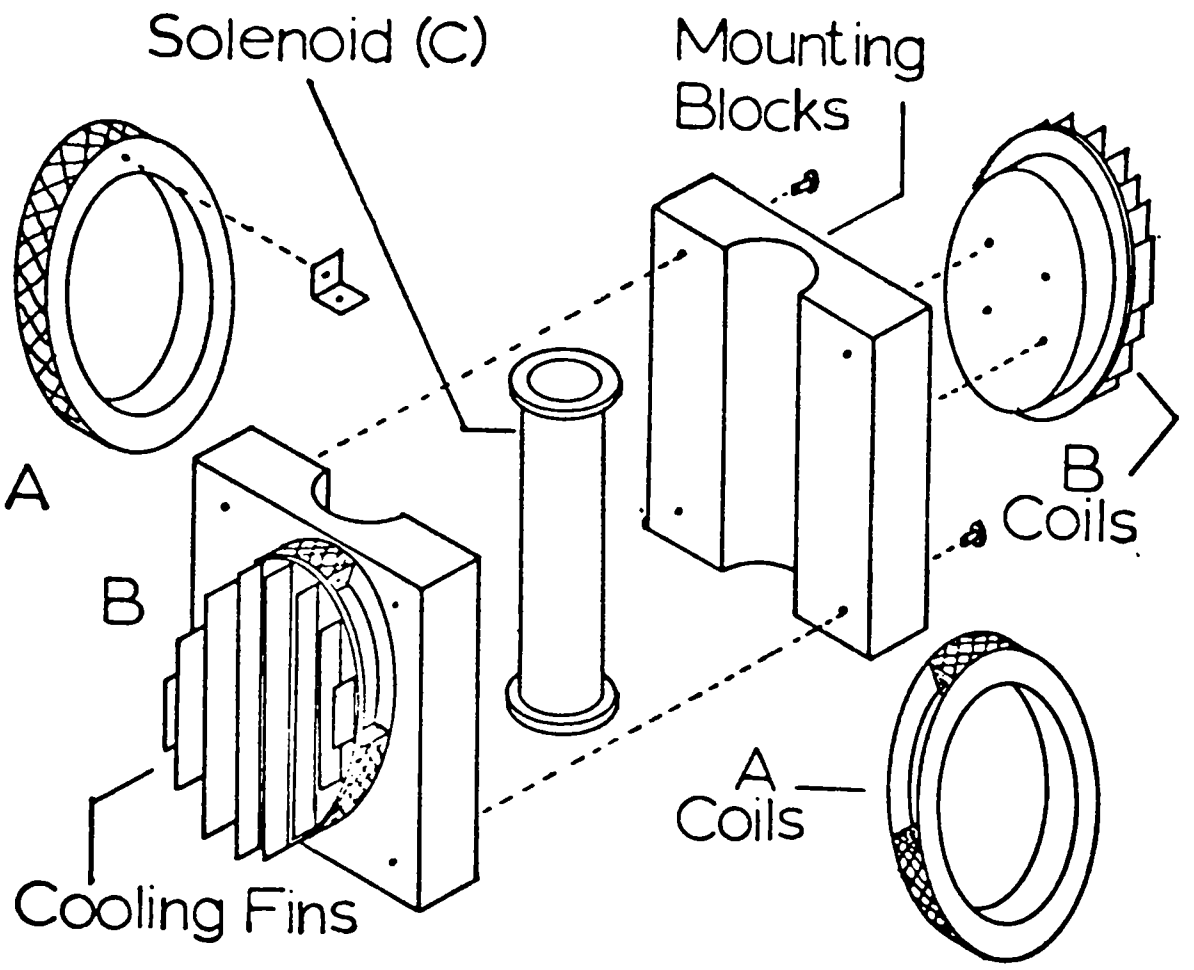
By making a series of measurements of this nature, for various currents and frequencies, the R.F. magnetic field generated by the upper coil was calibrated. The measured value was 6.48 Gauss/amp, constant for $0 < \text{freq.} < 6$ MHz.

4.7 UPPER STATIC MAGNETIC FIELD CONTROL UNIT

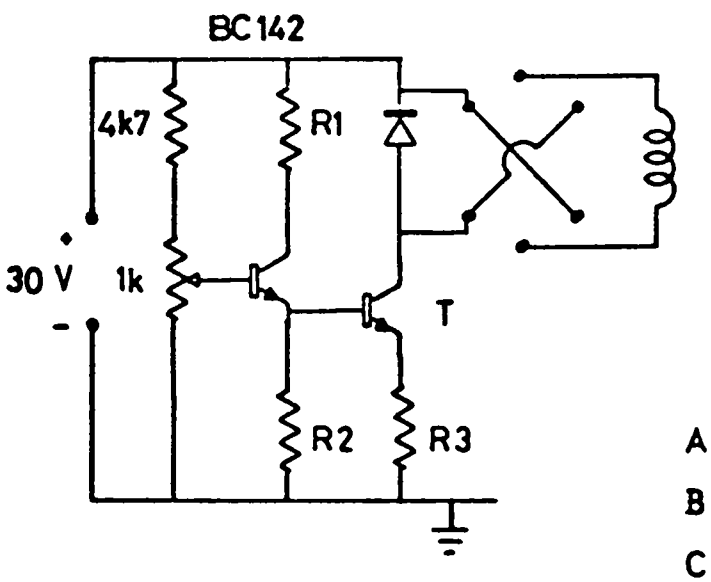
To correctly observe NQR powder spectra, a zero or known small, steady magnetic field must be provided in the region where irradiation at the quadrupole frequencies is to occur - in this case, around the upper irradiation coil of the apparatus -(the upper sample position).

As described in the section 'NMR Magnet', the stray field in the region of the upper coil is reduced to $\approx$ 8 Gauss by the large steel plate fitted above the magnet pole faces, about 4" below the upper sample position.

To reduce this field to zero, and to allow small fixed D.C. fields to be applied to the sample, the upper D.C. field control unit was constructed (Fig.4.20).



Construction



Power Supplies

	A,C	B
R1	1k5	470
R2	680	330
R3	6·8	2
T	TIP 29A	TIP 3055

Coils

A	1060	Turns	x 28 swg	in series	40 Ω
B	800	"	26 "	parallel	12 Ω
C	800	"	32 "	"	20 Ω

Fig. 4.20 : Field Control System

This consists of a solenoid, which can apply vertical fields (parallel to the R.F. irradiation field) up to 50 Gauss, and two sets of mutually perpendicular Helmholtz coils, which (a) cancel the stray 8 Gauss of the NMR magnet, with the option of generating a D.C. field parallel or anti-parallel to the NMR magnet field, of up to 35 Gauss, and (b) allow generation of D.C. fields of up to 100 Gauss perpendicular to the NMR magnet field.

The three sets of field coils are driven from constant-current sources; details of coil construction and power supplies are in the diagrams.

4.7.1 Field Calibration

Each field power unit is controlled by a ten-turn helipot, which allows precise, repeatable current settings to be obtained. Two Hall probe magnetometers, one with an axial field detector, one with a perpendicular field detector, were used to probe the magnetic field in the upper sample region, before insertion of the dewar and its associated equipment.

Since there are field gradients $\approx$ 1 Gauss/cm in the upper sample region, the probes had to be fixed firmly in place, and replaced in exactly the same position if removed. The reference position chosen was the geometric centre of the upper coil - where the centre of the sample would lie during experiments.

The three field control units were then adjusted together to produce a field $\leq$ 1 Gauss at that position. Since the three applied fields are mutually perpendicular, we know we then have a true zero field region at the centre of the sample. The sample itself is 2.5 cm long, so that, with a measured field gradient $\approx$ 1 Gauss/cm, the maximum field anywhere in the sample is $\sim$ 1.5 Gauss.

The 'zero field' condition corresponds to a near-zero current in both the vertical field solenoid and the 'perpendicular' Helmholtz coils.

Only the 'parallel' Helmholtz coils carry current - to offset the stray 8 Gauss of the main magnet.

We then proceeded to calibrate each field generator in turn, plotting 'Helipot Reading' against field as measured using the Hall probes, (keeping the other two field generators at the 'zero' setting while doing so).

As a further check on field settings, a series of small field NMR experiments were carried out. By setting up a field of ≈ 40 Gauss (say) and operating the whole spectrometer in the normal fashion, the direct absorption of R.F. by protons in this field can be observed. A measurement of the absorption centre frequency, with certain corrections as related elsewhere[32], gives a very accurate measure of magnetic field - knowing the proton gyromagnetic ratio of 4.258 kHz/Gauss. This check was done for both the vertical and perpendicular field units, since they are often used at high field settings. Any error in the zero of either of the other field units is negligible, since the fields add up via a square law, e.g.

	Setting	True Value
Field 1	40	40
Field 2	0	2
Field 3	0	3

Net 'true' field = $\sqrt{40^2 + 2^2 + 3^2}$ = 40.16 Gauss.

This is within the field tolerances set by the (unavoidable) field gradients of ± 1.5 Gauss over the sample region.

The 'zero' field set up in this way (i.e. 0 ± 1.5 Gauss over the sample in any 3 orthogonal directions) proved to be accurate, within error limits, at all subsequent 'zero field' checks made during day-to-day operation of the apparatus.

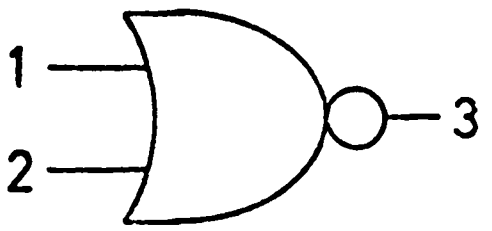
4.8 CHART RECORDER CONTROL UNIT

On receipt of a trigger pulse, the chart recorder control unit switches on two relays, and keeps them on for periods of approximately 3 and 4 seconds. The chart motor is held on for four seconds, while the output of the sample and hold gate (which holds the 90° pulse magnetisation measurement) is connected to the pen for the first three seconds. The resultant chart output consists of columns as shown in the sample of typical output (Fig.4.21).

The control unit makes use of a CD 4001 AE quadruple CMOS NOR gate chip, with associated components as shown in Fig.4.22.

An input edge turns the output on, and this stays on, after the input pulse is switched off, for a time determined by R and C, when it reverts to the stable off condition. The very high input impedance of a CMOS device allows large values of R to be used, and consequently small (non-electrolytic) capacitors can be used for C.

NOR GATE



NOR LOGIC

1	2	3
0	0	1
0	1	0
1	0	0
1	1	0

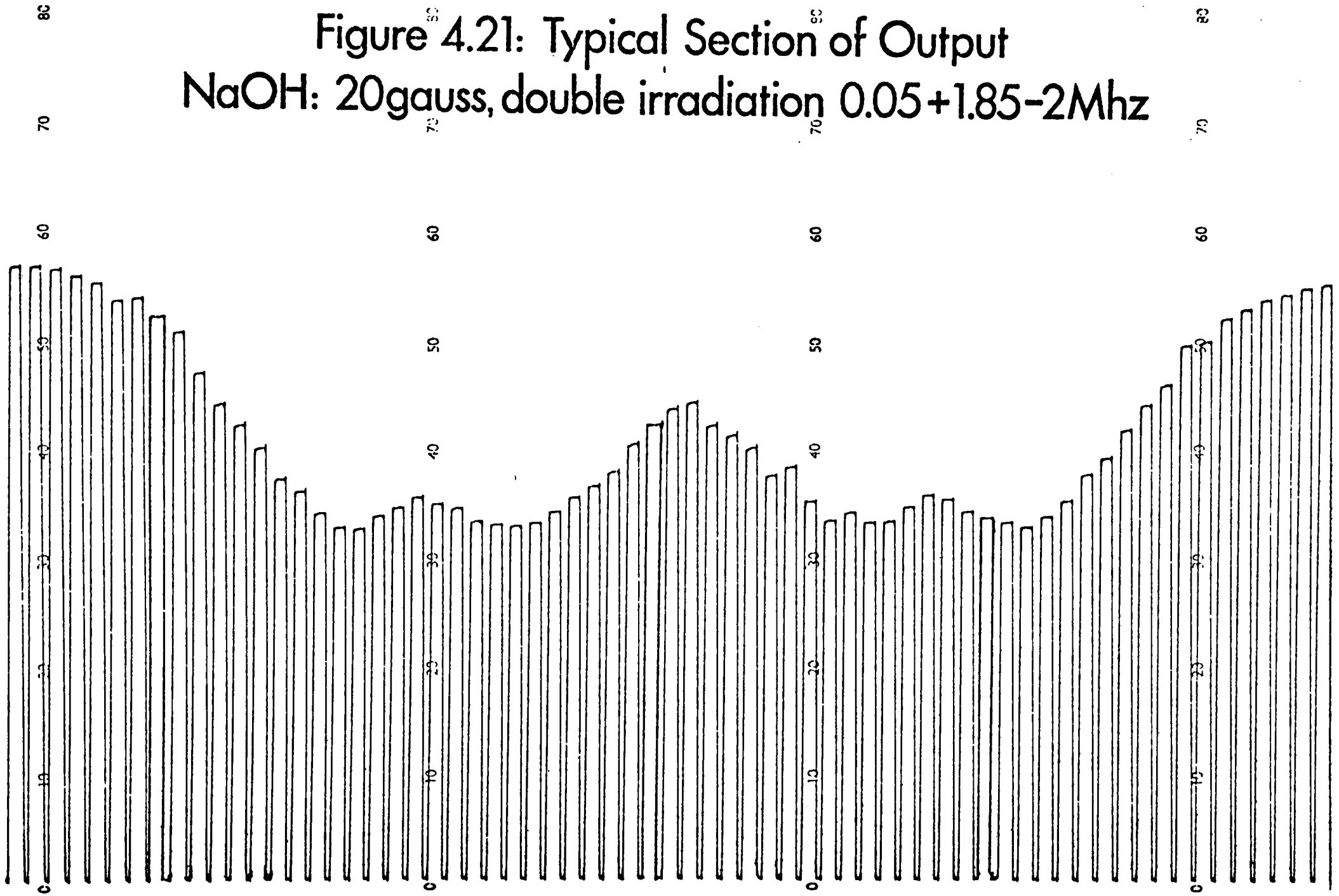
4.9 NMR MAGNET, MAIN FRAME, AND TRANSIT MECHANISM

4.9.1 NMR Magnet (Fig.4.23)

A 0.94 T permanent magnet was obtained from Swift-Levick & Co. Ltd (Sheffield) and modified in the factory by fitting a ½" thick by 12" wide mild steel plate across the magnet yoke above the pole faces. Access to the field is via a 3" dia. hole cut in the centre of the plate.

The plate reduces the stray field above it to ≈ 8 Gauss, which can

Figure 4.21: Typical Section of Output
NaOH: 20gauss, double irradiation 0.05+1.85-2Mhz



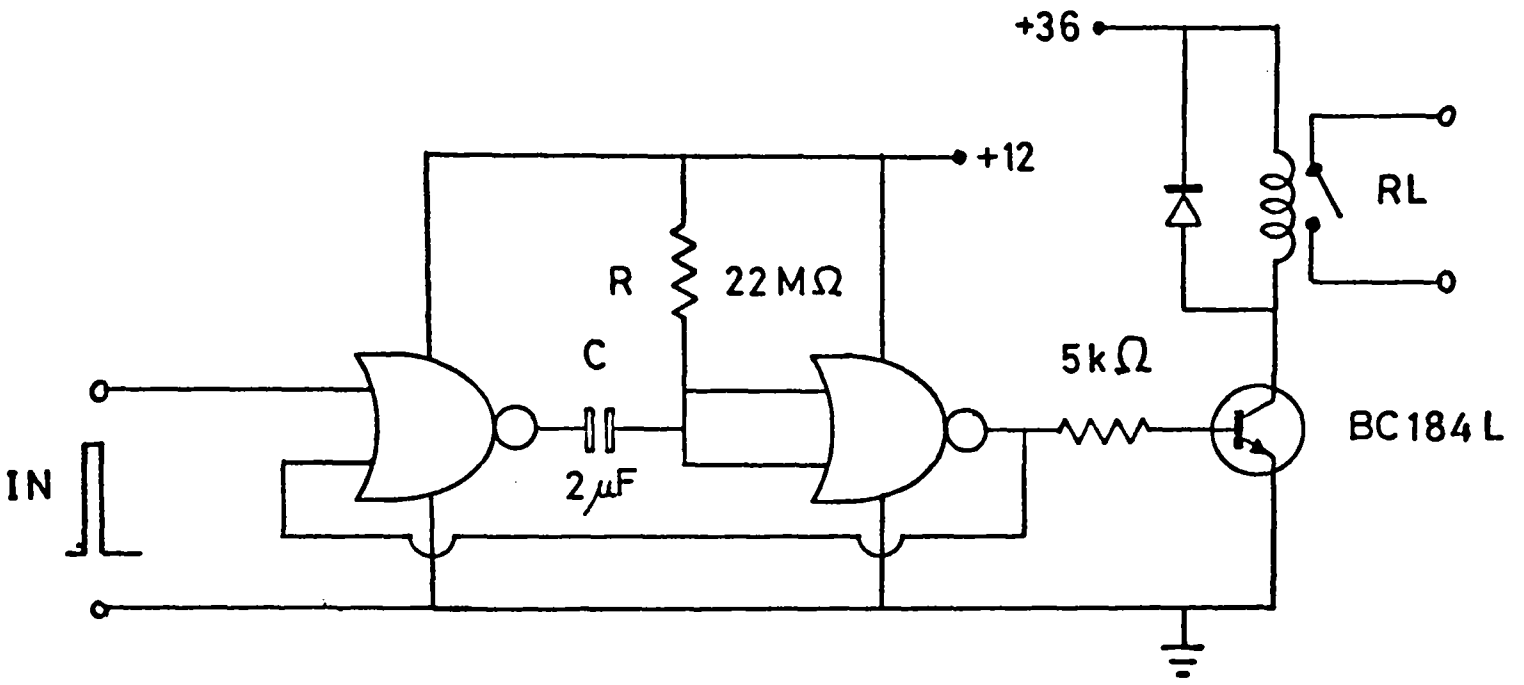


Fig.4.22: Chart recorder control unit
(one channel only shown)

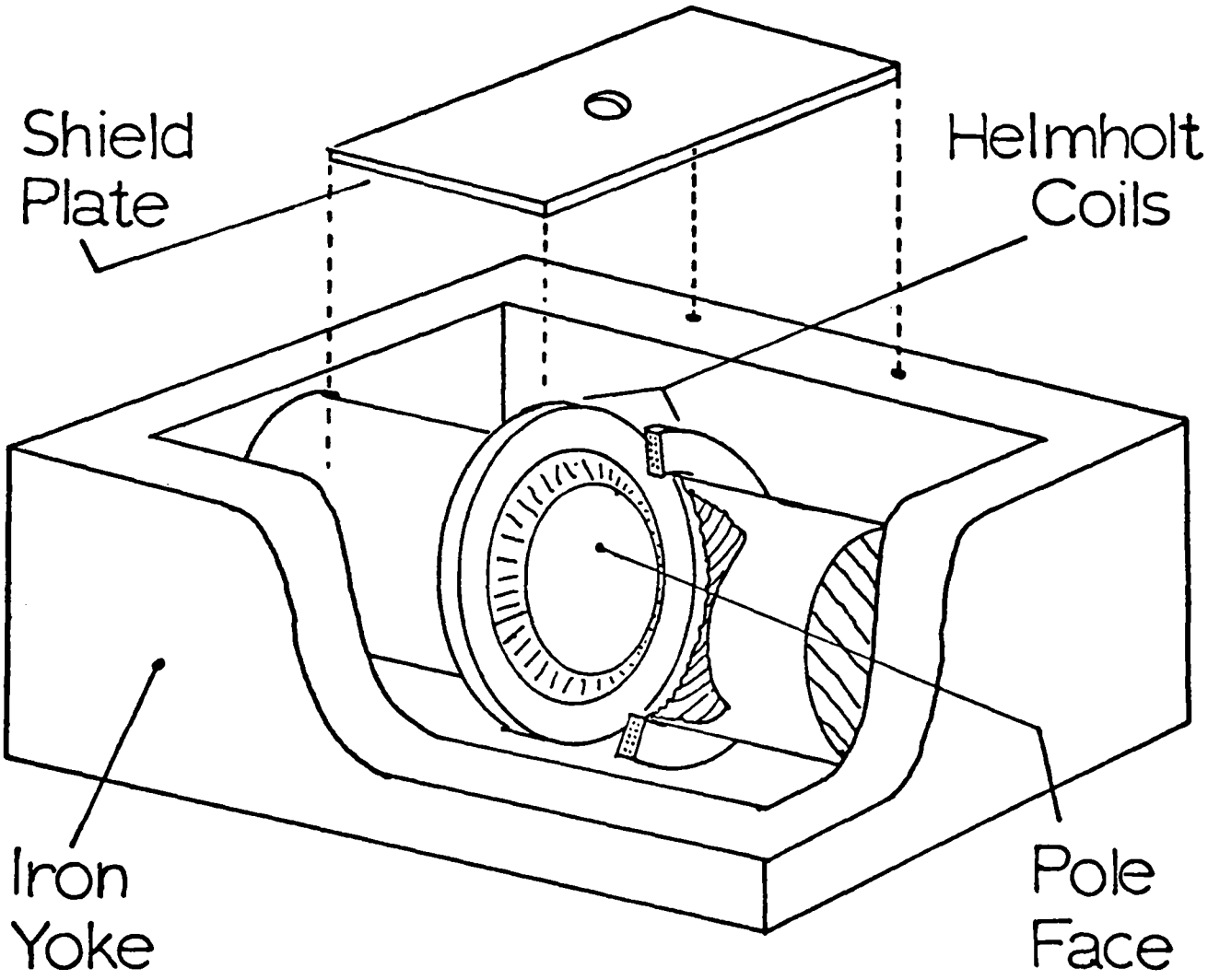


Fig.4.23 : 0.93 T Permanent Magnet

be easily cancelled by the upper field control coils. The stray field without the shield plate is ≈ 200 Gauss.

Some field homogeneity is lost by fitting this plate, but this is not important, since we only measure free induction decays ≈ T_2 ≤ 15 μs ($\Delta H \sim 2$ Gauss). Homogeneity remains relatively high, however, since up to 30 'wiggles' can be observed in the signal from a sample of rubber at room temperature.

Field Control. In order to tune the magnet to exactly 0.930 T (39.6 MHz for protons), some field variation is required. Coarse control is obtained by means of mild steel bars fitted across the magnet yoke below the pole pieces. Fine control is obtained via a pair of 12" diameter Helmholtz coils fitted around the magnet pole faces. These allow compensation for temperature effects on the magnet, which cause the field to decrease in summer and increase in winter.

To tune the field, the Minispec is set up for phase sensitive detection, and a sample of rubber inserted, at room temperature, into the spectrometer. The current in the Helmholtz coils is then varied (using a 10-turn helipot) until no wiggles are visible, and the free induction decay is maximised in amplitude.

When running normally, the Minispec is used in its 'diode detector' mode, and signals are almost independent of the temperature - caused shifts in field value, so that a weekly check on tuning is adequate to maintain optimum performance.

4.9.2 Apparatus Main Frame

The main frame of the apparatus is constructed entirely of ¼" thick 2" wide dural angle and channel, consisting of three main parts, viz:

(1) A stressed, welded table to support the NMR magnet, which weighs ~ 1500 kg, at a height of 33" above the ground.

(2) A vertical H frame, bolted to (1), which supports the dewar, sample transit mechanism, gas flow control valves and in addition supports some of the electronic equipment.

(3) A movable platform, which fits beneath the magnet and carries the storage dewar of liquid refrigerant. The platform slides on vertical rails and is driven by a hand operated hydraulic jack.

Assembly Notes

4" × 2" softwood beams were inserted between the table support beams and the magnet before the latter was lowered into place, in order to evenly distribute the load, and to allow the fitting of a wooden box which encloses the magnet completely on all four sides and above. The wooden enclosure keeps stray steel tools etc. from the magnet poles and allows the experimenter to climb on top of the magnet, for access to the upper parts of the apparatus. In addition, the magnet is partly shielded from draughts, etc., so that temperature stability of the field is aided.

The main apparatus dewar and attached sample transit mechanism is securely fixed to the vertical H frame by means of two stand-off fixing blocks, and is accurately located by the hole bored in the upper static field control unit. The position of the dewar is slightly adjustable by means of slots and spacing plates in the two mounting blocks.

4.9.3 Sample Transit Mechanism - Operation (see Fig.4.24)

The air solenoid valve is equivalent to a two pole change-over switch for compressed air. When 'off', air is directed to the top of the cylinders, the lower end being vented to atmosphere. The pistons are thus pushed downwards until the crossbar reaches the lower end stops. When switched 'on', the connections are reversed, and the pistons are driven up to the top end stops.

The Buffer amplifier is used, instead of a simple relay, to avoid switching the inductive load of the solenoid on and off rapidly, since this

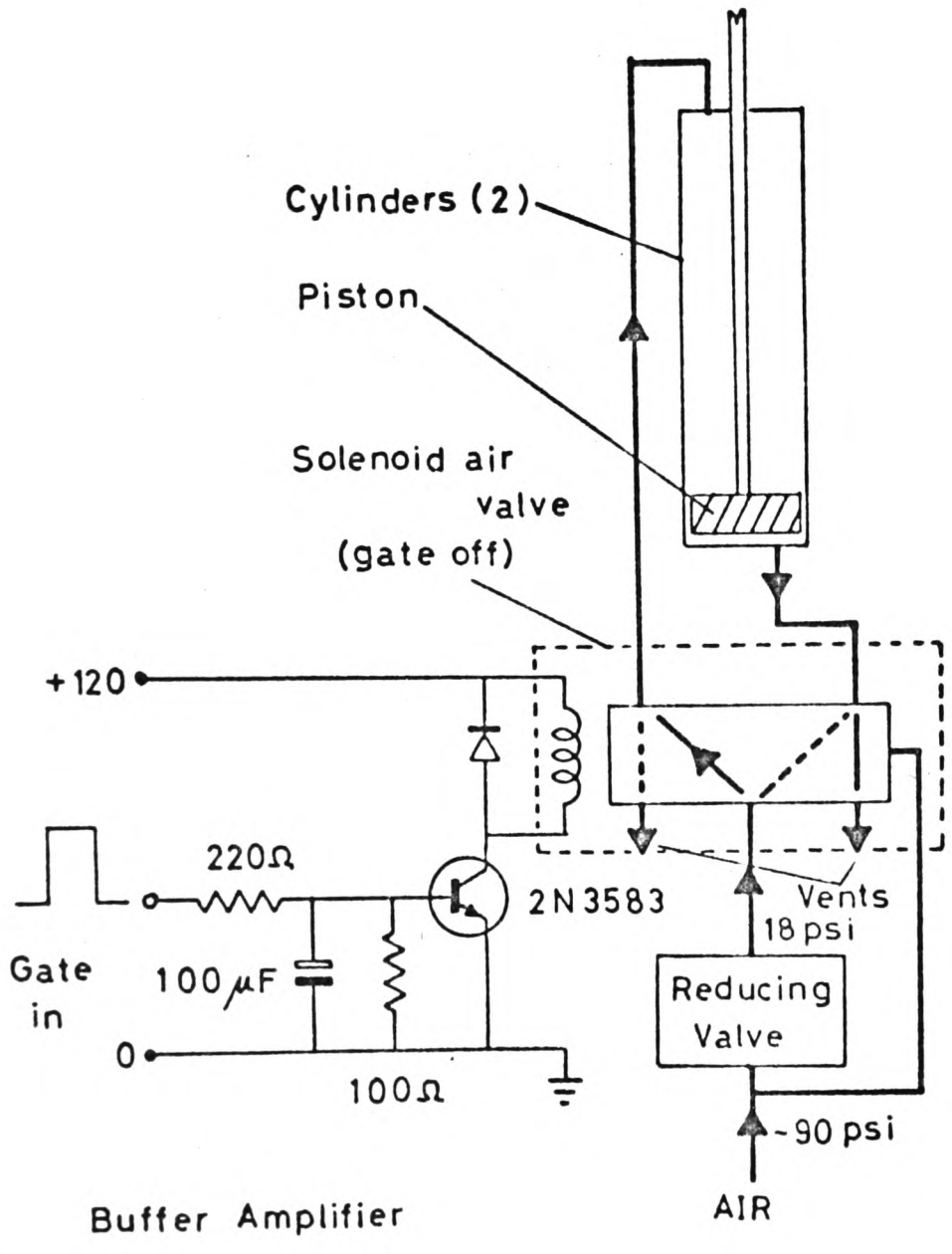


Fig. 4.24: Compressed air control system

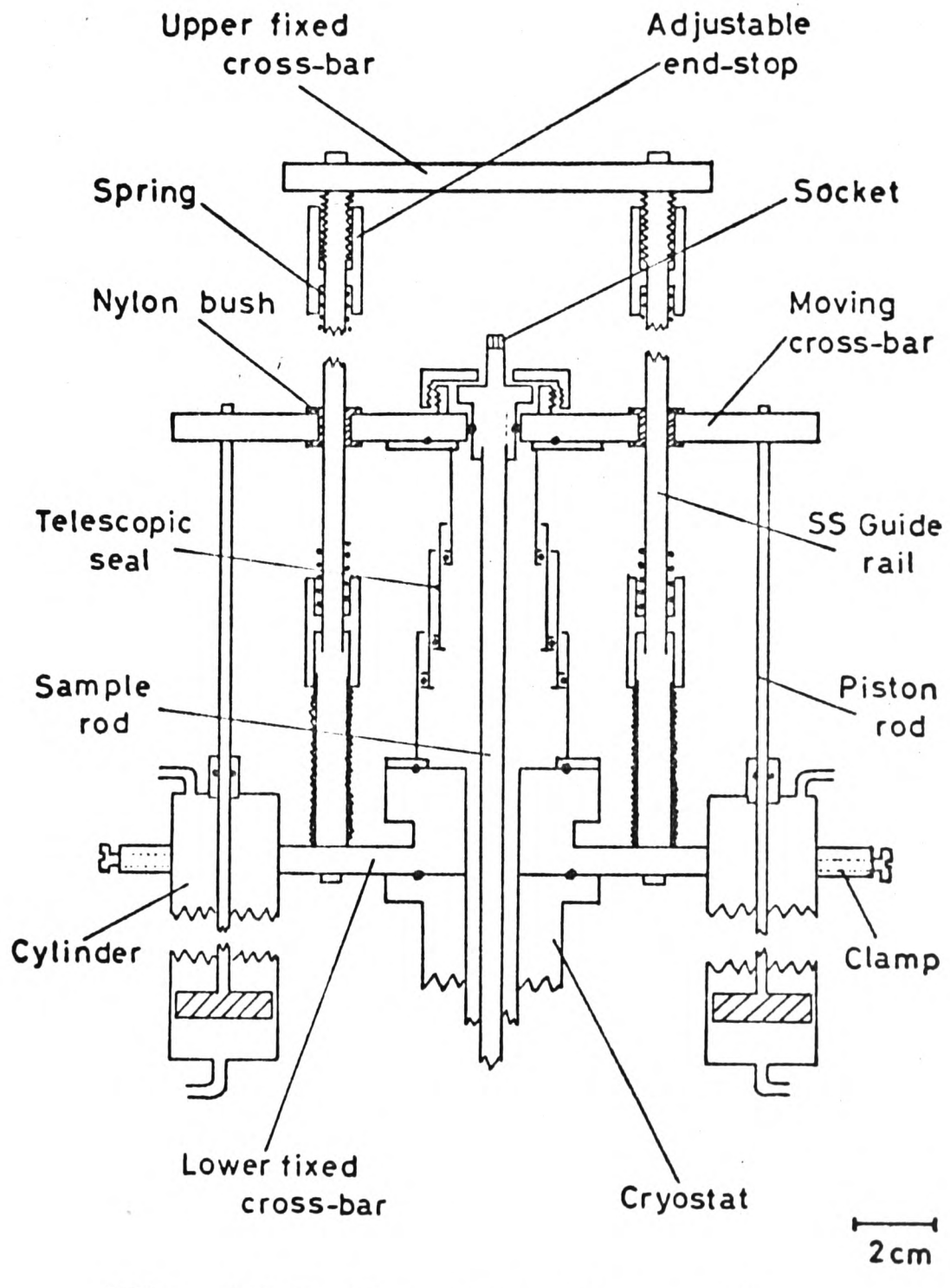


Fig. 4.25: Sample transit mechanism

causes undesirable high-voltage transients. The RC network on the input of the high-voltage transistor 2N 3583 ensures minimum switch on and off times $\sim \frac{1}{2}$ RC or ~5 ms, which are negligible, compared to the 1 sec → 60 sec usually used for the 'up' time.

Mechanical Construction (Fig.4.25)

The moving part of the apparatus is carried on two stainless steel guide rails, which have adjustable stops at both ends, and include springs to reduce the shock when the end stop is reached.

The two air cylinders are attached to the guide rails and to the dewar system via a fixed cross-bar and clamps. A second, moving, cross-bar is attached to the two piston rods and to the sample rod. The two rails pass through nylon bushes in the moving cross-bar, thus locating it.

The moving and fixed cross-bars are joined by a brass expanding telescopic tube which maintains a seal between the outside air and the experimental volume, which is filled with an exchange gas (helium, usually).

Sample Rod

This consists of a thin-walled stainless steel tube, fitted with brass plugs at either end. The lower end is hollowed-out and contains a silicon diode temperature sensor, held in place by araldite. The P T F E sample holder screws on to this plug, and also acts as the lower lateral location for the sample rod, since it is a close sliding fit inside the apparatus.

The upper end of the sample rod locates in the moving cross-bar, and contains a 4-pin socket by which the diode sensor is connected to its power supply and a digital volt-meter.

4.10 PERFORMANCE DATA : N Q R SPECTROMETER MARK II

Temperature Range:	4.2°K → 350°K
Quadrupole Irradiation: frequency	1 Hz - 8 MHz
Applied RF field	0 to 5 Gauss pp
Quadrupole D.C. Field:	
Parallel to RF field	0 to 40 Gauss
Perpendicular	0 to 90 Gauss
Total Cycle Time:	0 to 1000 seconds
Up (irradiation) Time:	0 to 1000 seconds
Transit Time Variation:	0.3 to 0.6 seconds
Maximum Run Time:	limited only by refrigerant supply
	N_2 - infinite
	He - 48 hours

Refrigerant Consumption:		Gas	Liquid
Not including direct storage dewar boil-off	N_2 at 217°K	300 cc/min	30 mℓ/hour
	N_2 at 77°K	1200 cc/min	120 mℓ/hour
including storage dewar	He at 20°K		180 mℓ/hour
	He at 4.2°K		250 mℓ/hour

Sample Volume:	1.5 cm^3
Transit Distance:	30 cm
Transit Time: (Typical)	0.5 sec

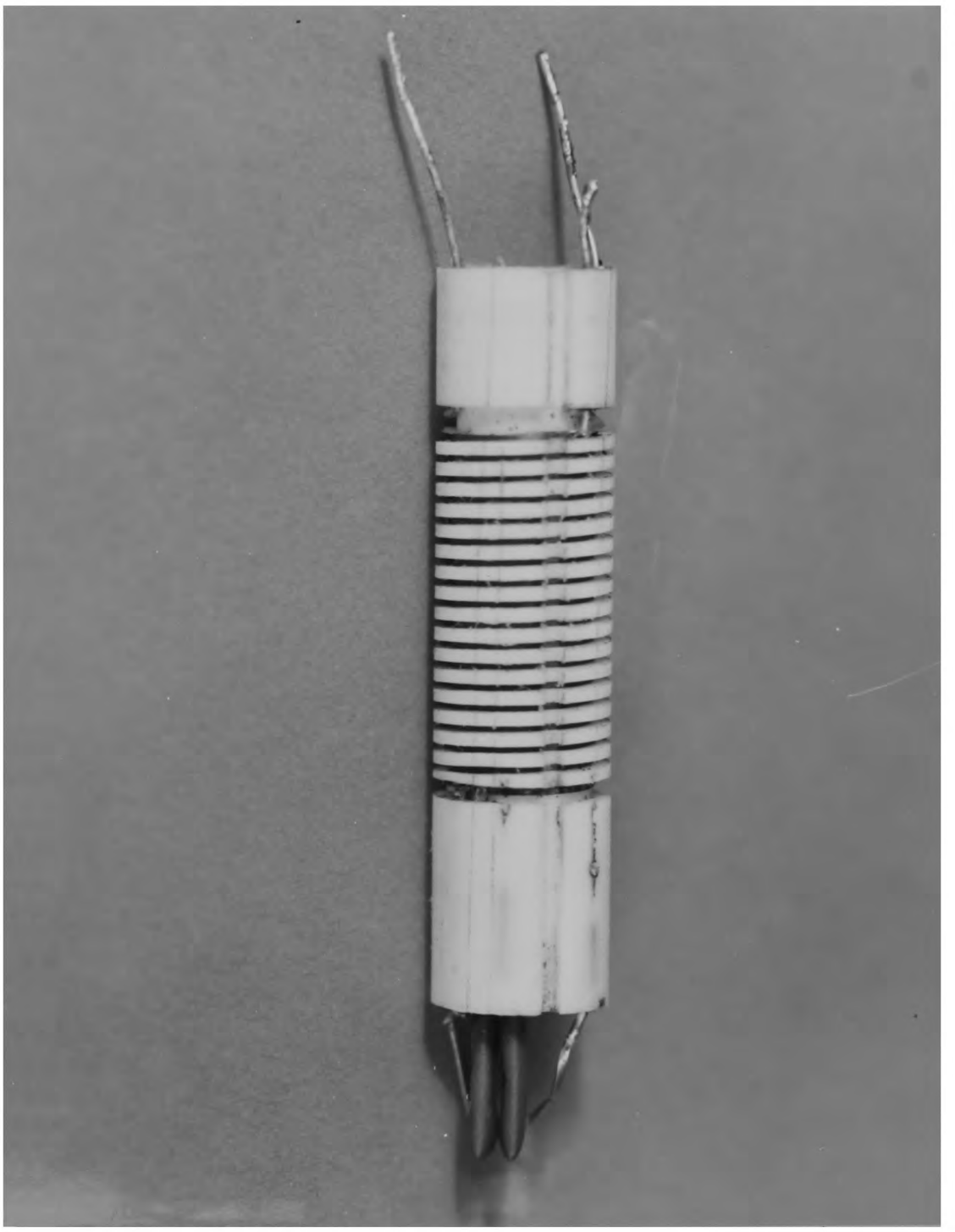


Plate 1
NMR COIL FORMER AND TANK CIRCUIT



Plate 2
CRYOSTAT - DEWAR VESSEL



Plate 3
CRYOSTAT - FLOW CONTROL INSERT

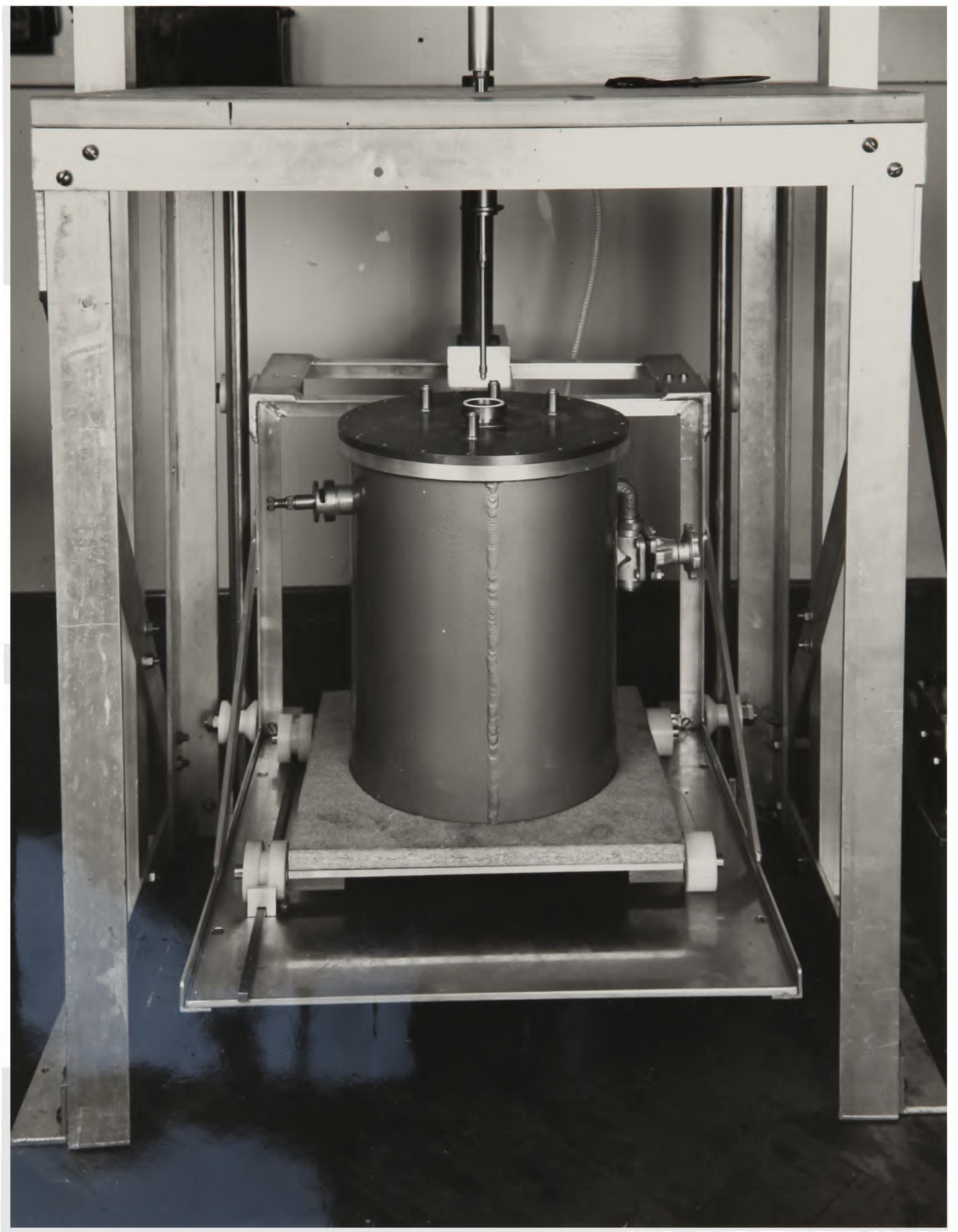


Plate 4

HELIUM STORAGE DEWAR AND HYDRAULIC LIFTING MECHANISM

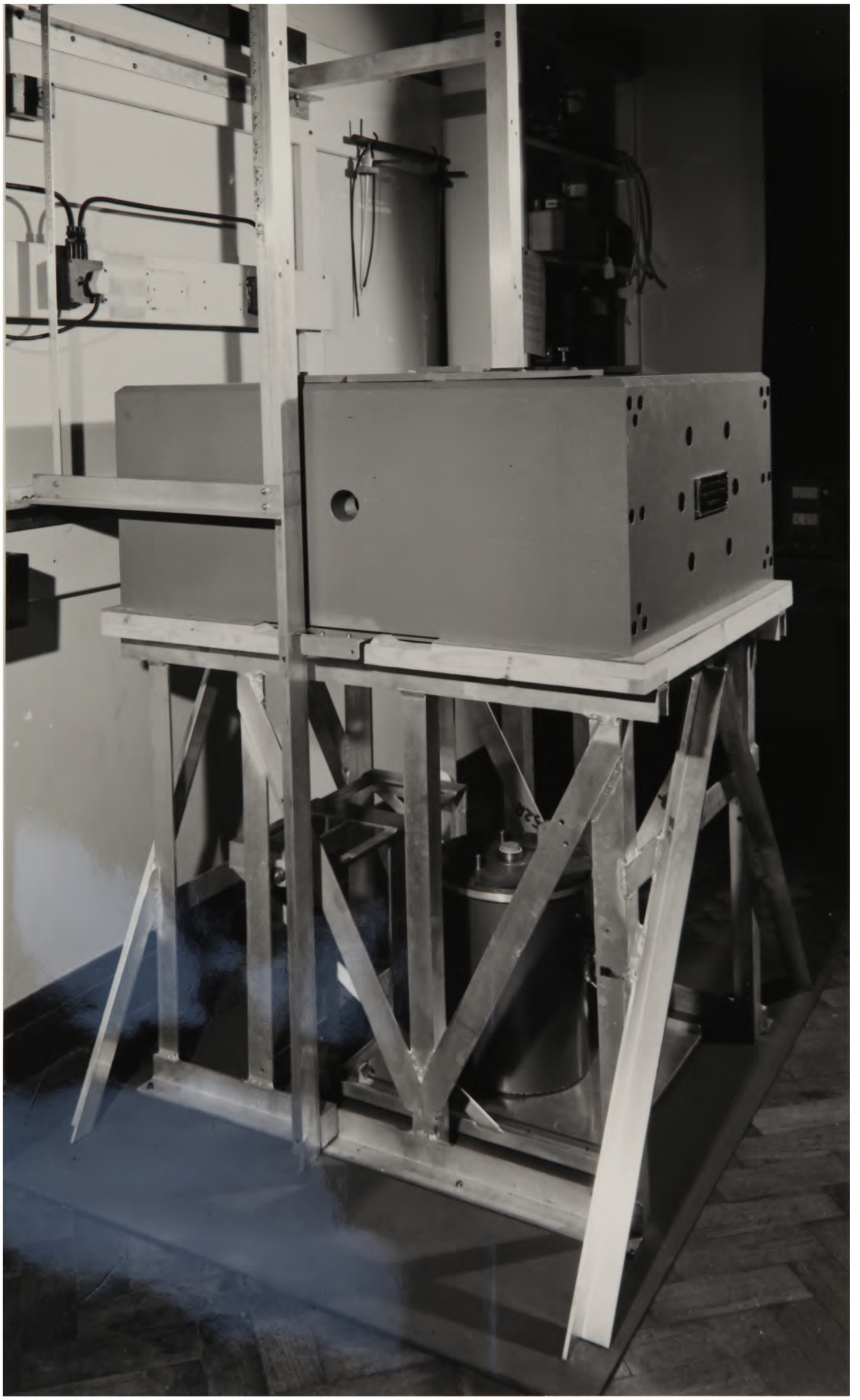


Plate 5

NMR MAGNET (DURING INSTALLATION)

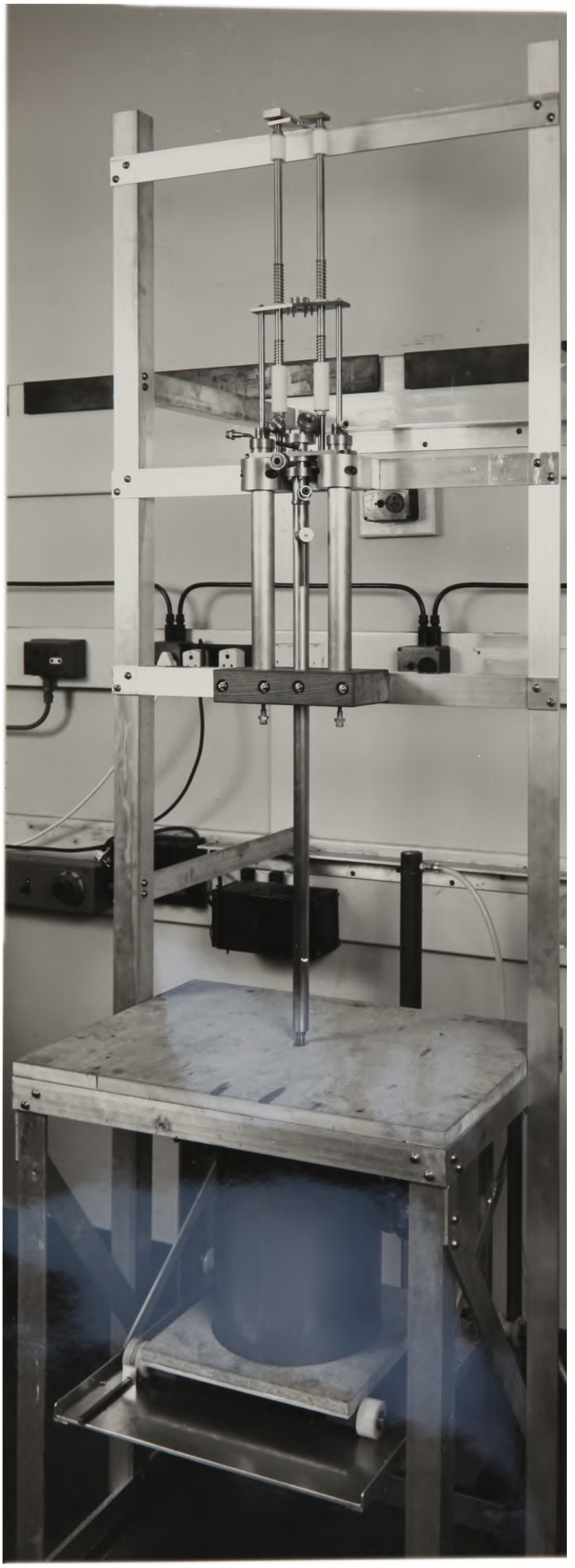


Plate 6
VIEW OF MAIN FRAME ASSEMBLY
WITHOUT THE MAGNET



Plate 7
SAMPLE TRANSIT MECHANISM, INTERNAL
SUPPORT TUBE AND RF COILS

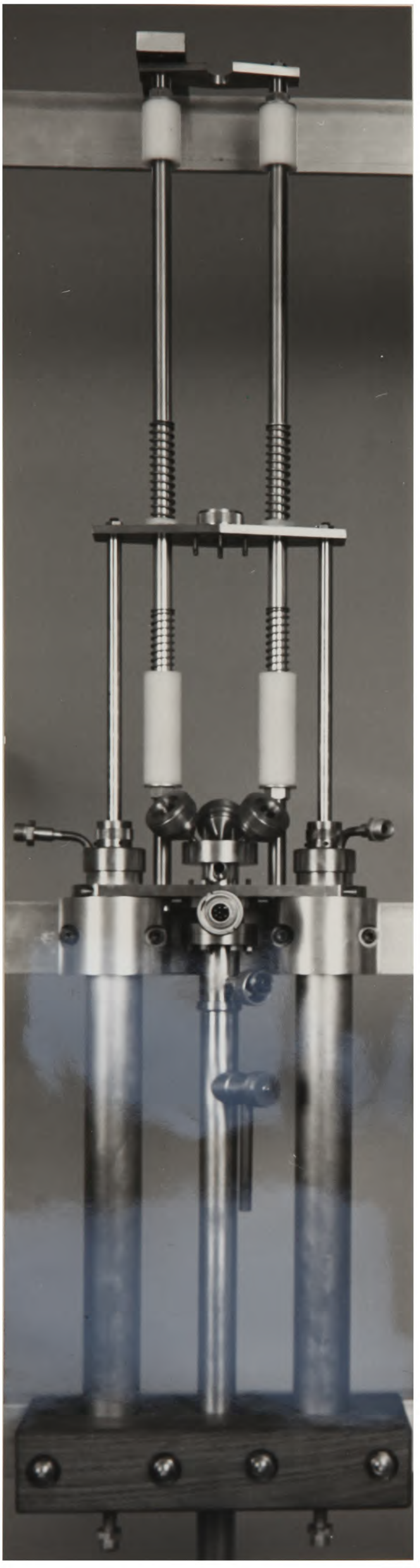


Plate 8
DETAILS OF TRANSIT MECHANISM AND
CRYOSTAT TOP PLATE CONNECTIONS



Plate 9
TELESCOPIC EXCHANGE GAS
SEALING TUBE

CHAPTER V

DOUBLE RESONANCE BY CONTINUOUS COUPLING

5.1 INTRODUCTION

In Chapter III, we gave a description of the technique of double resonance by level crossing (D R L C) , in which abundant P spins polarise rarer Q spins, to prepare them for examination during an irradiation pahse. Any absorption of power by the Q spins is then transferred to the P spins during a second level crossing, allowing detection of Q spin resonances by their effect on the P spin final polarisation. It is notable that no contact occurs between the P and Q spins during the irradiation period. Irradiating the Q spins to saturation will have a limited effect on the P spins, determined by the relative abundance of the two spin species (see Figs.3.8 and 3.9).

Double resonance with spin mixing by continuous coupling (D R C C) may occur whenever the P and Q spins are in some form of (spin) thermal contact during the irradiation phase. This contact can occur whenever a Q spin splitting is very close to the P spin splitting during the irradiation phase.

In Chapter III, page 39 , we introduced the idea of the proton dipolar bath. To summarise this, an assembly of protons in zero applied D.C. magnetic field will be able to absorb radiation in the frequency range $\sim 0 - 100$ kHz with a long 'tail' to it, such that weak absorption is detectable at low or moderate irradiation intensitities up to 300 kHz in some cases. It must be remembered that the dipolar bath is a tightly-coupled system, i.e. if energy is absorbed by one 'section' of the bath this is shared (in a time $\approx T_2$) with all the protons in the dipolar bath, so that a net rise in the spin temperature of the whole dipolar system occurs. In the 'tail' region there are few protons capable of absorbing energy at those high frequencies,

and each proton can only absorb energy at a maximum rate of 1 photon in a period $\approx T_2$. Given an 'infinite' supply of photons, the rate of absorption of energy is thus limited by the number of protons available which are capable of absorbing, and this tends to zero as frequency of irradiation tends to infinity.

Continuous coupling is thus of special importance to deuterium NQR. All deuterium resonances measured to date[4] have $\nu_0 < 50$ kHz and $\nu_+, \nu_- < 250$ kHz, but typically $\nu_+ \sim \nu_- \sim 150$ kHz. It is thus apparent that the ν_0 transition is always fully coupled to the proton dipolar bath, and that the ν_+ and ν_- transitions may also be coupled to the proton bath to some extent.

Continuous coupling also has an effect on nitrogen NQR, but can only occur via the ν_0 transition, because ν_+ and ν_- of all nitrogen resonances measured by our method to date[4] have $(\nu_+ >)\nu_- > 500$ kHz.

In this chapter, we first compute the effect of ν_0 coupling alone, and then proceed with an investigation of continuous coupling through ν_+ and ν_- in the model compounds H_2O (ice 1 h) and HCOOH (formic acid), in samples with small known amounts of D_2O and HCOOD.

5.2 CONTINUOUS COUPLING THROUGH ν_0 ALONE

We consider now the interaction between a three-level quadrupole system and a two-level P spin system when the P spin splitting is held equal to the smallest Q spin splitting throughout the irradiation phase. In particular, we examine the effect on the sensitivity of detection of the ν_+ and ν_- transitions of a spin 1 quadrupole, when $\nu_0 = \nu_p$, the proton frequency.

The argument may be generalised to the case of three Q spin levels chosen suitably out of N levels, and will be applied to the case of spin $\frac{3}{2}$ in Chapter VII.

The initial conditions are the same as at the end of the polarisation phase, given in Chapter III, page 45, and are summarised in Fig.5.1.

Irradiation is applied at the frequency ν_+ or ν_-, and the populations of the various levels change to a'', b'', c'', p''. We now consider how these are related to each other and to the original populations a', b', c', p'.

5.2.1 Irradiation of ν_+

Saturation occurs when $a'' = c''$ (no further absorption).

Coupling equilibrium is maintained by holding the ratio of the populations of levels A and B equal to the ratio of the populations of the P spin levels, i.e.

$$\frac{1 + a''}{1 + b''} = \frac{1 - p''}{1 + p''} \qquad (a'', p'', b'' \sim 10^{-5})$$

or $a'' - b'' = -2p''$, ignoring cross terms $\approx 10^{-10}$.

Conservation of spins ensures:

$$a'' + b'' + c'' = 0.$$

Solving these equations for a'', b'', and c'' we have

$$\begin{aligned} a'' = c'' &= -\tfrac{2}{3} p'' \\ b'' &= \tfrac{4}{3} p'' \end{aligned} \qquad \ldots (5.1)$$

Equilibrium is maintained by simultaneous flips of the P spin system and the levels AB. This process must conserve energy. The number of photons emitted (or absorbed) by levels AB must equal the number of photons absorbed (or emitted) by the P spins. ν_+ irradiation increases the population of level A (Fig.5.1), and hence tends to decrease the population difference between levels A and B. This process can be limited, if AB can emit photons, reducing A and increasing B. The photons are absorbed by the P spins, so that p' is decreased, and the equilibrium is thus maintained.

If we now define the quantities Δc and Δp:

$$\Delta c = c' - c''$$
$$\Delta p = p' - p''.$$

The populations of the various levels are then as shown in Fig.5.2. Saturation of transition AC ensures that $a'' = c''$ or:

$$Q(1 + a' + \Delta c) - 2P\,\Delta p = Q(1 + c' - \Delta c).$$

Simple rearrangement of terms gives:

$$\Delta c = \frac{c' - a'}{2} + \frac{P}{Q}\Delta p \qquad \ldots (5.2)$$

Equilibrium is maintained - the population ratio of levels A and B is kept equal to the population ratio of the 2P spin levels, i.e.

$$\frac{Q(1 + a' + \Delta c) - 2P\,\Delta p}{Q(1 + b') + 2P\,\Delta p} = \frac{1 - p' + \Delta p}{1 + p' - \Delta p} \quad .$$

Cross-multiplying, eliminating terms like $p'a' \approx 10^{-10}$, and noting that $2p' = b' - a'$, we can reduce this to:

$$\Delta c = \Delta p \left(4\,\frac{P}{Q} + 2\right) \qquad \ldots (5.3)$$

Combining this with equation (2), we then have

$$\Delta p = p' - p'' = \frac{c' - a'}{2}\left(\frac{Q}{3P + 2Q}\right)$$

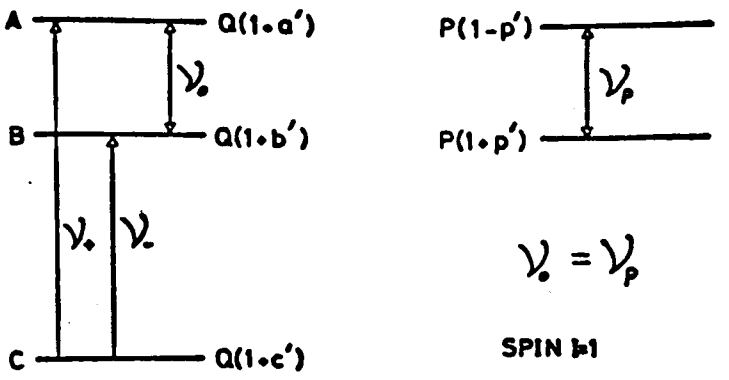
or

$$p'' = p' - \frac{Q}{2(3P + 2Q)}(c' - a') \qquad \ldots (5.4)$$

Since $(c' - a')$ is a positive quantity (see Fig.3.7), p' is <u>decreased</u> by irradiation of ν_+, as expected.

5.2.2 <u>Irradiation of ν_-</u>

This time, when saturation occurs, $b'' = c''$. To maintain the equilibrium of the population ratios this time, p' must <u>increase</u> to its new value p'', while b' increases to b''. Arguments similar to those of section 5.2.1 lead to:



$$-\frac{a'}{p}=\frac{3}{4}X^3+X \qquad \frac{p'}{p}=\frac{3}{4}X^3-\frac{1}{4}X^2+\frac{1}{2}X$$

$$\frac{b'}{p}=\frac{3}{4}X^3-\frac{1}{2}X^2 \qquad X=P/(P+Q)$$

$$\frac{c'}{p}=\frac{1}{2}X^2+X$$

$$a'+b'+c'=0$$

$$b'-a'=2p'$$

Fig.5.1: Populations after 3 level crossings

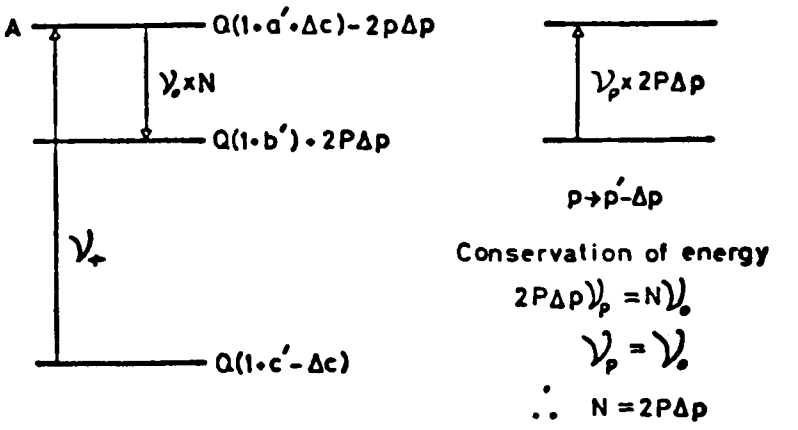


Fig.5.2: Irradiation of ν_+ while coupling ν_0

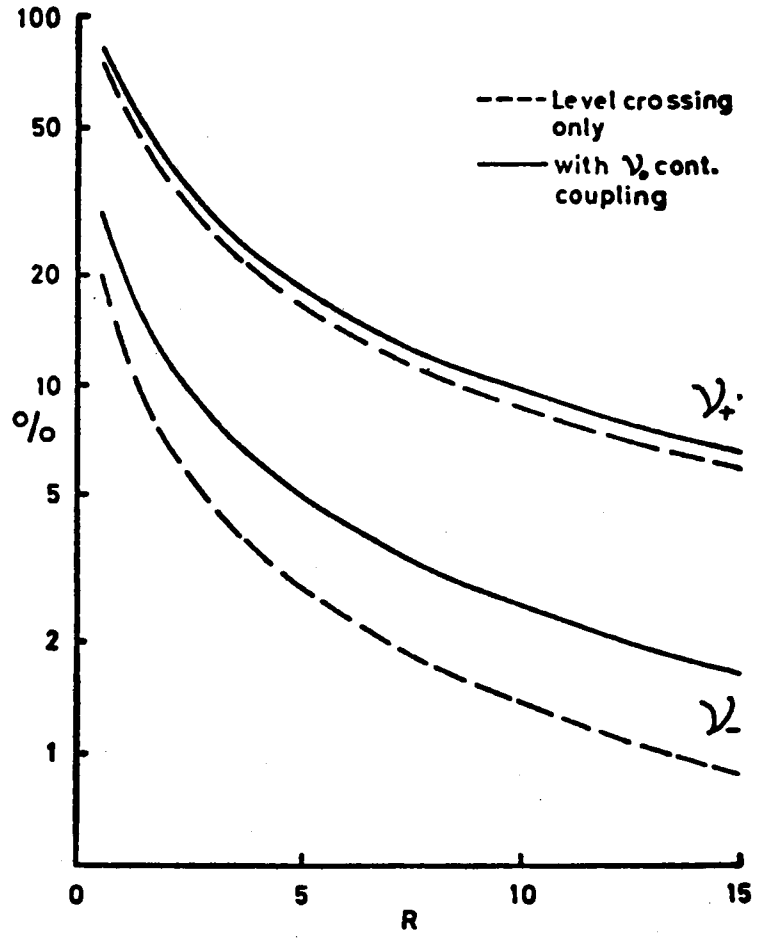


Fig.5.3: % of p''' destroyed by irradiation to saturation of ν_+ and ν_-, comparing the effect of continuously coupling ν_0 to the protons.

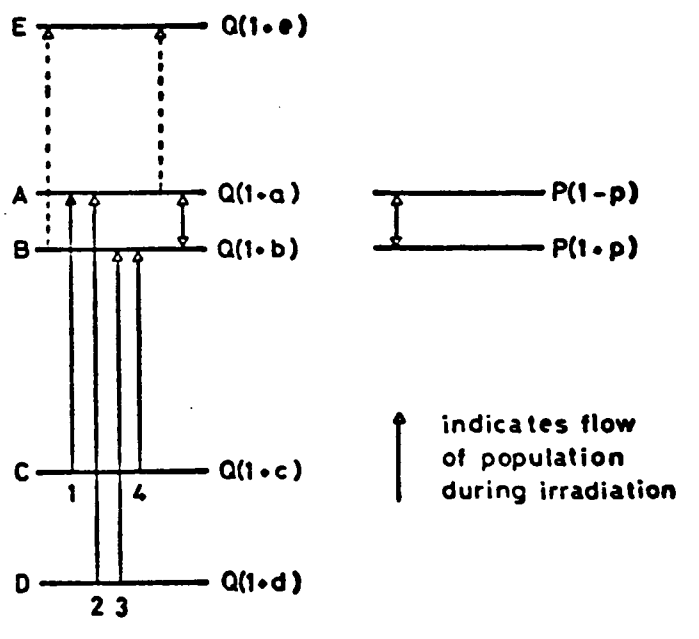


Fig.5.4: 5 levels of an N level system, AB coupled to P spins

$$a'' = -\tfrac{4}{3}\, p''$$
$$b'' = c'' = \tfrac{2}{3}\, p'' \qquad \ldots (5.5)$$

with

$$p'' = p' + \frac{Q}{2(3P + 2Q)}\,(c' - b') \qquad \ldots (5.6)$$

Since $(c' - b')$ is a positive quantity (see Fig.3.7), p' is increased by irradiating ν_-.

Measurement Phase

If we now employ equation (3.30), to calculate the value of p''', the amount of magnetisation left at the end of the experimental cycle, we can examine the effect of continuously coupling ν_0 to the protons, whilst irradiating either ν_+ or ν_-.

Defining: $p'''(0) = p'''(a', b', c', p') = p'''$ (no irradiation)

$p'''(\nu^+ \text{ or } \nu^-) = p'''(a'', b'', c'', p'') = p'''$ (irradiation)

The percentage absorption due to irradiating ν_+, for example, is then given by

$$A(\nu_+) = \frac{p'''(0) - p'''(\nu^+)}{p'''(0)} \times 100\%$$

similarly

$$A(\nu_-) = \frac{p'''(0) - p'''(\nu^-)}{p'''(0)} \times 100\% \ .$$

These variables are plotted in Fig.5.3 for a spin 1 quadrupole as a function of the spin number ratio

$$R = \frac{N_P}{N_Q} = \frac{2P}{3Q} \ ,$$

together with the absorptions obtained in the conventional manner of Chapter III, assuming no continuous coupling of ν_0.

Note: We assume throughout this section that T_{1D} of the protons is long, so that $p'' = p'$ if there is no continuous coupling. If T_{1D} is fast, and the levels AB are coupled to the protons, $p'' \approx 0$, $a'' \approx b''$ and the ν_+ and ν_- transitions become equally intense, exactly as if we doubly irradiated the ν_0 transition as described in Chapter III.

We see from Fig.5.3 that both the ν^+ and ν^- sensitivities, as revealed by the maximum percentage absorption obtained, are increased, but that the relative increase in ν^- is larger.

Interpretation

As in Chapter III, equation (3.30')

$$p''' = \pi(p'') + \Delta(a'',b'',c'').$$

For no continuous coupling $\pi(p'')$ is a constant (for long T_{1D}) and all changes in p''' are due to changes in Δ during irradiation.

There are two oppositely-acting effects when we couple in ν_0, viz the effects on π and the effects on Δ.

When we irradiate ν_+, we saw that p' decreases to p'', so that π is decreased. Irradiation of ν_- increased p' and hence increased π. Coupling of ν_0 however, tends to decrease the effect on Δ of irradiating ν_+, so that $\Delta(\nu^+$ saturated, continuously coupled) > $\Delta(\nu^+$ saturated, no coupling). Also, coupling ν_0 increases the effect on Δ of irradiating ν^-.

These two effects almost cancel out for ν^+ irradiation, but the net effect is that, for all R,

$p'''(\nu^+$ or ν^- saturated, coupled) < $p'''(\nu^+$ or ν^- saturated, not coupled). So that the absorptions $A(\nu^+)$ and $A(\nu^-)$ are larger with continuous coupling that without. One must note, however, that the calculated effect is not large.

If while continuously coupling ν^0, we also saturate the proton system with irradiation, so that $p'' = 0$, we then also keep the populations of levels A and B equal, i.e. $a'' = b'' = \frac{1}{2}(a' + b')$. Irradiation of ν^+ or ν^- makes $c'' = a''$ or b''. In either case, $a'' = b'' = c''$ which can occur only if all three are zero. Irradiation of either ν^+ or ν^- can thus destroy 100% of Δ. This is also true if we keep AB saturated, without affecting the P spins, and hence continuous coupling produces no new effect in this case.

5.2.3 Generalisation of Continuous Coupling to the Case of $I > 1$

If we have an N-level system, where $N > 3$, and two of the levels are almost degenerate, then we can treat the case of these two levels (alone) being continuously coupled exactly as in the case of spin 1 and coupling of ν_0.

Figure 5.4 shows five levels of an N-level system. We assume that levels A and B are coupled to the P spin bath. Transitions between level A and any other level lower in energy, such as C or D, can be treated exactly like a ν^+ transition, while any transitions between level B and levels below it are exactly analogous to a ν^-. In either case the lower level which does not take part in the transition remains unaltered in population.

Similarly, for levels above AB, such as E, transitions from A decrease its population, and may be treated similarly to a ν_- irradiation, while transitions from B to E tend to decrease the population of B, and may be treated like a ν^+ irradiation.

Slight modifications to the final calculated populations in this case will occur, since transitions from above AB tend to decrease the total population of (A + B) while transitions from below such as ν_+ and ν_- tend to increase the total population of (A + B).

These theories are used in the case of $I = \frac{3}{2}$ (a four-level system) in an applied magnetic field and are discussed for this case in Chapter VII.

5.3 CONTINUOUS COUPLING THROUGH ν_+ AND ν_-

It has been shown that the effect of continuously coupling ν_0 to the proton dipolar bath is a relatively small one, and that the maximum effect of irradiating a ν_+ or ν_- transition (to saturation) is still limited by the relative abundances of the P and Q spins.

For example, when $R = 10$ (10 times more P spins than Q spins) the maximum effect of irradiating a ν_+ transition to saturation is a 10% change in the final P spin magnetisation. However, it is easy to observe that one may, when investigating a sample of 10% D_2O in H_2O ($R = 9$) destroy 100% of the final P spin magnetisation by irradiating either ν_+ or ν_- to saturation. Some additional effect must be operative, and we will show that this is due to continuous coupling to the P spin bath through the ν_+ and ν_- transitions themselves.

One then has an effect that one may call full or complete continuous coupling, and it is this effect which leads to much higher sensitivities in deuterium NQR than are ever attainable for nitrogen NQR or any NQR by DRLC.

The limitation on sensitivity of DRLC for small numbers of Q spins, may be removed by arranging that the P and Q spin systems remain in good thermal contact during the irradiation phase. In these circumstances a small number of Q spins may continuously absorb power and pass most of it to the P spins without saturation occurring, until the total polarization of the abundant P spins has been destroyed. However, this thermal contact is difficult to achieve without adversely affecting the method as a detector of NQR. For example, if the P spin splitting were held equal, during the irradiation phase, to the Q spin splitting to be investigated, there would be continuous level crossing between the two systems and strong thermal contact would be maintained. However, the direct absorption of power by the P spins (being much more abundant and also probably having a larger transition probability due to their larger magnetic moment) would completely swamp the Q spin absorption and destroy the detection of NQR. If DRCC is to be effective, the two spin systems must be tightly coupled during the irradiation phase but the absorption of power must be predominantly through the Q spins.

That these conditions can readily be attained in practice is due to the frequency distribution of the density of states of an assembly of P spins in zero or small applied magnetic field. For an assembly of dipoles in zero applied field and coupled by magnetic dipole-dipole interaction, the absorption of power per second at frequency ν is proportional to[27,33]

$$A(\nu) = (h\nu) \cdot (h\nu/kT_S) \cdot f(\nu) \cdot B_1^2 \qquad \ldots (5.7)$$

The term $h\nu$ represents the energy per photon. The factor $(h\nu/kT_S)$, where T_S is the spin temperature of the assembly, is the relative probability of absorption over stimulated emission, or the population difference of the levels concerned. B_1 is the amplitude of the applied radio frequency irradiation field and $f(\nu)$ is the transition matrix element distribution function. $f(\nu)$ is maximum at zero frequency and is Gaussian in shape, being appreciable out to frequencies of order $(\gamma_P/2\pi)B_L$, where γ_P is the magnetogyric ratio of the spins. B_L is an effective internal field being the root of the mean squared internal field due to the dipole-dipole interaction among the P spins. Such an assembly is known as a dipolar bath and is tightly coupled by mutual spin flips, the whole assembly maintaining a single spin temperature T_S. If a small steady field B_0 is applied, $f(\nu)$ breaks up into peaks at frequencies 0; $(\gamma_p/2\pi)B_0$; $2(\gamma_p/2\pi)B_0$; $3(\gamma_p/2\pi)B_0$ etc. but for small applied fields, $B_0 < B_L$ the peaks are not resolved and the effect is simply to shift the broad peak of $f(\nu)$ slightly to higher frequency.

By arranging that the high frequency wing of $f(\nu)$ just overlaps in frequency the quadrupole transition of the Q spins to be detected, it is possible to ensure that $f(\nu)$ at ν_Q is sufficiently large to maintain good coupling between P and Q spins, but is not so large as to prevent the predominant absorption of power to be via the Q spins.

5.3.1 Experimental

As model compounds to investigate DRCC we have chosen frozen mixtures of HCOOD in HCOOH and of D_2O in H_2O. By using frozen liquids it is easy to obtain samples of accurately known deuterium concentration at a given site. All experiments were performed at 77 K.

In Fig.5.5 we display the measured absorption spectrum of the proton dipolar bath of both frozen HCOOH and frozen H_2O in zero applied magnetic field. For formic acid and ice the absorption may be represented approximately by a function of the form described above of $\nu^2 \exp(-\nu^2/2\sigma^2)$ with σ given by 20 kHz and 42.4 kHz respectively. The smaller proton-proton separation (r) in ice with the consequent increase in the strength of the dipolar interaction ($\alpha\, 1/r^3$) is responsible for its much broader dipolar absorption spectrum. Also indicated in Fig.5.5 are the positions of the deuterium NQR lines for HCOOD dilute in HCOOH (114.4 ± 0.2 kHz and 124.4 ± 0.2 kHz) and for HDO dilute in H_2O (166.9 ± 0.3 kHz and 154.0 ± 0.3 kHz). For formic acid the frequency separation between the NQR lines and the high frequency tail of the dipolar bath absorption in zero applied field is such that the detection of the NQR is characteristic of DRLC. In ice on the other hand there is sufficient frequency overlap to ensure DRCC and the characteristics of the two mechanisms can thus be compared in these two specimens. Furthermore, by the application of small steady magnetic fields during the irradiation phase, the dipolar bath spectrum of formic acid may be moved to higher frequency sufficiently to cause the NQR detection in this substance to become characteristic of DRCC with its much higher sensitivity. This enables us to compare the two mechanisms within the same sample and to contrast the results directly.

In Fig.5.6 we display the measured deuterium NQR spectra of 8% HCOOD in HCOOH in zero applied steady field ($B_0 = 0$) as the irradiation power level is increased. It is seen that the line depth soon saturates and the application of higher powers of irradiation merely tends to broaden the

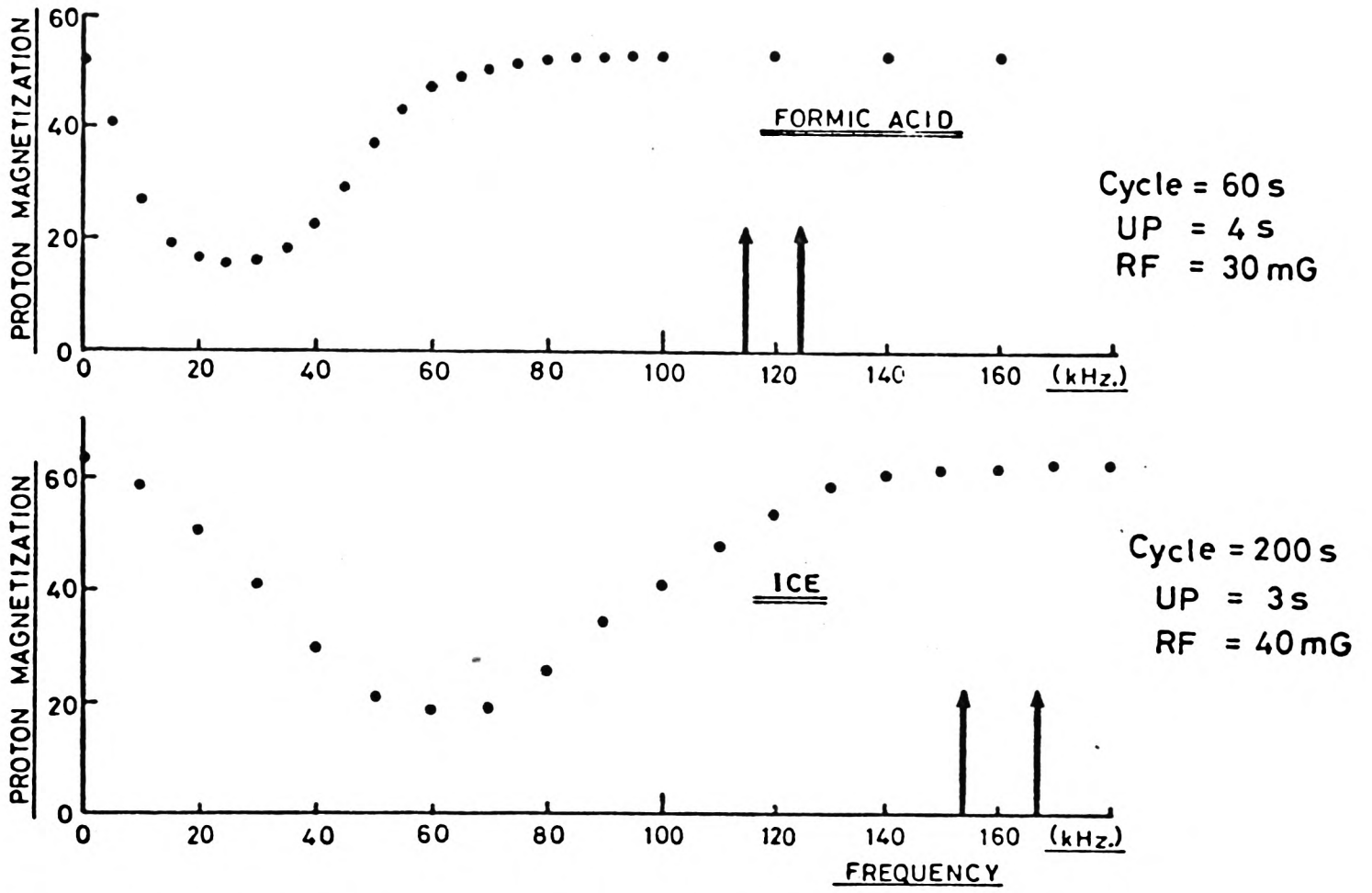


Fig.5.5: Proton dipolar bath spectra

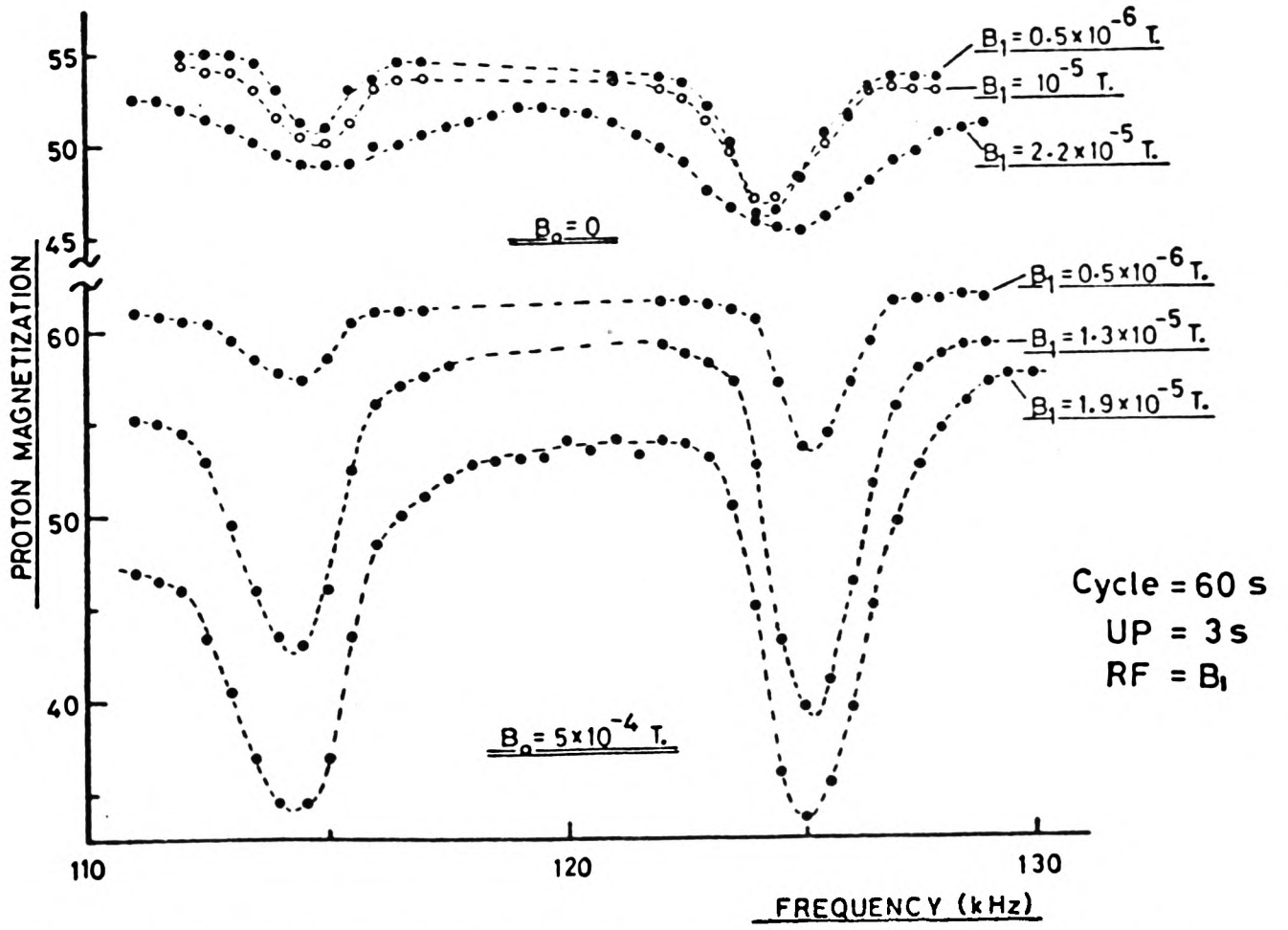


Fig.5.6: NQR Spectra of 8% HCOOD

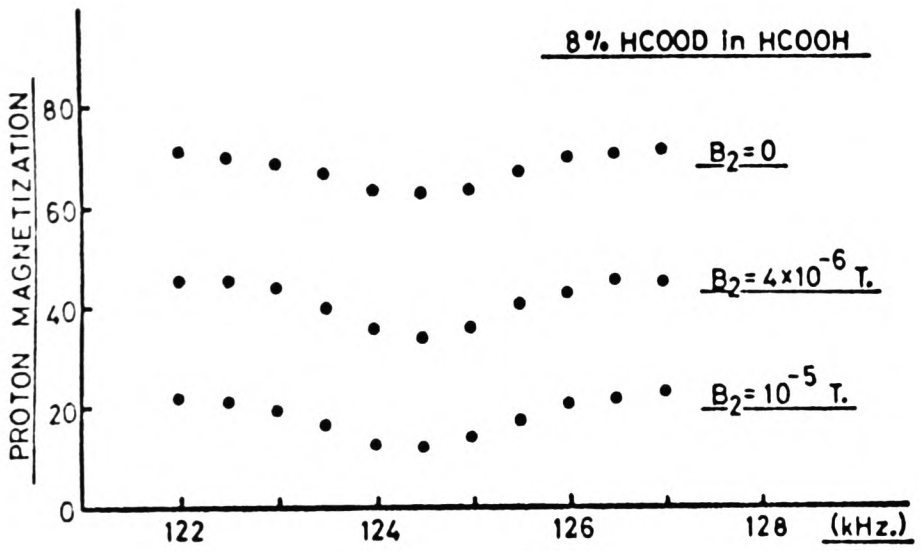
lines. This is characteristic of DRLC and reflects the finite number of Q spin flips that may occur under irradiation before saturation prevents further absorption.

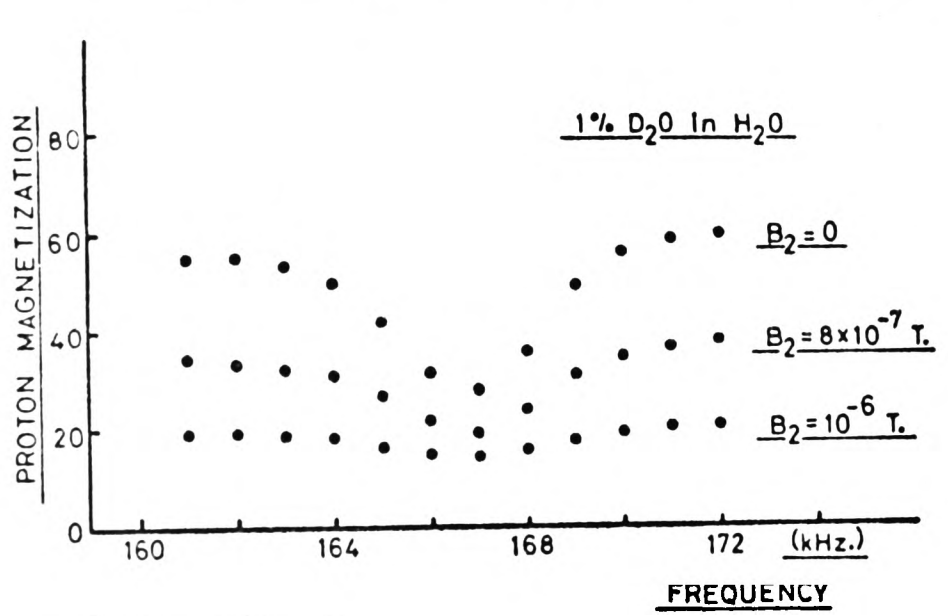
Also in Fig.5.6 we display the NQR spectra of the same sample taken under identical conditions except that a steady magnetic field of $B_0 = 5 \times 10^{-4}$ T (5 Gauss) was applied during the irradiation phase. In these cases the line depth increases with applied radiation power and no early saturation occurs. This behaviour is in marked contrast to that obtained with $B_0 = 0$ and is characteristic of DRCC with its much higher sensitivity. The presence of frequency overlap between the NQR lines and the high frequency tail of the dipolar bath absorption with $B_0 = 5 \times 10^{-4}$T may be observed by the baseline tilt of these spectra particularly at the highe powers of irradiation.

Even in zero applied steady field the deuterium NQR spectra of HDO dilute in H_2O is characteristic of DRCC and enables the NQR spec trum of very low deuterium concentrations to be measured as we shall see.

The single major difference between DRCC and DRLC is the thermal contact that is, or is not, maintained between P and Q spins during the irradiation phase. This difference is most graphically illustrated by using double irradiation as shown in Fig 5.7. This contrasts the behaviour of frozen mixtures of 8% HCOOD in HCOOH and 1% D_2O in H_2O when the irradiation phase, spent in zero applied steady field, is divided into two equal periods. During the first, the proton dipolar bath is irradiated directly at 50 kHz and with various irradiation field peak to peak amplitudes B_2 s as to heat directly the P spin bath to various extents.

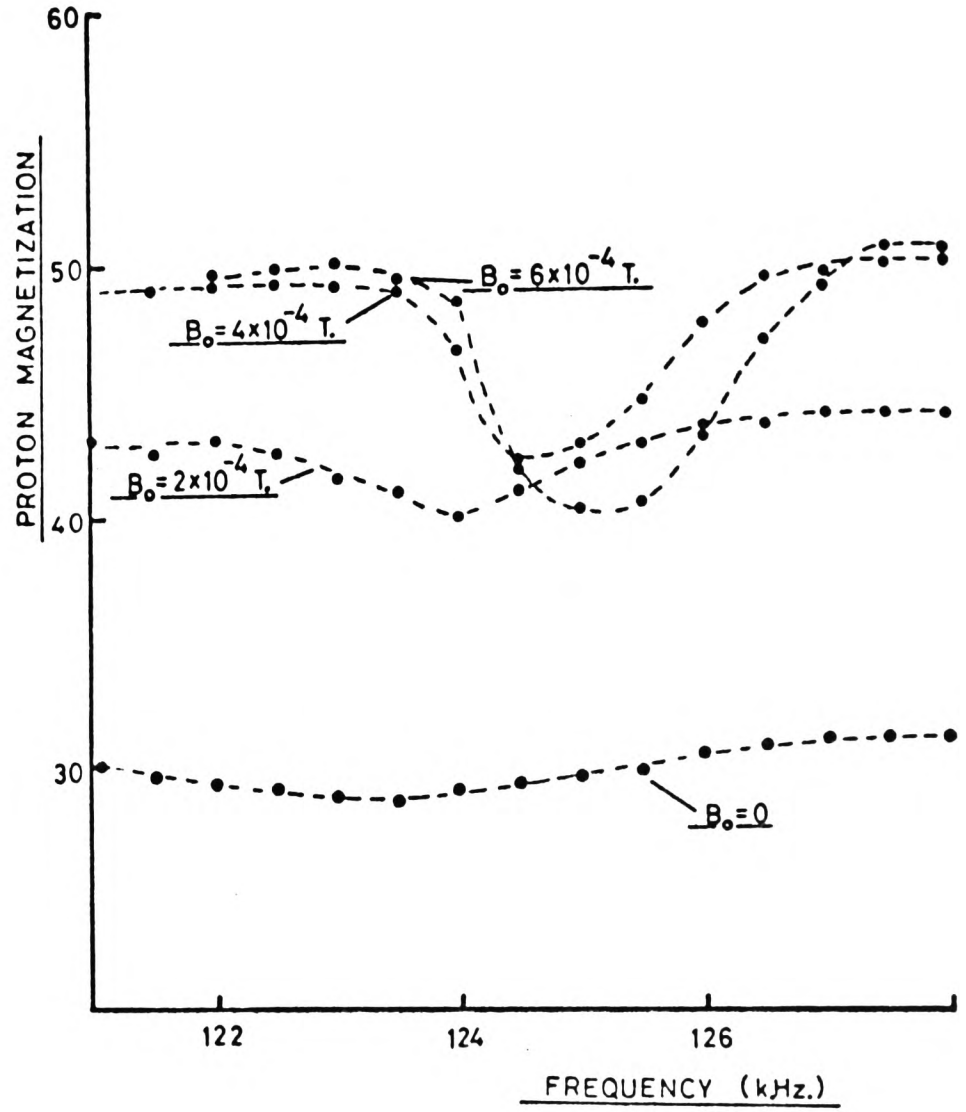
During the second period the Q spins are irradiated always at the same power level in order to detect the NQR. In the case of formic acid it is seen that prior heating of the P spins during the irradiation phase





	Cycle	UP	RF
HCOOH	60s	4s	100mG
H_2O	120s	60s	34mG

Fig.5.7: Double irradiation spectra



Cycle = 120s UP = 20s RF = 40mG

Fig.5.8: 1% HCOOD Spectra - effect of B_o

merely lowers the final proton magnetization measured but the NQR line intensity is not appreciably changed. This behaviour is characteristic of DRLC in that the NQR is signalled by the destruction of the polarization stored by the Q spins during the irradiation phase and that this polarization is immune from the radiant power absorbed directly by the P spins in the first half of the irradiation phase.

In direct contrast to this is the behaviour of the ice specimen displayed in Fig.5.7. Here the NQR signal diminishes in proportion to the measured total final proton magnetization. This is characteristic of DRCC. The irradiation during the first half of the irradiation phase, although aimed at the P spins, raises the spin temperature of <u>both</u> coupled spin systems. The net transition probability of the Q spins during the second period, being proportional to $1/T_S$, is diminished by the raising of T_S during the first period.

The final off-resonance P spin magnetization is also proportional to $1/T_S$. The very different durations of irradiation phase used for formic acid and ice reflect their markedly different zero field proton relaxation times.

The gain in sensitivity of detection of deuterium NQR in samples dilute in deuterium that may be obtained by the manipulation of the proton dipolar bath by the application of small magnetic fields so as to ensure DRCC rather than DRLC is illustrated in Fig.5.8. The specimen is a frozen mixture of 1% HCOOD in HCOOH and the NQR spectral line is measured with various steady fields B_0 applied during irradiation but with constant radiant power applied. As the steady field is increased from zero to 6×10^{-4} T (6 Gauss) the NQR line is seen to change from being barely discernable to being large. Two other features are noteworthy. The first is the increase in the off-resonance proton magnetization that occurs on applying steady fields from zero to 4×10^{-4} T. This is due to the lengthening

of the proton small field spin-lattice relaxation time. The second is the shift of the detected NQR line to higher frequency in applied magnetic fields. This shift is well understood[19] even in powder samples, but must be corrected for either theoretically or by taking spectra in several applied fields and extrapolating to zero applied field.

The field shift may be eliminated entirely by employing a time sharing technique. The small field B_0 is replaced by a half wave rectified sinusoidal field of low audio frequency ($\sim$20 Hz) and amplitude 6×10^{-4} T. The quadrupole resonance detection radiation at frequency ν_Q is gated in antiphase with the audio frequency field such that when one is applied the other is off. The Q spins are thus alternately heated and coupled to the P spins. The resonance is detected in zero applied field so that there is no field shift and also the direct absorption by the P spins is much reduced as the frequency overlap of the P spin bath in zero field is negligible. Because of the ν^2 dependence of the dipolar bath absorption there is negligible heating of the P spins by the low audio frequency field, despite its relatively large amplitude. This technique is the low frequency equivalent of DRLC with multiple level crossing[4] except that the amplitude of the audio frequency field applied to ensure coupling is only a fraction of that required for complete resonant level crossing.

Finally in Fig.5.9 we display the deuterium NQR spectra obtained in zero applied field of 5% and 0.1% D_2O in H_2O ice. The sensitivity is far in excess of any that would be obtained in these samples using DRLC. These spectra are obtained by stepping ν_Q through the required frequency range once, each cycle being terminated by a single sampling of the free induction decay. Enhanced signal-to-noise ratios may be obtained by averaging, for example by adding several such spectra obtained sequentially. The sloping baseline of the 0.1% spectrum shows the extent of direct proton bath absorption at the irradiation powers necessary in order to obtain discernible

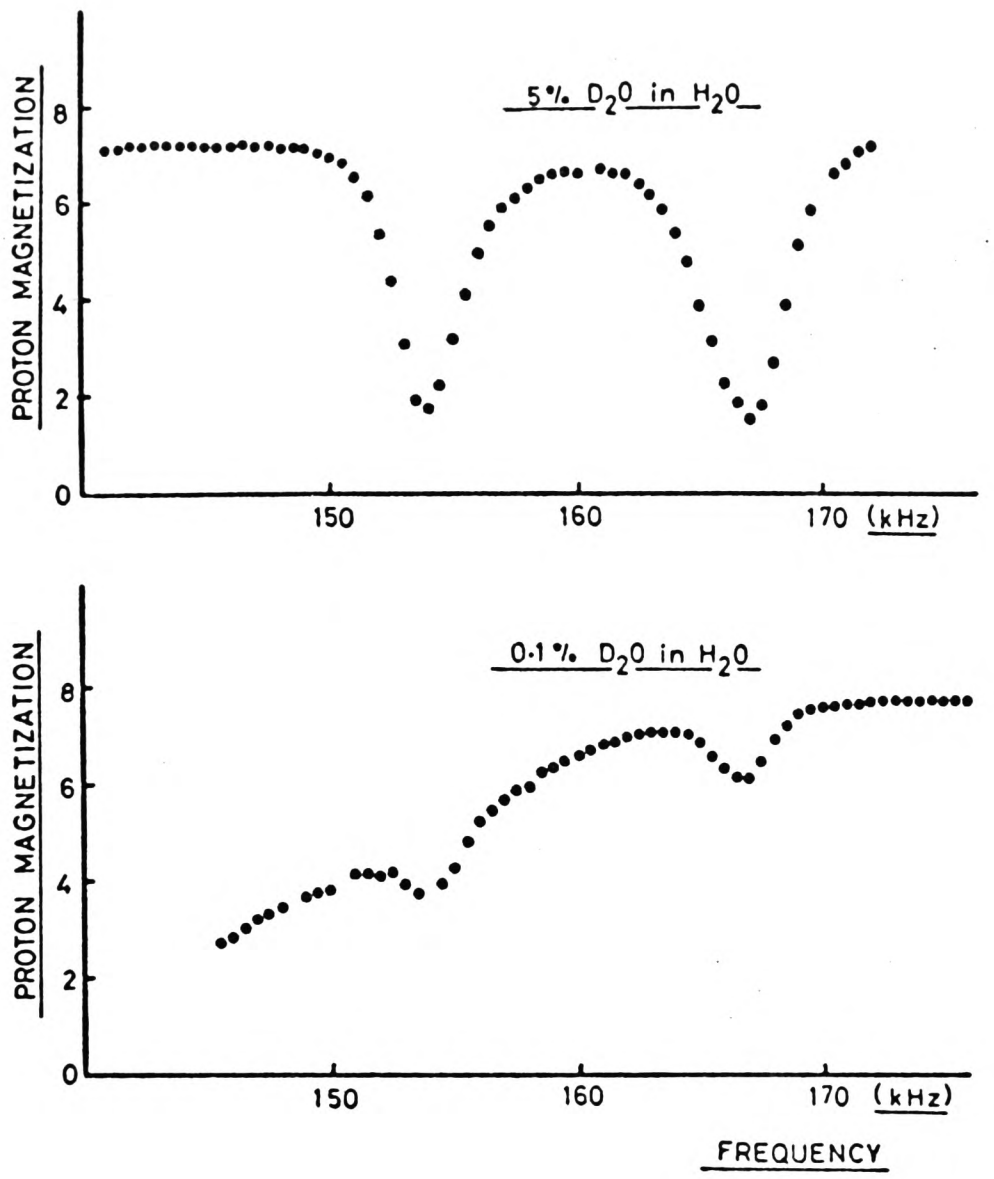


Fig.5.9:
HDO Spectra

Cycle = 300 s
UP = 60 s
RF = 26 mG (5%)
40 mG (0·1%)

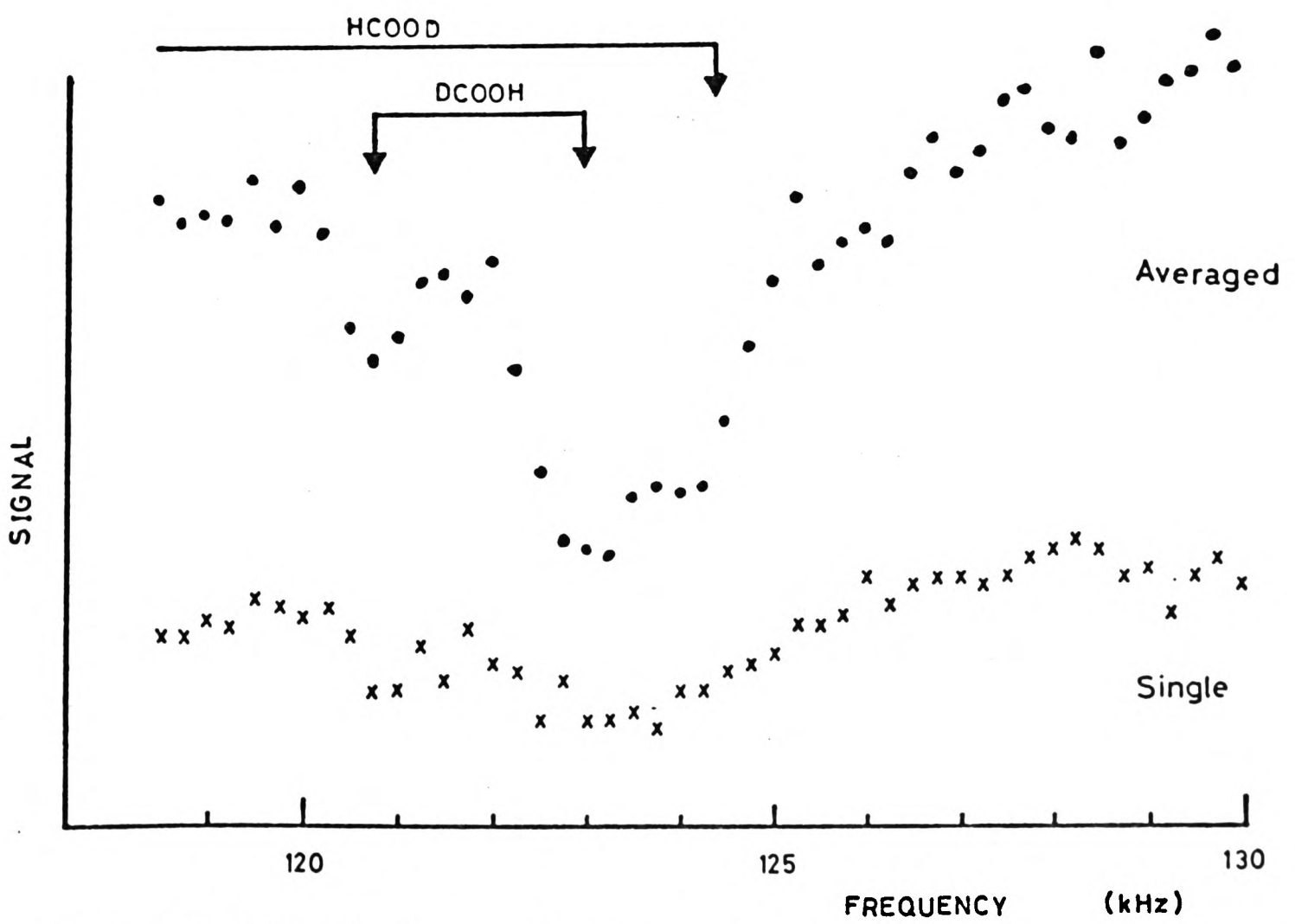


Fig. 5.10: Natural abundance ^2D spectra

absorption by the rare Q spins. It is this competitive direct absorption that finally limits the sensitivity of DRCC.

5.4 DETECTION OF NATURALLY ABUNDANT DEUTERIUM NQR

As an extension of the work outlined above, an attempt was made to detect signals from deuterium present only at natural abundance (0.0156%) in HCOOH and H_2O.

5.4.1 Natural Abundance ^2D Spectra in HCOOH

The spectrum obtained for HCOOH is shown in Fig.5.10. A time sharing technique was employed in which the dipolar proton bath and the deuterons were alternately thermally isolated from each other in zero applied steady field, and then thermally coupled by the application of a steady magnetic field of 14.5×10^{-4} T (14.5 Gauss). During the time spent in zero steady field, the sample was irradiated with a radio frequency field of peak-to-peak amplitude 5×10^{-5} T in order to detect the NQR spectrum of the deuterons. The alternation between resonantly heating the thermally isolated deuterons and placing them in thermal contact with the proton bath was arranged by applying the 'steady' field as a 10 Hz square wave. The time sharing technique, rather than simple continuous coupling, was employed so that magnetic field induced line shifts and direct absorption of radio frequency power by the proton bath are eliminated as we have described.

The statement made above that, in zero applied magnetic field, the deuterons and the proton dipolar bath are thermally isolated from each other is of course a considerable over-simplification. As we have discussed before, the two deuteron energy levels separated by an energy $h\nu_0$, ($\nu_0 = \nu_+ - \nu_-$ in the standard notation) are in fact continuously coupled to the proton dipolar bath even in zero applied field. This ν_0 continuous coupling does in fact affect the relative sizes of the detected NQR spectral lines but an understanding of it is not important in arriving at an explanation of the very high sensitivity obtainable using this DRCC technique.

Normal ANALAR formic acid was used to obtain Fig.5.10, and the experiment was performed at 77 K. The total cycle time was 100 secs and the total dwell time in low field (irradiation phase) was 10 secs each cycle. The result of a single sweep through part of the spectrum is shown as the lower trace in Fig.5.10 and the result of recording digitally and then adding five consecutively obtained spectra is shown as the upper trace in Fig.5.10. The signal-to-noise ratio of the single trace is about 2:1 and that of the composite trace is about 4:1.

The spectral line at 124.4 kHz together with another line (not illustrated) at 114.4 kHz, form the deuteron spectrum of HCOOD dilute in HCOOH, as we have shown previously with isotopically enriched samples of a few percent HCOOD in HCOOH. The corresponding quadrupole coupling constants for HCOOD dilute in HCOOH are $e^2qQ/h = 159.2 \pm 0.4$ kHz and $\eta = 0.125 \pm 0.01$. These are to be compared with the coupling constants previously obtained[4] for 100% deuterated HCOOD of $e^2qQ/h = 161.15 \pm 0.1$ kHz and $\eta = 0.122 \pm 0.001$, again taken at 77 K. There is thus a significant change between HCOOD diluted in HCOOH and pure HCOOD.

The remaining spectral lines in Fig.5.10 at 123.0 ± 0.3 kHz and 120.75 ± 0.3 kHz, form the deuteron spectrum of DCOOH diluted in HCOOH and lead to quadrupole coupling constants of $e^2qQ/h = 162.5 \pm 0.4$ kHz and $\eta = 0.03 \pm 0.01$. Unfortunately we have not previously measured 100% DCOOH so that the diluted to concentrated specimen comparison cannot be made. Values of the quadrupole coupling constants in 100% DCOOH and HCOOD have been previously reported [34], derived from deuterium NMR in single crystal specimens and the results obtained were:-

HCOOD, $e^2qQ/h = 165.1 \pm 2.7$ kHz, $\eta = 0.125 \pm 0.03$
DCOOH, $e^2qQ/h = 161.0 \pm 2.0$ kHz, $\eta = 0.040 \pm 0.025$.

The large errors quoted reflect the much greater difficulty of the NMR experiment compared with DRCC but the results are roughly consistent.

If we perform a similar experiment on pure frozen H_2O, we have somewhat less success. A spectrum like that of Fig.5.9 results, but with only a very slight change of background slope at each HDO line position. The competitive direct absorption by protons 'wins' in this case - the system is slightly over-coupled for detection of the HDO lines to be optimized.

Experiments were performed at 77°K on a range of D_2O/H_2O mixtures from 10% D_2O down to 0.05% D_2O, the latter being the lowest percent from which it was possible to obtain a recognisable absorption. Over this range, it was observed that (allowing for background slopes due to direct proton absorption) there was no shift in the ν^+ or ν^- lines. It was additionally observed that the size of an absorption line (as measured by its total area) was directly proportional to R.F. energy input (R.F. power × duration of irradiation) and to the amount of deuterium present (so long as no saturation effects occurred).

Direct absorption by protons (as judged by the background slope) was slightly more power-dependent - i.e. for the same total energy input, a longer irradiation period produced a lesser background slope. There is thus some small advantage in using longer irradiation periods when searching for dilute deuterium lines, if this is allowed by a sufficiently long T_{1D} for the protons.

These limitations on sensitivity of detection, at present around the 0.05% level, are only of academic interest. It is normally desirable to enrich one or a few sites, and to examine those sites in isolation, since a simpler spectrum then results. For most samples, deuterium concentrations of 5%-10% are most convenient, because the lines are readily observable and no deuteron-deuteron interactions are of importance.

5.5 CONCLUSION

This technique of D R C C should be applicable to the detection of deuterium N Q R in any proton-containing solid provided that the low field proton and deuteron spin-lattice relaxation times are a few seconds or longer. For most proton solids the proton-proton dipolar interaction is less than that of ice so that small steady fields B_0 of order $0\text{-}10 \times 10^{-4}$ T should be applied during the irradiation phase to ensure the optimum coupling between P and Q spins discussed above.

5.6 FACTORS AFFECTING NITROGEN N Q R SENSITIVITY

It has often been observed that one cannot obtain the sensitivity of detection as predicted in Chapter III and section 5.1. This can sometimes be attributed to unfavourable T_1's for either the protons or quadrupoles in the samples in question, and there is usually no way of improving these, except perhaps by performing experiments at different temperatures. In many cases the 'desirable' temperature (from the T_1 point of view) is experimentally unobtainable.

Generally speaking, however, it has been observed, that, when detecting nitrogen quadrupole resonance, it is almost always possible to obtain 'theoretical' sensitivity when working on $-NH_3^+$ or $-NH_2$ groups, while this is usually impossible in NH groups and it is always very hard to detect an N not directly bonded to an H. R.F. power levels of ~10 Gauss (peak-to-peak) are often required to detect -N lines while power ~ 0.1 Gauss pp are usually adequate for $-NH_3^+$ lines, even in the same compound.

One might suggest that, for some reason, most of the RF power fed into the upper coil of the apparatus is not reaching the nitrogen nuclei in the sample. For one explanation, and a possible solution, we return briefly to an earlier section.

In Chapter III, page 36, when discussing double resonance methods for detecting N Q R, we referred to double resonance with spin mixing in the rotating frame (D R R F) [2]. This relies on a process known as 'spin locking' for its sensitivity. As explained by EDMONDS[4], a sample containing P and Q spins comes to equilibrium in a large magnetic field B_0 (along axis OZ), the P spins acquiring a magnetisation M_0. A strong radiofrequency field B_1 is applied for a time $\tau_{90} = \pi/2\,\gamma_p B_1$ (a normal 90° pulse), so that, in the rotating frame of Chapter III, $OX'Y'Z$, M_0 precesses about B_1 until it lies along the axis OY' (see Fig.5.11). Immediately after this,

the amplitude of B_1 is maintained, but its phase is shifted by 90° in a time $\ll T_2$ so that, in the rotating frame, it too lies along OY'. REDFIELD[35] has shown that, in these circumstances, M_0 remains 'locked' to B_1 in direction and the two precess together in the laboratory frame. M_0 decays slightly to a value M_0' in a time $\approx T_2$, but thereafter decays only at a rate $\approx T_{1D}$.

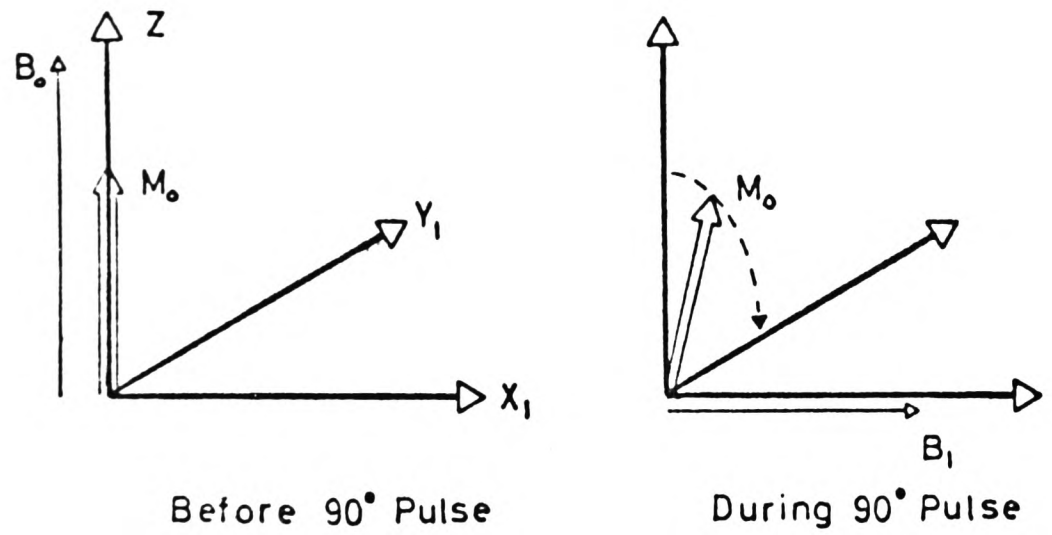
This spin locking effect (for a spin $\frac{1}{2}$ nucleus) means that the spin bath maintains its magnetisation M_0' for an unusually long time ($\sim T_{1D}$) while the R.F. field B_1 continues to exist. The spins do not give up energy, since no free induction decay is observed.

Conversely, one can say that the spins do not absorb any more energy from the R.F. field, since M_0' and B_1 remain always parallel.

One can build up the mathematical theory to show that a similar effect can happen for a spin 1 quadrupole nucleus in zero magnetic field. A rotating frame can be defined for such a nucleus[36], although it can no longer be pictured as a real rotation of coordinates. In such a rotating frame, an applied R.F. field at a quadrupole frequency ω_Q appears as a constant applied magnetic field B_Q'. If B_Q' (in the rotating frame) is made parallel to the quadrupole moment Q' (also in the rotating frame) . R.F. absorption is prevented by a similar spin-locking process. So long as B_Q' is not parallel to Q', R.F. absorption does occur, and all the other processes of the double resonance method proceed to allow detection of the quadrupole signal.

If, however, spin-locking does occur, then even application of very large R.F. fields will not increase the actual absorption by the quadrupoles (assuming always that ω_Q is a good sine wave).

The key to curing the spin-locking problem lies in the fact that power is absorbed if B_Q' is not parallel to Q'. Assuming that spin-locking



Before 90° Pulse

During 90° Pulse

Phase shift B_1

$M_o \rightarrow M_o'$ in $\sim T_2$

Fig.5.11: Spin locking (spin $\frac{1}{2}$)

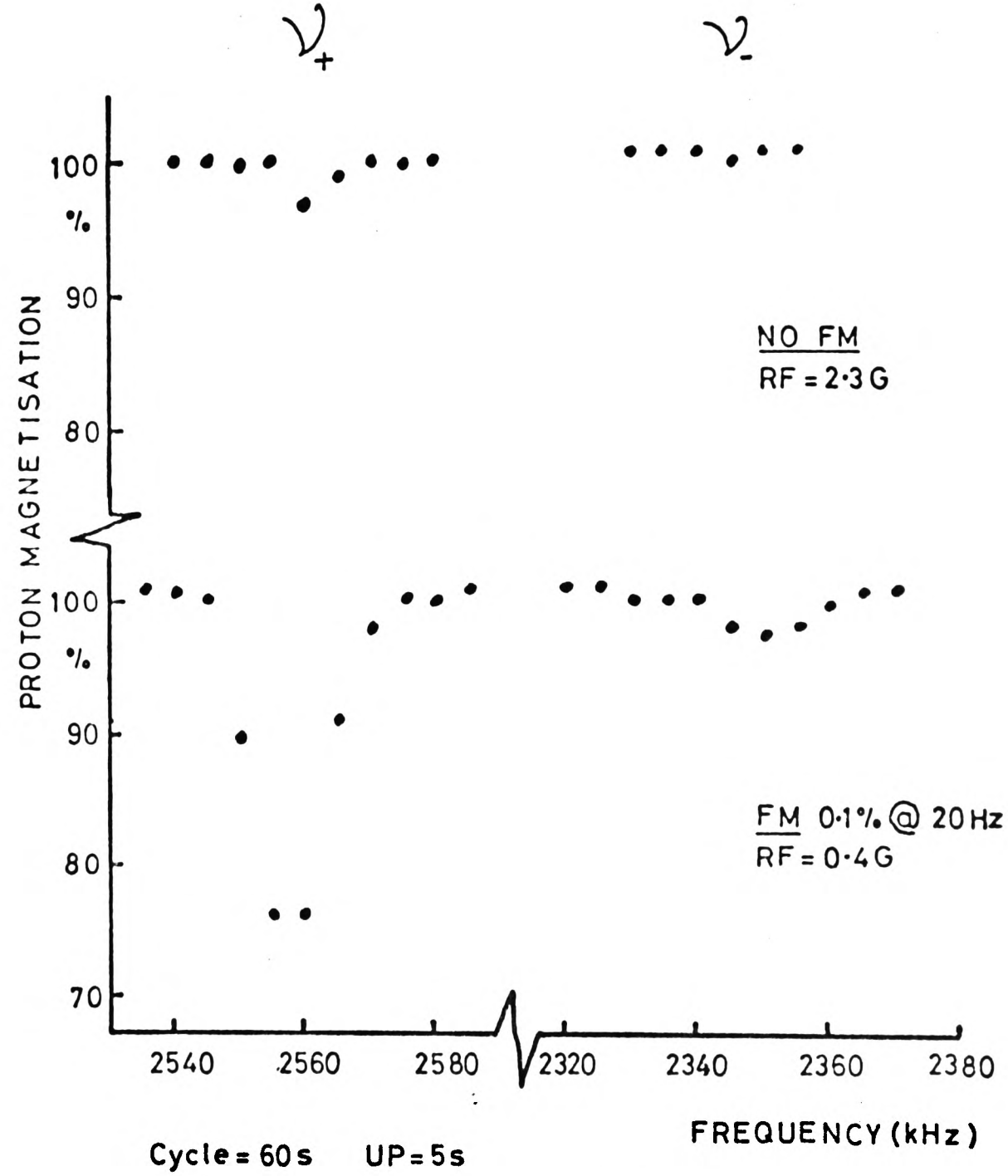


Fig.5.12: Effect of FM on NQR signals in Imidazole(-N)

has occurred ($B'_Q \parallel Q'$) a fast phase shift (in a time $< T_2$ quadrupole) of B'_Q by $\pi/2$ will allow absorption of power since then $B'_Q \perp Q'$.

The phase shift must be fast, since Q' can follow B'_Q if it changes slowly enough. After some time B'_Q is once again parallel to Q', and another phase shift must be applied. Needless to say, such fast, repeated phase shifts are somewhat difficult to generate experimentally, but it has been done[(2)].

Alternatively, one can apply a continuous phase shift, or frequency modulate ω_Q - which amounts to the same thing (if $\Delta\omega_Q <$ quadrupole line-width). F.M. is quite easy to arrange experimentally (note in apparatus section), and does produce useful effects, as outlined below, although it is not as effective as a true phase-shift oscillator system might be.

5.6.1 Experimental Observations

(Data from reference (4) are reproduced in Table 5.1).

Figures 5.12 and 5.13 show the spectra of the N and NH multiplets in Imidazole. The upper traces are taken using a conventional R.F. source, while the lower traces use a source frequency modulated at $f_0 \pm \Delta f$, where $\Delta f = 3\,kHz$, and the modulation frequency is 20 Hz. Other experimental conditions are kept constant - cycle time is 60 seconds and up time is 5 seconds, although a high R.F. intensity of 2.3 Gauss pp is required to produce a recognisable signal from the N site.

The improvement when using FM is immediately apparent: sensitivity for both ν^+ and ν^- is increased by a factor ~ 10, although the R.F. intensity is reduced to only 0.4 Gauss pp, (Fig.5.12). Fig.5.13 also shows considerable improvement, but with no change in R.F. intensity (0.4 Gauss in both cases). Measurements on $-NH_2$ and $-NH_3^+$ groups, however, reveal no improvement in sensitivity.

One may explain the above observations by postulating that spin-locking occurs readily to an isolated N, less so to an NH, and not at all

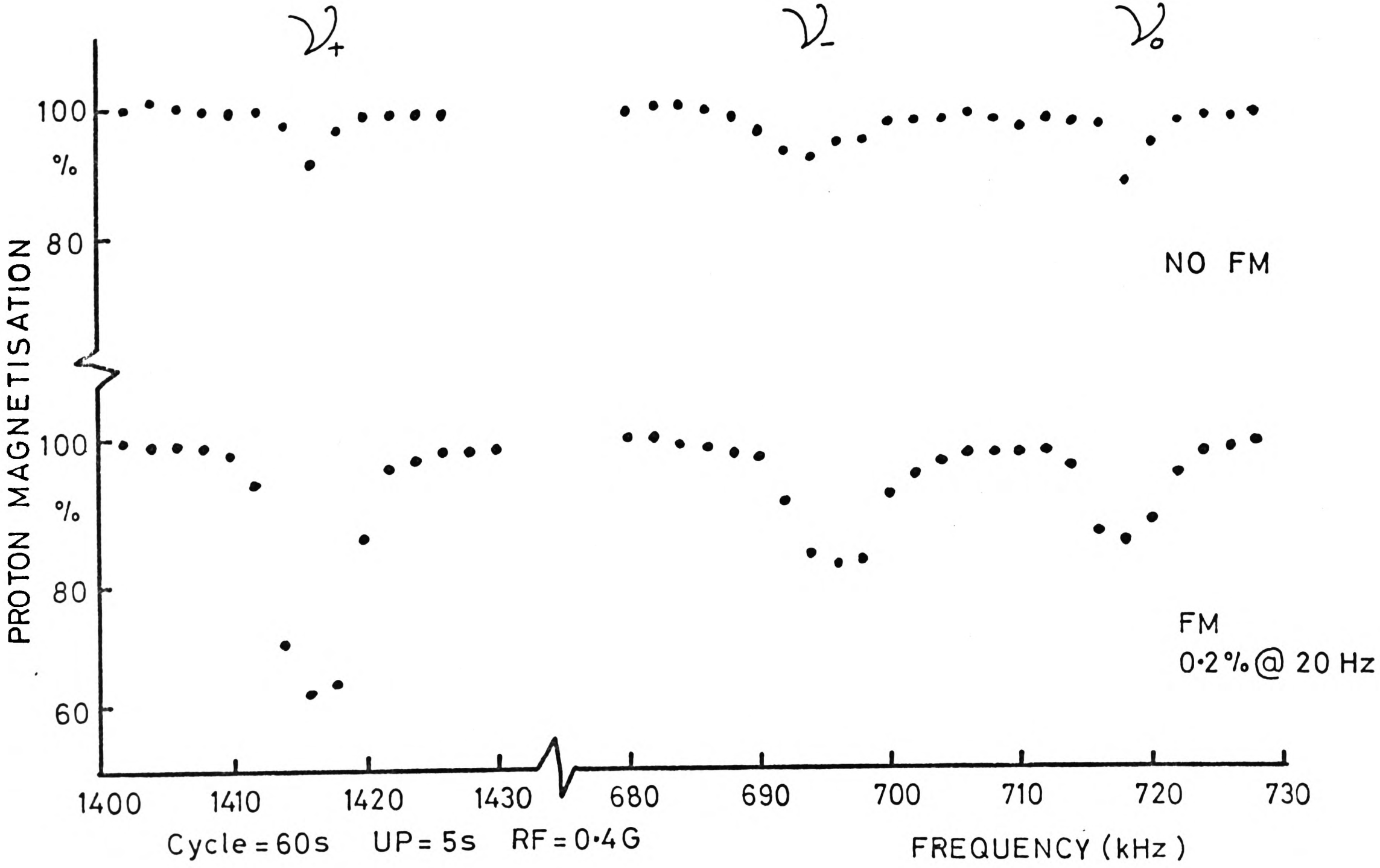


Fig. 5.13: Imidazole-effect of FM on -NH signals

to an $-NH_3^+$ or $-NH_2$. The immediate environment of an isolated N usually consists of atoms of ^{12}C (spin 0) with no magnetic moments, and hence any local magnetic fields at the N site are very weak. When an R.F. field B_Q is applied, it principally defines the magnetic environment of the quadrupole nucleus, and the quadrupole will readily lock on to such a field, if it oscillates at a quadrupole frequency.

A nitrogen bonded to two or three protons, however, experiences strong local fields due to their magnetic dipole moments; when an external R.F. field B_Q is applied, usually much weaker than the internal fields, the quadrupole moment is unable to lock on to B_Q, and the full possible absorption of power can occur.

An NH group is intermediate between the two extremes, since the dipole field of a single proton is proportionately weaker. Some spin locking occurs, but is not usually serious enough to cause detection problems, as in the case of an isolated -N.

FM has a secondary undesirable effect in that it broadens the quadrupole line. This broadening is a function of the frequency sweep Δf, and can be much reduced by making Δf sufficiently less than the quadrupole linewidth. Experience has shown that modulation frequencies in the range 4 Hz - 40 Hz are almost equally effective, and that any limitations seem to be mostly instrumental.

We found that a modulation frequency of 20 Hz, with $\Delta f = 0.1\%\ f_0$ (i.e. $\pm$ 3 kHz at 3 MHz) was ideal in most cases, and built a modulation unit to work under those conditions.

It must be remembered that use of FM does not improve sensitivity in the same way as continuous coupling. FM merely allows us to attain the sensitivity which we would theoretically expect from level crossing calculations. Continuous coupling changes the level crossing arguments, by

introducing additional connections between the proton bath (P spins) and quadrupoles (Q spins). For nitrogen NQR we may sometimes weakly connect the protons to the nitrogens via the ν_0 transition. For deuterium NQR, we always have this ν_0 connection, and additionally have some connection through the ν^+, ν^- transitions, so that all three deuterium levels are, to some extent, in contact with the proton spin bath. Additionally, the amount of such 'connection' may be altered by applying suitable magnetic fields.

Deuterium NQR will always be more sensitive than Nitrogen NQR (in this apparatus) simply because the width of the zero field proton bath is sufficient to encompass the whole span of the deuterium quadrupole energy levels. As a result, 'level crossing' calculations of sensitivity are almost meaningless in the case of deuterium.

5.6.2 Continuous Coupling of ν_0 and Nitrogen NQR

We have seen that continuous coupling of ν_0 alone should improve the sensitivity of detection of ν_+ and ν_-, relative to that obtainable by level crossing alone. We have additionally seen that the use of frequency modulation techniques 'improves' the sensitivity of ν_+ and ν_- transitions, but only by ensuring that quadrupole transitions are saturated by the irradiation - the total effect on the proton spin bath is still limited by the relative abundances of the P and Q spins.

To further investigate sensitivity limitations in nitrogen NQR, we carried out experiments on a number of model compounds, these being examples of $-NH_3^+$, $-NH$ and $-N$ groups. As shown for deuterium, application of small D.C. fields enhances the sensitivity of detection of quadrupole lines, by assisting the coupling between the quadrupole and dipole (proton) systems. We set out to investigate whether application of D.C. magnetic fields during the irradiation phase might enhance detection of ν^+ and ν^- lines, by coupling the ν_0 transition of the N to the proton spin bath.

It is important to remember that we can only couple ν_0 to the P spin bath. e^2qQ is always relatively large for nitrogen, so that ν_+ and ν_- cannot be coupled to the P spins except by application of a very large magnetic field (as during level crossing). Since we are concerned only with the effects of coupling ν_0 levels to the P spins, sensitivity will always be 'Q-spin saturation limited', and such methods are not applicable to NQR in samples with low concentrations of nitrogen, or other Q spins. We are mainly interested in achieving the theoretical sensitivity outlined in the first section of this chapter.

An examination of the available data[4] readily reveals that many nitrogen ν_0's lie in the range 50-400 kHz, if the nitrogen is bonded to either three, one or no hydrogens. NH_2 groups always have relatively large η and $\nu_0 > 400$ kHz. The existing apparatus has the facility to apply D.C. fields during irradiation of up to ~ 90 Gauss. Since this corresponds to a proton NMR frequency of ~380 kHz, it is not possible to attempt resonant coupling to nitrogens with ν_0 greater than this figure.

As suitable models we chose Imidazole and L-Histidine as examples of an isolated N in a carbon ring; indole as an example of an NH group in a carbon ring; and glycine and D-L serine as examples of the NH_3^+ group in amino acids. All the above have $\nu_0 < 380$ kHz.

All experiments were performed at 77°K. The known[4] values of ν_+, ν_- and ν_0 are given in Table 5.1, together with the value of static magnetic field B, such that $\nu_0 = \nu_p = \gamma_p B$ where γ_p = magneto-gyric ratio of protons/2π .

TABLE 5.1

(from reference (4))

Compound	Site	ν^+ (kHz)	ν^- (kHz)	ν_0 (kHz)	B (Gauss)
Imidazole	N	2556	2345.5	210.5	49.3
Imidazole	NH	1417	719.0	698.0	-
L-Histidine (mono)	N	2631	2411.0	220.0	51.8
Indole	NH	2305	(2030)	275.0	64.7
Glycine	NH_3^+	1093	780.0	313.0	73.6
D-L Serine	NH_3^+	949	875.0	(74)	(17.4)

The value of the 'background signal' (the net proton signal for $\nu_{IRR} \neq \nu_+$ or ν_-) increases somewhat as B increases from zero. In these samples, the proton T_{1D} is not, in general, long. However, as B increases, T_{1D} increases also (see Chapter VIII), so that the final measured magnetisation increases. In Chapter III, we wrote $p''' = \pi(p'') + \Delta(a'',b'',c'')$. $\pi(p'')$ is that part of p''' (the final measured magnetisation) which depends on p'', the P spin population difference at the end of the irradiation phase. If T_{1D} is infinite, then $p'' = p'$, the P spin magnetisation at the beginning of the irradiation phase. If $T_{1D} = 0$, $p'' = 0$ and $\pi(p'') = 0$. Thus as T_{1D} increases, p'' increases and hence $\pi(p'')$ increases, producing an increase in p''' (the measured magnetisation).

The ν^+ and ν^- lines were measured, keeping cycle time, up time and R.F. intensity constant, varying only the static field B. A comparison between the background and the region near the ν^+ and ν^- line centres gives a measure of the sensitivity of detection, so long as the other factors are held constant. Fig.5.14 shows the intensity of ν^+ and ν^- as a function of field for Imidazole and Mono-L-Histidine.

In both cases a dramatic increase in sensitivity occurs when the static field passes through its 'resonant' value. For Imidazole, the ν_-

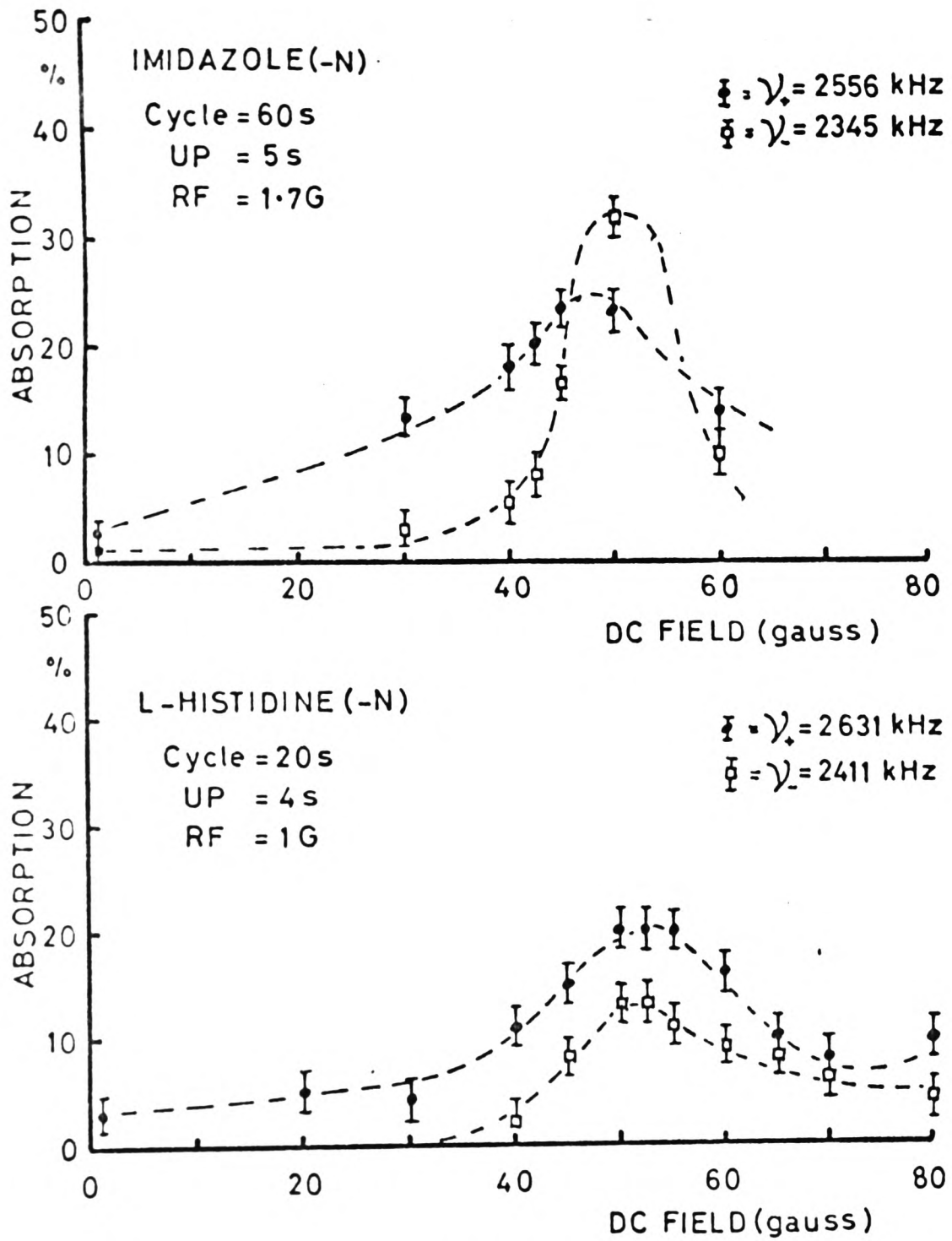


Fig. 5.14: Effect of ν_0 coupling (-N)

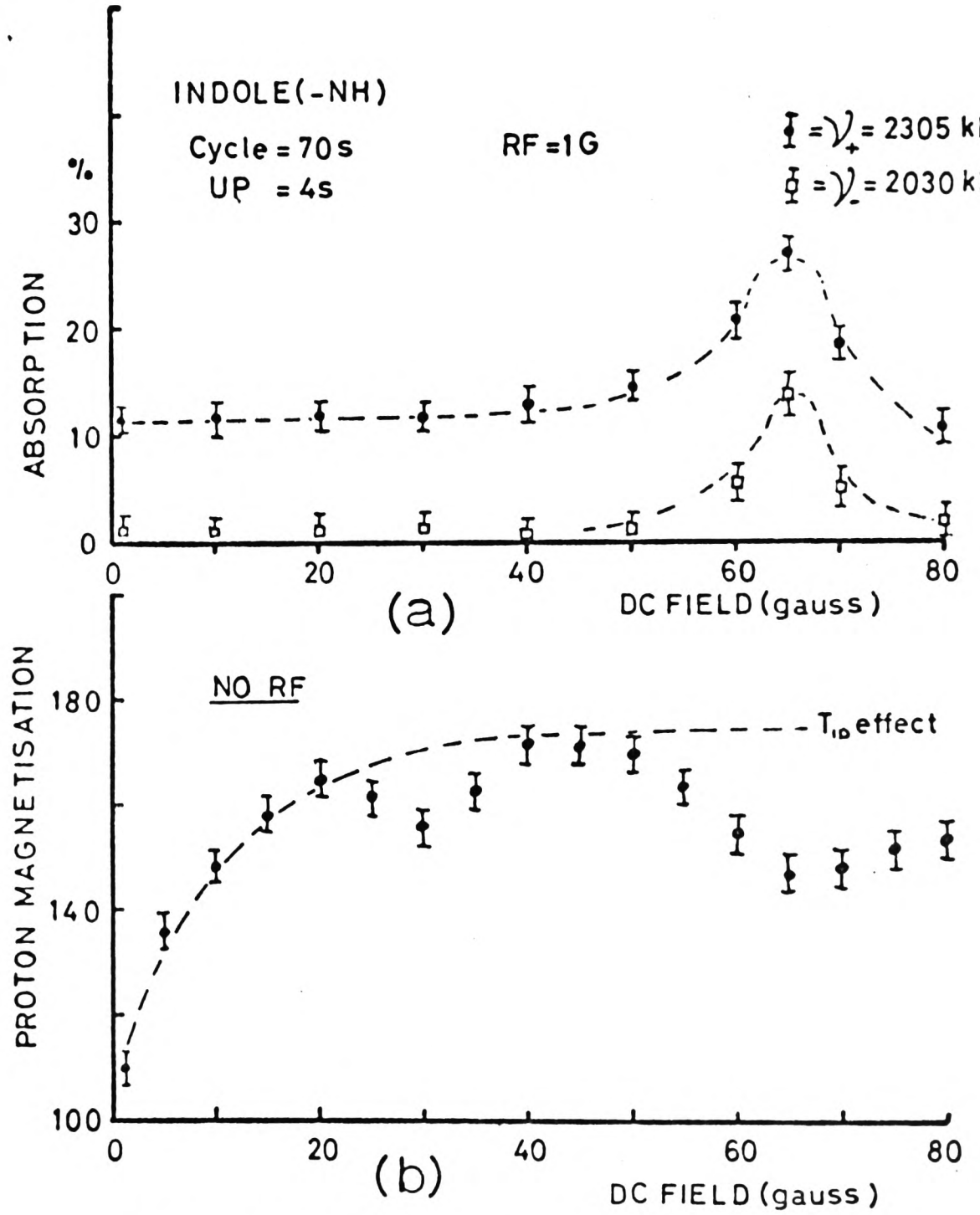


Fig. 5.15: ν_0 coupling effects in Indole (-NH)

line increases in intensity from zero (undetectable) to over 30% absorption, when it is in fact larger than ν_+. (But ν_- is a very sharp line in imidazole , so its area < area of ν_+.) The resonance effect is quite sharp, being fully effective only for B = 50 Gauss ± 10.

Figure 5.15(a) shows much the same effect in indole , the resonance in this case being at B = 65 ± 10 Gauss.

The results for glycine and D-L serine, Fig.5.16, must be taken as a pair. D-L serine, with its low ν_0, is continuously coupled even in zero field, and exhibits a high sensitivity for detection of ν^+ and ν^-. Increasing the applied field B decreases the sensitivity of detection. Glycine, conversely, has a large ν_0 , and application of large static fields is needed to produce continuous coupling. For these compounds, the range of fields suitable for continuous coupling is very wide - stretching out to 30 Gauss on either side of the resonant value. This may be due to the strong local fields generated by the protons in the $-NH_3^+$ group, which would have the effect of producing a broad spread of fields around any externally applied value.

The general conclusion, however, is a simple one. Continuous coupling of ν_0 can be induced by applying suitable D.C. fields in any nitrogen compound. We would expect the same to be true of an $-NH_2$ group, although it was not possible to examine this experimentally, due to the limitations of the apparatus.

Unlike ^2D , large fields can be applied to nitrogen compounds without adversely affecting the position or width of quadrupole lines, due to the large nitrogen quadrupole moment, (and the fact that the spin 1 nucleus is quenched). No significant shifts in line centres were observed during the compiling of this data.

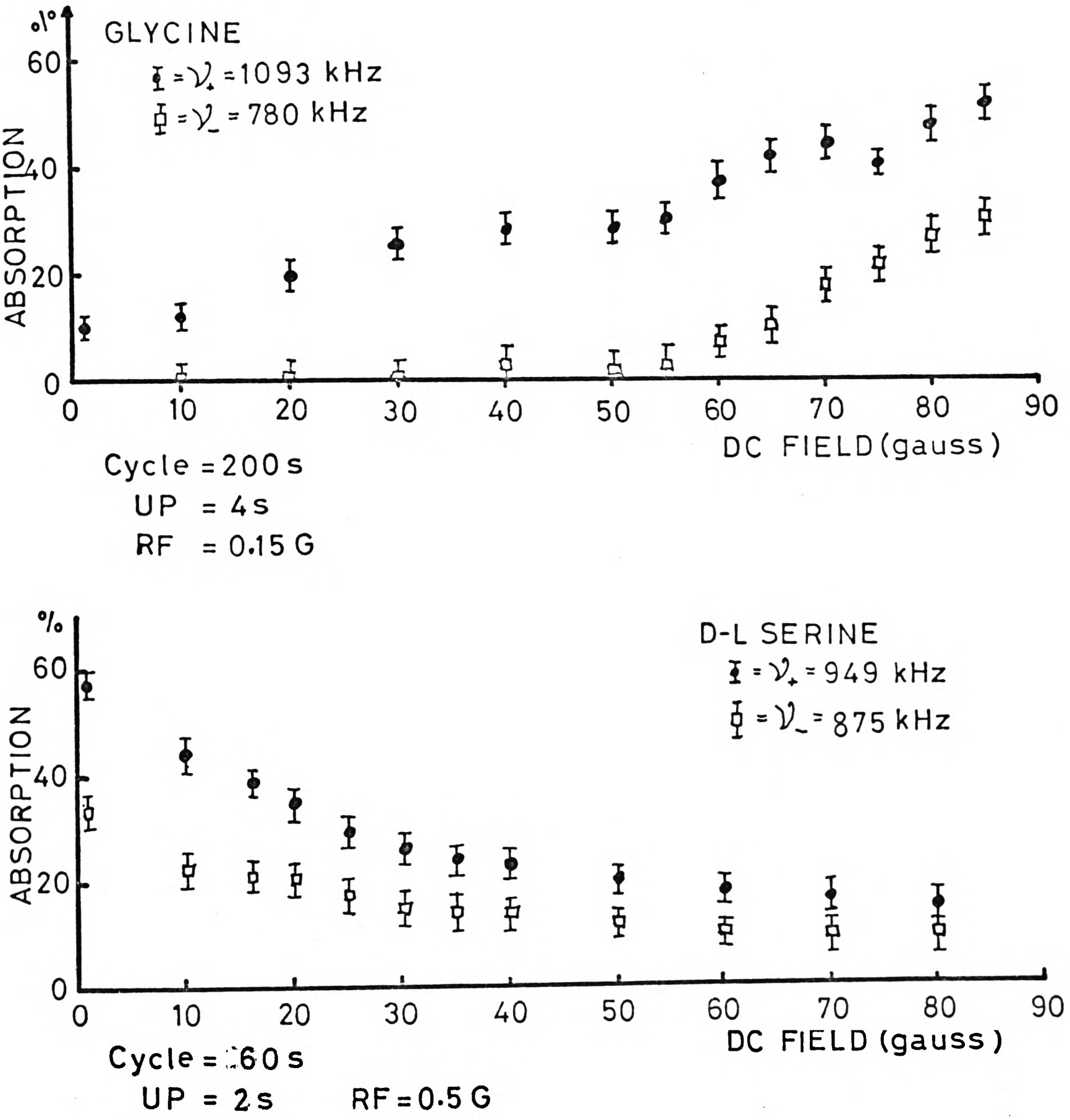


Fig. 5.16: Effect of ν_0 coupling on NQR in $-NH_3^+$ groups

An interesting effect was also observed in Indole, Fig.5.15(b). Using no irradiation, keeping cycle time and up time constant, the final proton magnetisation was measured, varying only the static field between cycles. The resulting graph shows dips when $B = \frac{\nu_0}{2\gamma_p}$ and $B = \frac{\nu_0}{\gamma_p}$, indicating that polarisation can pass between the P and Q systems when the above conditions on B are satisfied. The general 'background slope' may be attributed to the increase in proton T_{1D} with static field. This method has in fact been used for detecting ν_0 in certain double resonance experiments[37].

It can be seen that continuous coupling of ν_0 produces an apparent large increase in sensitivity of detection of ν_+ and ν_- in nitrogen NQR. However, this large improvement is mainly due to the fact that the zero-field sensitivity of all the above compounds except D-L serine is less than one would expect from basic theory. We have already seen that the use of F.M. irradiation also produces an apparent increase in sensitivity, due to the prevention, or partial prevention, of spin-locking effects.

The improvements in the cases of FM and resonant coupling of ν_0 are of a similar order of magnitude, and a comparison of the two effects shows that they are essentially the same in origin. Table 5.2 compares the effects for imidazole and indole. It can be seen that either coupling ν_0 or using FM and also saturating ν_0 (double irradiation) produce almost the same effect. Saturation of ν_0 (as shown earlier) tends to make ν_+ and ν_- equally sensitive. Making the P spin bath resonant with ν_0 thus seems to have two effects, viz:

(1) the P spins pump the ν_0 transition;

(2) the oscillating magnetic fields of the P spin dipoles with $\nu_p \approx \nu_0$ overcome the effects of spin locking in much the same way as FM or phase-shifting.

TABLE 5.2

The apparatus was initially adjusted to give the same zero-field zero-irradiation signal in both cases. (Signal = 110 units).

Compound	Group	Conditions			Net Absorbtion (arbitrary units)	
		Resonant Field	F M	ν_0 (Double Irradiation)	ν_+	ν_-
Imidazole	-N	NO	YES	NO	30	5
		YES	NO	NO	30	30 (narrow line)
		NO	YES	YES	25	18
Indole	-NH	NO	YES	NO	12	2
		YES	NO	NO	20	9
		NO	YES	YES	26	14

5.7 CONCLUSION

Nitrogen NQR sensitivity is always limited by the number of Q spins available, relative to the number of P spins. However, one cannot always achieve the theoretical sensitivity predicted by simple level-crossing theory, if simple low-power irradiation is used for searching for the quadrupole resonances.

However, if one can ensure true saturation of the quadrupole transitions ν_+ and ν_-, then one does indeed achieve the sensitivity predicted in Chapter 3, as slightly modified if necessary by the calculation at the beginning of this chapter (for ν_0 coupling). Experimentally, one can achieve this <u>either</u> by making ν_0 resonant with the P spin frequency (by applying a magnetic field during irradiation) <u>or</u> by using frequency-modulated R.F. to search for ν_+ and ν_-, while saturating ν_0 by a double irradiation technique.

Knowledge of these effects in nitrogen NQR has allowed investigation of several substances which give no usable results when special effects such as F.M. are not employed, (see Chapter VI).

CHAPTER VI

USES OF HIGH-SENSITIVITY NQR

6.1 INTRODUCTION

The improvements in detection of NQR signals which were described in Chapter V were used in two short studies. Continuous coupling in ^{2}D NQR allows the study of samples with relatively small amounts of deuterium. This was used to test the theories of earlier published work on fully deuterated compounds.

Secondly, an NQR investigation of the organometallic complex Lanthanum Nicotinate Dihydrate was carried out using F.M. techniques, after normal irradiation methods had failed to provide sufficient information for a complete analysis to be attempted.

6.2 D-D AND H-D INTERACTIONS IN AMIDE GROUPS AND WATER MOLECULES

In a paper which we shall refer to as I,[38] the deuterium quadrupole resonance spectrum of the fully deuterated amide group in acetamide, thioacetamide, nicotinamide and propionamide and that of D_2O as water of crystallization in L-serine hydrate, was published. A characteristic multiplet line structure was observed which was shown to be the result of magnetic dipolar interaction between two deuterons in very similar electric field gradients. The manner in which the dipolar interaction between the deuterons perturbs the energy levels of the two deuterons due to the quadrupole interaction and thus gives rise to the multiplet spectral line structure is indicated in Fig.6.1, which is reproduced from I.

Figure 6.1(a) shows the two sets of three energy levels of the two deuterons in similar electric field gradients. The levels are labelled in the conventional way (reference (4) and Chapter III) and the deuteron with the larger ν^+ frequency (higher Y level) is arbitrarily defined as 1.

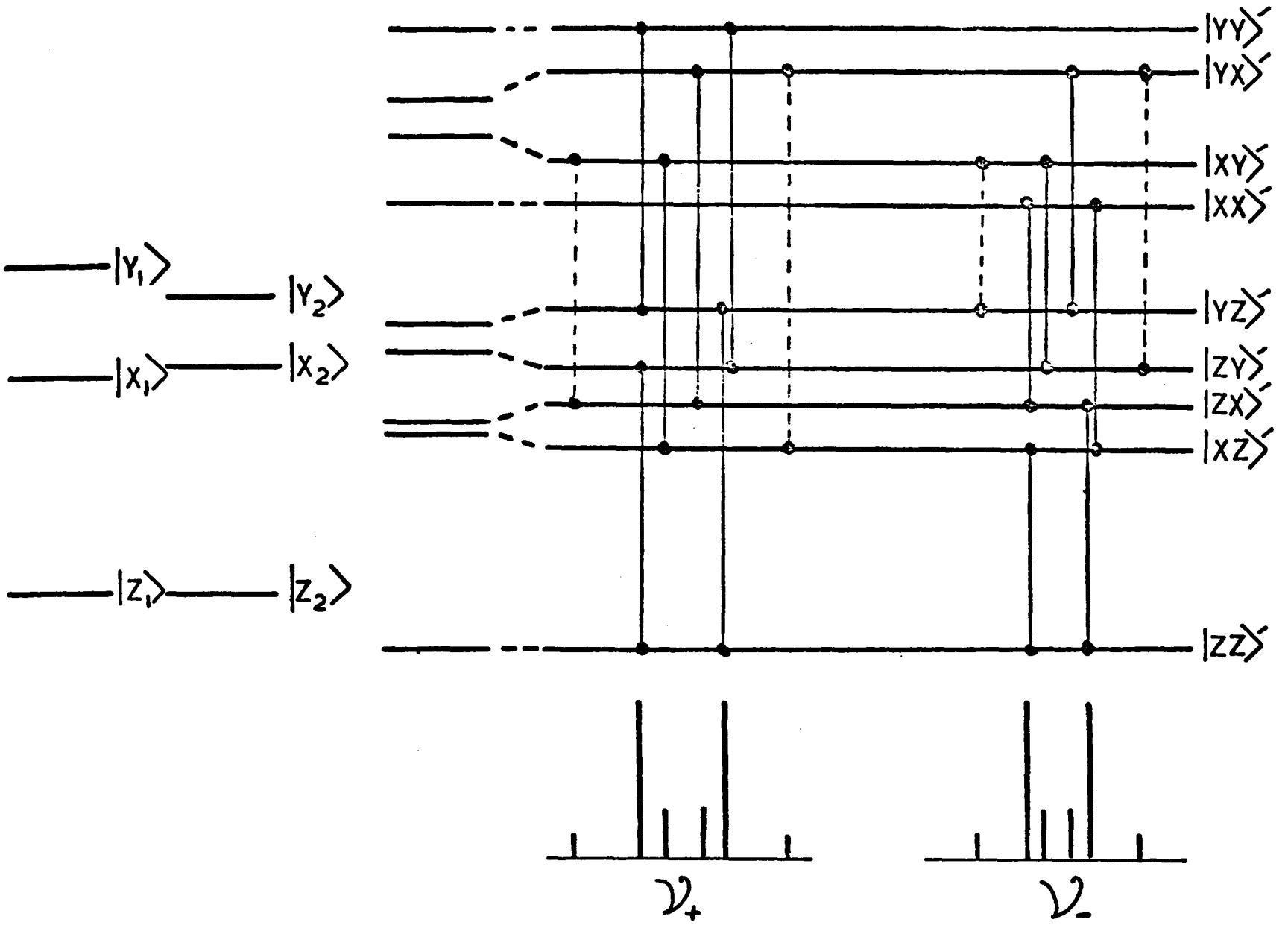


Fig.6.1:(a) Energy levels of 2 deuterons in similar EFG's

(b) Combined level diagram with no interactions

(c) Including magnetic dipolar interaction (ν_+, ν_- multiplets also shown)

Figure 6.1(b) shows the combined energy level scheme assuming no interactions. The notation $|XZ\rangle$ then represents a state in which nucleus 1 is in a state $|X\rangle$ and nucleus 2 is in a state $|Z\rangle$. In fact, due to their proximity in space, there is a magnetic dipole-dipole interaction between the two deuterons, which changes the energy levels as in Fig.6.1(c), the notation $|XZ\rangle'$ representing the perturbed energy level.

First-order perturbation theory predicts that the perturbed and unperturbed energy levels are related by an equation of the form (taking the YZ levels as an example):

$$E'(YZ),\ E'(ZY) = \tfrac{1}{2}\left[E(YZ) + E(ZY)\right] \pm \left[\left\{E(YZ) - E(ZY)\right\}^2 + 4|D_{YZ}|^2\right]^{\frac{1}{2}}$$

where $E'(YZ)$ represents the energy of the state $|YZ\rangle'$ and the terms D_{YZ} are given by relationships of the form

$$D_{YZ} = \langle YZ|\mathcal{H}_{DIP}|ZY\rangle = \langle ZY|\mathcal{H}_{DIP}|YZ\rangle = (\gamma_D^2 \hbar^2)/r^3\ F(\theta_0)$$

with $\mathcal{H}_{DIP}$ = full Van Vleck Dipolar Hamiltonian (reference (12), p.103).

γ_D = gyromagnetic ratio of the deuteron

r = distance between the two deuterons

θ_0 = $D\hat{O}D$ or $D\hat{N}D$ bond angle ($\phi = 0$)

and $F(\theta_0) =$ 1 for D_{XZ}

$$F(\theta_0) = -\left[2\cos^2\frac{\theta_0}{2} + \sin^2\frac{\theta_0}{2}\right] \quad \text{for} \quad D_{YZ}$$

$$F(\theta_0) = +\left[2\sin^2\frac{\theta_0}{2} + \cos^2\frac{\theta_0}{2}\right] \quad \text{for} \quad D_{XY}$$

We are only concerned with pairs of states whose separations are comparable with the matrix elements of the magnetic dipolar interaction (D), and hence only the shifts in the pairs of levels $|XZ\rangle$ and $|ZX\rangle$, $|ZY\rangle$ and $|YZ\rangle$, and $|XY\rangle$ and $|YX\rangle$ are of significance. The effects on states separated by larger energy differences will be small due to the large energy denominator in the admixture coefficient. Similarly, the dipolar interaction due to the neighbouring nitrogen nucleus (in amides) may also be ignored.

Making some assumptions about the directions of the principal components of the electric field gradient and about the geometry of the site, it was possible to reduce the six line multiplets to doublet lines which would be observed in the absence of magnetic dipolar coupling between the two deuterons. These frequencies for formamide at 77 K, acetamide at 77 K, acetamide at 300 K and D_2O in L-serine hydrate at 77 K are listed in the first column of Table 6.1. These results are taken from I except for those of formamide which we measured subsequently. At 77 K the ν_+ multiplet of formamide ($H.CO.ND_2$) consists of only two principal lines at 152.3 ± 0.1 and 158.05 ± 0.1 kHz whilst the ν_- multiplet consists of four resolved lines, principal lines at 136.95 ± 0.2 and 140.20 ± 0.2 kHz and weaker subsidiary lines at 134.6 ± 0.2 and 142.7 ± 0.2 kHz. The data in the first column of Table 6.1 were obtained by following the procedures laid down in I.

Given sufficient detection sensitivity, it is of course possible to eliminate the deuteron-deuteron interaction by using a specimen sufficiently dilute in deuterium. For example, if only 10% of the exchangeable protons are replaced by deuterons, then the probability that both proton sites in an amide group or water molecule are deuterated is only 1%. The dominant signals detected will be from N D H or H D O groups. The deuteron quadrupole resonance lines detected in formamide, acetamide and L-serine hydrate are listed in the second column of Table 6.1 using specimens in which the probability of deuteron substitution for a single exchangeable site was 5%, 10% and 20% respectively. In each case only two ν_+ lines and two ν_- lines were detected corresponding to the two slightly inequivalent deuteron sites. There is no multiplet structure as is to be expected in the absence of deuteron-deuteron interaction. On comparing the first two columns of Table 6.1, it is seen that the lines measured in the deuterium diluted samples have consistently higher ν_+ frequencies and consistently lower ν_- frequencies. We will now show that this is predominantly due to magnetic dipolar interaction between proton and deuteron.

TABLE 6.1

A comparison between the spectral lines obtained in samples 100% enriched and lightly enriched at the amide or water site. In each case the calculated effect of deuteron-deuteron or proton-deuteron interaction is allowed for.

Compound	Temperature [K]	Line	Line frequency measured in 100% D sample and corrected for D-D interaction [kHz]	Line frequency measured in sample dilute in deuterium [kHz]	Line frequency measured in dilute sample corrected for deuterium-proton interaction [kHz]	Difference $\nu_{conc} - \nu_{dilute}$ each corrected for interaction [kHz]
Formamide	77	ν_+	157.95 ± 0.2	158.6 ± 0.2	158.0 ± 0.3	0 ± 0.5
		ν_-	140.25 ± 0.2	139.8 ± 0.2	140.3 ± 0.3	0 ± 0.5
		ν_+	152.10 ± 0.2	152.5 ± 0.2	151.9 ± 0.3	+0.2 ± 0.5
		ν_-	136.95 ± 0.2	136.2 ± 0.2	136.7 ± 0.3	+0.3 ± 0.5
Acetamide	77	ν_+	154.77 ± 0.2	155.45 ± 0.2	154.8 ± 0.2	0 ± 0.4
		ν_-	137.30 ± 0.2	137.00 ± 0.2	137.5 ± 0.2	-0.2 ± 0.4
		ν_+	154.49 ± 0.2	154.65 ± 0.2	154.0 ± 0.2	+0.5 ± 0.4
		ν_-	139.34 ± 0.2	139.10 ± 0.2	139.6 ± 0.2	-0.3 ± 0.4
Acetamide	300	ν_+	155.44 ± 0.2	155.50 ± 0.3	154.9 ± 0.3	+0.5 ± 0.5
		ν_-	141.59 ± 0.2	141.50 ± 0.3	142.0 ± 0.3	-0.4 ± 0.5
		ν_+	154.93 ± 0.2	155.50 ± 0.3	154.9 ± 0.3	0 ± 0.5
		ν_-	138.45 ± 0.2	138.10 ± 0.3	138.6 ± 0.3	-0.2 ± 0.5
Water in L-Serine Hydrate	77	ν_+	186.79 ± 0.2	187.2 ± 0.2	185.5 ± 0.3	+1.3 ± 0.5
		ν_-	173.71 ± 0.2	173.0 ± 0.2	174.3 ± 0.3	-0.6 ± 0.5
		ν_+	184.23 ± 0.2	184.2 ± 0.2	182.5 ± 0.3	+1.7 ± 0.5
		ν_-	171.08 ± 0.2	170.3 ± 0.2	171.6 ± 0.3	-0.5 ± 0.5

Using the same notation as I, the Hamiltonian of the $I = 1$ deuteron in the electric field gradient is

$$\mathcal{H}_Q = K\left[3I_z^2 - I(I+1) + \eta\,(I_x^2 - I_y^2)\right]$$

where $K = e^2qQ/[4I(2I-1)]$. One set of eigenvectors and eigenvalues are

$$|X\rangle = [1/(2)^{\frac{1}{2}}](|+1\rangle - |-1\rangle); \quad E_x = (1-\eta)K$$

$$|Y\rangle = [1/(2)^{\frac{1}{2}}](|+1\rangle + |-1\rangle); \quad E_y = (1+\eta)K$$

$$|Z\rangle = |0\rangle \quad ; \quad E_z = -2K$$

where $|+1\rangle$, $|0\rangle$, and $|-1\rangle$ are the eigenvectors of the spin 1 quantized along the Z-axis. The coordinated axes are chosen as in I with the z-axis along the N-D or O-D bond, the X-axis perpendicular to the bond axis and in the D N H or D O H plane, and the Y-axis perpendicular to this plane.

We will assume that in zero applied magnetic field the two energy levels of the $S = \frac{1}{2}$ proton are degenerate but that there exists a magnetic dipolar interaction between the neighbouring proton and deuteron of the usual form.

$$\mathcal{H}_{DH} = (\gamma_H\gamma_D\hbar^2/r^3)\left[A + B + C + D + E + F\right]$$

where γ_H and γ_D are the gyromagnetic ratios of the proton and deuteron, r is the distance between them and $A = I_zS_z(1 - 3\cos^2\theta)$ etc. are the usual Van Vleck[12, p.103] terms. The line joining the deuteron to the proton makes polar angles θ and $\phi = 0$ in the set of axes O X Y Z defined above. Using the notation $|X\rangle\ |+\frac{1}{2}\rangle$ to represent the state in which the deuteron is in a state $|X\rangle$ and the proton is in a state $|+\frac{1}{2}\rangle$ we may write the Hamiltonian matrix of the coupled two spin system

	$\|Y\rangle\|+\frac{1}{2}\rangle$	$\|Y\rangle\|-\frac{1}{2}\rangle$	$\|X\rangle\|+\frac{1}{2}\rangle$	$\|X\rangle\|-\frac{1}{2}\rangle$	$\|Z\rangle\|+\frac{1}{2}\rangle$	$\|Z\rangle\|-\frac{1}{2}\rangle$
$\|Y\rangle\|+\frac{1}{2}\rangle$	$(1+\eta)K$	0	$\frac{1}{2}L$	N	$\frac{1}{2}(N+P)$	$M+U$
$\|Y\rangle\|-\frac{1}{2}\rangle$	0	$(1+\eta)K$	P	$-\frac{1}{2}L$	$M+V$	$-\frac{1}{2}(N+P)$
$\|X\rangle\|+\frac{1}{2}\rangle$	$\frac{1}{2}L$	N	$(1-\eta)K$	0	$\frac{1}{2}(N-P)$	$(U-M)$
$\|X\rangle\|-\frac{1}{2}\rangle$	P	$-\frac{1}{2}L$	0	$(1-\eta)K$	$(M-V)$	$\frac{1}{2}(P-N)$
$\|Z\rangle\|+\frac{1}{2}\rangle$	$\frac{1}{2}(N+P)$	$M+U$	$\frac{1}{2}(P-N)$	$M-U$	$-2K$	0
$\|Z\rangle\|-\frac{1}{2}\rangle$	$M+V$	$-\frac{1}{2}(N+P)$	$V-M$	$\frac{1}{2}(N-P)$	0	$-2K$

where

$$L = (1-3\cos^2\theta)\,\alpha \quad ; \quad M = -\tfrac{1}{4}(1-3\cos^2\theta)\,\alpha$$

$$N = P = -\tfrac{3}{2}(\sin\theta\cos\theta)\,\alpha \; ; \; U = V = -\tfrac{3}{4}(\sin^2\theta)\,\alpha$$

and

$$\alpha = (\gamma_H \gamma_D \hbar^2/r^3) \; .$$

In order to find the eigenvalues of the coupled spins, the matrix may be diagonalized or, because the dipolar interaction is small in comparison with the quadrupolar splitting, first order perturbation may be used with $\mathcal{H}_{DH}$ a small perturbation on $\mathcal{H}_Q$. For the amides we assume, as in I, an N-H bond length of 0.1 nm (1 Å) and a $D\hat{N}H$ angle of 124°, leading to $r = 0.177$ nm (1.77 Å) and $\theta = 152°$. The perturbed eigenvalues of the deuteron become

$$E'_y = E_y + 0.56 \times 10^3\,h$$

$$E'_x = E_x - 0.51 \times 10^3\,h$$

$$E'_z = E_z - 0.05 \times 10^3\,h$$

so that the effect of the HD interaction is to increase ν_+ by 0.61 kHz and to decrease ν_- by 0.46 kHz. Corrections for these shifts are applied in the third column of Table 6.1. For D_2O in L-serine hydrate, again using the values quoted in I of O-D bond length = 0.095 nm and $D\hat{O}H$ angle 106.6° we obtain

$$E'_y = E_y + 1.55 \times 10^3\,h$$

$$E'_x = E_x - 1.44 \times 10^3\,h$$

$$E'_z = E_z - 0.11 \times 10^3\,h$$

Thus in DOH we would expect the dipolar interaction to increase ν_+ by 1.66 kHz and to decrease ν_- by 1.33 kHz.

In the fourth column of Table 6.1 we list the difference between the line frequencies deduced in the concentrated specimen, correcting for dipolar deuteron-deuteron interaction, and the dilute sample, correcting for proton-deuteron interaction. For the amides it is seen that, to within the errors, the two sets of frequencies agree, so that the electric field gradient experienced by a deuteron at one site does not depend upon whether the other site is occupied by a deuteron or a proton.

For water in L-serine hydrate, there exists a systematic disagreement which indicates either that the corrections applied are in error, or that there is a difference of electric field gradient at one site depending on the occupation of the other by a proton or deuteron. It is known (appendix,(4)) that there is a substantial shift of the NQR of ^{14}N if a bonded proton is replaced by a deuteron. Often such differences are explained by the change in either thermally activated or zero-point motion due to the changing mass on deuteration. It has been shown previously that the quadrupole coupling constant e^2qQ/h of the deuteron depends predominantly upon the N-D or O-D distance[39], but this is of course dependent upon the hydrogen bond strength[40] and thus will be affected by motion even if the covalent bonds in the molecular group itself are regarded as rigid.

As a check on possible thermally activated motion effects, the spectra for L-serine hydrate and formamide both dilute in deuterium were repeated at 4°K, but no change from the results obtained at 77°K was detected. This does not, of course, rule out zero-point motion effects and it may well be that the apparent change in the D_2O to HDO spectra is due to motion of the relatively light water molecule that changes on deuteration.

Having determined the two ν_+ and two ν_- frequencies, as in Table 6.1, it is necessary to assign them to the two deuteron sites so that the quadrupole coupling constants may be deduced. Such an assignment was attempted in I using the measured intensity and splitting of the constituents of

a multiplet. With the high sensitivity of DRCC it is however possible to assign the lines directly and experimentally using nuclear double quadrupole resonance on the same 100% deuterated specimens used in I. Double quadrupole resonance is an example of the solid state effect in which two interacting deuteron spins simultaneously flip[40,4], absorbing a single radio-frequency photon. The transition probability for such a simultaneous flip is low, so that high sensitivity is required. If we label the two transition frequencies of the deuteron at site 1 as $\nu_+(1)$ and $\nu_-(1)$, with those for the deuteron at site 2 as $\nu_+(2)$ and $\nu_-(2)$, it is easily seen that the double quadrupole resonance spectrum may contain frequencies $\nu_+(1)+\nu_-(2)$, $\nu_+(1)+\nu_+(2)$, $\nu_-(1)+\nu_+(2)$ and $\nu_-(1)+\nu_-(2)$ but may not contain frequencies $\nu_+(1)+\nu_-(1)$ and $\nu_+(2)+\nu_-(2)$. In terms of the energy level diagram displayed as Fig.6.1(c), a frequency $\nu_+(1)+\nu_+(2)$ would represent a transition from the state labelled $|ZZ\rangle'$ to that labelled $|YY\rangle'$. As far as spectrum assignment is concerned, the important double quadrupole resonance spectral lines have frequencies $\nu_+(1)+\nu_-(2)$ and $\nu_-(1)+\nu_+(2)$, corresponding to transitions $|ZZ\rangle'$ to $|YX\rangle'$ and $|ZZ\rangle'$ to $|XY\rangle'$ in Fig.6.1(c). The frequencies of such transitions answer the question; if site 1 has by definition the higher ν_+ frequency, to which site should the higher ν_- frequency be assigned?

It is to be noted that double quadrupole resonance transitions take place between the energy levels of the coupled two deuteron system and that the energy levels are perturbed by the dipolar coupling. Thus the frequency $\nu_+(1)+\nu_-(2)$ does not correspond to the sum of the frequencies of principal lines in the ν_+ and ν_- multiplets. As may be seen in Fig.6.1(c), the frequency of the transition $|ZZ\rangle'$ to $|YX\rangle'$, which is $\nu_+(1)+\nu_-(2)$, is the sum of the frequency of a ν_+ multiplet principal line and a ν_- multiplet subsidiary line, or equivalently the sum of the frequency of a ν_- multiplet principal line and a ν_+ multiplet subsidiary line.

In Table 6.2 are listed the measured frequencies of the $(\nu_+ + \nu_-)$ double quadrupole resonance frequencies for some of the compounds studied in I. As in I they are 100% deuterated at the exchangeable proton sites by repeated crystallization from D_2O. For comparison are the frequencies of these lines predicted with the spectrum assignment deduced in I and also with the alternative assignment. Once again the results on formamide (measured since the publication of I) are included with the assignment procedure used to predict the double quadrupole resonance lines as laid down in I. For the water of crystallization in L-serine hydrate, one of the double quadrupole resonance lines is very weak and the agreement has to be judged on the basis of a single $(\nu_+ + \nu_-)$ line.

It is seen that in each case the assignment based upon the model postulated in I proved to be correct. The higher frequency ν_+ line is to be associated with the same deuterium site as the higher frequency ν_- line in acetamide at 300 K, formamide at 77 K and D_2O in L-serine hydrate at 77 K, whilst in acetamide at 77 K the higher frequency ν_+ line is to be associated with the lower frequency ν_- line. The change in acetamide with temperature is not so surprising as it would at first appear, as the frequencies of the two ν_+ transitions deduced in the absence of dipolar interaction are very similar, so that the ν_+ multiplet splitting is due almost entirely to the magnetic interaction.

The agreement lends further weight to the probability that the theoretical model, postulated in I to explain the multiplet structure, is substantially correct. The ν_+ to ν_- pairing used in Table 6.1 follows the confirmed assignment.

6.2.1 Conclusions

We have shown that valuable information may be extracted from a comparison of the NQR of the same compound highly and slightly enriched with deuterium, particularly as to deuterium-deuterium and proton-deuterium

TABLE 6.2

A comparison between the measured $(\nu_+ + \nu_-)$ double quadrupole resonance frequencies and those predicted, based upon (a) the assignment of the spectrum dictated by the theoretical model in I , and (b) the alternative assignment.

Compound	Temperature	Measured $(\nu_+ + \nu_-)$ double Quadrupole resonance frequencies [kHz]	Frequencies deduced from theoretical model assignment [kHz]	Frequencies deduced from alternative assignment [kHz]
Formamide	77	294.9 ± 0.05 292.4 ± 0.05	294.9 292.35	298.2 289.05
Acetamide	77	294.4 ± 0.05 291.5 ± 0.05	294.45 291.45	294.17 291.63
Acetamide	300	296.7 ± 0.1 293.6 ± 0.1	296.8 293.6	297.3 293.1
Water in L-Serine hydrate	77	359.1 ± 0.1 (355 ± 1)	359.1 356.7	361.7 354.1

interaction. Secondly, we have given an example in which the assignment of the measured deuterium spectrum may be decided using homo-nuclear double quadrupole resonance.

6.3 NQR SPECTRUM OF LANTHANUM NICOTINATE DIHYDRATE (LND)

The development of the use of FM in NQR was occasioned by a request from Prof. C.A. Hutchison Jnr, of Chicago University, to supply NQR data on the nitrogen sites in Lanthanum nicotinate dihydrate. He was carrying out an ENDOR study of that material, using Nd^{3+} as a dilutely substituted paramagnetic impurity, and wished to know the electric field gradient parameters of the ^{14}N nuclei in the nicotinate rings. Initial attempts with this substance produced only a few weak lines - insufficient for a full analysis.

However, following our study of spin-locking effects in nitrogen NQR, we applied frequency modulation and double irradiation techniques (as described in Chapter V), and succeeded in obtaining nine absorption frequencies. Using the identity $\nu_+ = \nu_- + \nu_0$, and observing intensity changes in the ν_+ and ν_- (high-frequency) lines while double irradiating the ν_0 (low frequency) lines, we were able unambiguously to assign the NQR spectrum to three different nitrogen sites, as shown in Table 6.3.

Having carried out the measurements and assignments at 77°K, the measurements were repeated at 4.2°K (since the ENDOR experiment was to be carried out at 5°K). All lines were considerably weaker at 4.2°K, and no ν_- lines were observed. In assigning lines to sites at 4.2°K, we assumed that only a small change in e^2qQ would occur with the change in temperature (we have observed only very small shifts in other NQR spectra when the temperature is lowered from 77°K to 4.2°K). The 4.2°K results, thus assigned, also appear in Table 6.3.

TABLE 6.3

NITROGEN NQR DATA ON LND (in kHz)

Temperature	Site	ν^+	ν^-	ν^0	e^2qQ/h	η
77°K	Site 1	3714 (±1)	2914 (±2)	800 (±2)	4418 (±2)	0.362 (±.002)
	Site 2	3521 (±1)	2813 (±2)	708 (±2)	4222 (±2)	0.335 (±.002)
	Site 3	3511 (±1)	2820 (±2)	690 (±2)	4220 (±2)	0.327 (±.002)
4.2°K	Site 1	3722 (±5)	(2917)	805 (±3)	4426 (±4)	0.364 (±.004)
	Site 2	3540 (±5)	(2825)	715 (±3)	4243 (±4)	0.337 (±.004)
	Site 3	3525 (±5)	(2840)	685 (±3)	4243 (±4)	0.323 (±.004)

6.3.1 Structure of LND

This has been determined by X-ray diffraction[41]. The main points of the structure relevant to this work lie in the estimated hydrogen-bond lengths between the N of the nicotinate ring and the H_2O units of the water of crystallisation. From the projection of the structure, Fig.6.2, reproduced from reference (41), we see that the complex LND is made up of a dimer $[La^{3+}(C_5H_4NCO_2^-)_3 \cdot (H_2O)_2]_2$ with a centre of symmetry between the two La^{3+} ions. Atoms or groups in Fig.6.2 designated by primed numbers or letters are related to unprimed units through the centre of symmetry.

Each La^{3+} ion is coordinated inside an 8-member cage of oxygens, two of which are in water molecules, two of which form part of one nicotinate carboxyl group, and the remaining four come, one from each of the other four nicotinate carboxyls. The remaining four nicotinate oxygens are linked to the other La^{3+} ion.

Dimers are interlinked in the crystal by hydrogen bonds between the N's of the nicotinate rings and the water oxygens of neighbouring dimers.

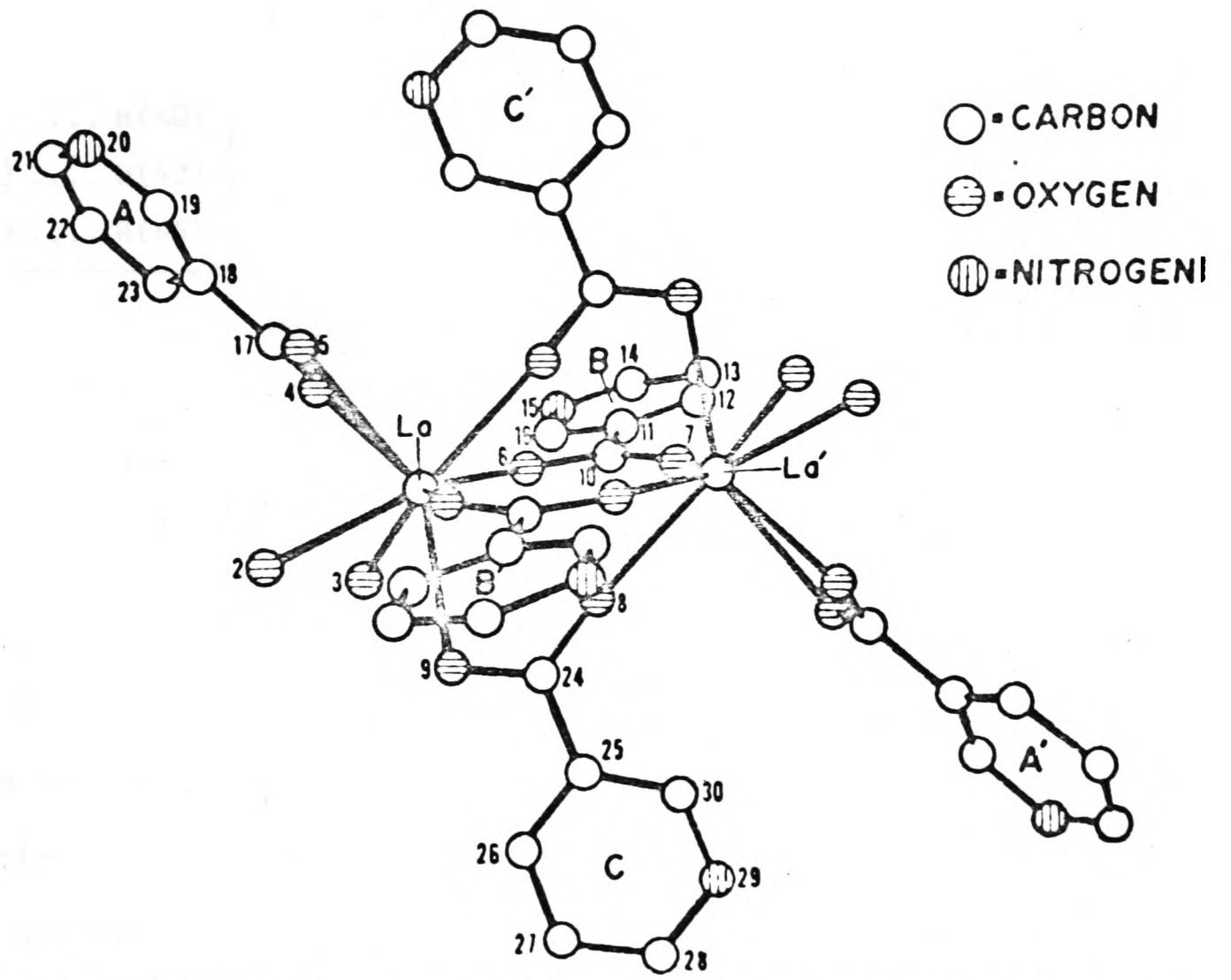


Fig.6.2: The structure of the molecular dimer of lanthanum nicotinate dihydrate determined by x-ray diffraction. The atoms are numbered according to the conventions employed in the x-ray studies; an atom related by the center of inversion to one designated by an unprimed number is denoted by the same number primed. The numbering conventions for the hydrogen atoms and the carbon or oxygen atoms to which they are covalently bonded, are as follows:

H(31) C(26)	H(39) C(19)
H(32) C(27)	H(40) O (2)
H(33) C(30)	H(41) C(14)
H(34) C(16)	H(42) O (3)
H(35) C(23)	H(43) C(13)
H(36) C(12)	H(44) C(22)
H(37) C(21)	H(45) O (2)
H(38) C(28)	H(46) O (3)

TABLE 6.4

Distances from N to neighbouring nuclei in L N D

(numbering as in Fig.6.2 and reference (41))

Bond	Length (Å) ±.05	Bond	Length (Å) ±.001
N(15) .... H(40)	1.9	N(15) .... O(2)	2.734
N(20) .... H(42)	1.8	N(20) .... O(3)	2.703
N(29) .... H(45)	2.2	N(29) .... O(2)	2.846
Bond	Water Molecules Length (±.05) Å	Bond	Water Molecules Length (±.05) Å
O(2) ..... H(40)	0.9	O(3) ..... H(42)	0.9
O(2) ..... H(45)	0.7	O(3) ..... H(46)	0.7

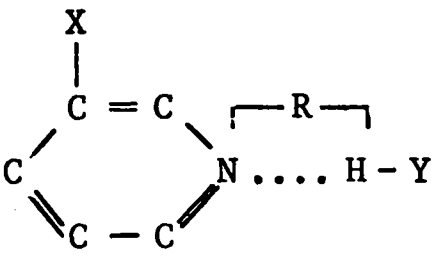
When we examine the structure of the immediate environments of the three different N-sites, we see that there are two very similar sites, and one in which the N .... H-O hydrogen bond is noticeably longer. Table 6.4 summarises the selected data for N sites. We also note that the nicotinate rings are almost identical at all three sites, with N-C bonds of 1.33 ± 0.01 Å and C-N-C angles of 117.1 ± 0.5°.

Since we have one site with a considerably larger e^2qQ than the other two, which form an almost identical pair, it seems reasonable to assign Site I of Table 6.3 to N(29) in Table 6.4.

The sites II and III of Table 6.3 have identical e^2qQ but differ slightly in η. N(15) and N(20) of Table 6.4 have hydrogen bonds of lengths 1.8 and 1.9 Å, ±.05 Å, so that they are almost identical, and one cannot assign sites II and III unambiguously on this basis alone.

6.3.2 Hydrogen-Bonding in Related Pyridine-ring Compounds

To aid assignment of sites II and III in L N D , we examined data from a number of related pyridine-ring compounds. These were Pyridine (gas and solid phases), nicotinamide and nicotinic acid. They all have the general form:



where R indicates the length of the hydrogen bond between the N of one unit and the H of the H-bond donor.

Table 6.5 summarises the known structures and NQR data on these compounds.

TABLE 6.5

NQR and structural data on Pyridine-ring compounds

COMPOUND Temp. = 77°K, except I		Structure			NQR Data		References	
		X	Y	R Å (±.05)	e^2qQ/h (±2)kHz	η ± .002	Structure	NQR
I	Pyridine (gas phase)	H	C	∞	4880 (±40)	0.405 (±.006)	-	43
II	Pyridine	H	C	?	4584	0.396	48	44
III	LND I	COO^-	$(H_2)O$	2.2	4418	0.362	41	-
IV	Nicotinamide	NH_2	$(H_2)N$	2.1	4360	0.350	45	46
V	LND II	COO^-	$(H_2)O$	[1.9]	4222	0.335	41	-
VI	LND III	COO^-	$(H_2)O$	[1.8]	4220	0.327	41	-
VII	Nicotinic Acid	COOH	(H)O(OC)	1.66	3769	0.281	47	46

NOTE: In estimating R for nicotinamide and nicotinic acid, we have assumed an OH or NH bond length of 1 Å, consistent with the known values for amino acids[49] and ice Ih[50].

It can be seen from Table 6.5 that, as a general trend in these related substances, e^2qQ and η of the ring-nitrogen decrease as the hydrogen-bonding of the N becomes stronger (R decreasing). The structure of the ring itself is only slightly altered when the side group X is changed. For example in Pyridine[48] the $C\hat{N}C$ angle is 117° 34' while in the three nicotinate groups of LND, the $C\hat{N}C$ angles are[41] 117° 36', 117° 6' and 116° 36'. The C-N bond lengths show only slight variations too: viz. Pyridine is 1.331 Å ± 0.002.

while the three nicotinate groups in L N D have C-N = 1.338, 1.336 and 1.330 Å(± .002). Thus it is reasonable to expect that the main differences between these substances, as far as the ring-nitrogen is concerned, will lie in the degree of external hydrogen-bonding. Table 6.5 may thus be interpreted to say that e^2qQ and η of the ring-nitrogen decrease as hydrogen bonding increases. If this is so for L N D, we may then assign L N D site II to N(15) and site III to N(20), to fit the general trend.

6.4 CORRELATION BETWEEN NITROGEN COUPLING CONSTANTS AND HYDROGEN BOND LENGTH IN PYRIDINE DERIVATIVES

It has been shown[42] that there is a correlation between hydrogen-bond length and deuterium e^2qQ in deuterated amino acids, for the cases of O and N as donor atoms and O as an acceptor, i.e. for O-D .... O and N^+-D .... O bonds.

In that paper, the authors demonstrated that a relationship of the form

$$e^2Qq = e^2Qq_0 - K/R^3$$

held for most of the amino acids studied. where

e^2Qq_0 = value of e^2Qq for no H-bonding
R = hydrogen bond length
K = constant.

They found that the values of e^2Qq_0 and K depended on whether the donor was an N or an O.

In the Pyridine derivatives, we are looking at the 'other end' of the hydrogen bond. The ring-nitrogen is an H-bond acceptor in these compounds, and its covalent bonds are almost identical in all the compounds considered, so that the hydrogen bonding mainly determines the details of the quadrupole coupling constants.

When we attempt to plot e^2qQ against $1/R^3$ for this series of compounds II - VII, we obtain Fig.6.3. The errors in R are large, due to the

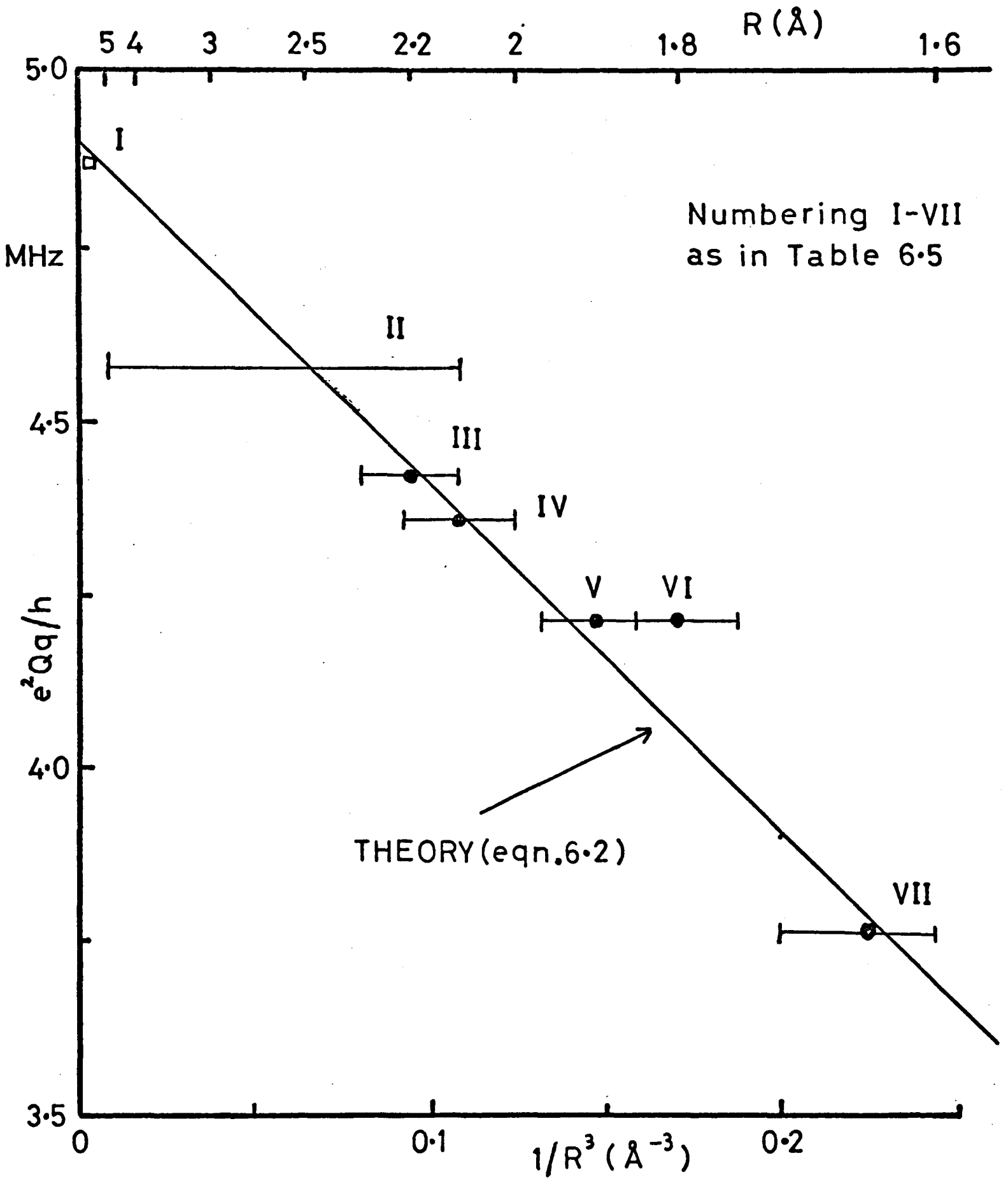


Fig. 6.3 : Correlation between e^2Qq and H-bond length for N in Pyridine rings

absence of good neutron diffraction data for these compounds. In estimating R in nicotinamide and nicotinic acid, we have assumed that the N-H and O-H covalent bonds are ~1 Å, consistent with the known values in amino acids[49] and ice Ih [50], and that the hydrogen bonds are straight. These are somewhat drastic assumptions, but, given these, Fig.6.3 demonstrates that a correlation does exist between nitrogen e^2Qq and hydrogen bond length in these pyridine derivatives of the form

$$e^2Qq = e^2Qq_0 - hK/R^n \qquad \ldots (6.1)$$

where $e^2Qq_0/h \approx 4900$ kHz

$$K \simeq 5000 \text{ kHz Å}^3 \qquad \ldots (6.2)$$

and $n \simeq 3$

If we attempt to fit the solid-state value if pyridine e^2Qq to this chart, we obtain an estimated N....H distance of ~2.6 Å. This weak bonding is consistent with other properties of pyridine, such as its low melting point of -42°C.

It is interesting to note that the intercept on Fig.6.3 for $\frac{1}{R} = 0$ ($R = \infty$) using equation 6.1 occurs at $e^2Qq/h = 4900$ kHz. From Table 6.5, we see that the value of e^2Qq/h for gas-phase pyridine is 4880 kHz, which would correspond to $R \to \infty$. We are of course neglecting temperature effects - all other measurements were performed at 77°K.

However, the values of e^2Qq for LND at 4.2°K reveal an almost negligible change compared to the values at 77°K (if our 4.2°K assignment is correct). However, the fact that the gas-phase result falls on the graph may be quite fortuitous, or it may indicate that there is relatively little difference in the environment of the N, as far as its covalent bonds are concerned, over the temperature range 4.2°K - 350°K.

6.5 CONCLUSIONS

By using F M irradiation techniques coupled with conventional double irradiation, we have succeeded in measuring and assigning the complete ^{14}N N Q R spectrum of Lanthanum Nicotinate Dihydrate (L N D).

We have also shown that the value of ^{14}N e^2Qq in pyridine derivatives is strongly affected by hydrogen bonding of the ring-nitrogen to neighbouring molecules in the crystal, and have obtained a correlation function to relate e^2qQ to the hydrogen bond length R.

CHAPTER VII

QUADRUPOLE RESONANCE IN SPIN $\frac{3}{2}$ NUCLEI

7.1 INTRODUCTION

Double resonance methods have been used before to examine quadrupole resonance in sodium compounds[9,4], but since only one resonance line is observed while in a zero applied D.C. magnetic field, it was not possible to determine both η and e^2qQ. Indeed, for any spin $\frac{3}{2}$ nucleus such as ^{23}Na, ^{39}K or ^{11}B, there is only one resonance line for zero D.C. magnetic field at a frequency

$$\nu_q = \frac{e^2qQ}{2h}\left(1+\frac{\eta^2}{3}\right)^{\frac{1}{2}}.$$

However, if a magnetic field is applied to a spin $\frac{3}{2}$ nucleus, the unquenched levels diverge with relatively large g-values, and a multiplet spectrum is produced (Fig.7.1). In general, different crystallites will have different energy levels, depending on the relative orientation of the EFG Principal Axes and the applied magnetic field direction.

For a given crystallite, the actual set of absorption frequencies depends on both γ for the nucleus and on η for the EFG, as well as on θ,ϕ (the orientation angles). Thus, for a powder, a broad set of overlapping lines is expected.

It has been found, however, that, under certain conditions, approximate values of η can be obtained for a powder specimen containing a spin $\frac{3}{2}$ quadrupole nucleus. The conditions are:

(1) A static field B_0 must be applied parallel to the usual irradiation field B_1. This results in a reduced set of allowed transitions (such as ν_1, ν_2 in Fig.7.1), such that, when transitions from different crystallites are added together, the powder spectrum will have resolvable features.

(2) The D.C. field B_0 must be of sufficient strength to separate the individual lines of the resulting multiplet by $\sim > \frac{1}{2}$ line-width, for analysis to be sufficiently accurate.

(3) The field B_0 also broadens the lines. Hence it must not be so strong as to broaden the lines until they merge and become unobservable.

Conditions (2) and (3) together require the quadrupole nucleus to have a relatively large γ, so that magnetic fields in the range 20-50 Gauss can produce adequate splittings. ^{23}Na and ^{11}B are suitable for this reason, while ^{39}K is much harder to work with.

The rest of this chapter develops the theory of nuclear quadrupole double resonance in spin $\frac{3}{2}$ powder samples, and describes some experiments on NaOH, $NaOH.H_2O$ and $NaOH.4H_2O$, which are used to test the theoretical predictions, as well as to acquire new data.

7.2 ZEEMAN NQR IN SPIN $\frac{3}{2}$ POWDERS

MORINO and TOYAMA[51] showed that, when conducting ZNQR (NQR in magnetic fields) experiments on spin $\frac{3}{2}$ powder specimens, it was desirable to apply a static magnetic field B_0 parallel to the normal irradiation (RF) field B_1. For small η, transitions at frequencies $\nu_q \pm \nu_L$ then became forbidden (where $\nu_L = \frac{\gamma}{2\pi} B_0$) while transitions at frequency $\nu_q \pm (1 \pm \eta)\nu_L$ were allowed.

Conversely, if B_0 is applied perpendicular to B_1, the transitions $\nu_q \pm (1 \pm \eta)$ are forbidden while transitions $\nu_q \pm \nu_L$ are allowed. Thus, if one is interested in measuring η, it is desirable to apply B_0 parallel to B_1.

As in the spin 1 case, only the components of B_1 parallel to the principal axes of the EFG are effective in causing transitions, and the transition probabilities of the four possible transitions in a given crystallite will depend on the relative angles of orientation of the EFG Principal Axes to the applied R.F. field B_1.

BROOKER and CREEL[52] extended this work so that the results were valid for all η. Their calculations are exact in η, but only to first order in B_0. Higher-order effects and finite linewidths modify the results somewhat, since fairly broad lines are the experimental norm.

7.2.1 Theory

We now summarise the theory as laid out in references (7, 51 and 52). The Hamiltonian of a quadrupolar nucleus in a magnetic field B_0 is given by:

$$\mathcal{H} = \mathcal{H}_Q + \mathcal{H}_z$$

where

$$\mathcal{H}_Q = \frac{e^2Qq}{4I(2I-1)}\left(3I_z^2 - I(I+1) + \eta(I_x^2 - I_y^2)\right)$$

as before, with I = nuclear spin and the coordinates (X,Y,Z) refer to the principal axes of the EFG; and

$$\mathcal{H}_z = -\gamma\hbar\,\underline{B}_0 \cdot \underline{I}$$

with $\gamma B_0 = \nu_L$ = Larmor frequency of the quadrupole nucleus.

Diagonalisation of $\mathcal{H}_Q$ for $B_0 = 0$ yields the energy levels for a spin $I = \frac{3}{2}$

$$\pm E_q = \pm\tfrac{1}{4}e^2Qq(1+\tfrac{1}{3}\eta^2)^{\frac{1}{2}}$$

and the single resonance frequency

$$\nu_q = \tfrac{1}{2}\frac{e^2Qq}{h}(1+\tfrac{1}{3}\eta^2)^{\frac{1}{2}}$$

So long as $\mathcal{H}_Q \gg \mathcal{H}_z$, we may use perturbation theory to obtain the four energy levels in non-zero magnetic field given by:

$$E_{4,3} = E_q \pm \frac{h\nu_L}{2\rho B_0}\left[(\rho-1+\eta)^2 B_{ox}^2 + (\rho-1-\eta)^2 B_{oy}^2 + (2+\rho)^2 B_{oz}^2\right]^{\frac{1}{2}}$$

$$E_{2,1} = -E_q \pm \frac{h\nu_L}{2\rho B_0}\left[(\rho+1-\eta)^2 B_{ox}^2 + (\rho+1+\eta)^2 B_{oy}^2 + (2-\rho)^2 B_{oz}^2\right]^{\frac{1}{2}}$$

where the plus signs refer to levels 4 and 2, (B_{ox}, B_{oy}, B_{oz}) are the components of B_0 along the EFG Principal Axes and $\rho = (1+\frac{1}{3}\eta^2)^{\frac{1}{2}}$.

There are, in general, six allowed transitions, but only the four 'quadrupole' transitions are of interest here. For one particular orientation of B_0, all the transitions are shown in Fig.7.1 (i.e. for one specially-oriented crystallite).

The two 'magnetic' transitions not considered here are of low frequency, and too broad (in a powder sample) to be of use in defining η. They are, however, important when we come to consider the effects of continuous coupling.

As explained by MORINO and TOYAMA[51], transitions 1 and 2 are much favoured when B_0 is applied parallel to B_1, the R.F. field, while transitions 3 and 4 are inhibited.

For a polycrystalline sample, the above expressions for the energy levels $E_1 \rightarrow E_4$ indicate that different crystallites will have transitions at different frequencies.

BROOKER and CREEL[52] obtained expressions for the above transition frequencies in terms of the polar coordinates (θ,ϕ) specifying the direction of B_0 relative to the E.F.G. Principal Axes, They assumed at first that any absorption was in the form of a δ-function and then found the critical points of the surface so defined in frequency-space by calculating those frequencies for which

$$\frac{\delta\nu}{\delta(\cos\theta)} = \frac{\delta\nu}{\delta\phi} = 0 \ .$$

They thus found that the singularities in frequency occurred at the points

$$\nu = \nu_q \pm \frac{2\nu_L}{\rho} \qquad \ldots\ (7.1)$$

$$\nu = \nu_q \pm \nu_L \qquad \ldots\ (7.2)$$

$$\nu = \nu_q \pm \frac{(1 \pm \eta)}{\rho}\,\nu_L \qquad \ldots\ (7.3)$$

Brooker and Creel then continued their calculation to find formulae for the transition probabilities of all these transitions for arbitrary

(θ,ϕ), and by means of a computer simulation, including a Gaussian line-shape rather than a δ-function, produced a set of predicted quadrupole line-shapes in magnetic fields.

The conclusions of their work were as summarised below:

A spin $\frac{3}{2}$ powder specimen will have a 6-line multiplet spectrum when subjected to a magnetic field B_0 and irradiated with an R.F. magnetic field $B_1 \parallel B_0$. The frequencies of the six lines are given by:

$$\nu = \nu_q \pm \frac{2\nu_L}{\rho} \qquad \ldots (7.1)$$

$$\nu = \nu_q \pm \frac{(1 \pm \eta)}{\rho} \nu_L \qquad \ldots (7.3)$$

where $\nu_L = \frac{\gamma}{2\pi} B_0$ = Larmor frequency of the nucleus and $\rho = (1 + \frac{1}{3}\eta^2)^{\frac{1}{2}}$ with η = asymmetry parameter of E F G.

Transitions given by equation (7.2) are always forbidden when $B_0 \parallel B_1$. For small η, the transitions of equation (7.1) are very weak, and (7.3) may be approximated by (for $\eta \leq 0.2$)

$$\nu = \nu_q \pm (1 \pm \eta)\, \nu_L \qquad \ldots (7.3')$$

as originally deduced by Morino and Toyama.

For intermediate η $(0.2 \leq \eta \leq 0.8)$, equation (7.3) applies but the transitions of equation (7.1) remain relatively weak. For $\eta \geq 0.8$, transitions (7.1) become significant.

Thus, in general, we expect to see a broad four-line multiplet when a spin $\frac{3}{2}$ quadrupole is examined while subject to a D.C. magnetic field B_0 applied parallel to the R.F. field B_1.

The line centres should diverge from the zero-field value ν_q at rates given by equation (7.3), dependent on both γ and η.

If we can measure all the lines given by equation (7.3) [and (7.1) if appropriate] as a function of applied D.C. field B_0, we should be able to determine both γ and η. Since γ is generally well known from other

experiments, this provides one check on the accuracy of the theory outlined above.

The slopes of the four lines given by equation (7.3) should be given by:

$$\frac{d\nu}{dB_0} = \pm \frac{(1 \pm \eta)}{\rho} \gamma/2\pi \qquad \ldots (7.4)$$

If we name the slopes $\lambda(++)$, $\lambda(+-)$, $\lambda(-+)$ and $\lambda(--)$ where $\lambda(++) = +\frac{(1+\eta)}{\rho}\gamma$ then we should have

$$\frac{\lambda(++)}{\lambda(+-)} = \frac{\lambda(-+)}{\lambda(--)} = \frac{1+\eta}{1-\eta} \qquad \ldots (7.5)$$

and

$$\lambda(++) + \lambda(+-) = -(\lambda(-+) + \lambda(--)) = \frac{\gamma}{\pi\rho} \simeq \gamma/\pi \quad \text{for small } \eta. \qquad \ldots (7.6)$$

As in most double resonance experiments, the intensities of the above transitions will depend mostly on level crossing effects. We must thus proceed to calculate the effects of level-crossing and continuous coupling in a four-level system.

7.3 LEVEL CROSSING AND THE SPIN $\frac{3}{2}$ NUCLEUS

The spin $\frac{3}{2}$ nucleus (e.g. ^{23}Na, ^{11}B, ^{41}K) is unquenched, and in general has a large magnetic moment, e.g. for ^{23}Na, γ is ~ 1.126 kHz/Gauss. In zero D.C. fields the spin $\frac{3}{2}$ Hamiltonian is easily solved (as shown earlier) to give two doubly degenerate levels, and a single allowed quadrupole transition frequency.

However, when a magnetic field is applied to a sample containing a spin $\frac{3}{2}$ nucleus, the degenerate energy levels diverge to give four independent energy levels, the splittings between pairs of levels being a function of γ, η (asymmetry parameter) θ and ϕ (the angles of orientation of the EFG principal axes relative to the applied field B_0). A full general treatment of the behaviour of these energy levels is possible[7], but the result is clumsy and extremely involved. The matrix of $\mathcal{H}_Q$ must be diagonalised for each value of θ and ϕ, and the process is best done numerically on a computer, as indicated in reference (52).

It is instructive to consider the special case of $\theta = \phi = 0$, i.e. for a single crystal, and to apply the results to NQR in Na OH, using the measured values of η, e^2qQ and spin ratio $N_p/N_Q = 1$. (We pre-empt the experimental section by giving both η and e^2qQ, but it is useful to obtain a feel for the numerical values in the problem.)

GRECHSHKIN and AINBINDER[7] give the four energy levels of a spin $\frac{3}{2}$ nucleus in a magnetic field B_0 as follows, for $\theta = \phi = 0^0$:-

$$\left.\begin{aligned} A &= \left\{ + \sqrt{\left(\frac{K}{6}+\frac{1}{4}\right)^2 + \frac{\eta^2}{48}} + \frac{K}{12} \right\} e^2qQ \\ B &= \left\{ + \sqrt{\left(\frac{K}{6}-\frac{1}{4}\right)^2 + \frac{\eta^2}{48}} - \frac{K}{12} \right\} e^2qQ \\ C &= \left\{ - \sqrt{\left(\frac{K}{6}-\frac{1}{4}\right)^2 + \frac{\eta^2}{48}} - \frac{K}{12} \right\} e^2qQ \\ D &= \left\{ - \sqrt{\left(\frac{K}{6}+\frac{1}{4}\right)^2 + \frac{\eta^2}{48}} + \frac{K}{12} \right\} e^2qQ \end{aligned}\right\} \quad \ldots (7.7)$$

where $$K = \frac{4\gamma hB_0}{e^2Qq} .$$

There are six possible transition frequencies, and these are plotted for the sodium nucleus in NaOH in Fig.7.2(a). The corresponding frequency of protons in the field B_0 is also plotted, showing that four level crossings occur in non-zero B_0.

The results for $\theta = \phi = \frac{\pi}{2}$ are very similar to $\theta = \phi = 0^0$. $\theta = \frac{\pi}{2}$, $\phi = 0$ is plotted in Fig.7.2(b). There are seen to be the same four distinct level crossings, levels BC and BD being separated by over 100 kHz when level crossings occur.

For arbitrary θ, ϕ, there are in general always four distinct energy levels (as shown) for the range of magnetic fields of interest for level crossings with protons (0 - 1 kG). In general too, there are always six distinct transition frequencies, as in Fig.7.2, differing only in the slopes of the lines AB, AD, etc.

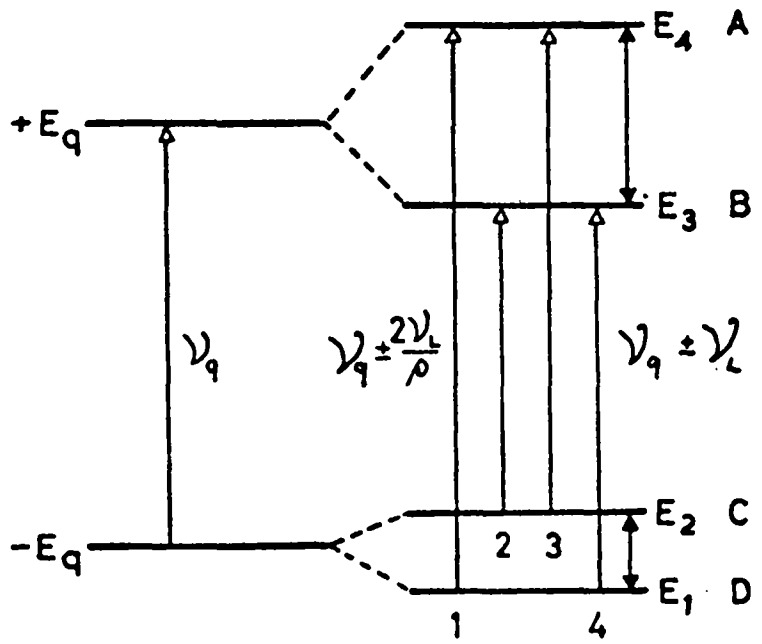


Fig.7.1: Energy levels of a spin $\frac{3}{2}$ nucleus when $B_0 \| Z$ axis of EFG

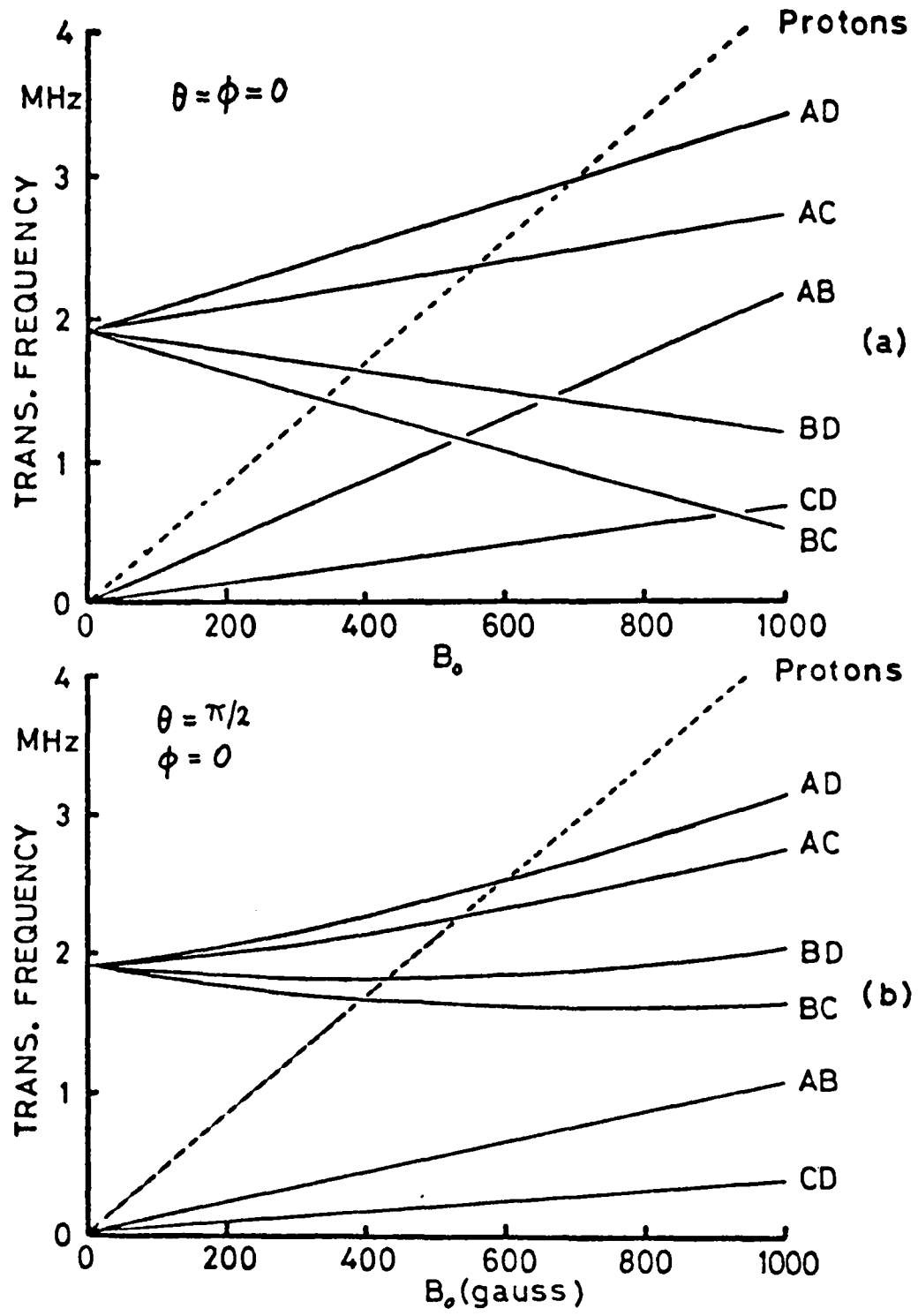


Fig.7.2: Transition frequencies of Na in NaOH

There is only one special case of interest, which occurs when

$$\sin^2\theta = 2/(3 - \eta \cos 2\phi)$$

In this case, the energy level equations become biquadratic

$$A,B,C,D = \pm e^2qQ \sqrt{\left(\frac{1}{16}\left(1+\frac{\eta^2}{3}\right)+\frac{5K^2}{144}\right) \pm \frac{K}{72}\sqrt{4(K^2+3\eta^2)+9(9-\eta^2)\cos^2\theta}}$$

There are then only four distinct transition frequencies. The transitions equivalent to AC and BD (Fig.7.2) become equal and independent of B_θ, and transitions like AB and CD become equal in frequency. Thus, in this case there are only three level-crossings ('Magnetic' transition AB/CD not being involved).

However, the two transitions AC and BD which merge in this special case involve two <u>separate</u> pairs of levels. As a result the population ratios $\frac{1+a}{1+c}$ and $\frac{1+b}{1+d}$ (Fig.7.3) become equal at that level crossing, being equal to the proton ratio at that time, $\frac{1-p}{1+p}$. Since no term a, b, c or d appears twice, the level crossing calculations are not changed for this crystallite, and the single transition that would be observed in such a crystallite (being a combination of AC and BD) would have an intensity given by the sum of the two individual transitions within it.

7.3.1 Level Crossing Calculations

We now calculate the populations of the four quadrupole energy levels of a spin $\frac{3}{2}$ nucleus, as a result of four distinct level crossings with a polarised proton system, and proceed to estimate observed line intensities as a result of these level crossings. We confine our interest to the 'Quadrupole' transitions, until we come to consider continuous coupling and double irradiation effects.

We first define population values as shown in Fig.7.3. As in the spin 1 case, we shall assume that, initially, $|a| = |b| = |c| = |d| = 0$, $|p| \sim 10^{-5}$, although the assumption is less valid in this case, due to the larger value of the gyromagnetic ratio of the Q spins.

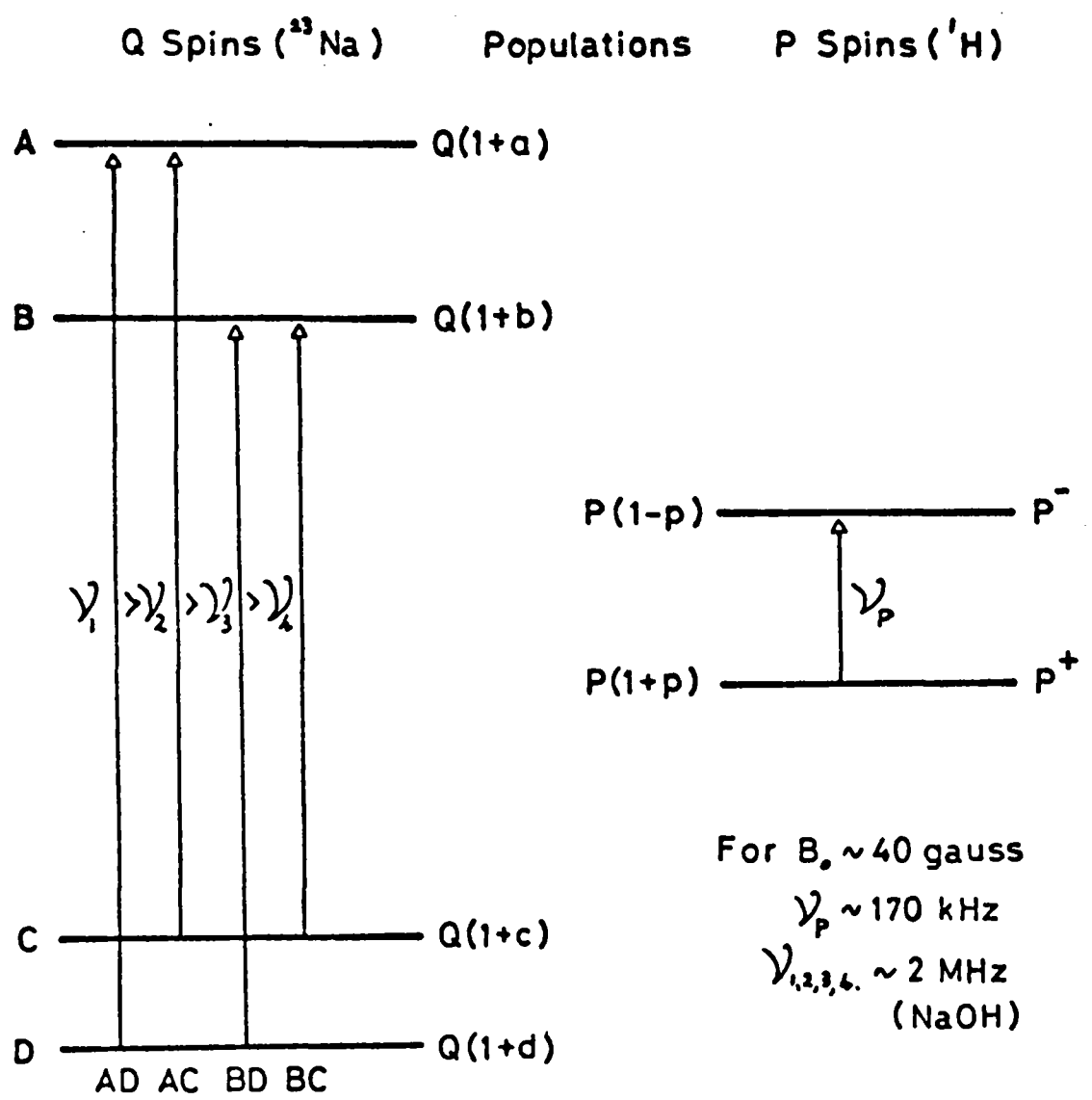


Fig.7.3: Energy levels and populations for spin $\frac{3}{2}$ in a magnetic field B_o

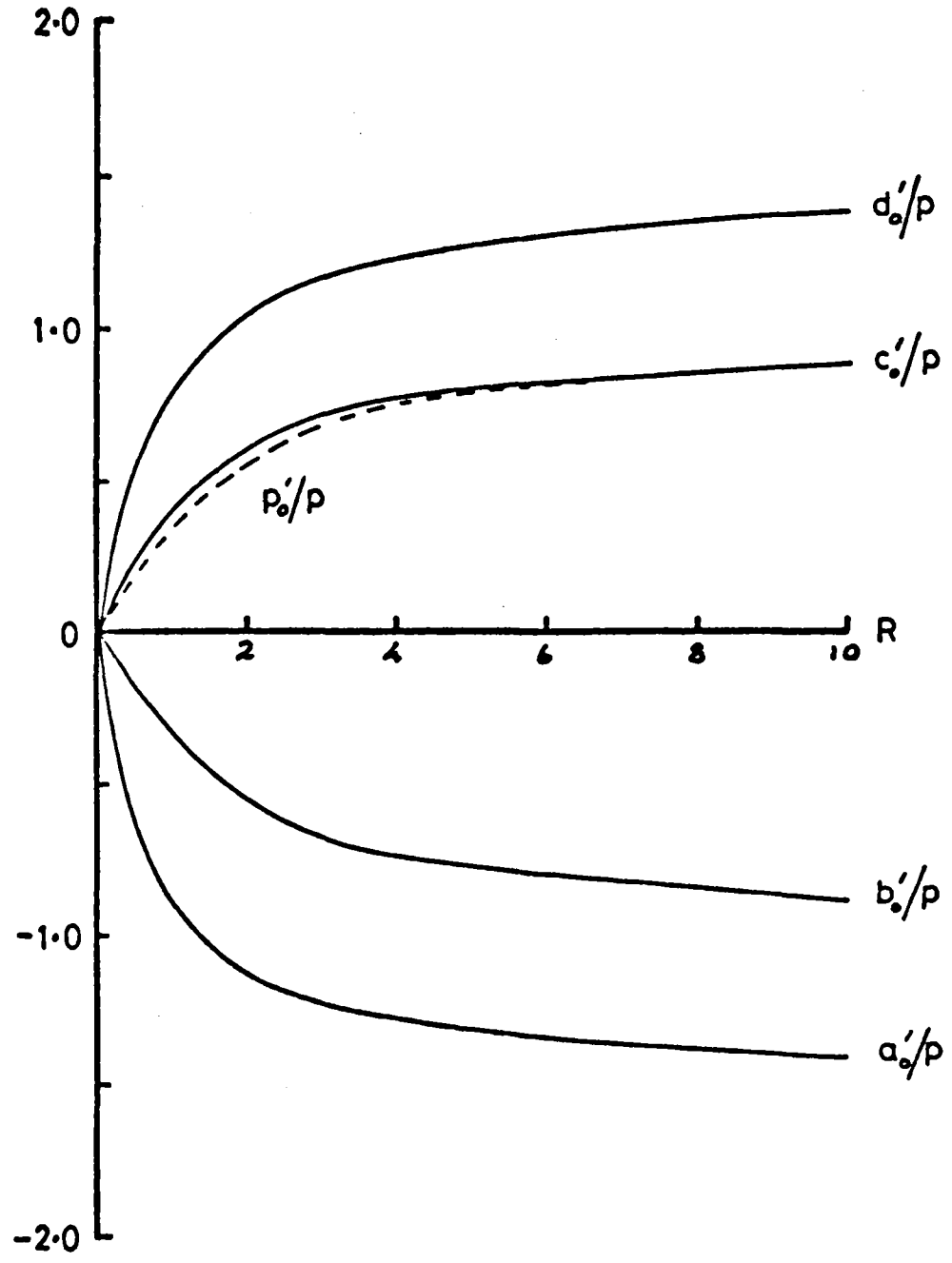


Fig.7.4: Spin $\frac{3}{2}$: populations after 4 level crossings with P spins. $R = N_P/N_Q$

(a) Polarization Phase

As B_0 decreases, four level crossings occur in turn, and we apply equations (3.28) successively to obtain the values a_0', b_0', c_0', d_0' and p_0' after the four level crossings. Analogous to equations (3.29), with $X = \frac{P}{P+Q}$ we then have:

$$\left.\begin{aligned} \frac{a_0'}{p} &= -X - \frac{X^2}{2} \quad : \quad \frac{b_0'}{p} = -\frac{X^4}{4} - \frac{X^3}{4} - \frac{X^2}{2} \\ \frac{c_0'}{p} &= \frac{X^4}{4} - \frac{X^3}{4} + X^2 \quad : \quad \frac{d_0'}{p} = X + \frac{X^3}{2} \\ \frac{p_0'}{p} &= \frac{X^4}{4} + \frac{3X^2}{4} \end{aligned}\right\} \quad \ldots (7.8)$$

The values of a_0', b_0', c_0', d_0' and p_0' are plotted in Fig.7.4, as a function of R, the spin number ratio, where

$$R = \frac{N_P}{N_Q} = \frac{2P}{4Q} = \frac{P}{2Q}$$

in this case.

(b) Measurement Phase

If we now irradiate the sample, so that the level populations are transformed into a'', b'', c'', d'' and p'', then we obtain a final P spin population p''' in the high field B_0 given by:

$$\left.\begin{aligned} p''' &= \pi''' + \Delta p''' \\ \text{where} \quad \pi''' &= \frac{X}{4}(2 - 3X + 7X^2 - 2X^3)\, p'' \\ \text{and} \quad \Delta p''' &= \frac{(1-X)}{2}\left\{-(1+X)a'' + \frac{X}{4}(4X^3 - 2X^2 - 9X + 1)\, b'' \right. \\ &\qquad \left. -\frac{X}{4}(2X^2 - 5X - 2)\, c'' + (X^2 + 1)\, d'' \right\} \end{aligned}\right\} \quad \ldots (7.9)$$

Firstly, we consider what happens if continuous coupling effects are ignored.

(c) Irradiation Phase (without continuous coupling)

During irradiation, p_0' is unaffected, but may decrease with time if T_{1D} is fast. We assume that $p'' = p_0'$ for simplicity. π''' is then a constant.

We consider the effect of irradiating each of the four quadrupole transitions to saturation. For example, if we irradiate the transition AD, then we make $a'' = d'' = \frac{1}{2}(a'_0 + b'_0)$, $c'' = c'_0$, $b'' = b'_0$ and calculate

$$\Delta p'''(a'', b'', c'', d'') .$$

If we then plot the percentage ratio

$$[\Delta p'''(0) - \Delta p'''(a'', b'', c'', d'')]/\Delta p'''(0)$$

where $\Delta p'''(0)$ is the value of $\Delta p'''$ for no irradiation ($a' = a'_0$ etc), we obtain Fig.7.5, which compares the effect of irradiation on the four transitions, and also plots the ratio $\Delta p'''(0)/\pi'''$, which indicates the maximum effect that irradiating the Q spins can have on the P spins.

As shown earlier, only certain ones of these four transitions are allowed for a given crystallite, depending on its orientation. The macroscopic effect is a sum of the contributions of different crystallites, but this does not detract from the predictions about intensities as calculated here, except to increase the 'effective' value of R (decrease the effective number of Q spins).

It can be seen that the sensitivity of detection of AD, the highest frequency transition, is the largest, with the possibility of destroying 80% of $\Delta p'''(0)$ when $R = 1$. The lowest frequency transition BC also has the lowest sensitivity, and the other two are intermediate, becoming equal in sensitivity for $R > 4$, with $\sim 47\%$ of $\Delta p'''(0)$ able to be destroyed.

7.3.2 Double Irradiation Effects

If we share the irradiation period between the quadrupole search frequency $\approx \nu_q$ and low frequency irradiation $\approx$AB or CD, we can predict sensitivities as follows. Since in low fields the P spin bath is broad, and extends over most of the range of AB and CD, we will always have $\pi''' = p' = 0$.

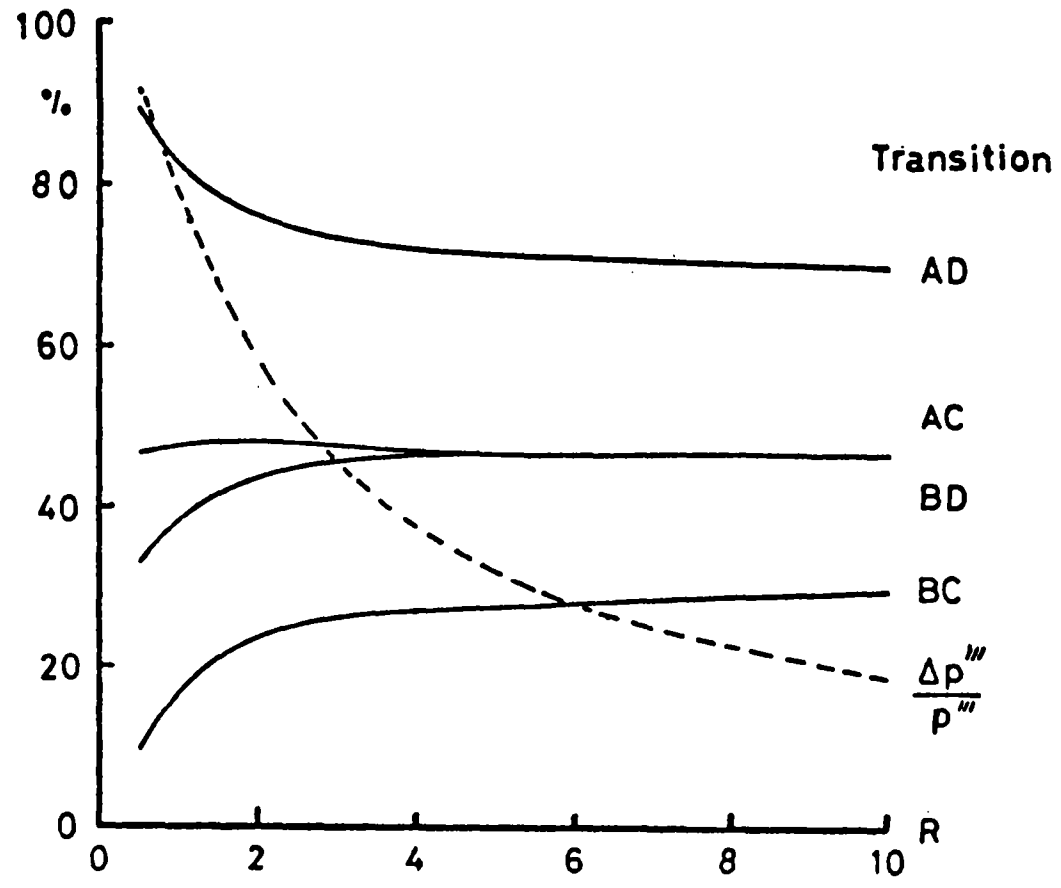


Fig.7.5: %ages of $\Delta p'''$ which may be destroyed by irradiation to saturation of transitions

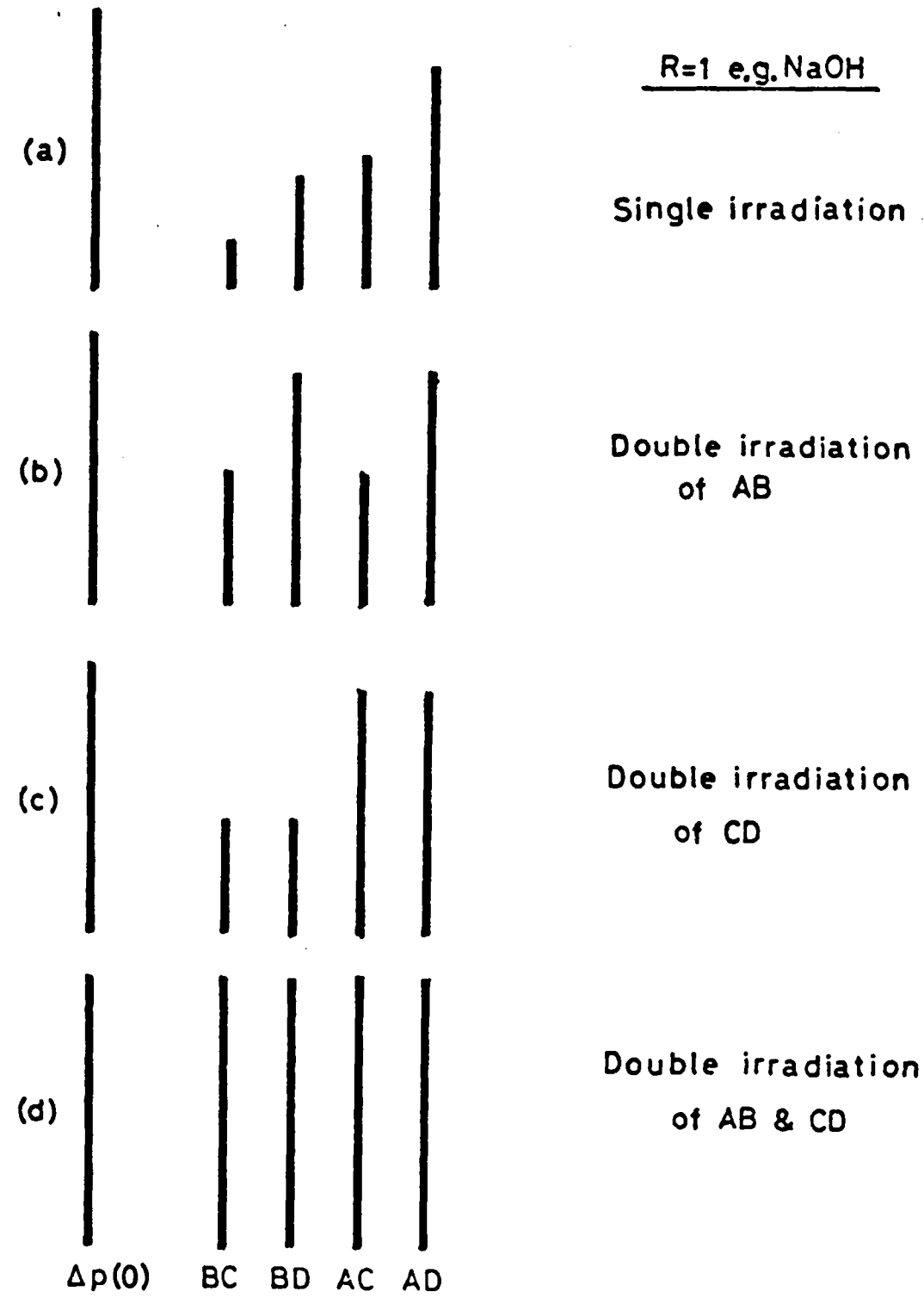


Fig.7.6: Effects of double irradiation - amounts of $\Delta p'''(0)$ affected in each case

(a) Irradiation of AB

If we irradiate AB, we keep $a'' = b''$. Irradiation also of AC or BC will then make $a'' = b'' = c'' = \frac{1}{3}(a_0' + b_0' + c_0') = -\frac{1}{3} d_0'$ and $d'' = d_0'$. AC and BC will be equally intense. Similarly, AD and BD will be equally intense, with $a'' = b'' = d'' = -\frac{1}{3} c_0'$ and $c'' = c_0'$. Noting that $d_0' > c_0'$ for all R, a simple calculation using equation (7.9) shows that irradiating AD or BD can destroy almost twice as much of $\Delta p'''(0)$ as irradiating AC or BC. (see Fig.7.6(b)).

(b) Irradiation of CD

Irradiating CD keeps $c'' = d''$. Thus irradiation also of AC or AD will make $a'' = c'' = d'' = -\frac{1}{3} b_0'$ and irradiation also of BC or BD will make $b'' = c'' = d'' = -\frac{1}{3} a_0'$. Again $b_0' > a_0'$ and a simple calculation shows that irradiating AC or AD destroys more of $\Delta p'''(0)$ than irradiating BC or BD.

(c) Irradiation of AB and CD together

This will always keep $a'' = b''$ and $c'' = d''$. Any other irradiation will result in one of (a'', b'') equalling one of (c'', d''). This can only occur if $a'' = b'' = c'' = d'' = 0$, and 100% of $\Delta p'''(0)$ can be destroyed by irradiating any transition.

These results are summarised in Fig.7.6.

One should note that, for small DC fields, it is not possible to separate AB from CD sufficiently to irradiate them separately, so that any double irradiation at or near the proton frequency ($\approx$ AB and CD) will tend to make all the quadrupole lines equally intense, as in Fig.7.6(d).

For larger DC fields ($\approx$ 30 Gauss) irradiation near the proton frequency will irradiate AB more effectively than CD, since $\nu(AB) > \nu(CD)$, and a spectrum like Fig.7.6(b) will result. Irradiation at a lower frequency will produce a spectrum like Fig.7.6(c).

7.3.3 Continuous Coupling Effects

When B_0 reaches very low values (~ 10 G), the 'magnetic quadrupole' transitions AB and CD become comparable with the proton splitting (Fig.7.2). Since splitting AB $\geq$ CD for all crystallites (by definition of A,B,C,D), splitting AB will be $\approx$ proton splitting for larger values of B_0 than will CD. Thus if B_0 drops to a small value >10 G, it is conceivable that levels AB couple to the protons more effectively than levels CD. However, as $B_0 \to 0$, CD also couples to the proton system.

(a) Effect of coupling levels AB only

If we define a', b' as the populations of levels A and B after continuous coupling, and a_0', b_0' as the populations before continuous coupling (after level crossing, as before), with p_0' and p' as the proton populations before and after continuous coupling, then we can relate these quantities by the equations:

$$\text{Coupling Equilibrium}: \quad \frac{1+a'}{1+b'} = \frac{1-p'}{1+p'}$$

$$\Rightarrow \qquad a' - b' = -2p'$$

(ignoring terms $a'p' \sim 10^{-10}$)

$$\text{Conservation of spins}: \quad a' + b' = a_0' + b_0'.$$

The continuous coupling population equilibrium (analogous to a thermal equilibrium) is established by a series of mutual spin flips between the P and Q spins, conserving energy (we consider splitting AB = proton splitting). Thus by conserving energy, we have:

$$P(2p_0' - 2p') = Q\{(b' - a') - (b_0' - a_0')\} .$$

Solving these equations, and using $R = P/2Q$, we deduce:

$$\left.\begin{aligned} a' &= \tfrac{1}{2}(a_0' + b_0') - p' \\ b' &= \tfrac{1}{2}(a_0' + b_0') + p' \\ p' &= \{p_0' + (b_0' - a_0')/4R\}/(1 + \tfrac{1}{2R}) \end{aligned}\right\} \qquad \ldots (7.10)$$

These equations are essentially the same as equations (3.28). Since levels CD are assumed unaffected, we also have

$$c' = c'_0 \ , \quad d' = d'_0 \ .$$

Irradiation Phase

During irradiation of a pair of quadrupole levels, say AD, the equilibrium of equations(7.10) would be disturbed. The equilibrium is maintained, however, by allowing mutual spin flips between levels AB and the P spins. As a result, the population of levels A , B and D, and the proton population, are all affected by irradiating AD.

Using the method of Chapter V, section 5.2, we can write down the equilibrium equations for the case of levels AB coupled to the protons throughout irradiation of AD (treated like ν^+):

$$\text{Population ratios:} \qquad a'' - b'' = -2p''$$

$$\text{Conservation of spins:} \qquad a'' + b'' + d'' = a' + b' + d' = -c'$$

$$\text{Saturation:} \qquad a'' = d'' \ .$$

Solving these for a'', b'' and d'', we obtain:

$$a'' = d'' = -\tfrac{1}{3}(2p'' + c') \qquad [c' = c'_0]$$

$$b'' = +\tfrac{1}{3}(4p'' - c')$$

To conserve energy for the mutual spin flips between levels AB and the P spins, we use equation (5.4)

$$p'' = p' - \frac{Q}{2(3P + 2Q)}(d' - a')$$

[with d' substituted for c'] .

And, since $R = \frac{P}{2Q}$ for the case of spin $I = \frac{3}{2}$, we may write this as

$$p'' = p' - \frac{1}{4(3R + 1)}(d' - a').$$

Similarly, by replacing c' for d' in the above equations, we obtain the effect of irradiating AC to saturation while AB is coupled to the proton dipolar bath.

In the same way, we may treat BD and BC like ν^- transitions, and obtain the effect of irradiating these transitions while AB is coupled to the proton bath.

The results of these calculations are given in Fig.7.7. The total amount of p''' that may be destroyed by irradiating the various transitions to saturation is plotted as a function of the spin ratio R. We see that the intensity of AC is now greater than that of BD for all R, but that all transitions are now more sensitive than expected from level crossing calculations alone. In plotting Fig.7.7, we have assumed that T_{1D} of the protons is long, so that no decay processes act to reduce p'''.

(b) Effect of coupling both AB and CD

We calculate this in much the same way as before, but we make certain assumptions to simplify the work. We assume that the P spin splitting = AB splitting = CD splitting, so that single-spin flips between any two of these systems conserve energy. This is only true in zero applied field (all splittings zero) but is approximately true in non-zero fields, given the width of the proton dipolar bath, (i.e. there are always some P spins for which the above condition is true). The equilibrium before irradiation is then controlled by the equations:

$$\text{Coupling:} \qquad \frac{1+a'}{1+b'} = \frac{1+c'}{1+d'} = \frac{1-p'}{1+p'}$$

$$\Rightarrow \qquad a'-b' = c'-d' = -2p'$$

$$\text{Conservation of spins:} \qquad a'+b' = a'_0+b'_0$$

$$c'+d' = c'_0+d'_0$$

$$a+b+c+d = 0 \quad \text{(always)}$$

Conservation of energy for the mutual spin flips leads to

$$P(2p'_0 - 2p') = Q\{[b'-a') - (b'_0 - a'_0)] + [(d'-c') - (d'_0 - c'_0)]\}$$

Solving these equations for a', b', c', d' and p', we obtain

$$
\left.
\begin{aligned}
a' &= \tfrac{1}{2}(a'_0 + b'_0) - p' \\
b' &= \tfrac{1}{2}(a'_0 + b'_0) + p' \\
c' &= \tfrac{1}{2}(c'_0 + d'_0) - p' \\
d' &= \tfrac{1}{2}(c'_0 + d'_0) + p' \\
p' &= \{ p'_0 + (b'_0 + d'_0)/2R \}/(1 + \tfrac{1}{R})
\end{aligned}
\right\} \quad \text{using} \quad R = \frac{P}{2Q} \; . \qquad \ldots (7.11)
$$

Irradiation Phase

Irradiation of either AC or BD now has no net effect on the P spins, because equilibrium can be maintained with the P spins merely by mutual flips between AB and CD. The equilibrium after irradiation to saturation in either case is given simply by

$$
\begin{aligned}
a'' = c'' &= - p'' \\
b'' = d'' &= + p'' \\
p'' &= p' \; .
\end{aligned}
$$

Irradiation of AD or BC, however, must alter the P spin populations in order to maintain equilibrium.

After performing the calculations as in the previous section, we obtain, for irradiation of AD to saturation:

$$
\begin{aligned}
a'' = d'' &= \tfrac{1}{2}(a' + d') = 0 \\
b'' &= b' + \frac{R}{R+1} \cdot \frac{(d' - a')}{2} \\
c'' &= c' - \frac{R}{R+1} \; \frac{(d' - a')}{2} \\
p'' &= p' - \frac{1}{R+1} \; \frac{(d' - a')}{4}
\end{aligned}
$$

and, for irradiation of BC to saturation

$$
\begin{aligned}
b'' = c'' &= \tfrac{1}{2}(b' + c') = 0 \\
a'' &= a' + \frac{R}{R+1} \; \frac{(c' - b')}{2} \\
d'' &= d' - \frac{R}{R+1} \; \frac{(c' - b')}{2} \\
p'' &= p' + \frac{1}{R+1} \; \frac{(c' - b')}{4}
\end{aligned}
$$

The results of these calculations are plotted in Fig.7.8,which gives the percentage of p''' that may be destroyed by irradiating each of the four

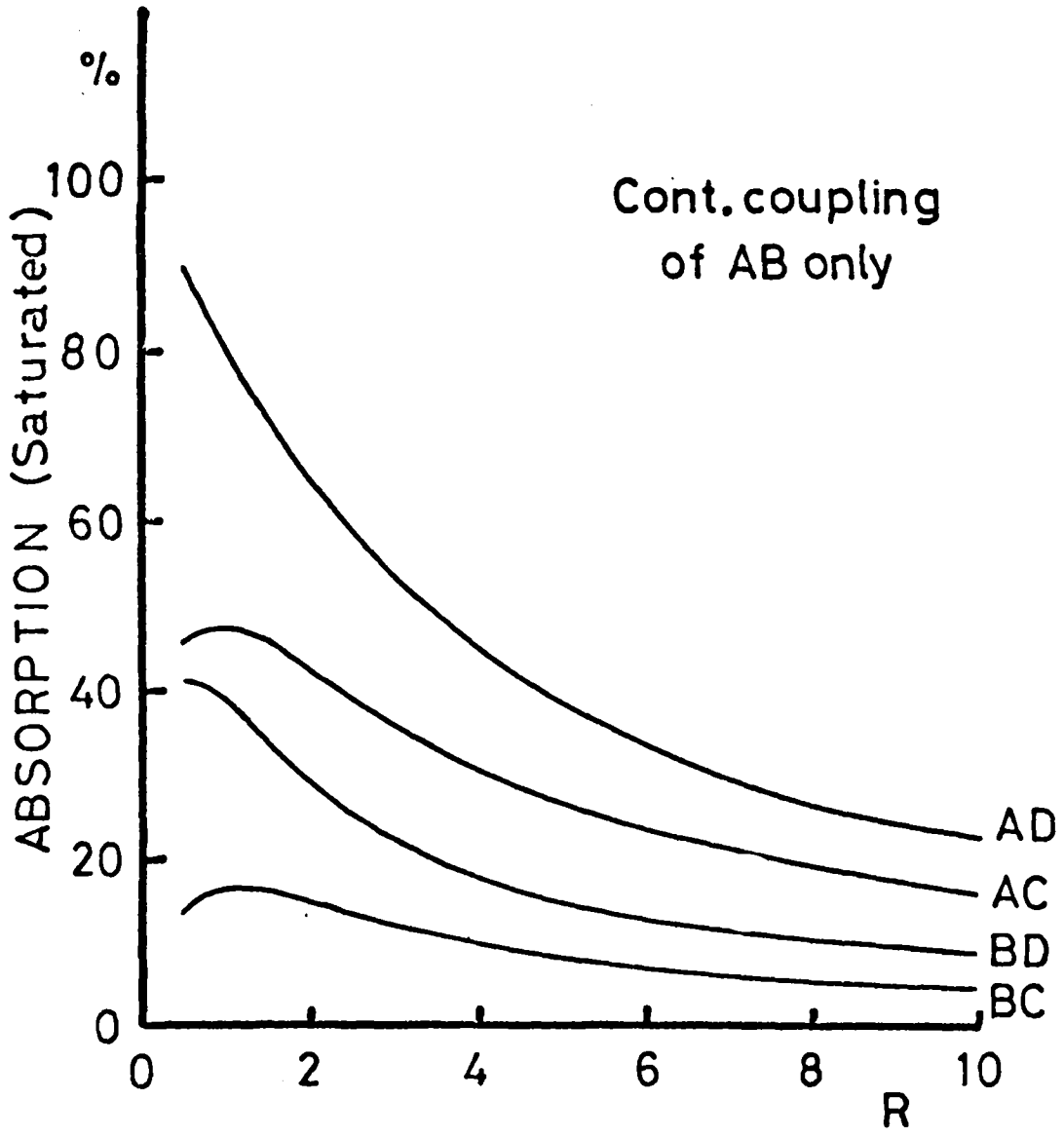


Fig.7.7

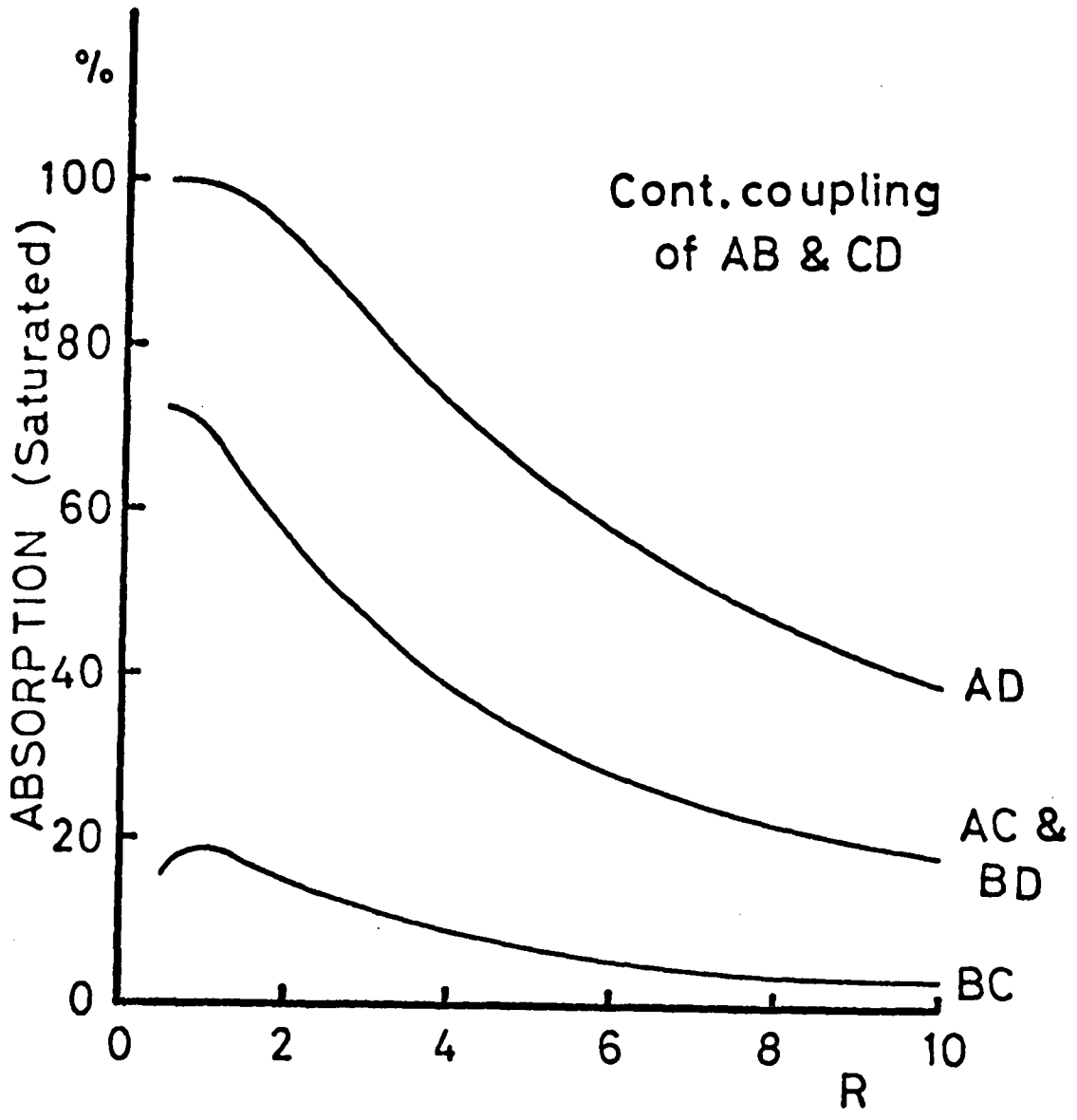


Fig.7.8

Amounts of $p'''(0)$ affected by (single) irradiation with continuous coupling

transitions to saturation, while coupling both AB and CD to the P spin bath.

Relative to Fig.7.7 (coupling of AB only) we see that AD is more intense, BC is about the same intensity, and in Fig.7.8, the common intensity of AC and BD is somewhat larger than the intensity of AC, the larger of the two in Fig.7.7.

To relate these results to real experiments, we must compare the relative intensities of the four transitions, as predicted in Figs.7.7 and 7.8, to the measured relative intensities. For low values of DC field, we expect Fig.7.8 to be true, and Fig.7.7 to hold for larger values of DC field. In fact, for all values of DC field such that the four lines are resolved, the experimental results resemble Fig.7.7, rather than Fig.7.8. From this we can conclude that, for such fields, the coupling between the P spin bath and levels CD is small while we expect that the coupling of levels AB is significant.

If we employ double irradiation techniques, and ensure that the P spins are always saturated ($p'' = 0$), we should obtain the same effects as calculated in the earlier section on double irradiation, assuming that we saturate levels AB as well as the P spins. The weak coupling of levels CD to the P spins means that they are little affected by such irradiation, except when the applied DC field is low.

7.4 EXPERIMENTAL INVESTIGATION OF NaOH AND ITS DERIVATIVES

As predicted by theory, a DRLC spectrum of a sample of NaOH (analar grade, from BDH at 97% pure) consists of a single spectral line when the static applied field is zero (measurements all at 77^0K).

The line is centred at 1920 ($\pm$ 2) kHz, and has a width at half height of 18 kHz. Fig.7.9 also shows the same sample, scanned using double irradiation at 50 kHz. The irradiation period is divided between continuous

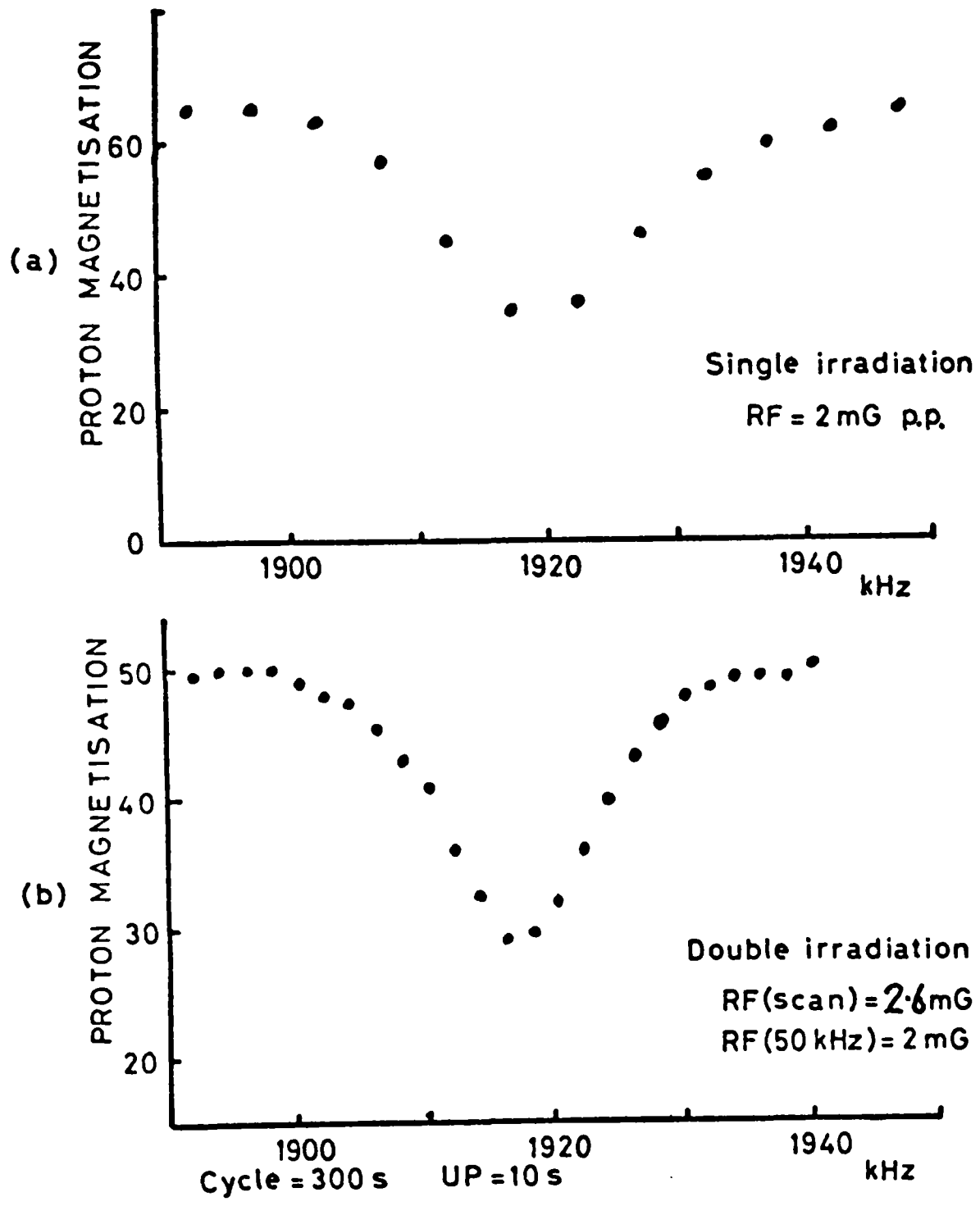


Fig.7.9: Zero-field NQR signals in NaOH

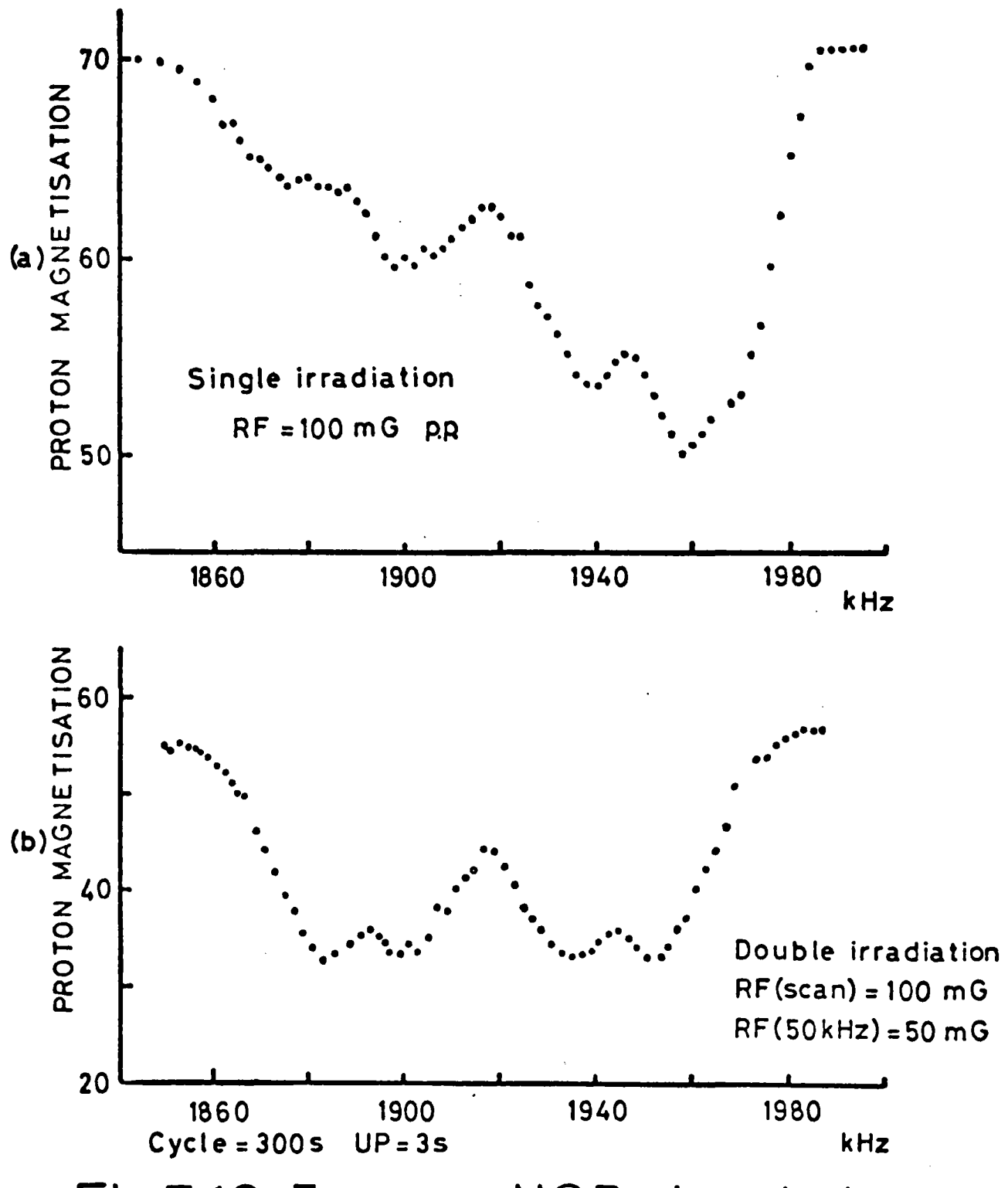


Fig.7.10: Zeeman NQR signals in NaOH for B_o = 23 gauss

50 kHz at intensity 2.6 milli-Gauss (peak-to-peak) and a scanned R.F. frequency of 2.0 milli-Gauss peak-to-peak.

The double irradiated spectrum reveals a shift in line centre to 1917 kHz and slight narrowing of the line to 14 kHz. This effect is due to dipole-dipole coupling between the protons and sodium nuclei in the small internal fields of the sample. This coupling favours transitions in which a proton and a sodium both simultaneously absorb a photon, at a frequency of $\nu_{Na}(\text{true}) + \nu_{H}(\text{local field})$. The true sodium line is thus broadened and shifted to the high frequency side. This 'proton satellite' effect is also observed in spin 1 nuclei (see N-H satellites and especially $N\text{-}H_2$ satellites[4,53]), but is stronger (in zero field) for unquenched nuclei such as ^{23}Na and ^{17}O (spin $\frac{5}{2}$). [The lower satellite $\nu_{Na}(\text{true}) - \nu_{H}(\text{local field})$ is always much weaker.]

Double irradiation at 50 kHz destroys all the proton magnetisation remaining in zero field (after level crossings), and thus prohibits the protons from absorbing at the quadrupole satellite frequency. Only the sodiums can then absorb power, thus revealing the true quadrupole line centre. Care must always be taken with unquenched quadrupolar nuclei to eliminate satellite effects. It is often advantageous to double irradiate when examining spin 1 nuclei such as nitrogen, even though this satellite effect is much weaker. The effect is fairly small in NaOH, but samples containing proportionately more protons exhibit larger apparent shifts, because the Na line is weaker.

Having obtained the true zero field value of the quadrupole absorption frequency, we proceed to examine spectra in which a constant static magnetic field is applied to the sample during irradiation, aligned parallel to the R.F. irradiation field.

Figure 7.10(a) shows the spectrum obtained with a static field of 23 Gauss. One notes that there are four overlapping lines which increase in

intensity with increasing frequency - this agrees with the predictions of the level crossing theory for spin $\frac{3}{2}$. Fig.7.10(b) shows the effect of double irradiation on this same spectrum. The relative intensities of the lines are considerably changed, as was predicted by the level crossing theory, and the overall sensitivity increased (as judged by the total area beneath the absorption curve). Using double irradiation in this way, always at a frequency $\approx \frac{\gamma(Na)}{\pi} \cdot B_0$, where B_0 is the static applied field, it is much easier to resolve the centres of the four spectral lines, over the range of 10 Gauss $\leq B_0 \leq$ 40 Gauss. Without double irradiation, resolution is barely possible, and then only in the region near B_0 = 25 Gauss.

Having obtained spectra as in Fig.7.10(b) for a variety of values of B_0, curve-fitting is carried out in order to estimate the true line centres of the four overlapping lines. A representative sample of this is shown in Fig.7.11. Symmetric absorption curves of appropriate amplitude are drawn on top of the experimental spectrum, and positioned so that, when added together, they give the observed spectrum. This process can be done by computer, but it is simpler in this case to do the operation by hand and eye. Two or three iterations usually produce a satisfactory and unique answer, from which line centres and maximum errors can be accurately estimated.

The four fitted curves are of slightly different amplitudes in this case. Full continuous coupling predicted that all four lines would be equally intense, but the calculation assumed that all the transitions were driven to saturation. If the lines are not fully saturated, and if different transitions saturate at slightly different rates (different R.F. intensities) then some differences are to be expected.

When this curve-fitting has been done, the results are plotted on to a graph (Fig.7.12), showing line centre frequency as a function of field. It is immediately observed that the four lines diverge linearly with increasing field from the true zero-field value.

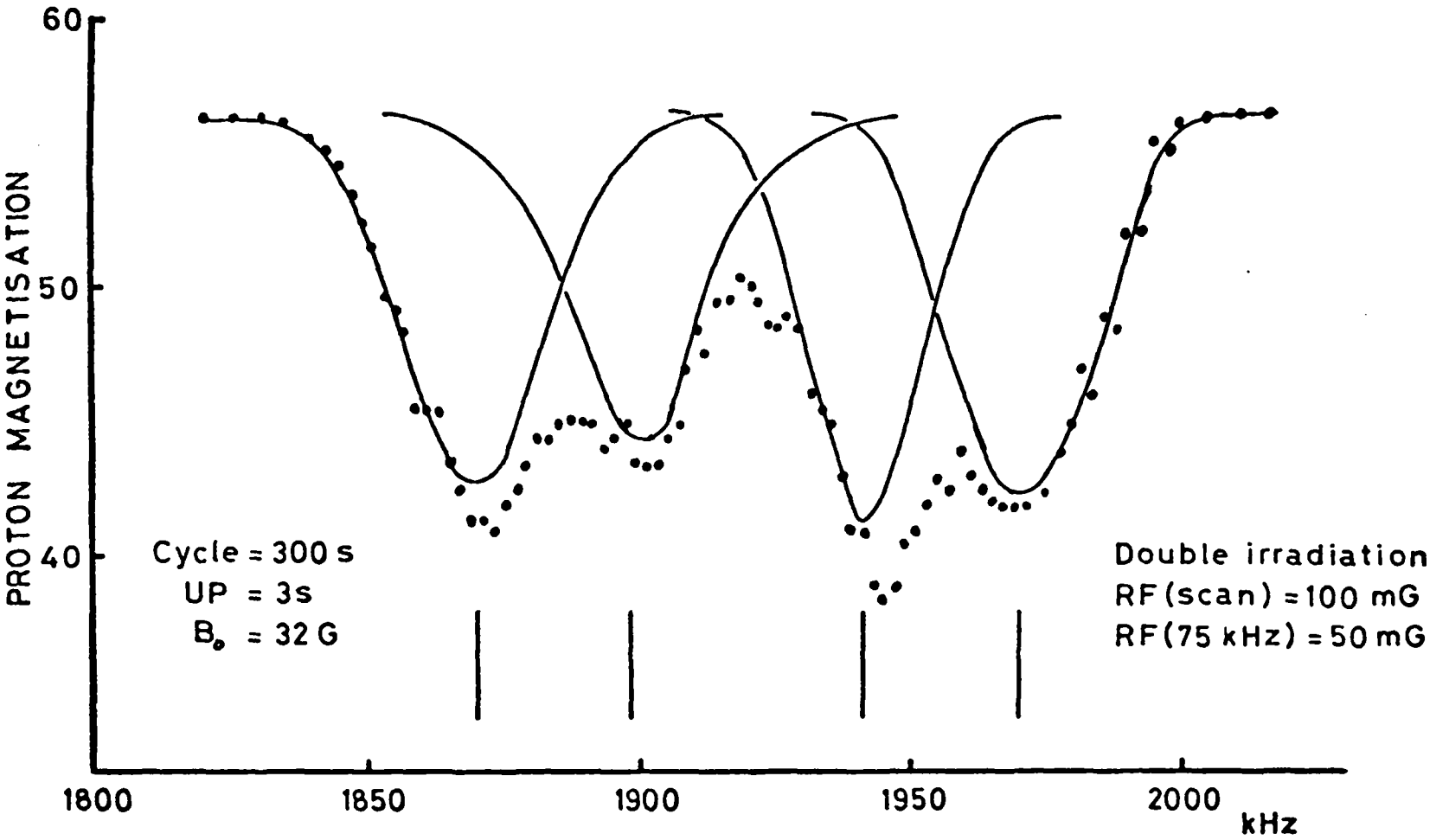


Fig. 7.11: ZNQR in NaOH - Curve fitting example

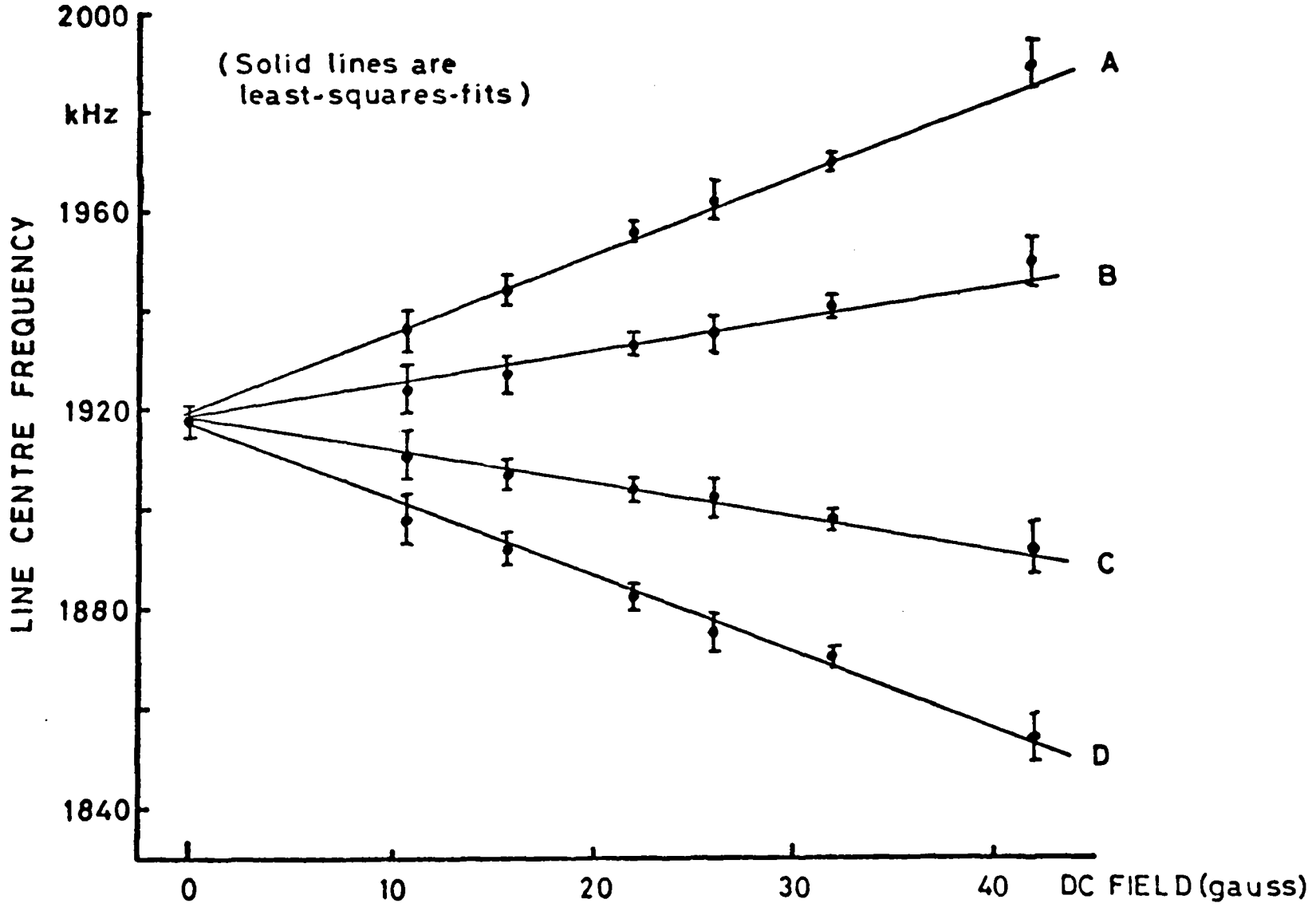


Fig. 7.12 : ZNQR in NaOH - Magnetic field shifts

A simple least-squares-fit program on a PDP8 computer gives the values of the slopes of the lines in Fig.7.12, with their expected errors. When these slopes are compared with the theoretical predictions of section 7.2, Table 7.1 is the result.

TABLE 7.1

Line (Fig.7.12)	Slope kHz/Gauss (± .07)	η deduced (± .07)	γ deduced (± .07) kHz/Gauss
A	+ 1.56	0.41	1.13
B	+ 0.65		
C	- 0.66	0.40	1.12
D	- 1.53		

The deduced value of γ compares with γ = 1.126 kHz/Gauss as published by VARIAN[54], and agreement is well within experimental errors. The deduced values of η agree [within the errors], and we can thus quote an η of 0.4 ± 0.07 for the Na^+ ion in crystalline NaOH. Knowing η, we can deduce e^2qQ from the zero-field absorption frequency, since

$$\nu_q = \frac{e^2qQ}{2h}\left(1 + \tfrac{1}{3}\eta^2\right)^{\frac{1}{2}} .$$

7.4.1 Comparative Studies

Very little work has been done on the quadrupole resonance of sodium. The only reported values for a hydrogen-containing sodium compound refer to sodium thiosulphate. A single crystal NMR study[55] revealed η's of 0.334 and 0.41 for the two sodium sites in the molecule (e^2qQ/h = 2260 kHz and 830 kHz).

A Zeeman NQR spectrum of this compound was produced, but the low ratio of sodiums to hydrogens made observation very difficult. Only the lower frequency line was observed (at 415 kHz ± 2) in zero field. Field splitting produced four lines, barely resolvable from noise, indicating an intermediate value of η (0.2→0.8) - no more could be said than that. It was apparent that η was not zero or one, as either a two-line or three-

line spectrum would have been obtained in these cases. This is 'confirmation' of a sort. The Zeeman NQR value agrees with the single-crystal NMR value within experimental accuracy, but that accuracy is very limited.

Given this degree of confirmation, we proceeded with the investigation of the NaOH complexes; in the event of an unreal result - either γ wrong or $\eta > 1$ - being produced, the theories would be disproved. Otherwise, the information might be of value, and circumstantial evidence of this type adds weight to the theory.

It is noted that the Zeeman NQR method in powders using double resonance for detection is not absolutely proved by experiment. All we can say is that the theory given in section 7.3 is consistent with the data taken in this section, and no unexplained results have so far been obtained.

7.4.2 The Hydrates of NaOH

It is well-known[56] that NaOH forms several complexes with water and the crystal structures of some of these are known.

To begin our investigation, we made up samples of $NaOH/H_2O$ mixtures, including several of the complexes. This was done by adding weighed amounts of deionized H_2O to weighed amounts of NaOH, and gently heating the mixture until the whole sample became liquid. (The complex $NaOH.H_2O$ = '50%' sample, has a melting point of 64.3°C.) The sample was then poured into the PTFE sample container and allowed to set, before proceeding with the measurements, which were all performed at 77°K. Samples with >60% NaOH could not be prepared in this way.

One sample of ≈ 80% NaOH was made by evaporating water from a 50% sample under vacuum at ~ 100°C. The water content was estimated by comparing the relative strengths of the Na NQR signals characteristic of NaOH and $NaOH.H_2O$.

Using the Bruker as a simple pulsed NMR spectrometer, we measured the spin-lattice relaxation times of the protons in the samples at 77°K in a field B_0 = 1 Tesla, and present the results in Fig.7.13.

It can be seen immediately that the proton T_1 is only long (i.e. ≥ 1 minute) at or near the stoichiometric complexes $NaOH.4H_2O$, $NaOH.3\frac{1}{2}H_2O$, $NaOH.H_2O$ and for ≥ 70% NaOH. (We use the molecular % notation; where $NaOH.H_2O$ = 50% NaOH, $NaOH.4H_2O$ = 20% NaOH, etc.).

Since our double-resonance method relies on a long proton T_1 for successful operation, we are thus limited to studying the above mixtures only.

We next proceeded with an Na-NQR study of the 20% and 50% NaOH mixtures, and, following the procedures laid down in section 7.4, we obtained the data shown in Table 7.2. Despite several attempts, we were unable to distinguish between $NaOH.4H_2O$ and $NaOH.3\frac{1}{2}H_2O$ (from the Na-NQR point of view) and thus we only give the figures for $NaOH.4H_2O$.

To complete the study, in collaboration with an undergraduate, H. Steele, we prepared partly deuterated samples of NaOH, $NaOH.H_2O$ and $NaOH.4H_2O$, by using a mixture of 20% D_2O in H_2O instead of pure H_2O. The NaOH/NaOD sample was made by evaporating the 50% sample at 300°C under vacuum for 12 hours, until the Na resonance at 1203 kHz became undetectable, and only the NaOH resonance at 1917 kHz remained.

TABLE 7.2

Sodium NQR data on NaOH and its Hydrates

% NaOH	Complex	$\nu_q \pm 2$ (kHz)	e^2qQ/h (±10) (kHz)	$\eta \pm 0.08$
100	NaOH	1917	3728	0.4
50	$NaOH.H_2O$	1203	2253	0.6
20	$NaOH.4H_2O$	684	1124	0.75

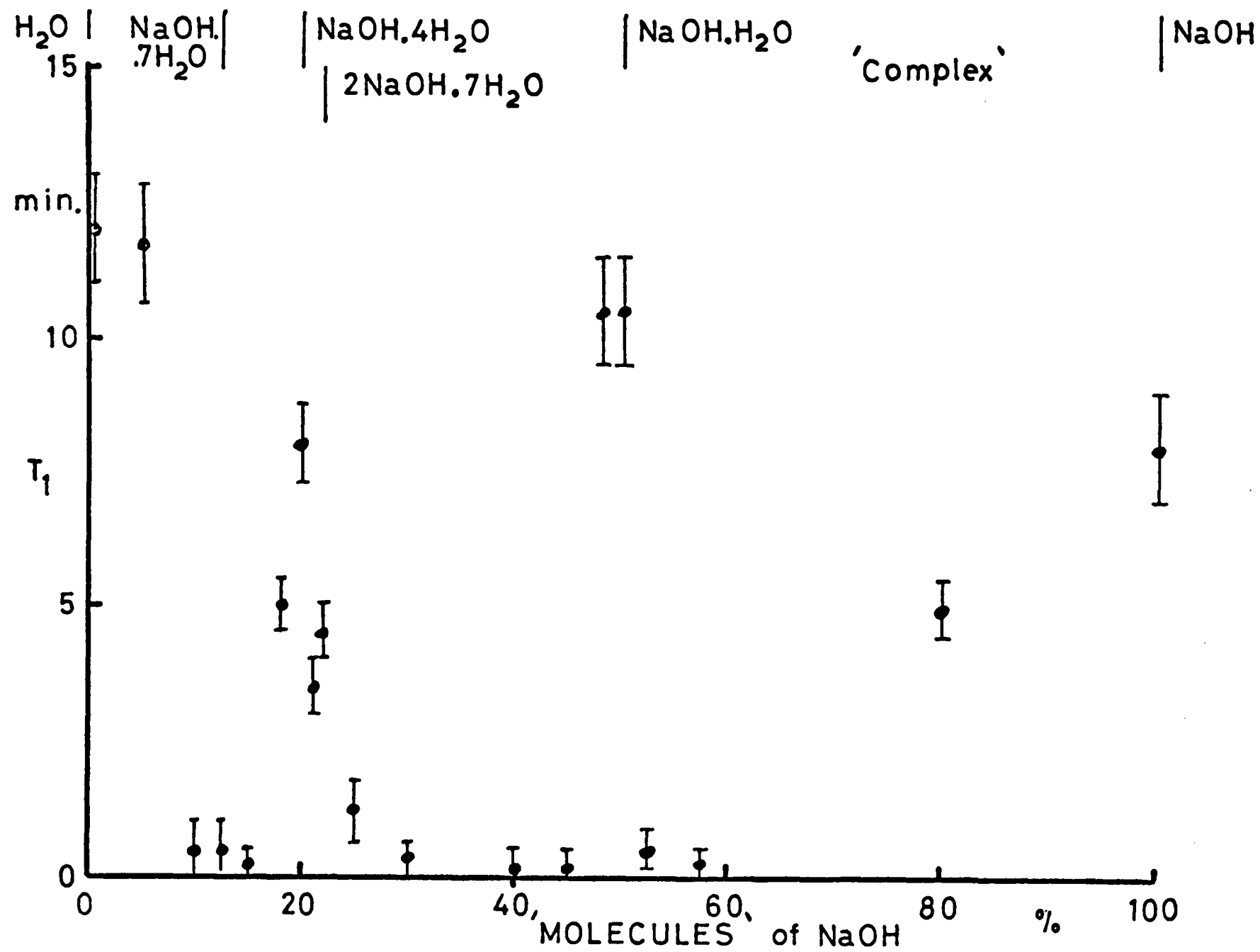


Fig.7.13 : Variation of proton T_1 in $NaOH/H_2O$ mixtures

TABLE 7.3

Dilute Deuterium NQR Data on NaOH and its Hydrates

Complex	Site	ν_+ (± 1 kHz)	ν_- (± 1 kHz)	e^2Qq/h (± 2 kHz)	η (± .01)
NaOH	OD^-	211	207	278	0.03
$NaOH.H_2O$	OD^-	202.5		270	0
	HDO	140	131	181	0.10
$NaOH.4H_2O$	OD^-	202		270	0
	HDO (I-IV)	141	132	(182)	(0.10)
		162.5	147	(214) Av	(0.16) Av
		171.5	153		
		173	157		
H_2O [63]	HDO	167	154	214	0.12,

The deuterium NQR data, taken by H. Steele, are presented in Table 7.3. Assignment is unambiguous except for $NaOH.4H_2O$, where there are four different water molecules (see structure section). It was not possible to obtain enough additional data to group the observed lines into $\nu_+ \nu_-$ doublets, but a possible assignment for some of the eight observed lines is indicated by the dotted lines and bracketed values of e^2Qq and η in Table 7.3. This assignment is based on structural considerations.

We shall now describe some of the relevant points of the structures of these materials, as taken from the literature, before returning to the assignment argument.

7.4.3 Structures of NaOH and its Hydrates

These materials are all ionic, and the electrostatic effects of the ions Na^+ and OH^- mean that nearest-neighbour considerations are not adequate when attempting to estimate quadrupole coupling constants for an Na^+ ion site. If one were to attempt such a calculation, one would need to take account of the large Sternheimer anti-shielding factor of the Na^+ ion (≈ -4 [59]).

One may, however, make some comparisons between the quadrupole and structural data from the symmetry point of view alone.

NaOH The structure has been determined by neutron diffraction[57] at room temperature. NaOH has two phases, but only the α-phase, stable below 299°C is of interest here.

The solid is made up of close-packed NaOH groups in a monoclinic lattice, with apparently no hydrogen bonding. The basic unit is linear, arranged Na-O-H, with Na-O = 2.301 Å, and O-H = 0.918 Å. The radii of the ions are ~1 Å for Na^+ and 1.35 Å for an O^{2-}, so that the H is 'embedded' inside the OH^- ion.

The H is so close to the O in the OH^- ion, that its electrostatic environment is almost wholly determined by the electron distribution of the oxygen. Since an O^{2-} ion has the electron structure $1s^2 2s^2$, it is spherically symmetric and the ionic charge is concentrated at the nucleus. When we add an H^+ ion to the O^{2-} to make up an OH^- ion, the electron shells will redistribute themselves about the two nuclei, but it is apparent that only the O-H axis is unique. Thus, from the point of view of the D, the principal axis of the field gradient (V_{zz}) will point along the OD axis, while $V_{xx} \sim V_{yy}$ due to the axial symmetry and $\eta \approx 0$. In NaOH, there are other Na^+ ions near the D (Na(1) ... H(2) ~ 3 Å), and these apparently are sufficient to reduce the symmetry slightly from pure axial, since $\eta = 0.03$.

There is an asymmetric arrangement of charges around the Na^+ ion. $\eta = 0$ would require axial symmetry and $\eta = 1$ requires that (say) the Na^+ ion lie at the centre of a regular tetrahedron of charges of two different sizes, there being two charges of each size, and that the rest of the crystal repeat this symmetry.

The arrangement of ions around the Na^+ is monoclinic with nearest OH^- ions at 2.301 Å, 2.428 Å and 3.790 Å and nearest Na^+ ions at 3.101 Å and 4.100 Å. This clearly does not correspond to $\eta \approx 0$ or $\eta \approx 1$ and we conclude that $\eta = 0.4$, as measured, is not unreasonable. We also note

that all Na^+ ions are equivalent, corresponding with our single site as determined by NQR.

To check temperature variations, we remeasured NaOH at the highest possible (limited by T_1) temperature. At 217°K, $e^2qQ/h = 3516$ kHz and $\eta = 0.5 \pm 0.15$. There is thus no significant change in η when the temperature is reduced to 77°K, although e^2Qq does increase as the temperature is lowered, in agreement with the vibrational mode theories of LUCKEN[18] and BAYER[58].

We thus feel justified in using the room-temperature structural data to argue in favour of the 77°K quadrupole data.

$NaOH.H_2O$ This structure has been determined by X-ray diffraction[60]. The solid is made up of a series of infinite sheets, linked by weak hydrogen bonds ~ 3.11 Å long between the layers.

Each layer is constructed of linked, distorted tetrahedra, consisting of an Na^+ ion surrounded by four oxygens, some of which are water molecules. The tetrahedra share edges and corners to make up the infinite sheet of $NaOH.H_2O$.

There is, again, only one distinct Na^+ site and there are two oxygen sites, but it is not known which is the OH^- and which is the H_2O.

The additional uncharged water molecules evidently help to shield the H in the OH^- ion from external electrostatic effects, as shown by the low value of $\eta \sim 0$ for OD^-.

The Na^+ site is at the centre of a distorted tetrahedron with Na - O(1) = 2.30 Å and Na - O(2) = 2.35, 2.39 and 2.41 Å. This arrangement is more 'cubic' than NaOH, but the corners of the tetrahedron differ in type - some are OH^- and some are H_2O. Thus the more 'cubic' lattice ensures a reduction in e^2Qq while the differences inside the tetrahedron imply a larger value of η, compared to NaOH.

$NaOH.4H_2O$. This structure has also been determined by X-ray diffraction[61,62], and is considerably more complicated that the others given above.

The crystal has a single Na^+ site, a single OH^- site and four different H_2O sites. Each Na^+ ion is surrounded by a cage of ~ 5 H_2O molecules, and each OH^- ion is surrounded by ~ 6 H_2O molecules, the whole lattice being a network of $(Na^+)\,5\,H_2O$ and $(OH^-)\,6\,H_2O$ units, sharing certain water molecules and thus being bound together by ionic forces and hydrogen bonds.

The Na^+ site is more nearly cubic (as judged by distances to OH^- sites) and this correlates with the further reduced value of e^2Qq. The charge differences between OH^-, H_2O and neighbouring Na^+ again ensure that $\eta \neq 0$, and a tendency for $\eta \to 1$ as $e^2Qq \to 0$ is not unreasonable. If we consider a system of Na^+OH^- very dilute in H_2O, we might expect an extended cubic 'lattice' of Na^+ and OH^- to be formed, rather like Na^+Cl^-, with H_2O as an electrically-neutral medium. Such a system would have $e^2Qq \sim 0$, but if $e^2Qq > 0$ due to a slight distortion from cubic symmetry, then $\eta \sim 1$. We would thus predict for the Na^+ ion, that $e^2Qq \to 0$ and $\eta \to 1$ as the concentration of $NaOH$ in H_2O is decreased.

Once again OD^- has $\eta = 0$ and e^2Qq almost unchanged. The additional hydration helps to shield the OH^- ion from other electrostatic charges.

7.4.4 Water Molecules and Assignment of the HDO Spectrum of $NaOH.4H_2O$

There are four different water molecules in the structure, and eight distinct quadrupole lines in the range 132 - 173 kHz. We observed that in $NaOH.H_2O$, there is only one pair of lines corresponding to an HDO, indicating that the two possible deuteron sites on the HDO molecule must be equivalent (as in ordinary ice Ih [63]).

Given that there are four water sites and eight lines, we thus feel justified in saying that each water molecule has two equivalent deuteron sites, with two lines (ν_+ and ν_-) for each water molecule.

If we name the four water sites $O_I \ldots O_{IV}$ as in reference (62), we note certain points about the structures of the sites. All the nearest neighbours of O_{IV} are H_2O's or OH^-. The hydrogen bonding network is similar to that of ice. The O_{II} site is shared between two neighbouring Na^+ ions, in a similar way to the shared edges of the tetrahedra in $NaOH.H_2O$.

We note from the quadrupole spectrum that there are two lines, at 141 and 132 kHz, which are very similar to the two lines in $NaOH.H_2O$ at 140 and 131 kHz. It may thus be justifiable to group these two as a $\nu_+ \nu_-$ pair and relate them to the site O_{II}, because of its similarity to the H_2O site in $NaOH.H_2O$.

If we sum the remaining six lines we obtain an average e^2qQ/h of 214 kHz (identical to that in ice[63]) and if we group them into ν_+ and ν_- as in Table 7.3, we obtain an average η of 0.16, which is somewhat larger than the value for ice.

We may stretch the argument a little further, if we link the lines at 171.5 and 153 kHz into a $\nu_+ \nu_-$ pair associated with site O_{IV}, since this pair most resembles ordinary ice lines. Almost equally likely, however, is the pairing of the lines at 162.5 and 153 kHz.

The assignment of lines in this way is of little value, considering the uncertainties involved, but further work with samples highly-enriched in deuterium may allow a more rigorous analysis, through observation of nuclear double quadrupole resonance lines (as in Chapter VI, p.139).

7.5 CONCLUSIONS

We have taken the Zeeman NQR theories of MORINO et al[51,52] and applied them to the double resonance technique, successfully predicting the form of the observed spectra under both single and double irradiation.

Using this method we have measured the quadrupole spectra of the Na^+ ion in environments of differing hydration, and related the results to the known structures by symmetry arguments.

Measurement of the dilute deuterium spectra has also fitted with the structural information, although a complete analysis of the NaOH.4HDO spectrum was not possible.

CHAPTER VIII

RELAXATION TIMES AND RELATED PROBLEMS

8.1 INTRODUCTION

From the description of our experimental method, it is evident that we rely on certain relaxation times to be 'long' if a given sample is to be examined by the double resonance method.

Using the terminology of Chapter II, we may summarise the requirements, and the reasons for them.

8.2 RELAXATION TIMES AND THE D R L C METHOD

8.2.1 Proton (P-Spin) Spin-Lattice Relaxation Time T_1

This must be 'long' compared to events that happen during the experimental cycle, but not too long compared to realistic cycle times. For example, a realistic maximum cycle time is ~ 15 minutes. When longer than this, the experiment takes an excessively long time to complete. If a sample proton $T_1 \approx 4$ hours, then the spins cannot acquire a significant magnetisation in a time $\approx$ 15 minutes, and sensitivity is lost, due to this small initial magnetisation. Long T_1's are not usually a problem, however.

A 'short' T_1 is a time $\approx$ 'up time' — the time for which the sample is removed from the large polarising magnetic field. Experimentally, up-time can be varied over the range 1.5 - 1000 seconds (typically 2-10 seconds). If T_1 is (say) $\approx$ 1 second, then the protons in the sample can demagnetise as it is removed from the field and remagnetise as it is returned to the magnetic field. In this case, level crossing does not effectively polarise the Q spins, and the amount of final polarisation measured which depends on the history of the Q spins (in zero field) is small compared to the amount due to simple remagnetisation of the P spins as they return to the large field. This makes the signal/noise ratio very low.

Thus, for practical purposes, $T_1 \geq 5$ seconds (approximately) is a T_1 lower limit on the P spins, if the method is to work.

8.2.2 Proton Dipolar T_1 (T_{1D})

It is often found that the spin-lattice relaxation time as measured in a zero or small D.C. field is factors (or orders of magnitude) faster than the 'high-field' value T_1. Some reasons for this will be suggested later, but since our experiment moves the sample into a zero-field region for a period $\geq$ 1 second (typically), there may be a T_{1D} restriction, even if T_1 is long. For example, if we are attempting deuterium NQR with the deuterium continuously coupled to the protons then a fast proton T_{1D} will ensure that all the polarisation of the protons and deuteriums will disappear in a time $\approx T_{1D}$, and the only component in the final measured magnetisation will be that due to proton remagnetisation during the return to high field — there is then no 'signal' to detect. For nitrogen NQR, however, a fast T_{1D} may be unimportant, or even useful.

8.2.3 Q Spin Relaxation Times

During the 'Polarisation Phase', the Q spins acquire polarisation from the P spins. If the Q spins relax rapidly back to thermal equilibrium with the lattice (short T_1) then the populations of their energy levels cannot be affected by irradiation, and we again detect no 'signal' after the return to the large field, except for polarisation that resides in the P spins throughout the irradiation phase and/or remagnetisation. Short Q spin T_1's are very rare, and have not affected any of this work.

8.2.4 T_1 and the NQR Experiment

There are thus two combinations that allow experiments to proceed:

(a) Long T_1, Long T_{1D}, Long $T_1(Q)$: the 'normal' conditions. We may destroy the P spin magnetisation if we wish by direct irradiation of the P spins while in zero field (at $\sim$ 50 kHz say). Sensitivity is high.

(b) Long T_1, Short T_{1D}, Long $T_1(Q)$: Provided T_{1D} only becomes 'short' for values of magnetic field lower than that necessary for level-crossing with the Q spins, this is much the same as (a), if the P spin magnetisation is destroyed by direct irradiation while in zero field. However, if T_{1D} is 'short' when level crossing occurs, the polarisation phase may be ineffective, remagnetisation becomes troublesome and sensitivity is lost, or the experiment becomes impossible. Thus a short T_{1D} can often be useful for a DRLC experiment. However, a fast T_{1D} rules out DRCC (i.e. deuterium NQR) because the P and Q spins form one thermal system. The fast T_{1D} 'shorts out' the Q spins and makes $T_1(Q)$ also fast ($T_1(Q) \sim T_{1D}$ for DRCC) so that detection is impossible.

8.3 FACTORS AFFECTING T_1 AND T_{1D}

Much work has been (and is being) done on the factors affecting spin-lattice relaxation times. There are several useful theories concerning relaxation, and much useful information can be extracted from measurements of T_1's by means of these theories.

For our purposes, we are only concerned with whether T_1 is 'long' or 'short', as indicated above. An understanding of the factors affecting T_1 is useful from the point of view of choosing fields of study that will be profitable, i.e. choosing samples that are likely to produce results from the NQR experiment.

T_1 describes the rate at which energy is exchanged between the spins and the lattice. For example, when an assembly of magnetic dipoles such as protons are placed in a large magnetic field, they will acquire a total net magnetisation M_0 at a rate T_1, where the size of M_0 depends on the value of the applied field and the lattice temperature, among other things. To understand T_1, we must understand the mechanisms by which energ is exchanged between the nuclear spin system and the lattice, so that they may come to equilibrium. We can divide the mechanisms broadly into two

types — paramagnetic relaxation and phonon-induced relaxation, which includes any mechanism involving changes in the orientations of atoms or molecules in a lattice.

We are concerned here only with solid materials, and consequently will confine our attention to those relaxation mechanisms which are active in solids.

8.3.1 Paramagnetic Relaxation[64]

According to ABRAGAM[12, p.378], a nuclear spin $\underline{I}$ and an electronic spin $\underline{S}$ will have a dipolar coupling involving combinations of the two operators. Among the various terms in this coupling operator, there is the term

$$C = -\tfrac{3}{2} \sin\theta \cos\theta \, e^{-i\phi} S_z I_+$$

where θ and ϕ define the direction of the vector joining $\underline{S}$ and $\underline{I}$ relative to the applied field.

He shows that this operator can induce a flip in the nuclear spin without a flip of the electron spin (which would require much more energy) and that the nuclear T_1 as a result of such processes alone is given by

$$\frac{1}{T_1} = \frac{2}{5} \frac{S(S+1)}{\tau} \left(\frac{H_e}{H_o}\right)^2 \quad \text{(ignoring angular dependence)}$$

where τ = longitudinal electron relaxation time ('electron T_1')

H_o = applied D.C. field

H_e = electronic field $\approx \gamma_s \hbar S/r^3$

and γ_s = electronic gyromagnetic ratio

r = distance between electron and nucleus.

This shows that, for small numbers of paramagnetic centres, nuclear dipoles close to a paramagnetic centre will relax much more rapidly than those further away. However, nuclei close to a paramagnetic centre will experience a shift in their resonant frequency, due to the local magnetic field of the unpaired electron, and will thus tend to become decoupled from the nuclear spin system as a whole. As it stands this theory is inadequate

to explain observed T_1's in dilute paramagnetic materials.

The 'volume of influence' of a paramagnetic centre is given by the volume around it up to a distance $\sim r_0$, where r_0 is the value of r for which $H_e = H_L$, the local (nuclear) dipole-dipole field. This 'volume' may be asymmetric - see reference (65). Information is carried beyond this radius by a spin-diffusion process among the nuclear dipoles, carried out by mutual spin-flips of the nuclei. This process is characterised by a diffusion constant D and the derived expression for T_1 is then

$$\frac{1}{T_1} = 4\pi N b D \qquad \ldots (8.1)$$

where N = number of paramagnetics/unit volume

and $b \sim a\left(\frac{H_o^e}{H_o}\right)^{\frac{1}{2}} (W\tau)^{-\frac{1}{4}} \sim a.$

with a = internuclear spacing

H_o^e = electronic field at distance $r = a$ from ion.

W = probability of the nuclear 'flip-flop' process.

There are elaborations of this theory, but they do not concern us here. We note mainly that the length of T_1 is inversely proportional to the concentration of paramagnetic impurities and T_1 is directly proportional to $\sqrt{H_o}$. Since electronic relaxation times τ are very short ($\sim 10^{-5}$ sec), very low concentrations $\sim 10^{-4}$ % have a significant effect on T_1, and $T_{1D} < T_1$, even if no other effects are considered, such as spin-spin interactions in zero field.

T_1 will increase as the temperature is lowered due to changes in D and τ, but ABRAGAM[12, p.388] shows that there is only a factor 2 difference in T_1 when the temperature is lowered from 300°K to 77°K in a single crystal of LiF, for example; see reference (66).

Paramagnetic impurities are often of use to us to shorten the T_1 of certain samples. As stated, very long T_1's are inconvenient experimentally, and addition of a few p p m of a paramagnetic impurity such as

Mn^{++} will often reduce T_1 to a few minutes. So long as the concentration N is low, most of the structure is almost unaffected by the presence of the impurity, since nuclei at a distance $r > r_0$ from the paramagnetic centre experience the impurity ion only through spin diffusion effects.

In general, however, paramagnetic relaxation is of only secondary importance to NQR, since we normally work with extremely pure diamagnetic substances; of far more importance are the various phonon-induced relaxation processes.

8.3.2 Phonon-Induced Relaxation

The references[67] give a range of current work on the theory of, and experiments on, phonon-induced relaxation mechanisms, but the details do not directly concern us — we seek only a general understanding.

(a) Lattice Vibrations and Phonons

Vibrations in a solid are usually characterised[68] by the phonon spectrum, which is simply the Quantum-Mechanical description of the lattice vibrational modes. If a crystal contains N_0 units (atoms), each with three degrees of freedom, then there are $\approx 3\ N_0$ normal modes of vibration with $3\,N_0$ characteristic frequencies $\omega_1, \omega_2, \ldots, \omega_{3N_0}$. Since N_0 is a very large number for real crystals, a continuum of ω's is usually assumed, extending from $\omega = 0$ up to a cut-off value $\omega \sim \Omega$ such that

$$\int_0^{\Omega} \sigma(\omega)\,d\omega = 3N_0 \qquad \ldots (8.2)$$

where $\sigma(\omega)d\omega$ is the mode distribution function, or the number of modes between ω and $\omega + d\omega$.

The Debye approximation assumes a propagation velocity v which is independent of direction or polarisation. Then

$$\sigma(\omega) = \frac{3V}{2\pi^2}\ \frac{\omega^2}{v^3} \qquad \ldots (8.3)$$

(V = volume of crystal).

(b) Spin-Phonon Coupling: [See ABRAGAM[12, p.404]]

If we have a set of spins in a magnetic field, characterised by a resonant frequency ω_s, various spin-phonon interactions may occur. The spins can emit a photon ω_s which the lattice absorbs by creating a phonon $\omega_L = \omega_s$, conserving energy (direct process). Alternatively, an interaction occurs where a phonon ω_1 is transformed into a phonon ω_2 by absorbing ω_s, where $\omega_2 = \omega_1 + \omega_s$ (Raman process). Because of the distribution of phonons, very few have $\omega = \omega_s$, but many pairs of phonons can be chosen such that $\omega_2 - \omega_1 = \omega_s$. Abragam shows that Raman processes are by far the most important in their effect on T_1 and that T_1 varies with temperature $\sim \theta^n$ where n lies in the range 2-7, depending on the temperature range under consideration.

Phonons are quantum-mechanical entities and each lattice mode can be said to consist of a set of equally-spaced energy levels $(n + \frac{1}{2})\hbar\omega_L$, with allowed transitions $\Delta n = \pm 1$. Such modes can then be characterised by an activation energy E_a where (with T = temperature)

$$\frac{n}{N_0} \propto \exp\left(\frac{-E_a}{kT}\right) \qquad \ldots (8.4)$$

If $E_a \gg kT$, $n \sim 0$, and the mode is inactive.

8.3.3 The T_1 Minimum Prediction

If we consider the effects of the lattice vibrations on a microscopic scale, we can say that any spin will experience a magnetic field which varies as a random function of time, as a result of the vibrations of its neighbours, and that this time-varying field can induce transitions between the energy levels of the spin, under suitable conditions.

The random function is limited by a correlation time τ_c. Roughly speaking, if we know the magnetic field at an instant t_1, then we can predict the field at a later time, t_2, and the probability of a successful prediction depends on $\tau = t_2 - t_1$. If $\tau \ll \tau_c$ we have a large probability of success while for $\tau \gg \tau_c$ we have very little probability of success.

This probability of success is called the auto-correlation function $G(\tau)$ [reference (12), p.270]

$$G(\tau) = \overline{H_q(t).H_q(t+\tau)}$$

where $q = x, y, z$

H = field at one spin due to its neighbours

t = time

Then $G(0) = \overline{H_q^2}$

and $G(\tau) = 0$ for $\tau \gg \tau_c$

$G(\tau)$ is a real, even function

$G(-\tau) = G^*(\tau) = G(\tau)$.

We now also introduce the spectral density function $J(\omega)$, which is the Fourier transform of $G(\tau)$

$$J(\omega) = \int_{-\infty}^{+\infty} G(\tau)\, e^{-i\omega\tau}\, d\tau \qquad \ldots (8.5)$$

$$\simeq 2 \int_{0}^{\tau_c} e^{-i\omega\tau}\, d\tau \qquad \ldots (8.5')$$

$J(\omega) = J(-\omega)$ and describes the distribution of frequencies which give rise to the random field variation in much the same way as (8.3) describes the distribution of phonons, but in a much more general way, since we have made no assumptions about crystal structures, wave velocities etc. We have only assumed that the field $H(t)$ is a stationary random function of time: i.e. it has a mean squared value $\overline{H^2(t)}$ which is a constant in time. The shape of $J(\omega)$ is as shown in Fig.8.1.

$$J(\omega) \sim \text{constant} \sim J(0) \quad \text{for} \quad \omega < \frac{1}{\tau_c}$$

$$J(\omega) \sim 0 \quad \text{for} \quad \omega > \frac{1}{\tau_c}$$

$$J(\omega) \simeq \frac{\tau_c}{(1+\omega^2\tau_c^2)} \quad \text{for} \quad \omega \sim \frac{1}{\tau_c}$$

Approximately [reference (12), p.426]

$$\int_{-\infty}^{\infty} J(\omega)\, d\omega \simeq \frac{2}{\tau_c} J(0) \qquad \ldots (8.6)$$

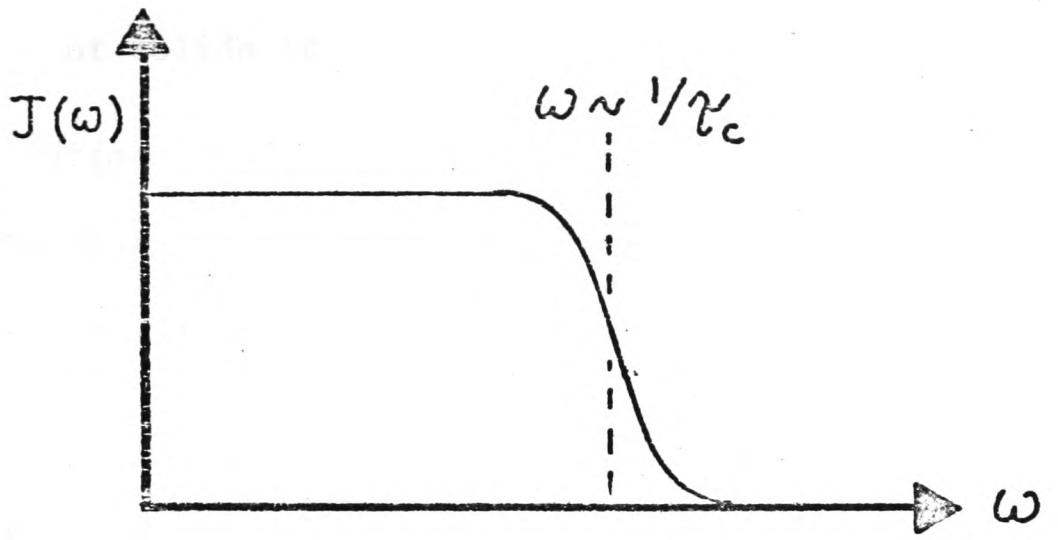


Fig.8.1

For liquids, this theory leads to the correct prediction of motional narrowing (the reduction of NMR linewidth as the temperature rises). If the rigid lattice linewidth is $\overline{\Delta\omega_0^2} = \gamma^2 \overline{B^2}$, then the observed linewidth is given by

$$\Delta\omega \simeq (\overline{\Delta\omega_0^2})\, \tau_c .$$

Narrowing occurs if $(\overline{\Delta\omega_0^2})^{\frac{1}{2}} \tau_c < 1$.

Motional narrowing is often of significance in solids also, even well below the melting point. We are, however, concerned with the origins of T_1 and T_{1D} in solids.

Spin-lattice relaxation is determined principally by the values $J(\omega_0)$, where ω_0 is the Larmor frequency (T_1 in a high field), and $J(\omega_D)$ where $\omega_D \approx 0$ and only dipole-dipole interactions are of significance (for T_{1D}).

The variation of T_1 and T_{1D} with temperature is thus reduced to the variations of $J(\omega)$ and τ_c with temperature. Such theories are varied and complex, and many may be found in the references (12) and (67) where they are successfully used to predict the properties of a wide variety of materials.

We do not delve into these theories, by we will attempt to explain some of our results qualitatively on the basis of $J(\omega)$ and τ_c. We will illustrate the method by explaining the minimum which is often observed

in the T_1 of solids as the temperature is varied.

Equations (8.2) and (8.3) describe a distribution of phonons $\sigma(\omega)$ which is similar in many ways to $J(\omega)$. We may make the comparison more quantitative and write

$$\int_{-\infty}^{\infty} J(\omega)\,d\omega \simeq \frac{2}{\tau_c} J(0) \sim \text{constant}.$$

Then $J(0) \propto \tau_c$.

As the temperature θ rises, phonons are redistributed, τ_c decreases and hence $J(0)$ decreases.

Figure 8.2 shows $J(\omega)$ for three different temperatures θ, and the fixed Larmor frequency ω_0. For θ_{low}, $\frac{1}{\tau_c} \ll \omega_0$, coupling is weak and T_1 is long. For θ_{high}, $\frac{1}{\tau_c} \gg \omega_0$, coupling is strong, but $J(\omega_0)$ is small and T_1 is intermediate in length. However, for θ_{med}, coupling is strong and $J(\omega_0)$ is large. T_1 is thus a minimum near this temperature.

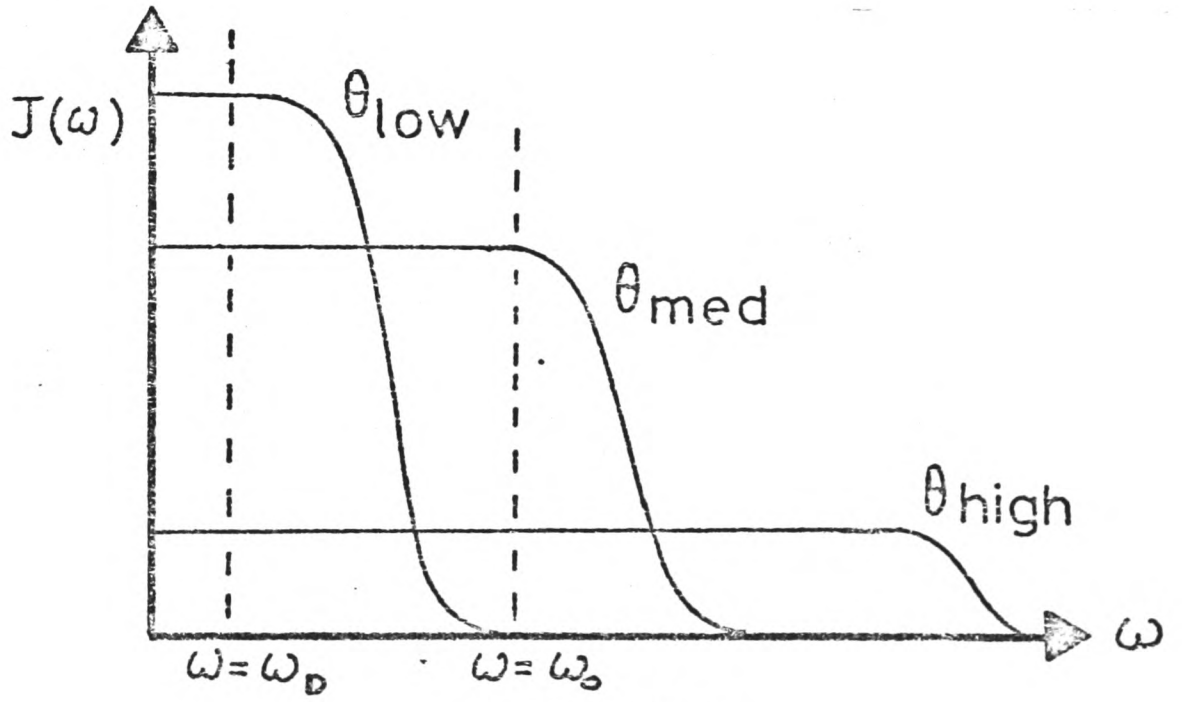


Fig. 8.2

A T_1 minimum of this type has been observed in many materials[69].

The above also shows in one way why T_{1D} is always $\leq T_1$ and usually $T_{1D} \ll T_1$. $J(\omega)$ for $\omega = \omega_D \sim 0$ is almost always large, even if $J(\omega_0)$ is very small. Indeed Fig.8.2 would predict a steady decrease in T_{1D} as the

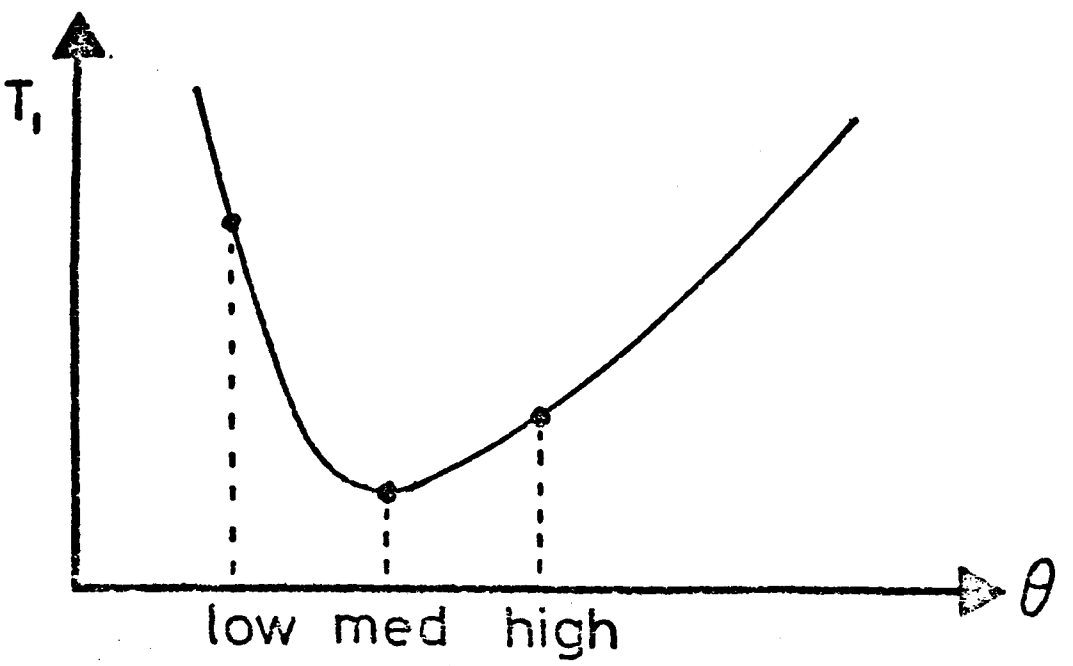


Fig.8·3

temperature falls, due to the increase in $J(\omega_D)$. GOLDMAN[36, p.55] shows that $T_{1D} \leq \frac{1}{2} T_1$, for example, but this is only an upper limit.

T_{1D} should go through a minimum as T_1 does, but this minimum will be at a much lower temperature. T_{1D} is only 'long' if the temperature is very low, below the T_{1D} minimum point. However, we have seen (Chapter II) that isentropic demagnetisation can induce very low spin temperatures, much below the lattice temperature. This much reduces the coupling between the spins and the lattice, and hence T_{1D} may be relatively long, although $T_{1D} < T_1$ always.

8.4 EXPERIMENTAL OBSERVATIONS

Since we had seen that T_1 should increase as we lower the temperature below the T_1 minimum point, we built the new spectrometer to work at 4.2°K, in the hope that this would increase T_1's of certain samples to a usable length (> ~ 10 secs) compared to T_1 at 77°K. In this hope we were mostly disappointed.

Long-chain molecules such as polyglycine, polyalanine, nylon, rubber and polystyrene had T_1's ≈ 1 second at 4.2°K (and 77°K). Small molecules such as ethanol and acetic acid also had very fast T_1's (due to low-frequency oscillations in the CH_3 group, perhaps?), as did zinc-porphyrin.

The only exception so far discovered was Collagen. Certain, but not all, samples of this hydrated protein[73] had a $T_1 \sim 30$ seconds at 4.2°K (5 seconds at 77°K) and we did succeed in obtaining a spectrum for HDO hydrated to the molecule. We only observed the normal HDO (ice Ih) lines, however, with a broad unstructured background absorption extending between 148 and 200 kHz. This we attributed to poor crystal structure. No nitrogen lines could be observed.

One other small success was with solid ammonia NH_3. At 4.2°K, this had a $T_1 \sim 30$ secs and a $T_{1D} \sim 1$ second. Due to the large value of e^2Qq for nitrogen, however, level crossings occur in a high field and the nitrogen T_1 is 'long'. Thus we were able to measure $e^2Qq/h = 3168 \pm 1$ kHz, $\eta \leq 0.002$ in agreement with other observations[70]. Because of the fast T_{1D}, however, we would not expect deuterium NQR to be possible, and did not pursue it.

The difference between T_1 and T_{1D} is well illustrated by ice Ih. We measured the HDO spectrum over the range 4.2°K - 140°K (noting very little change in spectral line frequencies) and observed that, although T_1 is almost constant (~ 15 minutes for tap-water), T_{1D} varies rapidly. At 77°K, $T_{1D} \sim 5$ minutes, but this decreases rapidly up to 140°K, where it becomes < 3 seconds, and NQR becomes unobservable (see Table 8.1).

TABLE 8.1

NQR in HDO (10% D_2O in H_2O)

Temp. °K	4.2	77	85	100	120	140
ν^+ kHz ± .2	166.9	167.0	166.9	166.8	167.0	167.2
ν^-	153.7	153.9	154.0	154.2	154.3	154.3
T_{1D} (secs)	~ 300	~ 300	~ 60	~ 30	~ 10	~ 3

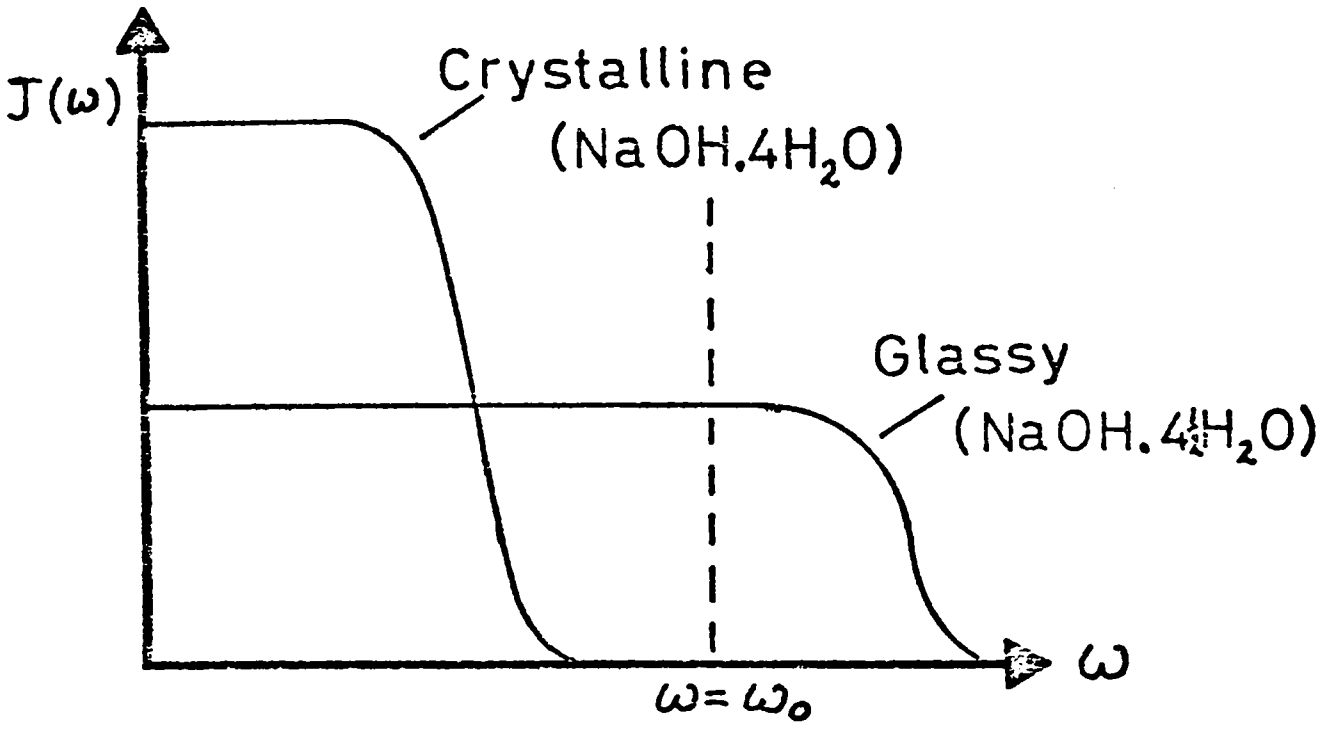


Fig.8.4

T_{1D} is some function of temperature over this range $\sim \frac{1}{T^N}$, but the mechanism is unclear. Tap-water has sufficient paramagnetic ions to induce some paramagnetic relaxation, but further investigation is required.

To explain the variation in T_1 for $NaOH/H_2O$ mixtures (Chapter VII) we need more detailed theories, since all measurements were made at 77°K. Stoichiometric mixtures form a good crystal structure, while intermediate mixtures with >50% water perhaps form a more glassy substance when frozen. Glasses are in many ways similar to liquids, and a very short correlation time is typical of liquids. Small τ_c corresponds to a small J(0) as before, and we may suggest Fig.8.4 as a way of explaining the difference in T_1 between (say) $NaOH.4H_2O$ and $NaOH.4\frac{1}{2}H_2O$.

8.5 CONCLUSION

In general, T_1 does not change much between 4.2°K and 77°K. Most changes happen for temperatures >77°K [69]. Since T_{1D} effects occur in dipolar fields ~20 G ~ 100 kHz (at most) for protons, we are concerned with thermal phonons with an equivalent temperature $\sim 10^{-5}$ °K. One could thus only totally eliminate phonon effects by going below this temperature, which is not possible in an apparatus of this type.

We must content ourselves for now with the facts of nature and make the best use we can of those compounds which do have sufficiently long T_1's at 4.2°K or above, given that only a few compounds show much difference between 77°K and 4.2°K.

Long-chain molecules have many low-frequency vibrational modes, especially if there is no hydrogen bonding. Molecules of almost any type with a $-CH_3$ group have fast T_1's (< 5 sec) at 4.2°K. One example of this is the comparison between ethyl alcohol (CH_3CH_2OH) plus water mixtures ($T_1 \sim 100$ ms) and ethylene glycol ($OH\,CH_2\,CH_2\,OH$) plus water ($T_1 \sim 30$ sec). Strong hydrogen bonding seems to cause long T_1's. $-NH_3^+$ groups in amino acids show T_1 minima at ~350°K [69] and most amino acids have $T_1 \sim$ minutes at 77°K. Benzene, although T_1 is long, has a very fast T_{1D} at 77°K, while its slightly H-bonded relative, pyridine, has $T_{1D} \sim 5$ sec.

Thus it seems that the best advice one could give to a would-be experimenter in Nuclear Quadrupole Double Resonance is to choose short hydrogen-bonded molecules with no $-CH_3$ groups or paramagnetic ions, until a new method is devised for coping with short T_1's.

CHAPTER IX

SUCCESSES, FAILURES AND THE FUTURE

9.1 GENERAL CONCLUSIONS

The work described in this thesis has, in general, been aimed at improving the DRLC and DRCC techniques and applying these improvements to open up new areas for research.

To this end, a better understanding of the nature of continuous coupling in deuterium has allowed the detection of signals from even naturally abundant (.015%) deuterium in certain samples, and easily from samples dilute (10%) in deuterium. Application of these ideas to nitrogen NQR produced a useful improvement in sensitivity, where we had previously been limited by spin locking or perhaps inhomogeneous N lines. The development of FM techniques followed directly from this.

One of the original aims of this work, viz. to lengthen the proton T_1's of certain samples so that they would be tractable to the DRLC method, has met with only limited success. Many samples do exhibit an increase in T_1 when the temperature is reduced from 77°K to 4.2°K, but in most cases the increase is not sufficient. Often one finds that T_{1D} is an order of magnitude shorter than T_1, effectively preventing the use of this technique in such samples.

However, the full temperature facility does allow the study of the variation of quadrupole coupling constants with temperature and the effects of any phase changes that may occur (see reference (74)). One may also perform NQR experiments at a temperature suitable for cross-correlation with other experimental data (as with Lanthanum Nicotinate Dihydrate).

The development of Zeeman NQR is of special interest in the study of sodium, since this plays an important part in many biological reactions.

9.2 LIMITATIONS OF THE APPARATUS

The present apparatus works very reliably at temperatures above 77°K, using liquid nitrogen. It also works well at 4.2°K; however, one notices large fluctuations in temperature as a result of the up-and-down mechanical motion of the sample. Given suitable flow rates etc., one can ensure a stable temperature cycling regime, and the PTFE sample container (being a good insulator), plus the heat capacity of the sample itself, will ensure that actual variations in sample (as opposed to sensor) temperature are kept to a minimum, see Fig.9.1.

However, such mechanical heat inputs would severely affect an apparatus intended to work at 2°K or below, to such an extent that stable operation below 4°K may well be impossible. One must therefore look for other ways of defeating the 'T_1 problem'.

9.3 FUTURE DEVELOPMENTS

The present apparatus takes ~ 500 msec to move a sample from high to low field, irradiates it for a time $\geq$ 500 msec and takes ~ 1 sec to return to the high field. A total time $\geq$ 2 seconds is thus spent away from the high field region, and as a result, samples with T_{1D}'s of ~5 sec or less cannot be examined in this apparatus, since remagnetisation swamps the quadrupole-related signal.

To be able to study more samples one must either (a) increase T_1 and T_{1D} to a suitable value, or (b) decrease the zero-field time. One may, in theory, accomplish (a) by decreasing the operating temperature, but experience has shown that a drop from 77°K to 4.2°K is usually not sufficient, and temperatures below 4.2°K would be very difficult, if not impossible, to attain while moving the sample mechanically. One may only accomplish (b) by a redesign of the mechanical section of the apparatus, or by the elimination of mechanical motion.

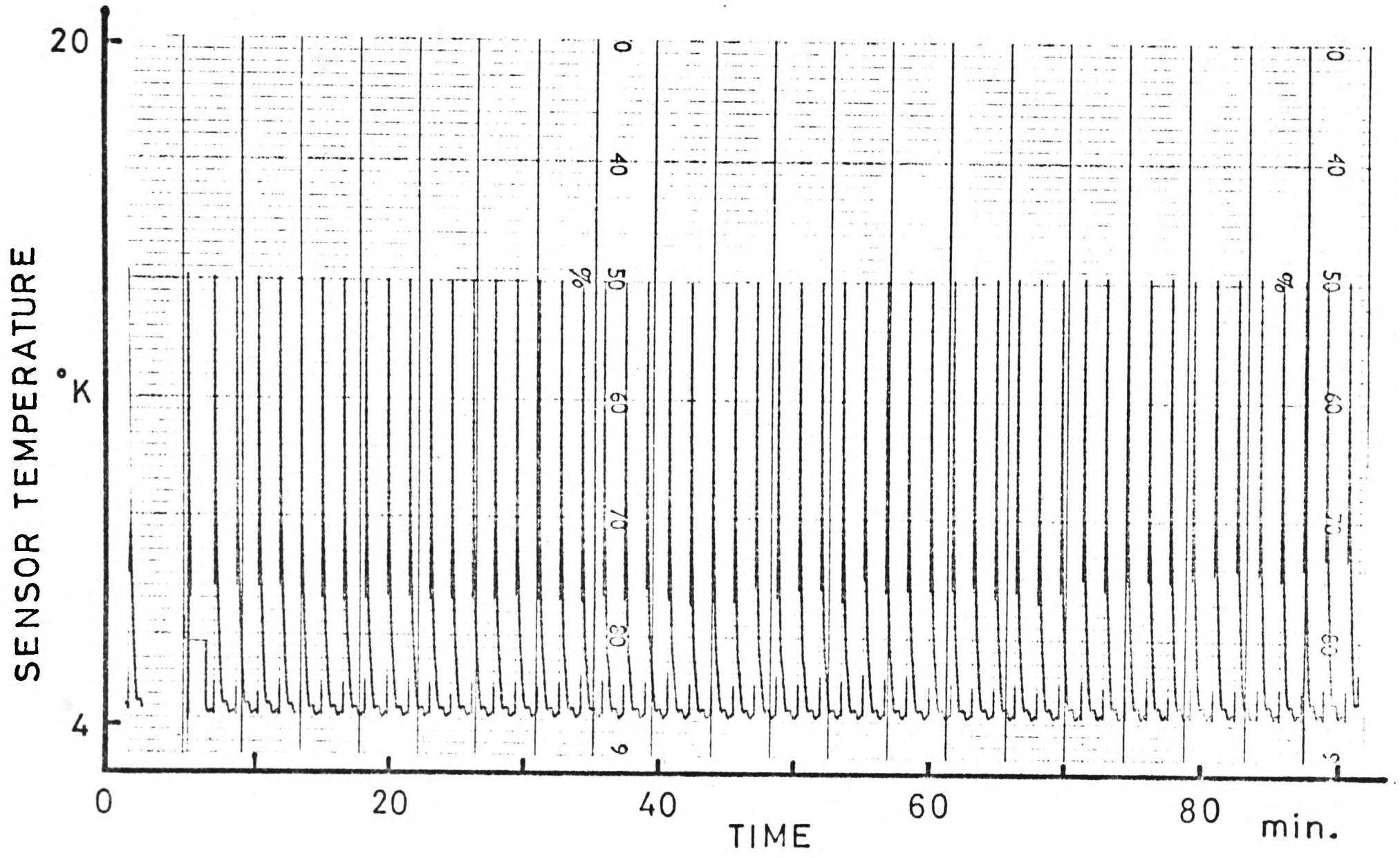


Fig.9.1: Temperature variation during an experiment (cycle =100 s, UP =1 s)

9.3.1 The Single Transit Spectrometer

The single transit spectrometer, an idea of Prof. Hahn, is one possible method. The system consists (Fig.9.2) of two magnets, separated by a suitable distance, say ~ 50 cm. One (magnet A) is a small permanent magnet forming part of a simple NMR spectrometer designed to measure magnetisation (usually of protons) by means of a 90° Pulse. Magnet B is a high field superconducting polarising magnet. Between the two, one arranges for a suitable zero-field region, where one installs the quadrupole irradiation coil. The sample begins in coil B, where it is magnetised. It is then fired up into magnet A, say by using a blast of compressed gas. One must arrange suitable control pulses so that (1) the quadrupole RF is switched on for perhaps 10 msec and off as the sample passes through the zero field region, and (2) the 90° pulse is applied when the sample reaches the correct spot in magnet A. To complete the cycle, the sample 'bullet' is stopped and returned to magnet B.

Since this method involves no accelerations while in zero field, one may arrange for the minimum time to be spent in the transit/irradiation phase. The 'speed limit' for this method involves the dynamics of spin-spin coupling, but one may make some simple assumptions about level crossing to arrive at a theoretical maximum speed. If we assume that level crossing occurs while the proton and quadrupole lines overlap, and that the spin-thermal equilibrium is established in a time $\sim T_2$ then we calculate as follows:

Typical proton linewidth	$\sim$ 100 kHz	
Typical quadrupole linewidth	$\sim$ 20 kHz	(Nitrogen)
	$\sim$ 2 kHz	(deuterium)
	$\ll$ Proton linewidth	

Quadrupole linewidths at B_L, the field at which level crossing occurs, will be larger than these, but we may take the overlap region to be $\approx$ 120 kHz. This corresponds to a range of magnetic fields (for protons) $\approx$ 25 Gauss.

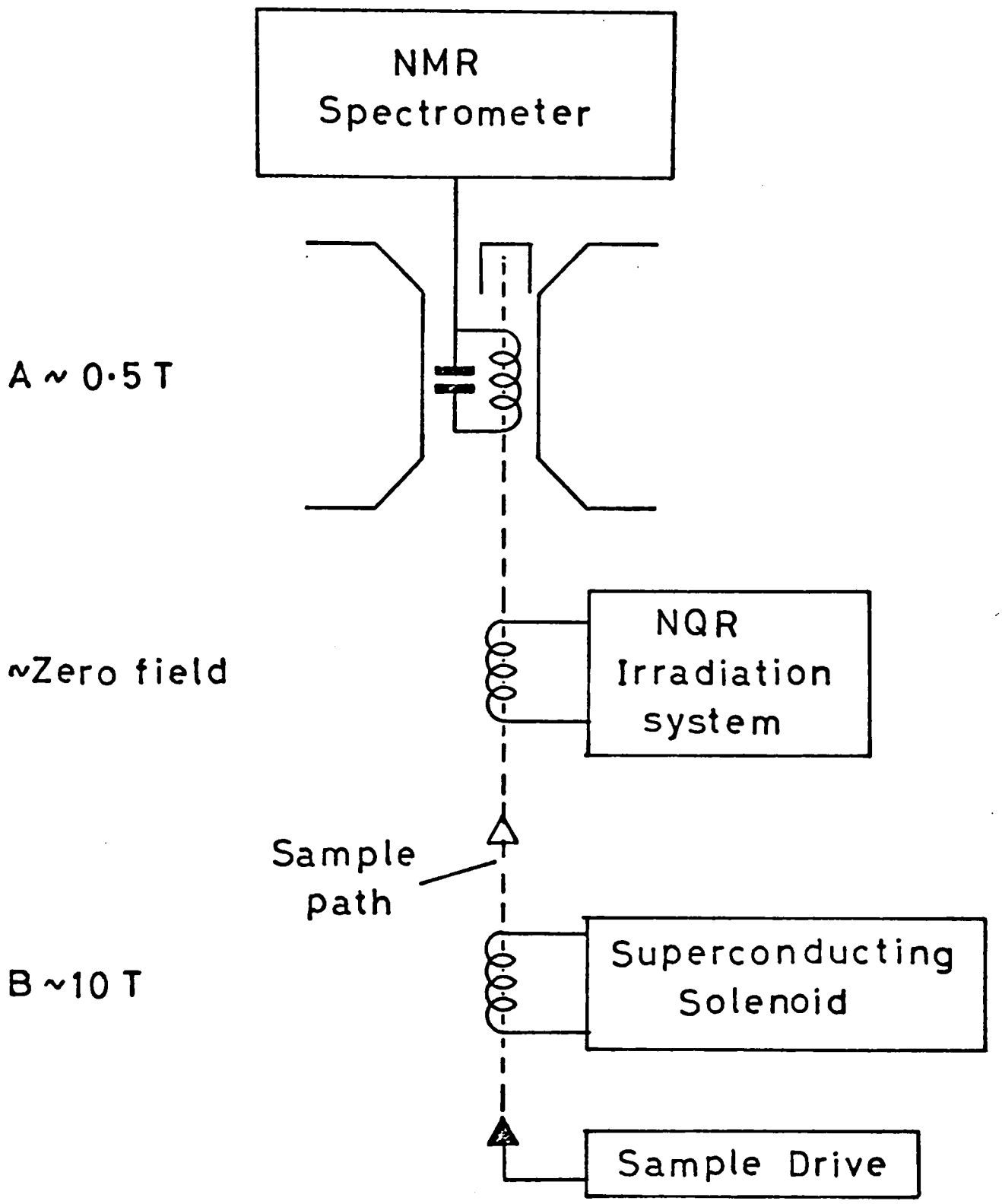


Fig.9.2: Single transit NQR spectrometer

T_2 in many solids is typically $\approx$ 20 μsec, so that we may say that $\frac{dB}{dt}$ for $B \simeq B_L$ must be $\leq$ 1 kG/msec, if we are to ensure that the proton and quadrupole lines are to overlap for a time $\sim T_2$. This is necessarily an upper limit, and more detailed calculations may well produce a lower figure than the above (see ABRAGAM, reference (12), p.154).

The present apparatus moves the sample from a field $\sim$ 10 kG (1 Tesla) to zero field in a time $\sim$ 0.5 second. If this were a linear change, then $\frac{dB}{dt}$ = 0.02 kG/msec. Sample transit speed could be increased by a factor $\sim$50, before the 'speed limit' was encountered. If this were accompanied by a proportional decrease in the T_1 limit, we would be able to take spectra from samples with $T_1 \geq$ 100 msec.

The field profile need not be linear. One might arrange for $\frac{dB}{dt}$ to be higher than the limit for $B \gg B_L$, allowing even faster transits. If one used a superconducting solenoid for magnet B, then large fields $\sim$ 10 T are easily obtainable and might be desirable in order to produce larger initial magnetisation of the protons (or other P spins). This would of course mean an increase in the minimum transit time, but careful design of the field profile could reduce this effect to a minimum.

9.3.2 High-Speed Passage

We have recently seen[71] a description of a system very similar to ours, except that the sample is contained in a 'bullet' which is fired up and down inside the cryostat by compressed gas, with automatic triggering of the 90° pulse and of the quadrupole irradiation.

A minimum transit time $\sim$ 150 msec is reported and a T_1 lower limit $\sim$ 400 msec. The author believed he could reduce this to $\sim$ 200 msec by further improvement of his system. We have not yet seen any NQR data from a sample with such a fast T_1.

9.3.3 Electromagnetic Field Switching

This is another way one might consider when designing an NQR double resonance apparatus. If one used an electromagnet as the source of the NQR field (either superconducting or conventional) one could, in theory, switch the field on and off, rather than move the sample. This would allow lower temperatures to be stably obtained, and could be done rapidly, up to the field 'speed limit' outlined earlier.

There are, however, practical difficulties which are apparent when one lists the experimental requirements.

(a) NMR field – this must be large (~ 1 T), repeatable (± 10 G) and fairly homogeneous (± 10 G over the sample for T_2 ~ 20 μsec).

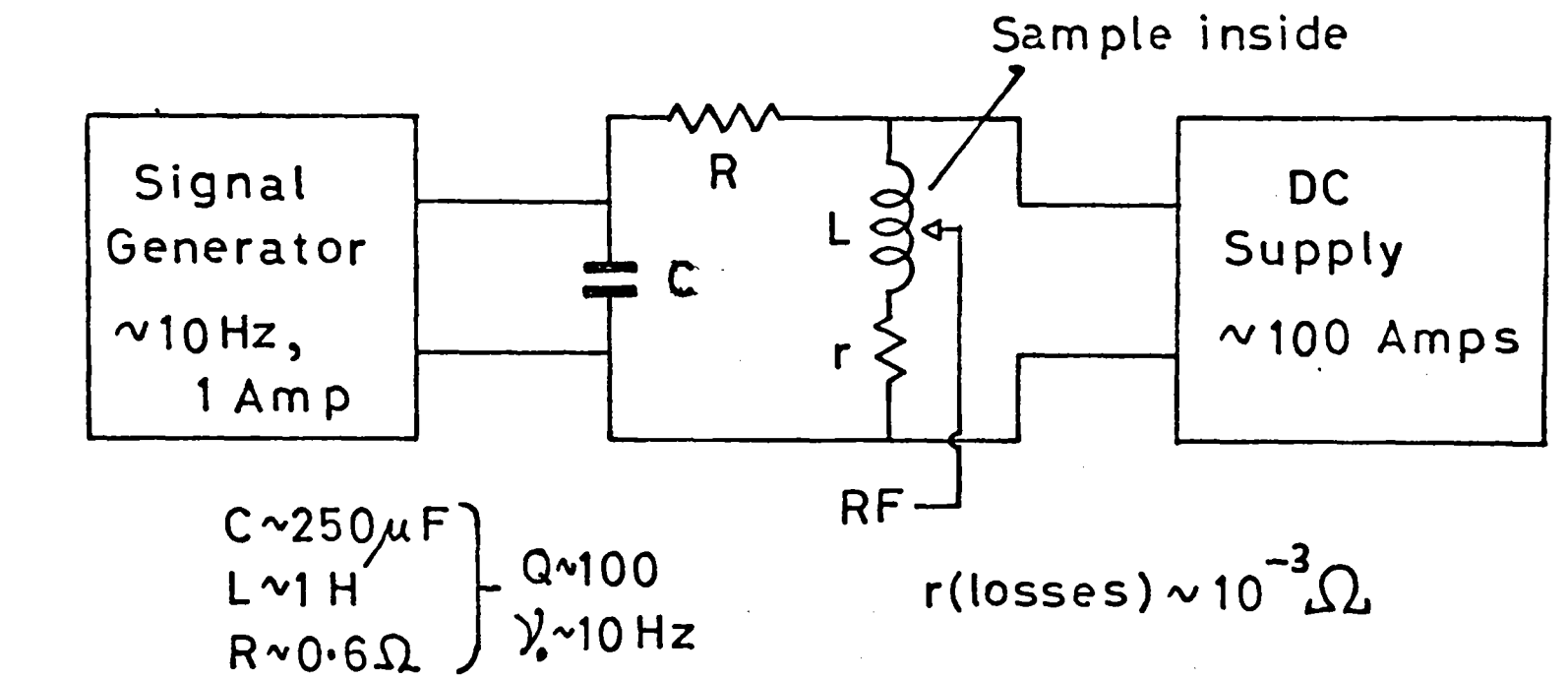
(b) NQR field – this must be zero (± 1 G) and ideally variable up to ~ 100 G. Gradients over the sample must similarly be ≤ 1 G.

(c) Field switching times – rapid switching is essential.

(a) and (b) require a high degree of stabilised current control. (a) will require a large net circulating current I perhaps ≈ 100 amps. (c) will result in a large $\frac{dI}{dt}$ as the field is switched on and off. The resultant back emf would be very large in any conventional system. The eddy current generated in a metal cryostat might also give cause for concern, through heating of the cryostat walls, by limiting dB/dt (by Lenz's law), and by affecting the value of the NMR field.

One possible way round these difficulties would be to use a tuned magnetic circuit, see Fig.9.3.

The solenoid forms the inductance of a tuned circuit, resonant at ~ 10 Hz, or a little lower. If the circuit Q is set at ~ 100 (easily obtainable if the solenoid is superconducting) then 1 amp of drive current from the signal generator becomes ~ 100 amps in the solenoid (Appendix 1),



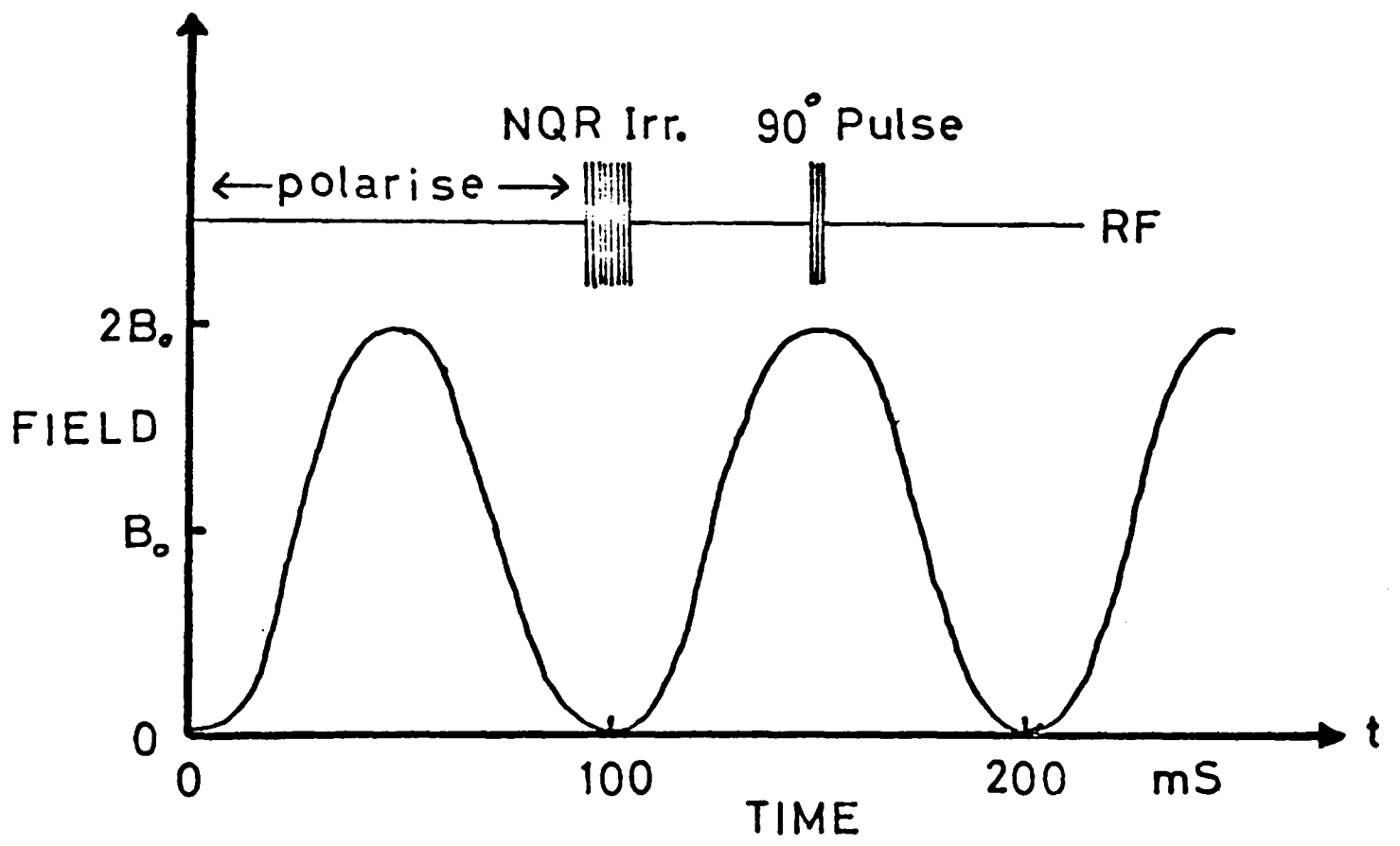


Fig.9.3: Electromagnetic field switching for NQR

which is usually adequate to generate a field of ~ 1 T over the small sample volume, for the NMR part of the experiment.

The 100 amp D.C supply provides 'back-off', so that the net field value is given by

$$B = B_0 \ (1 - \cos \omega_0 t) \ .$$

(One might alternatively use a separate static magnetic field, but the magnetic forces between it and the solenoid might be too large.)

$$\frac{dB}{dt} = \omega_0 B_0 \sin \omega_0 t$$

$$\sim 0 \quad \text{when} \quad \omega_0 t \sim 0, \pi, 2\pi, \text{ etc.}$$

Thus,

$$\frac{dB}{dt} \sim 0 \quad \text{when} \quad B = 0, \ 2B_0 \ .$$

For our experiment, this condition is ideal, since we apply the 90° pulse at the maximum field value $2B_0$ and NQR irradiation when $B \sim 0$.

When $\omega_0 t \approx 0$, we can approximate $\cos \omega_0 t$ by:

$$\cos \omega_0 t \ \approx 1 - \tfrac{1}{2}(\omega_0 t)^2 \ .$$

Then

$$|B| \simeq \frac{B_0}{2} (\omega_0 t)^2 \quad \text{for} \quad B \approx 0.$$

If we now calculate the time τ for which $B = 0 \pm 2$ Gauss, or $B = 2B_0 \pm 2$ Gauss, with $\nu_0 = 10$ Hz so that $\omega_0 = 2\pi\nu_0 = 62.8$ rad/sec , $2B_0 \sim 1$ T for NMR, we find $\tau \sim 1$ msec.

Compared to a 90° pulse of ~ 5 μsec , this is very long. The time-span is still long compared to quadrupole T_2's $\sim$ 100 μsec and so we can also irradiate the quadrupoles effectively.

The maximum rate of change of field occurs at $B \sim B_0$ and $\frac{dB}{dt} (B = B_0) = \omega_0 B_0 \sim 0.3$ kG/msec which is still below the coupling speed limit $\left[\frac{dB}{dt} (B = B_L)\right.$ will usually be lower$]$.

The equivalent transit time from $B = 2B_0$ to $B = 0$ is 50 msec, which is adequate for almost any T_1. Several complete cycles each of $\sim$100 msec can be used to build up the initial magnetisation, before carrying out the irradiation plus measurement phases. If necessary for T_{1D} reasons, one

could apply an additional small field ~ 200 G during the polarisation cycles, which is removed just before irradiation and measurement.

One would have to design a single R.F. coil arrangement for applying both the 90° pulse and the quadrupole irradiation (which would not be easy) and the timing of the control unit of the experiment would be very critical.

Furthermore, one would have to design a helium cryostat to contain the solenoid, R.F. coil etc. with the capacity to dissipate the large heat input due to A.C. losses in the solenoid coil. The cryostat would also have to be non-metallic, to avoid eddy current problems, but glass cryostats are quite suitable.

The technical problems associated with such an apparatus as is outlined above would be large, but not insuperable. Considerable care would be required in the design of the superconducting solenoid, and suitable power supplies would have to be constructed. A suitable capacitor bank, capable of storing the large amounts of energy involved, might have to be constructed. The problems of field regulation and repeatability would not be minor. However, I feel that such a system is feasible, especially given recent advances in very high current transitor technology (Lucas are developing a 200 amp 25 volt device). Such a system, I feel, might be the long-term solution to the T_1 problem, but might require several years of development. I have not carried out any experiments in this area, but superconducting magnet technology in this laboratory has advanced to the stage where such a design can be realistically contemplated. A design for a low frequency A.C. solenoid has been published[72] and some new superconductors have much lower A.C. losses.

9.4 EPILOGUE

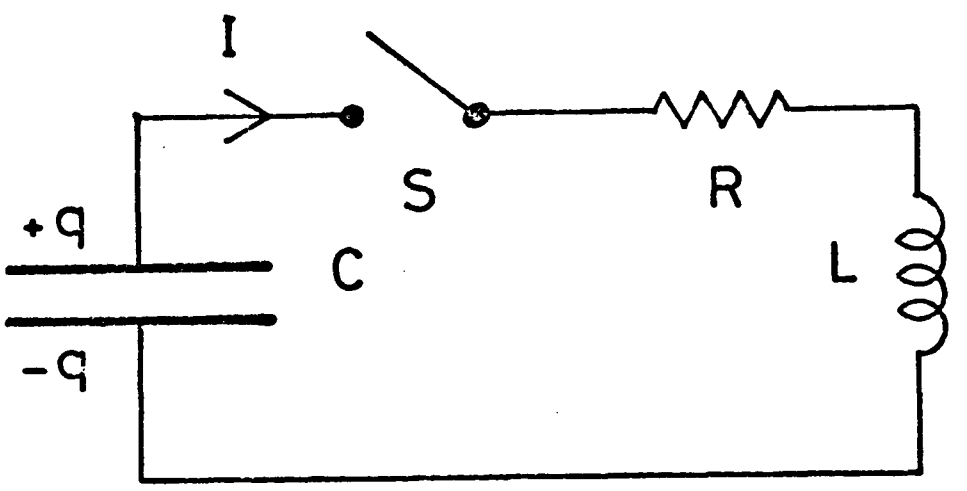
The future of low frequency pure NQR as an everyday analytical tool, in the way NMR now is, will be assured if the 'T_1 problem' can be solved in one of the ways outlined or in some other way. Otherwise the method will be restricted to those samples with suitable T_1's, and will remain only a specialised research tool. Even as such, there is much work yet to be done, many possible deuterium derivatives of simple compounds have yet to be studied, and NQR can provide useful information for the theoretical chemist who wishes to test his molecular wavefunction calculations. The present apparatus is simple in concept and relatively inexpensive to construct (see Appendix 2) from standard components. Several groups around the world have recently begun work with versions of our apparatus, and the next few years should see a great expansion in the available amount of low-frequency NQR data.

APPENDIX 1

TUNED CIRCUITS

This derivation is based on Bleaney and Bleaney[11]

A.1 DAMPED OSCILLATIONS - Consider the circuit:-



The switch is closed at time $t = 0$. We analyse the subsequent behaviour of the circuit.

Total voltage around circuit is zero: Summing the voltages on the elements

$$L\frac{dI}{dt} + IR + \frac{q}{C} = 0 \qquad \ldots (A.1)$$

and $I = \frac{dq}{dt}$ $\quad\therefore\quad$ $L\frac{d^2I}{dt^2} + R\frac{dI}{dt} + \frac{I}{C} = 0$ $\qquad \ldots (A.2)$

The general solution of this equation is of the form:

$$I = \exp\left[-(R/2L)t\right]\left\{A e^{nt} + Be^{-nt}\right\} \qquad \ldots (A.3)$$

where

$$n^2 = \left(\frac{R}{2L}\right)^2 - \left(\frac{1}{LC}\right)$$

But $I = 0$ at $t = 0$ $\therefore$ $A = -B$.

For an oscillatory solution, n is imaginary, i.e. $\frac{1}{LC} > \left(\frac{R}{2L}\right)^2$.

Then

$$I = A\exp\left[-(R/2L)t\right]\sin\omega t \qquad \ldots (A.4)$$

where

$$\omega^2 = \frac{1}{LC} - \frac{R^2}{4L^2} .$$

If

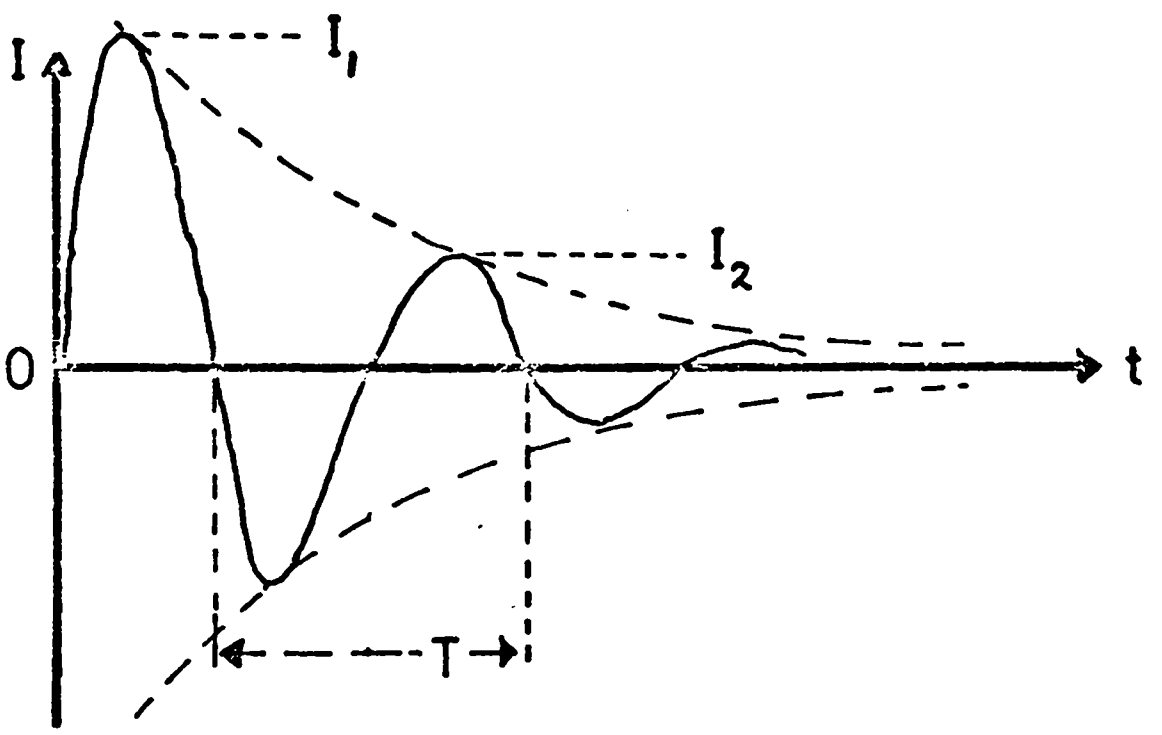
$$\sqrt{\frac{1}{LC}} \gg \frac{R}{2L} \qquad (R \text{ small}) .$$

then

$$\omega \simeq \sqrt{\frac{1}{LC}}$$

the natural frequency of oscillation.

The resultant variation of I with time as as shown:



When R is small (low damping) the period T of the oscillations is given by

$$T = \frac{2\pi}{\omega} \approx 2\pi\sqrt{LC} \quad . \qquad \ldots (A.5)$$

The amplitudes of successive maxima are related by the ratio, known as the logarithmic decrement K:

$$K = \frac{I_{m+1}}{I_m} = \exp\left(-\frac{TR}{2L}\right) \qquad \ldots (A.6)$$

i.e.

$$\log_e \frac{Im}{I_{m+1}} = \frac{TR}{2L} = \pi R\sqrt{\frac{C}{L}} .$$

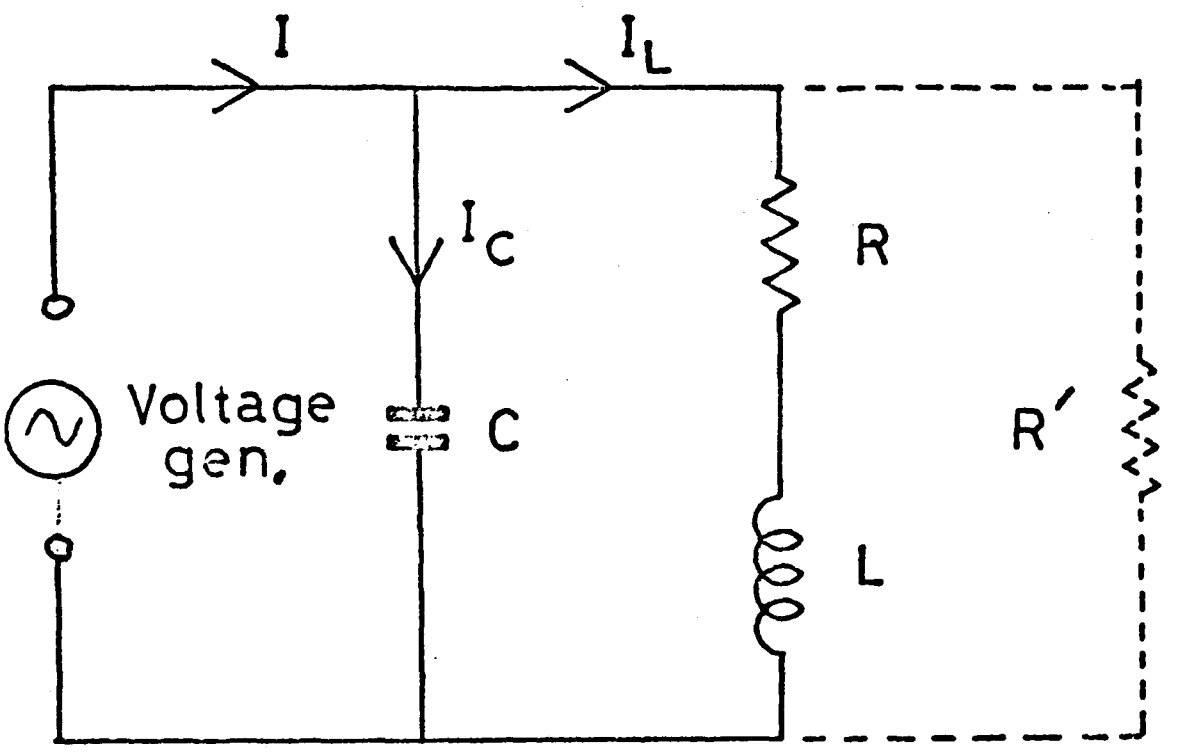
The quantity $R\sqrt{\frac{C}{L}}$ is defined to be $1/Q$, and is a measure of the damping in the circuit. Q is usually known as the quality factor of the circuit.

N.B. After Q cycles, the current drops to $1\frac{1}{2}\%$ of the first maximum. This time may be taken as the period for which the circuit 'rings'. Using

$\omega_0 = 1/\sqrt{LC}$

$$Q = \frac{1}{R}\sqrt{\frac{L}{C}} = \omega_0 L/R = \frac{1}{\omega_0 RC} \qquad \ldots (A.7)$$

A.2 PARALLEL TUNED CIRCUIT - DRIVEN BY A GENERATOR



Admittance $Y = 1/Z$ is given by (ignoring R' for now)

$$\underline{Y} = j\omega C + \frac{1}{R + j\omega L} = j\omega C + \frac{R - j\omega L}{R^2 + \omega^2 L^2} \qquad \ldots (A.8)$$

The resonance point of this circuit may be taken as the value of ω where $\underline{Y}$ is real.

Then
$$C - \frac{L}{R^2 + \omega^2 L^2} = 0 \quad \text{or} \quad 1 - \frac{L}{C(R^2 + \omega^2 L^2)} = 0$$

i.e.
$$\frac{L}{C} = R^2 + \omega^2 L^2$$

or
$$\omega^2 = \frac{1}{L^2}\left(\frac{L}{C} - R^2\right) = \frac{1}{LC} - \frac{R^2}{L^2}$$

$$= \frac{1}{LC}\left(1 - R^2 \cdot \frac{C}{L}\right) \qquad \ldots (A.9)$$

using
$$\omega_0 = \frac{1}{\sqrt{LC}} \quad \text{and} \quad Q = \frac{1}{R}\sqrt{\frac{L}{C}}$$

from part 1:

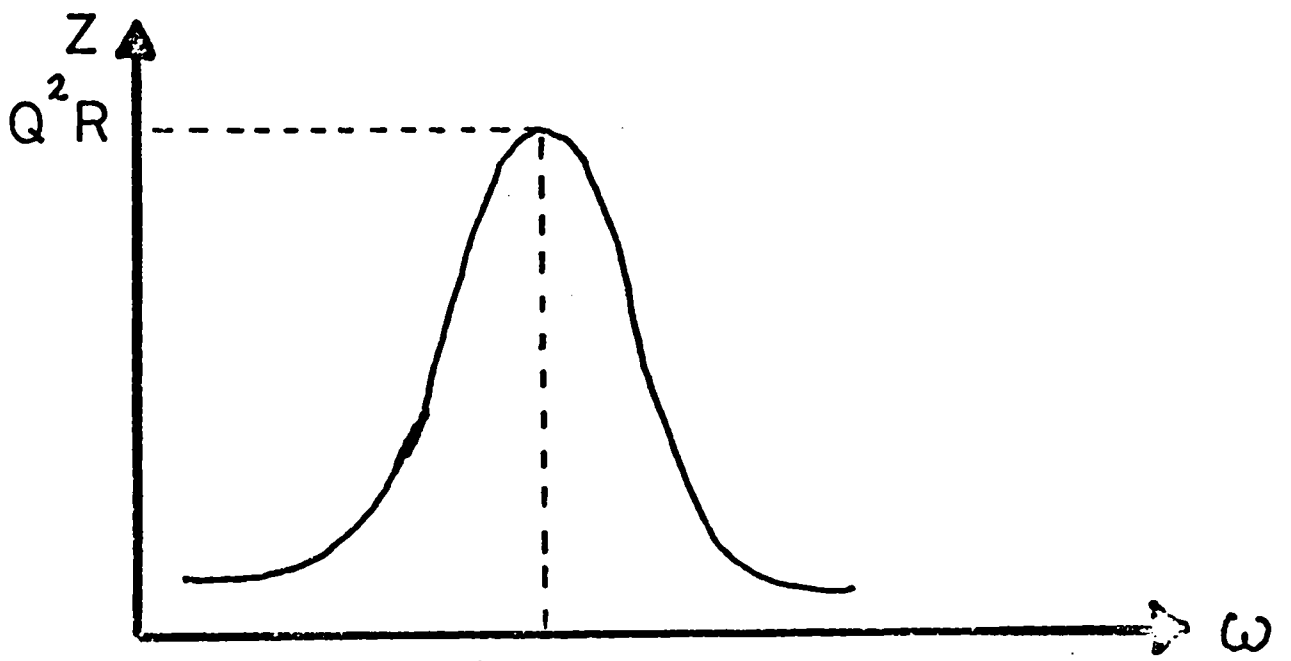
$$\omega = \omega_0 \left(1 - \frac{1}{Q^2}\right)^{\frac{1}{2}} \qquad \ldots \text{ (A.10)}$$

$$\simeq \omega_0 \quad \text{if} \quad Q \quad \text{is large.}$$

At the resonant point,

$$\underline{Y} = \frac{R}{R^2 + \omega_0^2 L^2} = \frac{RC}{L} = \frac{1}{Q^2 R}$$

or $Z = Q^2 R$; the impedance presented to the oscillator is Q^2 times the series resistance R, and is a maximum at resonance.



The series resistor R is thus equivalent, at resonance, to a resistor R' in parallel with the reactive elements, with $R' = Q^2 R$.

So we have alternative formulae for the Q of a <u>parallel resonant circuit</u> using R', as follows

$$Q = R' \sqrt{\frac{C}{L}} = \frac{R'}{\omega_0 L} = \omega_0 R' C \ . \qquad \ldots \text{ (A.11)}$$

At resonance, the current drawn from the generator is a minimum, and is given, in modulus, by

$$|I| = VY_0 = VRC/L \ .$$

The current in the capacitor is given, in modulus, by

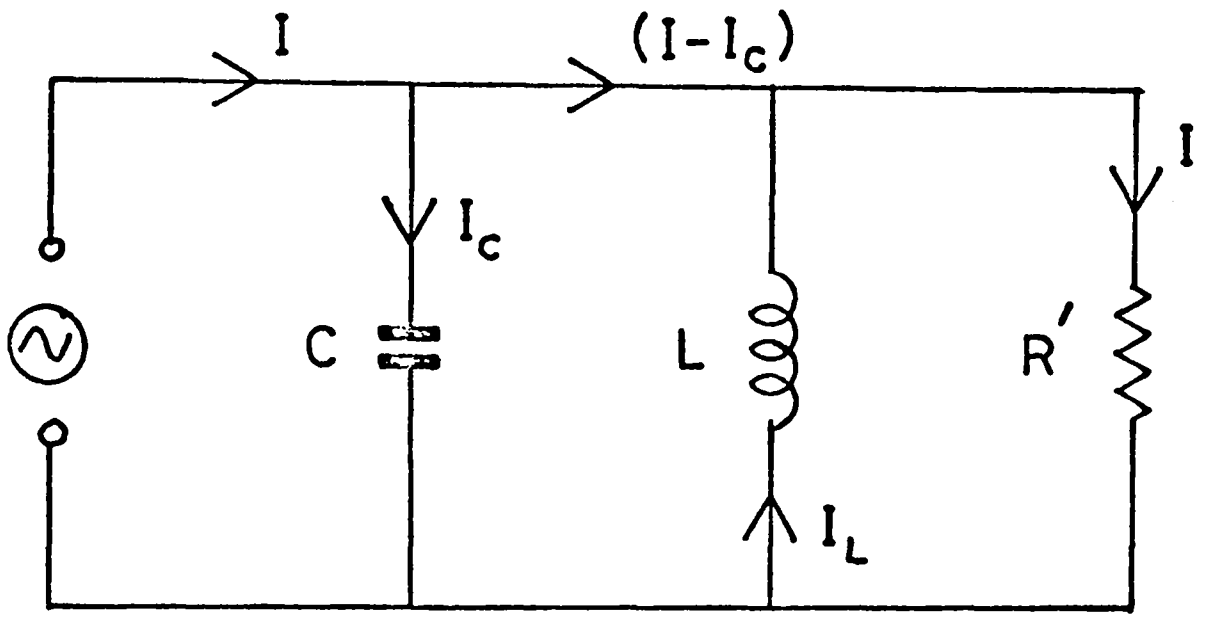
$$|I_C| = VY_C = V\omega_0 C.$$

Thus

$$\left|\frac{I_c}{I}\right| = \frac{\omega_0 CV}{RCV/L} = \omega_0 \frac{L}{R} = Q \qquad \ldots \text{(A.12)}$$

i.e. the current I drawn from the generator is amplified by the tuned circuit into a circulating current QI, in the resonant circuit.

Looking from the point of view of an ideal L and a parallel resistor R'



$$I_c = I_L = QI$$

(1) Use in a NMR Circuit

Application of a 90° Pulse - A current I drawn from the R.F. transmitter becomes a current QI in the inductance L. This generates a larger magnetic field inside L than would be possible without a tuned circuit since (very approximately) the coil is a solenoid and the axial field inside a solenoid is given by

$$H = k\,m\,I\ ,$$

where I is the current, m is the turn density, and k is a form factor depending on the length of the solenoid ($k = 1$ for an infinite solenoid).

(2) Detection of the Free Induction Decay

The precessing nuclear spins induce an e.m.f. $\mathcal{E}$ in the coil at the Larmor frequency ω_0, by Faraday's law of induction. ABRAGAM[12] shows (pp.71-72) that, if the coil is connected to a capacitor so that the circuit is resonant at ω_0, then a voltage $V = Q\mathcal{E}$ is initially generated across the terminals of the coil, which may be picked up by the detector system. Noise with $\omega \neq \omega_0$ is not amplified in this way and is thus rejected by the tuned circuit; only signal and that part of the noise spectrum with $\omega = \omega_0$ passes on to the receiver/detector stage.

An order of magnitude calculation[12] then shows that the magnitude of the voltage V for protons in water at room temperature in a coil of diameter 1 cm with 10 turns resonant at 42.6 MHz with a Q of 100 is given by

$$V = Q\mathcal{E} \approx 0.08 \text{ volts.}$$

In our case we have $Q \approx 25$ and a filling factor of less than unity, but V is still ≈ 10 mV. When we consider solid samples (short T_2), the size of the signal is further reduced due to the inevitable decay during the receiver dead time.

(3) Dead Time

As shown earlier, a tuned circuit 'rings' for $\approx Q$ cycles after the generator is shut off. This means that, for $\simeq Q$ cycles after a 90° pulse, the free induction decay cannot be detected because of these dying oscillations, e.g. for

$$\nu_L = 4 \times 10^7 \text{ Hz}, \quad Q = 40$$

$$Q \text{ cycles} = 1 \text{ μsec} = T_R.$$

This is not important, as long as T_R is short compared to T_2. It is also evident that higher Q's may be used if we increase ν_L (i.e. use a stronger magnetic field B_0).

The spectrometer receiver is normally kept switched off for $\approx Q$ cycles after the end of the 90° pulse, in order to avoid saturation of the preamplifier. Fig.A.1 shows a typical oscilloscope trace of a 90° pulse and detected free induction decay. The integrator gate period is also shown.

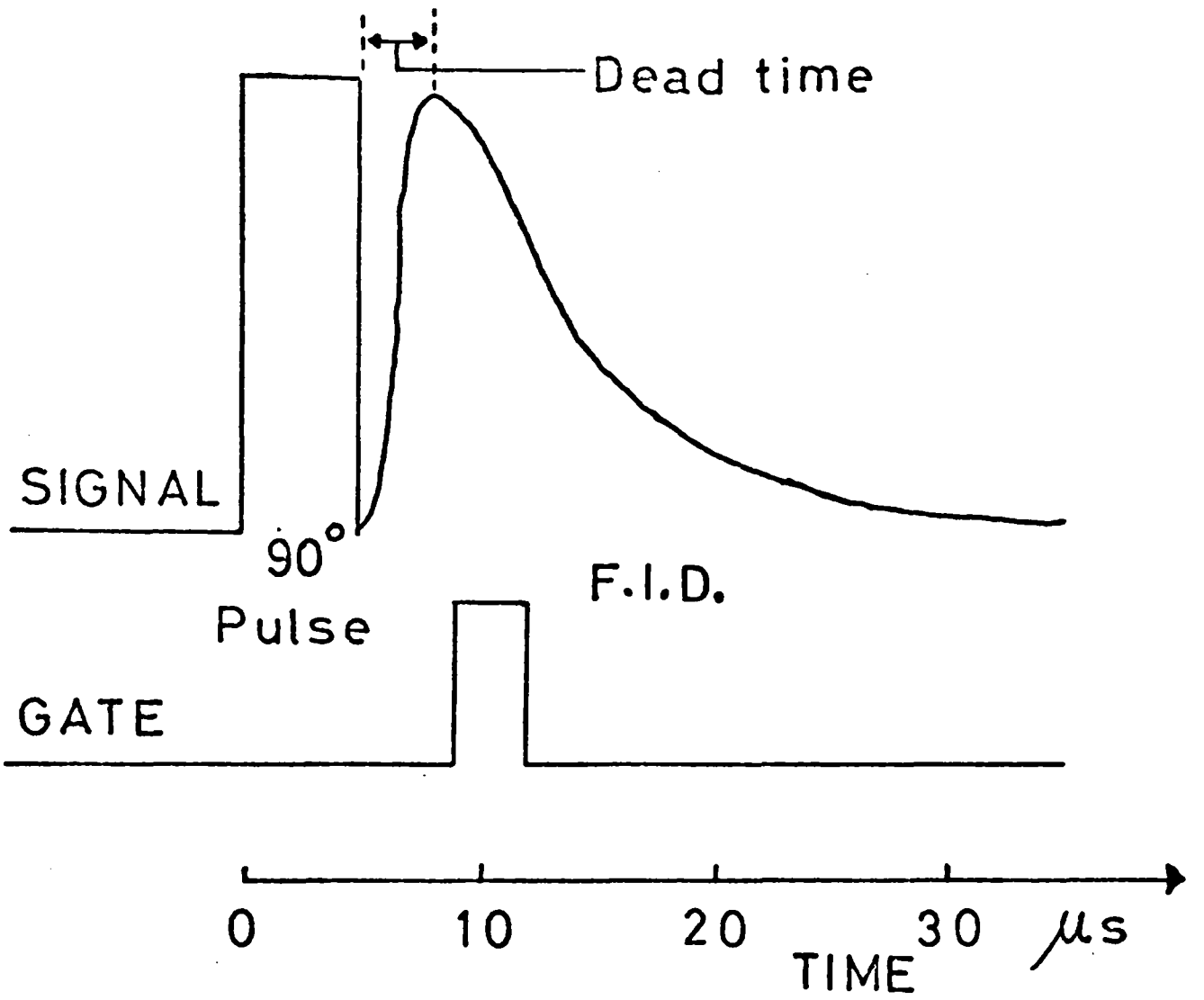
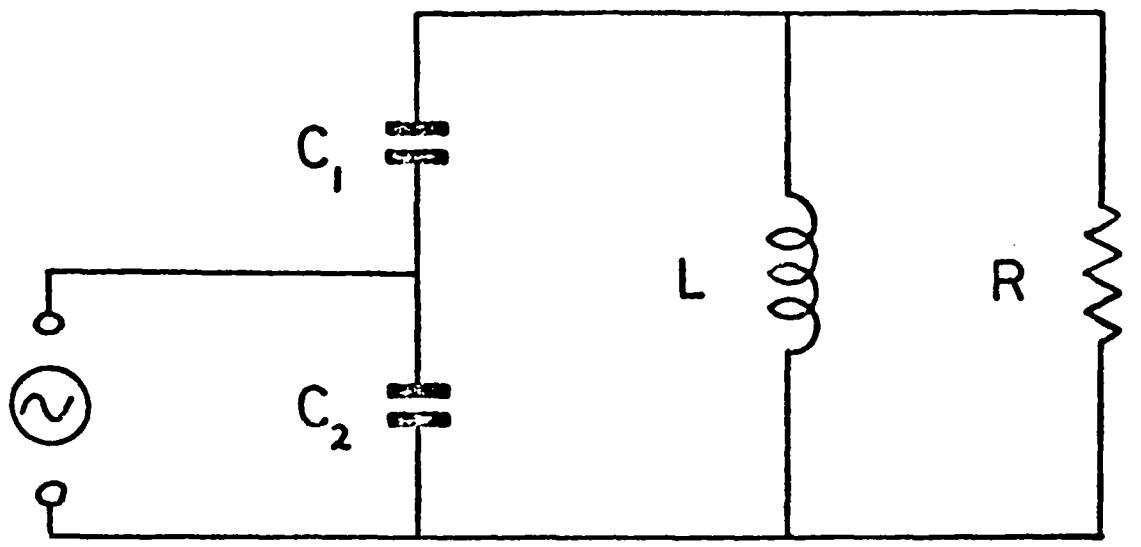


Fig. A.1

A.3 TANK CIRCUIT USED IN NMR DETECTION SYSTEM (after Bruker)

The impedance of a parallel tuned circuit at resonance is given by R'. But $Q = R'/\omega_0 L$, where R' is the parallel resistance. For large Q and large L, this necessitates a large value for R'. The output of the Minispec transmitter is matched at $50\,\Omega$, however, and if $R' = 50\,\Omega$ Q is unacceptably small. We thus need some form of impedance matching between the tank circuit and the transmitter. The circuit shown below has suitable properties.



R represents all losses in the circuit, as well as resistance

C_1 and C_2 form an impedance matching transformer

We now analyse the behaviour of this circuit. Let $C = \frac{C_1 C_2}{C_1 + C_2}$:

The self-resonant frequency of the circuit is then (as before)

$$\omega_0 \simeq \frac{1}{\sqrt{LC}} . \qquad \ldots (A.13)$$

The admittance Y is given by

$$Y = j\omega C_2 + \left(\frac{1}{j\omega C_1} + \frac{Rj\omega L}{R + j\omega L} \right)^{-1} \qquad \ldots (A.14)$$

This may be written as

$$Y = \frac{\left[j\omega R(C_1 + C_2 - \omega^2 L C_1 C_2) - \omega^2 L (C_1 + C_2) \right] \left[R(1 - \omega^2 L C_1) - j\omega L \right]}{\omega^2 L^2 + R^2 (1 - \omega^2 L C_1)^2}$$

The real part of Y is

$$\mathrm{Re}(Y) = \frac{\omega^2 LR(C_1 + C_2 - \omega^2 L C_1 C_2) - \omega^2 LR(C_1 + C_2)(1 - \omega^2 L C_1)}{\omega^2 L^2 + R^2 (1 - \omega^2 L C_1)^2} \qquad \ldots (A.15)$$

The imaginary part of Y is

$$\mathrm{Im}(Y) = \frac{\omega R^2 (C_1 + C_2 - \omega^2 L C_1 C_2)(1 - \omega^2 L C_1) + \omega^3 L^2 (C_1 + C_2)}{\omega^2 L^2 + R^2 (1 - \omega^2 L C_1)^2} \qquad \ldots (A.16)$$

As before, we take $\mathrm{Im}(Y) = 0$ at resonance, i.e.

$$R^2 (C_1 + C_2 - \omega^2 L C_1 C_2)(1 - \omega^2 L C_1) + \omega^2 L^2 (C_1 + C_2) = 0.$$

Putting $C = \frac{C_1 C_2}{C_1 + C_2}$, this may be rewritten as

$$(1-\omega^2 LC)(1-\omega^2 LC_1) + \omega^2 \frac{L^2}{R^2} = 0 \qquad \ldots (A.17)$$

For an ideal circuit, $R = \infty$ and ω is given by

$$\omega_1 = \frac{1}{\sqrt{LC}} \quad \text{or} \quad \omega_2 = \frac{1}{\sqrt{LC_1}} \qquad \ldots (A.18)$$

There are two resonant frequencies, but $\omega_1 \to \omega_2$ as $C_2 \to \infty$. We shall refer to ω_1 as the 'parallel mode', and ω_2 as the 'series mode', since C_1 and L form a series resonant current when $C_2 = 0$.

For R large but finite, the expressions for ω_1 and ω_2 are still approximately true.

Rewriting (A.17) we have

$$\omega^4 L^2 CC_1 + \omega^2 L\left(\frac{L}{R^2} - C - C_1\right) + 1 = 0 \qquad \ldots (A.19)$$

Putting in the values used in our circuit: $L \sim 6 \times 10^{-7}$ H, $R \approx 5 \times 10^3\ \Omega$ $C \approx C_1 \approx 3 \times 10^{-11}$ F, we have

$$\frac{L}{R^2} \sim 2.4 \times 10^{-14} \ll C, C_1$$

We can thus approximate (A.19) by

$$\omega^4 L^2 CC_1 - \omega^2 L(C + C_1) + 1 = 0 \qquad \ldots (A.20)$$

$$\therefore \quad \omega^2 L = \frac{(C + C_1) \pm (C - C_1)}{2CC_1}$$

$$= \frac{1}{C_1} \quad \text{or} \quad \frac{1}{C}$$

i.e. $$\omega_1 = \frac{1}{\sqrt{LC}}, \quad \omega_2 = \frac{1}{\sqrt{LC_1}}$$

as above.

The real part of Y may be rewritten as

$$\mathrm{Re}(Y) = \frac{\omega^2 LR(C_1 + C_2)[(1-\omega^2 LC) - (1-\omega^2 LC_1)]}{\omega^2 L^2 + R^2(1-\omega^2 LC_1)^2} \qquad \ldots (A.21)$$

(a) Series Mode

For $\omega = \omega_2$, $\omega^2 = \frac{1}{LC_1}$: $C = \frac{C_1 C_2}{C_1 + C_2}$

$$\mathrm{Re}(Y) = \frac{R\left(\frac{C_1 + C_2}{C_1}\right)\left(1 - \frac{C}{C_1}\right)}{L/C_1}$$

$$= \frac{R}{L}(C_1 + C_2)\frac{C_1}{(C_1 + C_2)}$$

$$\mathrm{Re}(Y) = \frac{RC_1}{L} \qquad \ldots (A.22)$$

Thus for the series mode, with $R = 5 \times 10^3 \Omega$, $C_1 = 3 \times 10^{-11}$ F , $L = 6 \times 10^{-7}$ H .

$$\mathrm{Re}(Y) = \frac{5 \times 10^3 \times 3 \times 10^{-11}}{6 \times 10^{-7}} = 2.5 \times 10^{-1}$$

$$\mathrm{Im}(Y) = 0$$

$$\therefore \quad Z = \frac{1}{Y} = 4\Omega.$$

This is not well matched to the transmitter.

(b) Parallel Mode

$$\omega = \omega_1 : \quad \omega^2 = \frac{1}{LC} : \quad C = \frac{C_1 C_2}{C_1 + C_2}$$

$$\mathrm{Re}(Y) = \frac{R\left(\frac{C_1 + C_2}{C}\right)\left(\frac{C_1}{C} - 1\right)}{\frac{L}{C} + R^2\left(1 - \frac{C_1}{C}\right)^2}$$

$$= \frac{R\left(\frac{C_1 + C_2}{C_2}\right)^2}{\frac{L}{C} + R^2\left(\frac{C_1}{C_2}\right)^2}$$

$$= \frac{1}{R}\left\{\frac{\left(\frac{C_1 + C_2}{C_2}\right)^2}{\frac{L}{R^2 C} + \left(\frac{C_1}{C_2}\right)^2}\right\}$$

$$= \frac{1}{R}\left\{\frac{\left(\frac{C_1 + C_2}{C_1}\right)^2}{\frac{L}{R^2 C}\cdot\left(\frac{C_2}{C_1}\right)^2 + 1}\right\}$$

$$= \frac{1}{R}\left(\frac{C_1 + C_2}{C_1}\right)^2 \left(\frac{1}{Q^2}\left(\frac{C_2}{C_1}\right)^2 + 1\right)^{-1}$$

$\frac{L}{R^2C} = \frac{1}{Q^2}$ for a parallel tuned circuit: $C_2/C_1 \approx 7$ in our case, and $Q \approx 30$, thus $\frac{1}{Q^2}\left(\frac{C_2}{C_1}\right)^2 \approx 0.05$.

Thus

$$\mathrm{Re}(Y) \approx \frac{1}{R}\left(\frac{C_1 + C_2}{C_1}\right)^2 \qquad \ldots (A.23)$$

$$\mathrm{Im}(Y) = 0$$

$$\therefore \quad Z = R\left(\frac{C_1}{C_1 + C_2}\right)^2$$

C_1 and C_2 thus form an impedance transformer which matches the high impedance of the tuned circuit at resonance to the low impedance of the transmitter/receiver line.

Putting in the values used in this case, $C_1 \approx 30\,\mathrm{pF}$, $C_2 \approx 220\,\mathrm{pF}$, $R \approx 5\,\mathrm{k\Omega}$,

$$\therefore \quad Z \approx 75\,\Omega .$$

This is not a perfect match, but it is much better matched than the 'Series Mode'.

Comparing the power absorbed by the circuit in each Mode: Bleaney gives the voltage standing wave ratio of a load Z connected to a line of impedance Z_0 as:

$$\frac{V_{reflected}}{V_{input}} = \frac{Z - Z_0}{Z + Z_0}$$

The power reflected by the load (not absorbed) is given by

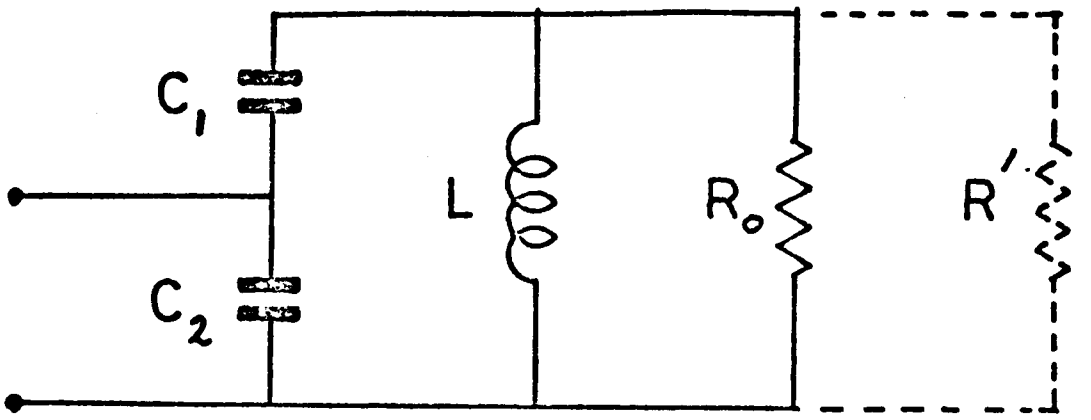
$$P_R \propto \left(\frac{Z - Z_0}{Z + Z_0}\right)^2$$

For $Z_0 = 50\,\Omega$, $Z = 75\,\Omega$, $P_R = \left(\frac{25}{125}\right)^2 = \frac{1}{25} = 4\%$

$Z = 5\,\Omega$, $P_R = \left(\frac{45}{55}\right)^2 = 67\%$

Losses

Losses in the inductance and capacitance may be considered as an additional parallel resistor, R'.



The net parallel resistance, R, is given by

$$\frac{1}{R} = \frac{1}{R_0} + \frac{1}{R'}$$

The Q of any parallel resonant circuit is given by

$$Q = \frac{R}{\omega_0 L} \qquad \ldots(A.11)$$

If we define, for the above circuit,

$$Q_{ideal} = \frac{R_0}{\omega_0 L}$$

$$Q_{coil} = \frac{R'}{\omega_0 L}$$

Then $$\frac{1}{Q_{total}} = \frac{1}{Q_{coil}} + \frac{1}{Q_{ideal}}$$

Voltage Requirements

The current flowing in the circuit at resonance is given approximately by $I = QI_0$, where I_0 = current drawn from the transmitter.

With $Q \approx 30$, we can ignore I_0 and say that the same current I flows in C_1 and C_2. Then

$$V_{c1} = \frac{I}{j\omega C_1}$$

$$V_{c2} = \frac{I}{j\omega C_2}$$

$$\therefore \quad \frac{V_{c1}}{V_{c2}} = \frac{C_2}{C_1} \simeq 7 \ .$$

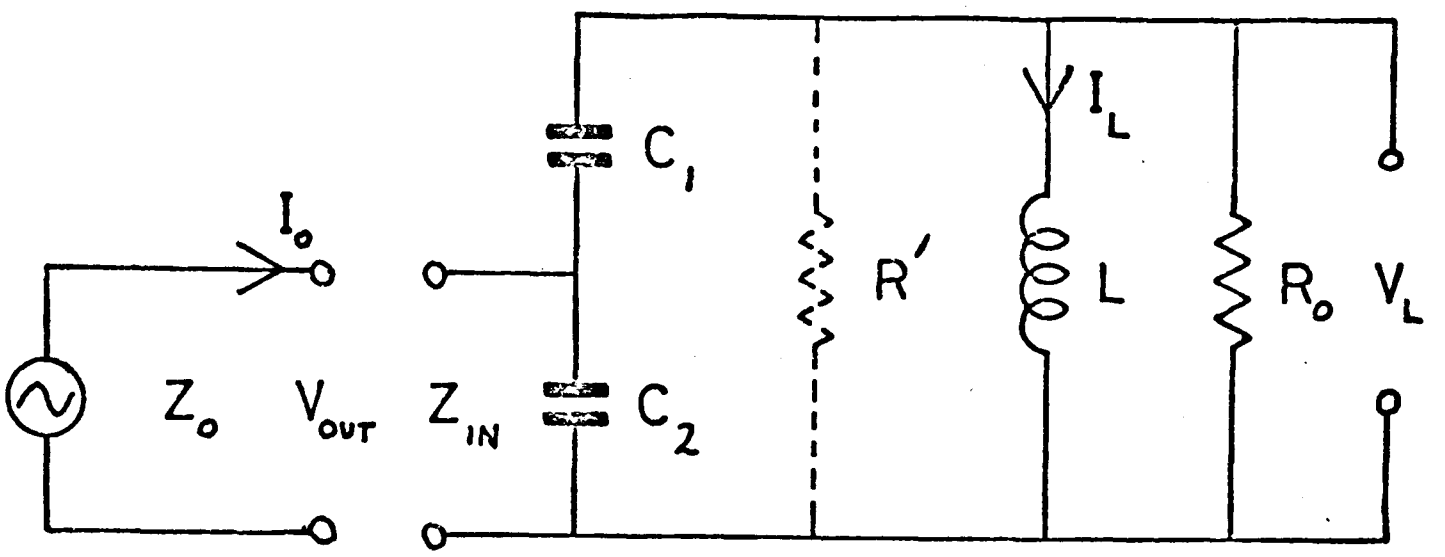
But $V_{c2} = V_{applied}$ from transmitter $\simeq$ 150 volts

$\therefore$ $V_{c1} \simeq$ 950 volts. $-c_1$ must be a high voltage type.

V_L, the voltage across L, $= V_{c1} + V_{c2}$

$= 1100$ volts

A.4 SUMMARY



$$C = \frac{C_1 C_2}{C_1 + C_2}$$

V_{out} = 150 volts peak $\quad C_1 \sim 30$ pf $\quad L = 6 \times 10^{-7}$ H

Z_0 = 50 Ω $\quad C_2 = 220$ pF $\quad R_0 = 10^4$ Ω

$I_0 \sim 3$ amps

Net parallel resistor $R = \dfrac{R_0 R'}{R_0 + R'} \sim 5 \times 10^3\,\Omega$

$$\nu_0 = \frac{\omega_0}{2\pi} = \frac{1}{2\pi\sqrt{LC}} \approx 4 \times 10^7\ \text{Hz}$$

$$Q = \frac{R}{\omega_0 L} \approx 25$$

$$Z_{in} = \left(\frac{C_1}{C_1 + C_2}\right)^2 R \simeq 75\,\Omega \qquad (\omega = \omega_0)$$

$$V_L \simeq \left(\frac{C_2 + C_1}{C_1}\right) V_{in} \simeq 1\ \text{kV}$$

$$I_L = QI_0 \simeq 90\ \text{amps}$$

The figure A.2 shows the predicted values of Re(Y), and Im(Y) as a function of frequency. C_1 (variable) has been chosen to give $\nu_0 \simeq 39.5$ MHz.

Equations (A.15) and (A.16) were used, with no approximations.

$R_{eff} = 3\,k\Omega$ gives the best match - R_{eff} is the sum of R and the effects of other losses in the circuit.

Using $Q = \dfrac{R_{eff}}{\omega_0 L}$, $Q = 20$ in this case, which is close to the measured value of 25.

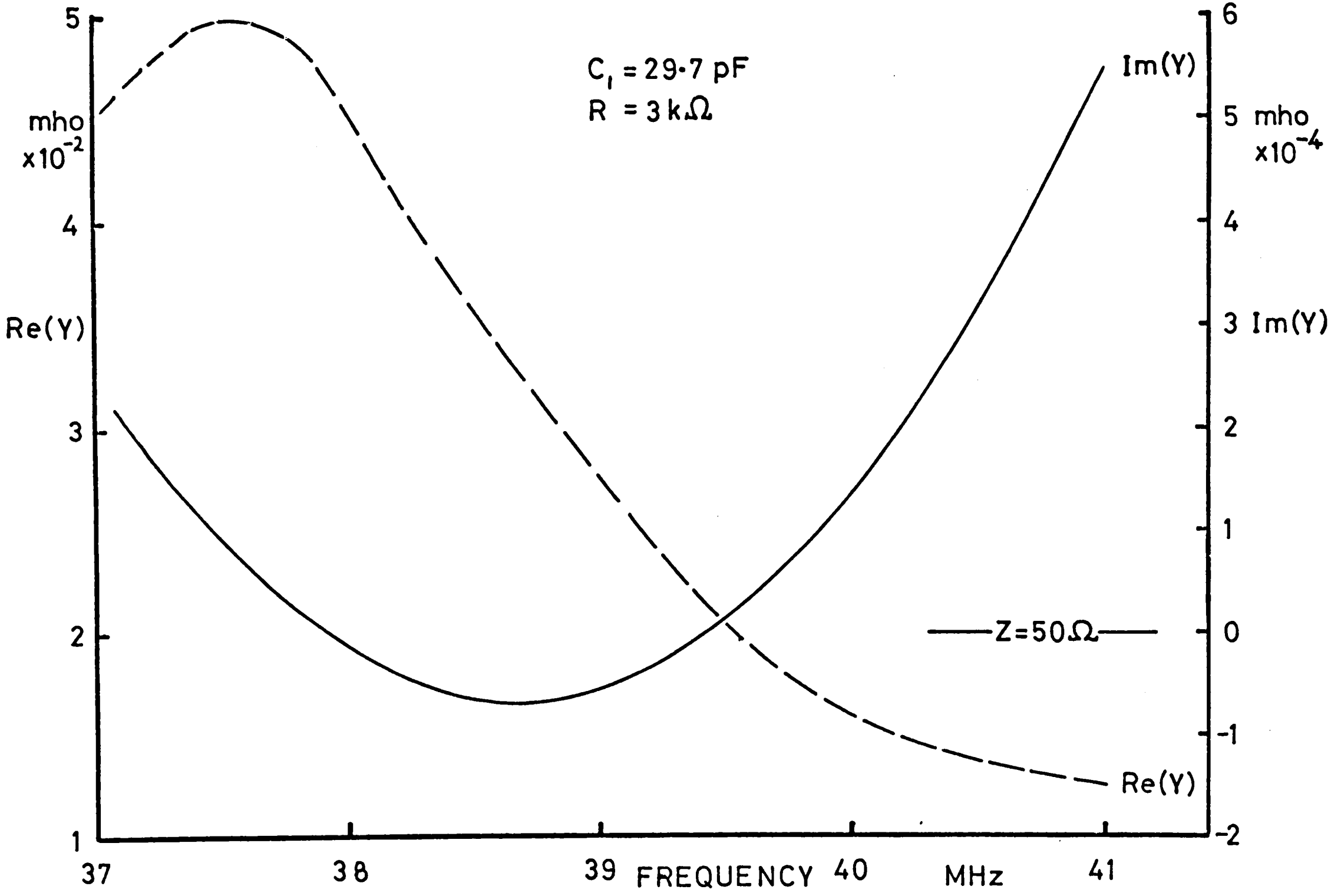


Fig. A.2 : Response of Tank circuit (theoretical)

APPENDIX II

LIST OF COMPONENTS

List of components and their cost (at May 1976) used in the NQR spectrometer.

Basic Units	Supplier (if external)	Cost (£)
Magnet	Swift-Levick & Co.	1000
Minispec	Bruker	6500
Cycle Controller (components & Labour)		1500
Synthesiser	Pacific Measurements Inc.	1000
Calculator + Interface	Advance Instruments	30
R.F. Amplifier (Components)		20
Cryostat & Transit Mechanism (est. labour)		1000
Circulation Pump	Compton	250
Chart Recorder	Honeywell	700
Framework and other essentials		500
		£12,500

Accessories	
Vacuum Pumping System	£ 400
Dewars (1) Glass	20
(2) Metal (helium)	500
Oscilloscope	500
Biomation	900
	£ 2,320

REFERENCES

(1) DEHMELT and KRÜGER, Naturwiss., 37, 111 (1950)

(2) HARTMANN and HAHN, Phys. Rev., 128, 2042 (1962).

(3) KOO, J.C., Ph.D. Thesis, University of California, Berkeley (1969).

(4) EDMONDS, Phys. Rep., 29C, 233-290 (1977).

(5) EDMONDS, HUNT, MACKAY and SUMMERS, 'Advances in Quadrupole Resonance' Heyden, London, (1974), p.145.

(6) EDMONDS, Proc. 18th Ampere Congress, Nottingham, (1974) p.13.

(7) GRECHSHKIN and AINBINDER, Sov. Phys. Uspekhi, 6, 566 (1964).

(8) ARNOLD, DHARMATTI and PACKARD, J. Chem. Phys., 19. 507 (1951).

(9) MACKAY, A.L., D.Phil. Thesis, University of Oxford, (1975).

(10) EDMONDS and MAILER, J. Mag. Res., 26, 93 (1977).

(11) BLEANEY and BLEANEY, 'Electricity and Magnetism'. 2nd ed., O.U.P. (1965).

(12) ABRAGAM, 'Principles of Nuclear Magnetism', O.U.P., (1961).

(13) ANDREW, 'Nuclear Magnetic Resonance', C.U.P., (1956).

(14) POUND, Phys. Rev., 81, 156 (1951).

(15) COHEN and REIF, Solid State Phys., 5, 321 (1957).

(16) RAMSEY, 'Nuclear Moments', Wiley, New York, (1953), pp.16-21.

(17) DAS and HAHN, 'Nuclear Quadrupole Resonance Spectroscopy', chpt. I, Academic Press, London, (1958).

(18) LUCKEN, 'Nuclear Quadrupole Coupling Constants', Academic Press, London (1969).

(19) NEGITA, J. Chem. Phys., 44, 1734 (1966).

(20) SMITH, J.A.S. ed., 'Advances in Quadrupole Resonance', vol.1, Heyden, London (1974).

(21) PETERSEN and OJA, 'Advances in Quadrupole Resonance', vol.1, Heyden, London (1974), p.179.

(22) BARNES, 'Advances in Quadrupole Resonance', vol.1., Heyden, London, (1974), p.335.

(23) WITANOWSKI and WEBB, eds., 'Nitrogen NMR', Plenum Press, London, (1973).

(24) REDFIELD, Phys. Rev., 130, 589 (1963).

(25) SLUSHER and HAHN, Phys. Rev., 166, 332 (1968).

(26) HSIEH, KOO and HAHN, Chem. Phys. Lett., 13, 563 (1972).

(27) WRIGHT, Phys. Rev., 76, 1826 (1949).

(28) LOWE and TARR, J. Phys. E., 1, 320 (1968).

(29) CAMPBELL, HERBERT, WARWICH and WOODGATE, J. Phys. E., 9, 443 (1976).

(30) CLARENDON LABORATORY, Data Sheet E.W.581.

(31) TAYLOR, BOOTH and ALLEN, J. Phys. E., 7, 105 (1974)

(32) SUMMERS, C.P., D. Phil Thesis, University of Oxford, (1975).

(33) ANDERSON, Phys. Rev., 125, 1517 (1962).

(34) ADRIAENSSENS and BJORKSTAM, J. Chem. Phys., 56, 1223 (1972).

(35) REDFIELD, Phys. Rev., 98, 1787 (1955)
130, 589 (1963)

(36) GOLDMAN, 'Spin Temperature and Nuclear Magnetic Resonance in Solids', O.U.P., (1970).

(37) JONES and DAYCOCK, J. Phys.C, 4, 765 (1971).

(38) EDMONDS, HUNT and MACKAY, J. Magn. Res., 20, 505 (1975).

(39) EDMONDS and SUMMERS, Chem. Phys. Lett., 41, 482 (1976).

(40) EDMONDS, GOREN, MACKAY, WHITE and SHERMAN, J. Magn. Res., 23, 505 (1976).

(41) MOORE, GLICK and BAKER, J. Am. Chem. Soc., 94, 1858 (1972).

(42) HUNT and MACKAY, J. Magn. Res., 15, 402 (1974).

(43) SØRENSEN, J. Mol. Spec., 22, 325 (1967).

(44) GUIBÉ, 'Nuclear Quadrupole Coupling Constants', Academic Press, London (1969).

(45) WRIGHT and KING, Acta. Cryst., 7, 283 (1954).

(46) WHITE, A.A.L., (Private communication)

(47) WRIGHT and KING, Acta. Cryst., 6, 305 (1953).

(48) LIQUORI and VACIAGO, Ric. Sci., 26, 1848 (1956).

(49) KOETZLE and LEHMAN, 'Hydrogen Bonding', (ed. Schuster), North-Holland, Amsterdam, (1974)

(50) RABIDEAU, FINCH and DENISON, J. Chem. Phys., 47, 544 (1968).

(51) MORINO and TOYAMA, J. Chem. Phys., 35, 1289 (1961)

(52) BROOKER and CREEL, J. Chem. Phys., 61, 3658 (1974).

(53) EDMONDS, HUNT and MACKAY, J. Magn. Res., 9, 66 (1973).

(54) VARIAN, N.M.R. Tables, 5th ed., (1965).

(55) ITOH, KUSAKA and YAMAGATA, J. Phys. Soc. Japan, 9, 209 (1954).

(56) WYCHOFF, 'Crystal Structures', Interscience, Wiley, London (1963).

(57) STEHR, Z. Kristallogr., 125, 332 (1967).

(58) BAYER, Z. Phys., 130, 227 (1951).

(59) LANGHOFF and HURST, Phys. Rev., 139A, 1415 (1965).

(60) WUNDERLICH, Acta. Cryst., 10, 462 (1957).

(61) HEMILY, Acta. Cryst., 10, 37 (1957).

(62) BEUERSKENS and JEFFREY, J. Chem. Phys., 41, 924 (1964).

(63) EDMONDS and MACKAY, J. Magn. Res., 20, 515 (1975).

(64) BLOEMBERGEN, Physica, 15, 386 (1949).

(65) WOLFE, Phys. Rev. Lett., 31, 907 (1973).

(66) WINTER, C.R. Acad. Sci., 249, 2192 (1959) (quoted in ref.(12)).

(67) ALLEN, ANDREW and BATES, eds., 'Proc. of 18th Ampere Conference', Nottingham University, (1974).

(68) KITTEL, 'Introduction to Solid State Physics', Wiley, London (1971).

(69) ANDREW, HINSHAW, HUTCHINS and SJÖBLOM, Proc. of 18th Ampere Conference, Nottingham University (1974), p.269.

(70) LEHRER AND O'KONSKI, J. Chem. Phys., 43, 1941 (1965).

(71) BOLLMAN, E., Diplomarbeit, Freie Universität Berlin (1977)

(72) HUDSON, RAMAGE and JONES, J. Phys. E., 9, 1106 (1976)

(73) CHAPMAN, DANYLUK and McLAUCHLAN, Proc. Roy. Soc., Lond., B178, 465 (1971).

(74) WHITE, A.A.L., D. Phil. Thesis, University of Oxford, (1977) (To be submitted).